Republic of Iraq
Ministry of Higher Education
and Scientific Research
University of Babylon
College of Engineering
Mechanical Engineering Department

Enhancement of Heat Exchanger for Thermal-Hydraulic Performance Using Copper Foam.

A Thesis

Submitted to the College of Engineering, University of Babylon in Partial Fulfillment of the Requirements for the Award of the Degree of Doctor of Philosophy in Engineering/ Mechanical Engineering/Power

By

Ahmed Mohammed Hassan Abdalirees

Supervised by

Prof. Dr. Adil Abbas Alwan Al-Moosawy

Prof. Dr. Hameed Kadhem Hamzah

2023A.D **1444 A.H**

بسم الله الرحمن الرحيم

﴿ وَلَوْلَا فَضْلُ اللَّهِ عَلَيْكَ وَرَحْمَتُهُ لَهَمَّتْ طَائِفَةٌ مِنْهُمْ
أَنْ يُضِلُّوكَ وَمَا يُضِلُّونَ إِلَّا أَنْفُسَهُمْ وَمَا يَضُرُّونَكَ مِنْ
شَيْءٍ وَأَنْزَلَ اللَّهُ عَلَيْكَ الْكِتَابَ وَالْحِكْمَةَ وَعَلَّمَكَ مَا
لَمْ تَكُنْ تَعْلَمُ وَكَانَ فَضْلُ اللَّهِ عَلَيْكَ عَظِيمًا ﴾

صدق الله العلي العظيم

سورة النساء أية ﴿١١٣﴾

Certification

We certify that this thesis entitled ***"Enhancement of Heat Exchanger for Thermal-Hydraulic Performance Using Copper Foam"*** was prepared by ***Ahmed Mohammed Hassan*** under our supervision at the University of Babylon in a partial fulfilment of the requirements for the degree of Doctor of Philosophy in Mechanical Engineering/ Power.

We recommend that this thesis be forwarded for examination in accordance with the regulation of the University of Babylon.

Signature:

Name: ***Prof. Dr. Adil Abbas AL-Moosawy***

Title: Supervisor

Date: / /

Signature:

Name: ***Prof. Dr. Hameed Kadhem Hamzah***

Title: Supervisor

Date: / /

Examining Committee Certification

We certify, that we have read this thesis entitled "**Enhancement of Heat Exchanger for Thermal-Hydraulic Performance Using Copper Foam"** and as an examining committee, examined the student "**Ahmed Mohammed Hassan ",** in its content and that in our opinion it meets the standard of thesis for the degree of Doctor of Philosophy in Mechanical Engineering/ Power.

Signature:

Name: ***Prof. Dr. Adil Abbas AL-Moosawy***
Title: Supervisor
Date: / /2023

Signature:

Name: ***Prof. Dr. Hameed Kadhem Hamzah***
Title: Supervisor
Date: / /2023

Signature:

Name: ***Prof. Dr. Qusay Rasheed Abd Al-Amir***
Title: Member
Date: / /2023

Signature:

Name: ***Prof. Dr. Riyadh S. Salah Al-Turaihi***
Title: Member
Date: / /2023

Signature:

Name: ***Prof. Dr. Isam Mejbel Abed***
Title: Member
Date: / /2023

Signature:

Name: ***Prof. Dr. Alaa Abbas Mahdi***
Title: Member
Date: / /2023

Signature:

Name: ***Prof. Dr. Qasim Saleh Mahdi***
Title: Chairman
Date: / /2023

Approval of Mechanical Engineering Department
Head of the Mechanical Engineering Department

Signature:

Name: ***Assist Prof. Dr. Samer M. Abdul Haleem***
Date: / /2023

Approval of the College of Engineering
The Acting Dean of the College of Engineering

Signature:

Name: ***Prof. Dr. Laith Ali El- Anzy***
Date: / /2023

Dedication

I would like to express my gratefulness to my biggest supporters, to the reason of where I am and where I will be, my father, and mother.

Ahmed 2023

Acknowledgments

Deepest appreciation for the almighty Allah for the modest assistance in all aspects of my preparation of this work. My sincere thanks and respect to my supervisors ***Prof. Dr. Adil Abbas AL-Moosawy*** and ***Prof. Dr. Hameed Kadhem Hamzah*** who never hesitated in helping me to achieve this.

I also thank all staff and members of the College of Engineering /Mechanical Engineering Department at the University of Babylon for being the greatest cooperators. Finally, thanks to ***Mr. Hussain Hamzah Rashid*** in mechanical engineering laboratories.

Ahmed 2023

Abstract

Due to its high porosity as well as a high specific surface area, the use of open cell metallic foam in heat transfer applications has received increasing interest. In present study, the dynamic and thermal performance of heat exchanger composed of copper foam incorporated in a fan coil was experimentally and numerically analyzed.

Fan coil unit heat exchanger is designed with 2 TR cooling load. Different flow conditions are tested to reach the appropriate design that covers the required cooling load. The heat exchanger designing process is carried out by using the effectiveness–NTU method and the SOLIDWORK 2022 software to determine the tube length and the form of the heat exchanger. Through experimental work, copper foam is used as a porous medium, which is placed instead of the traditional aluminum fins. The comparison between the two heat exchangers, one with fins and the other with copper foam, is done under different conditions. Reynolds number of the inlet air ranged from 22650 to 235000. A comparison is made between the thermal and dynamic performance of copper foam and fins by calculating several parameters, including effectiveness of heat exchanger, thermal resistance, heat transfer coefficient, Nusselt number, Colburn factor, friction factor, and area goodness factor. In theoretical work, COMSOL Multiphysics 6.0 software is used to analyze the flow through heat exchanger with metal foam. Darcy-Brinkman-Forchheimer model is used to represent the momentum equation inside the metallic foam (a porous medium). A local thermal equilibrium is used to solve the energy equation through the porous medium

Through experiments, it is found that the water entry temperature equal to 10 ^{o}C is the most appropriate to give better thermal performance

and depends mainly on the diameter of the tube that is designed. The flow rate of cold water through the tube depends on the cooling load, so through experiments it is found that the flow of 4 LPM covers the required cooling load. Experimental results show for the low air velocity that the heat transfer coefficient is almost equal for both types and with a small difference for the fins, while the difference in the heat transfer coefficient increases with the increase in the inlet air velocity. Colburn factor is higher in the case of the heat exchanger with copper foam than in the conventional fins, where it is equal to 0.1959 for the copper foam and 0.1186 for the fins. Area goodness factor is higher in the case of fins than its value in the case of copper foam by 16.8%. Different porosity values are taken during the study, ranging from 0.88 to 0.98, while the velocity of inlet air of the heat exchanger ranged from 1 m/s to 10 m/s. The theoretical results show that increasing porosity from 0.88 to 0.98 leads to a decrease in the heat transfer coefficient by 39% in the case of velocity 10 m/s and by 30% in the case of velocity 1 m/s. Pressure drop decreases by 32% when increasing the porosity from 0.88 to 0.98 at an air inlet velocity of 10 m/s.

A comparison is made between the experimental and the theoretical results, where it is found that the deviation error between the experimental and theoretical results of heat transfer coefficient is 19.1 % when Reynolds number equal to 22650, 19.2% at Reynolds number equal to 120800, and 19.2% at Reynolds number equal to 218940.

Nomenclature

Notation	Description	Units
A	Cross section area	m^2
B	Surface to volume ratio	m^2/m^3
C_F	Drag factor Coefficient	-
c_p	Specific heat	J/kg. ^oC
df	Fiber diameter	m
dp	Pore diameter	m
D	Diameter	m
f	Friction factor	-
g	Gravity acceleration	m/s^2
H	Heat exchanger height	m
W	Heat exchanger width	m
h	Heat transfer coefficient	$W/m^2\ ^oC$
j	Colburn factor	-
k	Thermal conductivity	W/m.^{o}C
K	Permeability	m^2
L	Thickness of porous medium in the direction of flow	m
$\dot{m}$	Mass flow rate	kg/s
Nu	Nusselt number	-
p	Pressure	Pa
Pr	Prandtl number	-
Q	Heat transfer rate	W
q'''	Heat generation	W/m^3

r	tube radius	m
Re	Reynolds number	-
T	Temperature	^{o}C
t	Time	s
u	x-velocity	m/s
U	General velocity term	m/s
v	y-velocity	m/s
V	Intrinsic average velocity	m/s
x	Cartesian x-axis direction	m
y	Cartesian y-axis direction	m
Greek symbols		
∇	Laplace operator	
Δ	Difference	
ε	Effectiveness	-
φ	Porosity	-
μ	Dynamic viscosity	m^2/s
ρ	Density	kg/m^3
σ	Normal stress	Pa
α_{sf}	specific surface area	m^2/m^3
Abbreviations		
AG	Area goodness factor	
FCU	Fan Coil Unit	
FEM	Finite Element Method	
HVAC	Heat, Ventilation, and Air Conditioning	
LTE	Local thermal equilibrium	

LTNE	Local thermal non equilibrium	
PEC	Performance Evaluation Criteria	
PPI	Number of pores per inch	
SIMPLE	Semi-Implicit Method for Pressure Linked Equations	
Subscripts		
e	Effective	
f	Fluid phase	
in	Inlet	
o	Outlet	
s	Solid phase	
tube	Wall of tube	

Contents

CHAPTER ONE

INTRODUCTION

Chapter One: Introduction

In many engineering applications, the process of transferring heat between two mediums occurs in a device called a heat exchanger. This transfer can occur either through direct contact or through a solid wall separating the mediums. Heat exchangers are also used in various equipment such as condensers, evaporators, economizers, fan coil units (FCUs), and radiators. The thermal performance of a heat exchanger depends on several factors, including the materials used, the medium (water or air), the device configuration, and the flow rates of water and air. Increasing the thermal performance of a heat exchanger can result in significant cost savings during both manufacturing and operation of the device [1]. When designing or predicting the performance of a heat exchanger, it is necessary to consider the total heat transfer rate and its relationship to various process variables. These variables include the geometry of the heat exchanger, the arrangement of flows, the materials used, and the design configurations such as tube sizes, geometry, operating conditions, and operational costs. An optimal design for a heat exchanger should provide the maximum heat transfer rate with a low pressure drop. A high pressure drop in the heat exchanger would require a larger pump size to overcome the flow resistance, resulting in increased system costs [2].

1.1. Heat Exchangers

It can be defined as a device that is used to transfer thermal energy (enthalpy) between two or more fluids, between a solid surface and a fluid, or between solid particulates and a fluid, at different temperatures and in thermal contact. In heat exchangers, there are usually no external heat and work interactions. Typical applications involve heating or cooling of a fluid stream and evaporation or condensation of single or multicomponent fluid streams. In a few heat exchangers, the fluids exchanging heat are in direct

contact. In most heat exchangers, heat transfer between fluids takes place through a separating wall or into and out of a wall in a transient manner. In many heat exchangers, the fluids are separated by a heat transfer surface, and ideally, they do not mix or leak. Many applications make use of them, including heating, ventilation, and air conditioning systems (HVAC), power generation, and manufacturing systems. A variety of heat transfer equipment, such as condensers, evaporators, economizers, and radiators, is generally referred to as heat exchangers. The design of heat transfer processes results in a wide range of shapes and sizes for heat exchangers. Shah and Sekulic [3] classifying the heat exchangers as seen in figure (1-1).

1.2. Crossflow Heat Exchanger

In this type of exchanger, as shown in figure (1-2), the two fluids flow in directions normal to each other. Typical fluid temperature variations are idealized as two-dimensional and are shown in figure (1-3) for the inlet and outlet sections only. Thermodynamically, the effectiveness for the crossflow exchanger falls in between that for the counter flow and parallel flow arrangements. The largest structural temperature difference exists at the ‘‘corner’’ of the entering hot and cold fluids, such as in figure (1-3). This is one of the most common flow arrangements used for extended surface heat exchangers, because it greatly simplifies the header design at the entrance and exit of each fluid. [3].

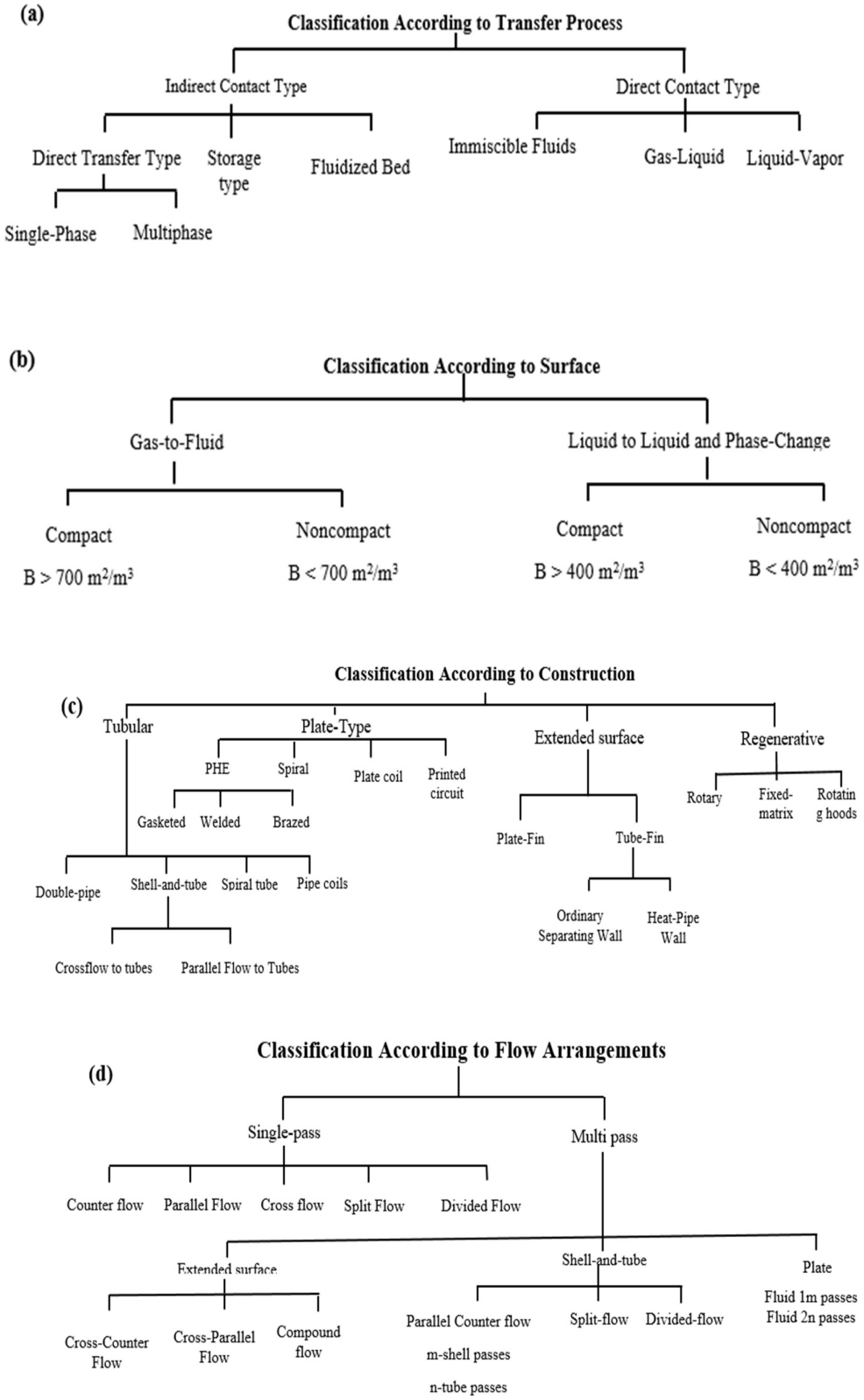

Figure (1- 1) classification of heat exchangers. Ref. [3].

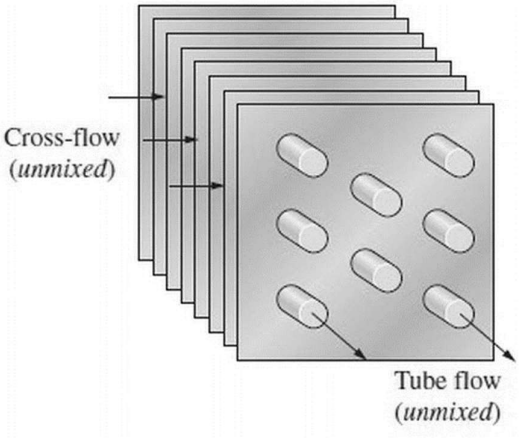

Figure (1- 2) (a) plate-fin unmixed–unmixed crossflow heat exchanger; (b) serpentine (one tube row) tube-fin unmixed–mixed crossflow heat exchanger.

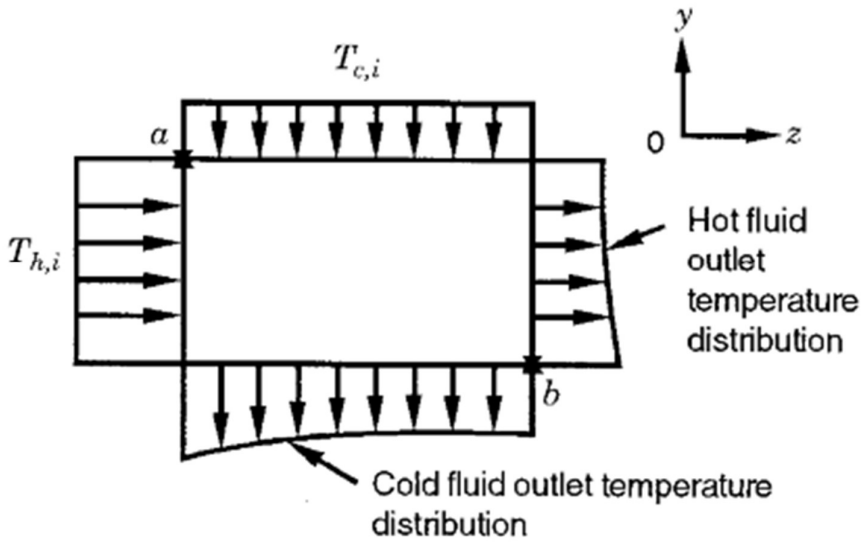

Figure (1- 3) temperature distributions at inlets and outlets of an unmixed–unmixed crossflow heat exchanger Ref.[3].

1.3. Fan Coil Unit (FCU) Operating Principle

A fan coil unit (FCU) is a part of an HVAC system used in residential, commercial, and industrial buildings. These devices consist of a heating or cooling coil and a fan. Typically, a fan coil unit is not connected to the ductwork, and is used to control the temperature in the space where it is installed, or serve multiple spaces. Control can be achieved either manually through the use of an on/off switch or by utilizing a thermostat.

Fan coil units are more cost-effective to install compared to ducted or central heating systems with air handling units, owing to their simplicity. However, they have the potential to generate noise since the fan is located within the same space. These units can be found in various configurations, such as horizontal (ceiling mounted) or vertical (floor mounted) [4].

The basic Fan Coil Unit (FCU) is manufactured using galvanized steel, which consists of a back panel, side panels, spigot panel, fan deck assembly, heat exchanger, drain tray assembly, filter, electrics assembly and access panels. In general, any FCU primary inputs are the flow rate of air, air temperature, the flow rate of liquid and its temperature, whereas heat transfer rate, pressure drop and noise level are the primary outputs that need to be analyzed. The basic operation of FCU uses re-circulated air which is air pulled into the FCU using the fan deck assembly. The heat exchanger has either cold or hot water circulating through the tubes, depending on what is required. The air which is drawn across the heat exchanger is then cooled or heated and expelled through various ducts, which are attached to the spigot panel into the room below which is seen in figure (1-4). Various sensors and controls systems are used with the FCU to control the temperature in the room. [5].

A centrifugal fan draws the air across the heat exchanger which will have either cold or hot water through the copper tubes; this is then expelled into the room as seen in figure (1-5).

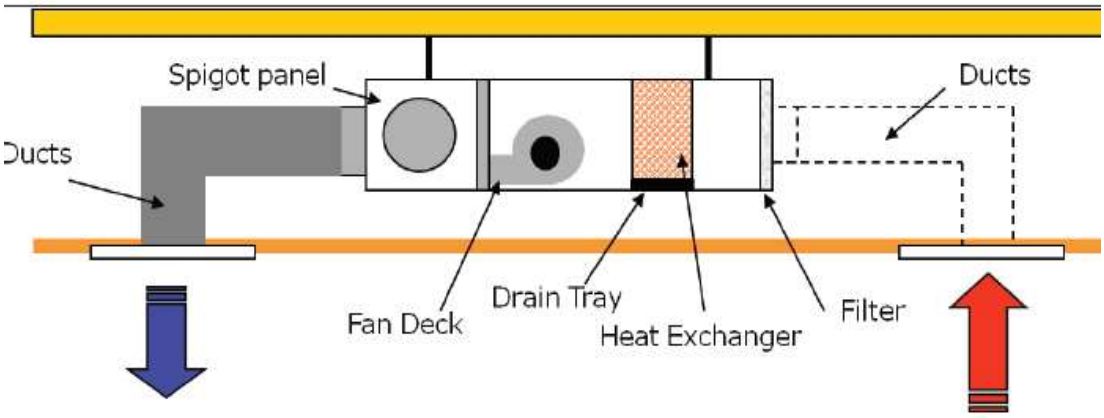

Figure (1- 4) operation of a fan coil unit. Ref. [4]

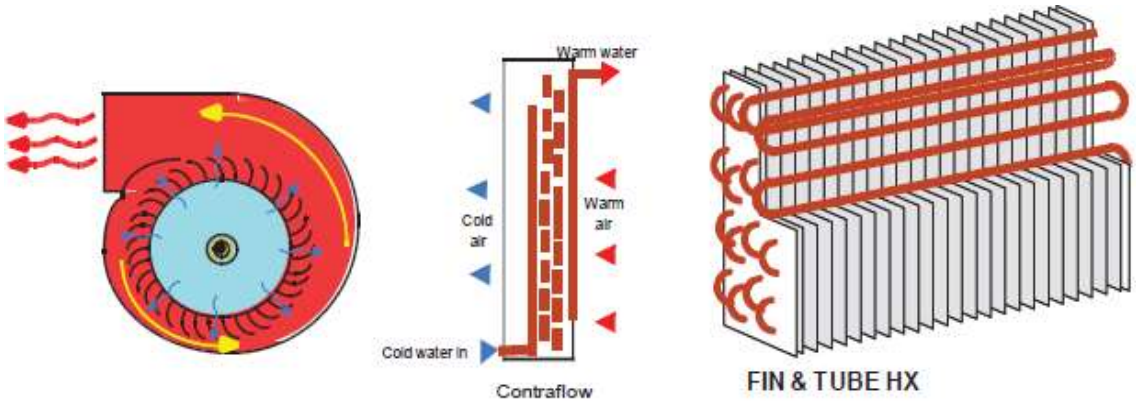

Figure (1- 5) fan operation. Ref.[5].

1.4. Cross-Flow Heat Exchanger and Enhancement Methods

The performance of the heat exchanger can be improved through several methods, as can be observed in figures (1-6). These methods are considered passive as they do not require an external power source. Passive methods are commonly employed to enhance heat transfer in the heat exchanger due to their independence from an external power source. Typically, the heat transfer surface area can be modified [6], and vortex generators can be added into the flow path [7]. These methods induce flow instability, leading to an improvement in heat transfer efficiency. Recently, metallic foam has been utilized in combination with cross-flow heat

exchangers to increase the heat exchange area and introduce flow instability, thereby improving heat transfer, as shown in figure (1-6).

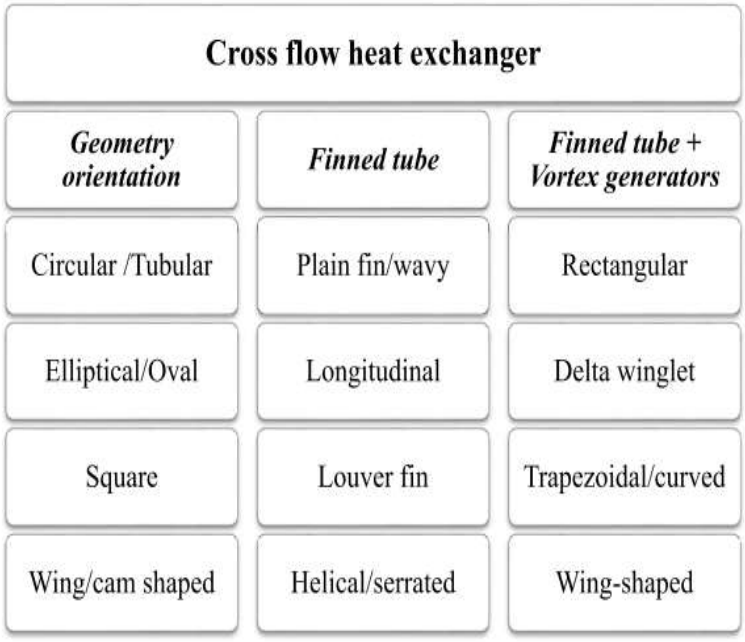

Figure (1- 6) methods for increasing the thermal performance of a cross flow heat exchanger. Ref. [8]

1.5. Metallic Foam

Metal foam is a porous medium that is formed using one of the metals such as aluminum, copper, steel, nickel and other metals. The foam consists of multiple open cells with hexagonal faces as shown in figure (1-7). The metal foam contains several variables, the most important of which are The pore diameter d_p which represents the diameter of the hollow cell and strut diameter d_f which represents the diameter of ligaments.[9]. The density of pores, which is measured by the number of pores within a length of one inch (PPI), which often ranges from 5 to 100 PPI, the lower PPI this means that the size of the pores is large. As for the other characteristic, which is porosity, which represents the ratio of the void volume to the volume of the solid part within the porous medium that ranges from 80%– 99%.[10].

Metal foam is one of the methods used to improve the thermal performance of heat exchangers due to its good thermal and physical properties. Where the metal foam increases the heat exchange area, as well as disrupts the boundary layer, thus increasing the Nusselt number, and then the thermal performance increases. In addition, the metallic foam has a high permeability and thermal conductivity and is also characterized by its light weight and therefore suitable for use with heat exchangers.

1.6. Motivation of This Study

Optimization of the heat exchangers itself as well as cost saving, and faster design and development processes are often referred to as heat transfer augmentation, enhancement or intensification. Main gains in thermal performance are usually achieved by increase in convective heat transfer by reducing thermal resistance. However, better thermal performance usually is coming at a cost of increased pressure drop across the heat exchanger and therefore increases energy requirement during operation. This could be partially compensated for by smaller designs and overall device miniaturization of the heat exchanger unit. Therefore, design and development of new type of heat exchangers is often an act of balancing competing requirements and different objectives at different stages of the design process.

1.7. Objectives of the Study

The main objective of this thesis is to study the thermal performance of cross flow heat exchanger used in fan coil unit (FCU). The study objectives can be formulated as follows: -

1- Design and fabrication of the rig for cross flow heat exchanger to determine the thermal performance parameters like the effectiveness of

heat exchanger, thermal resistance, heat transfer coefficient, Nusselt number, Colburn factor, friction factor, and area goodness factor.

2- Development of more efficient design for cross flow heat exchanger with metallic foam to improve (FCU) thermal performance. Determine Optimal Heat Exchanger Design Parameters. The study aimed to identify the ideal cold water flow rate and water inlet temperature for achieving the best performance of the heat exchanger.

3- Investigate Heat Transfer Coefficient: The study aimed to analyze the effect of air inlet velocity on the heat transfer coefficient for heat exchangers with fins or copper foam.

4- Evaluate Colburn Factor and Thermal Resistance: The study compared the Colburn factor and thermal resistance of heat exchangers with copper foam and conventional fins.

5- Analyze Pressure Drop: The study examined the pressure drop in heat exchangers with copper foam and conventional fins.

6- Investigate Porosity Effect: The study analyzed the impact of porosity on heat transfer coefficient, Colburn factor, and pressure drop.

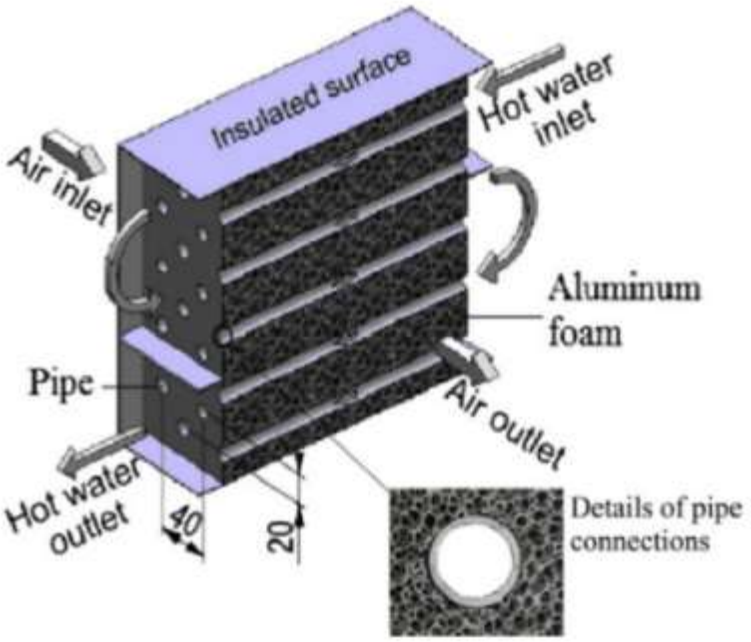

Figure (1- 7) open cell aluminum foam heat exchanger. **Ref.[11].**

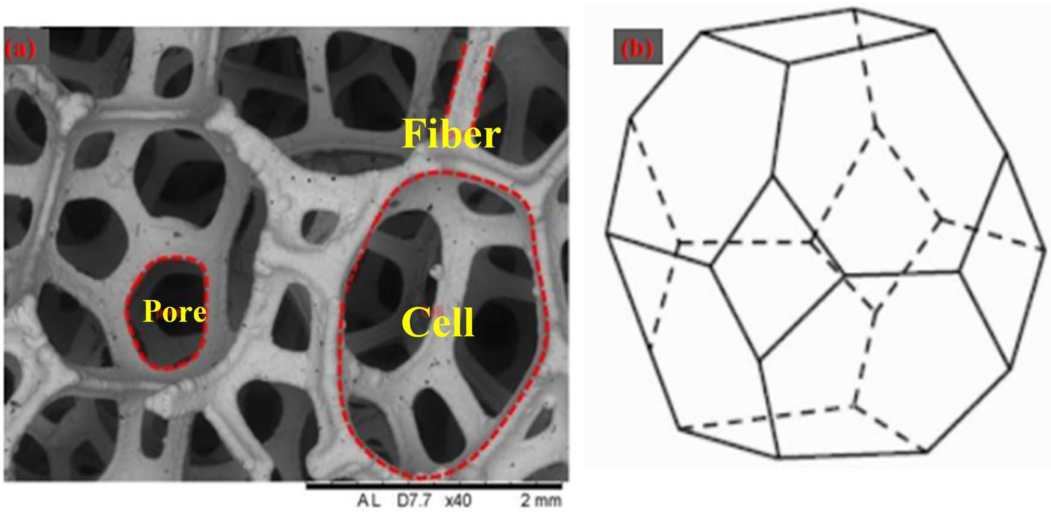

Figure (1- 8) (a)metal Foam Structure, (b) unit cell representation. **Ref. [12].**

CHAPTER TWO

LITERATURES

REVIEW

Chapter Two: Literature Review

Metal foams present a number of interesting material properties for the development of compact heat exchangers, specifically: a very high surface to volume ratio, strong mixing capability, low weight and high toughness. Quite a large number of technical papers have already been presented in the open literature reporting on the development of a heat exchanger using metal foams. In the subsequent literature survey, some of the previously published results will be listed, focusing on the application of (metal) foam to enhance the heat transfer rate. Several researchers have investigated the behavior of heat transfer in metallic foam theoretically and experimentally.

2.1. Experimental studies

Klett et al. 2000, [13] conducted an experimental study on an open cell graphite foam with a cross-flow heat exchanger that was utilized for heat recovery in vehicles. The foam had a density of 0.2-0.6 g/cm^3, providing it with a lightweight property, along with a surface area greater than 4 m^2/g. Water was employed as the cooling fluid with a flow rate of 11.34 LPM, while the air flow rate in the experimental setup ranged from 140 LPM to 420 LPM. Two heat exchanger designs were employed to minimize the pressure drop. The results demonstrated that heat transfer coefficients of the foam-based heat exchanger could be up to two orders higher than those of conventional heat exchangers.

Kim et al. 2000, [14] conducted an experimental investigation on the utilization of porous fins in cross flow plate heat exchangers. The study involved a comparison between louvered fins and porous fins in terms of thermal and dynamic performance. The porous fins were made from 6101-aluminum alloy foam. Various geometrical properties of the foam were

studied, including pore per inch (PPI) ranging from 10 to 40, porosity ranging from 0.89 to 0.96, and the number of fins ranging from 1 to 6. The flow conditions ranged from $270 < Re < 2050$. The results indicated that the friction factor was significantly lower for low-permeability porous fins. However, at high Reynolds numbers, the friction factor increased for porous fins. The researchers explained this observation by stating that increasing the pore density led to a decrease in the j-factor.

Boomsma et al., 2003, [15] studied experimentally the aluminum foam with compact heat exchanger used in electronic cooling application. 6101-T6 aluminum open cell foam with a cell diameter of 2.3 mm and a pore density of 40 PPI was utilized in the study. Two porosity values, 0.92 and 0.95, were considered. The aluminum foam exhibited a thermal conductivity of 218 W/m·K and a surface to volume ratio of 10,000 m^2/m^3. The flow conditions involved coolant velocities ranging from 0 to 2 m/s. Both water and a water-ethylene glycol mixture with a concentration of 50% were used as coolant fluids. The heat flux applied in the experiments reached up to 688 kW/m^2. Several parameters were investigated, including Nusselt number, pressure drop, friction factor, Colburn j factor, pumping power, and thermal resistance. The results showed that the heat exchanger with foam thermal resistance were two to three times lower than conventional heat exchanger with same value of pumping power.

Tadrist et al., 2004, [16] analyzed experimentally the transport properties such as friction factor, Nusselt number, effective thermal conductivity, permeability, and entrance length for both stacked fibers, and metallic foams. The foam made from aluminum with (10,20, and 40PPI). The fiber made from copper and bronze with porosity range from 0.38 to 0.92. Both materials were employed as replacements for fins in a cross-flow compact heat exchanger. The objective was to identify the optimal

parameters of the porous medium in order to maximize heat transfer while minimizing pressure drop. The results demonstrated a significant increase in thermal performance accompanied by a low pressure drop, indicating a favorable trade-off between the two factors.

Tian et al., 2004, [17] detailed experimentally the thermal and dynamic performance for different materials such as metallic foam, periodic cellular topologies metal, textile laminate, and brazed wire screen, which used as a heat dissipation medium. Pure copper material was utilized for all configurations in the study. The flow conditions encompassed an air flow velocity ranging from 1 to 10 m/s, corresponding to Reynolds numbers between 700 and 1000. Various parameters were investigated, including the effect of flow orientation, pore shape, porosity, and open area ratio. The thermal and dynamic performance of the system was assessed by establishing the relationship between Nusselt number, Reynolds number, and friction factor. The results showed that friction factor depends mainly on pore size, open area ratio, flow direction. Heat transfer depends mainly on solid conduction, forced convection, porosity, surface area.

Jamin and Mohamad, 2007, [18] presented experimentally the comparison between different configuration of aluminum fins and carbon foam. An external surface was utilized to mitigate the thermal resistance at the solid-gas interface. The experiment was conducted in the vertical direction with the surface being heated. The carbon foam was 61% porosity, and $7.5*10^{-13}$ permeability. The range of Re which used in their study was 7000 to 40,000. The results showed the aluminum fins gave heights value of Nu, which about three times greater than carbon foam. Carbo foam fins give pressure drop lower than aluminum fins, but higher than carbon sleeves.

Tzeng, 2007, [19] explained experimentally the aluminum foam with copper conductive pipe as a heat sink. Four models were employed for the cooling system: (1) a model without a conductive pipe, (2) a model with a copper conductive pipe, (3) a model with air gaps in front, and (4) a model with lateral arc gaps. Air was used as the working fluid, with Reynolds numbers ranging from 883 to 4416. The aluminum foam had the following dimensions: 10 PPI pore density, 0.97 porosity, 2.52 W/m·K thermal conductivity, and a permeability of $2.5x10^{-7}$. The study investigated the distribution of Nusselt number throughout the system, as well as the average Nusselt number and pressure drop across the porous medium. The results showed the conductive pipe with aluminum foam was very effective thermal performance. They found correlation equation for all four models, and they found the pressure drop through porous medium and pumping power.

Bonnet et al., 2008, [20] found the relation between foam geometrical parameter and flow parameter experimentally. Copper, nickel, and nickel-chrome alloy were utilized as foam materials with various pore sizes ranging from 500 to 5000 μm, and porosities ranging from 0.87 to 0.97. The working fluid employed in their study consisted of air with velocities ranging from 0 to 20 m/s, and water with velocities ranging from 0 to 0.1 m/s. Pressure drop in the foam was measured experimentally using 12 pressure sensors. The effect of compressibility on permeability and inertia coefficient was investigated. The results demonstrated that even at low velocities, compressibility strongly influenced the flow parameters. It was observed that the permeability and inertia coefficient were independent of the nature of the fluid, and the permeability was proportional to the square of the pore size, while the inertia coefficient was inversely proportional to the pore size.

Cavallini et al., 2008, [21] proposed experimentally the thermal and dynamic performance of two samples of Aluminum foam with 5 and 40 PPI. They used air mass flow rate range from 0.01 to 0.025 kg/s. Foam was employed to facilitate heat distribution from an electrical heater with power ranging from 25 to 40 kW/m2. The obtained results yielded empirical correlations for pressure gradients. It was observed that the heat transfer coefficient was dependent on the mass flow rate but not on the heat flux, irrespective of whether it was for the 40 PPI or 5 PPI samples. Al foam with 40 PPI gave better thermal performance than 40 PPI. The wall temperature is higher for 40 PPI samples than 20 PPI sample. The samples with 40 PPI gives higher pressure drop than 5 PPI sample.

T'Joen et al., 2010, [22] described experimentally the single row cross flow heat exchanger with aluminum foam. An aluminum tube with aluminum foam (4-8mm thickness) was utilized and its performance was compared with that of helical fins. The foam had two different pore per inch (PPI) values, namely 10 and 20, and various porosity levels of 0.19, 0.93, and 0.95. The air velocity ranged from 1 to 8 m/s. The results indicated that increasing the height of the foam led to an increase in pressure drop, while simultaneously reducing thermal resistance. It was observed that air only penetrated the external small layer of the foam, so increasing the foam height resulted in decreased thermal performance. Additionally, the study revealed that the benefits of foam were superior to those of helical fins at velocities greater than 4 m/s.

Kamath et al., 2010, [23] reported an experimental study on flow assisted mixed convection in aluminum metal foams of different pores per inch (PPI) with high porosity in the range of 0.9 to 0.95. With a view to delineate the flow regimes, experiments are conducted for Richardson number (Ri) range of $0.001 \leq Ri \leq 700$. Based on a parametric study with a

large number of experimental data, a correlation for Nusselt number of the porous medium as a function of Richardson number, Peclet number, and the porosity was developed. In order to quantify the enhancement of the heat transfer rate with the use of porous medium, correlations for (i) Nusselt number and (ii) ratio of heat transfer rate with and without porous medium have also been developed. The enhancement ratio is always more than one which clearly indicates that metal foams have good heat transfer enhancement capability.

Mancin et al., 2011, [24] showed an experimental study to investigate the heat transfer coefficient and pressure drop during single-phase air heat transfer through four metal foams with 10 pores per inch (PPI). The foams had different porosities and foam core heights, with core heights of 40 mm and 20 mm, respectively. The experiments were conducted in an open-circuit wind channel with a rectangular cross-section. To analyze the effect of foam core height on heat transfer, three constant heat flow rates (250 W, 325 W, and 400 W) were applied at the bottom plate of the samples. The air mass velocity was varied between 0.005 and 0.025 kg m^{-2} s^{-1} at atmospheric pressure. The pressure drops during airflow through the samples were measured using a high-accuracy differential pressure transducer. The experimental results were presented in terms of heat transfer coefficient, normalized mean wall temperature, pressure gradient, permeability, and inertia coefficient. These results were compared to the predictions of two different models.

Muley et al., 2012, [25] reported open-cell porous metal foams with compact heat exchangers due to their increasing availability and improved thermal performance. In recent years, considerable research has been conducted on use of metallic and nonmetallic foams to further improve performance of state-of-the-art heat exchangers. A brief review of nickel–

chromium and stainless-steel foam heat exchanger technology and of recent efforts on their manufacturing techniques for a liquid-to-air heat exchange application was presented. Measured heat transfer and pressure drop data for foam heat exchangers and their comparison with performance of a conventional wavy plate-fin heat exchanger were discussed. Technical challenges and risks associated with foam heat exchangers were discussed, along with recommendations for future development.

Nawaz and Jacobi, 2017, [26] reviewed the comparison between the thermal-hydraulic performance of aluminum and copper metal foam heat exchangers with the same geometry under dry and wet operating conditions. Heat exchanger consisting of round tube with annular layer of metal foam have been considered. Experiments have been conducted using a closed-loop wind tunnel to measure the heat transfer performance and pressure drop. The impact of base metal (aluminum and copper) on the heat transfer rate has been evaluated at varying air flow rates and upstream relative humidity. It has been found that due to similar geometry (flow depth, face area, pore size) both aluminum and copper foam samples have comparable pressure drop under dry conditions. However, the pressure gradient was noticeably different for two samples under wet operating conditions. An obvious difference in heat transfer rate for aluminum and copper metal foam heat exchangers was observed under both dry and wet operating conditions. The findings have been explained in terms of the impact of the thermal conductivity of base metal and condensate retention.

Chen et al., 2018, [27] studied the tube bundles wrapped with metallic foam in air-breathing engine as the compact heat exchanger due to its low density and high specific surface area. The enhanced thermal performance of metallic foam is crucial to design of staggered tube bundles with metallic foam fins. The results indicate that: 1, with increase of

porosity, Nusselt number increases because of stronger penetrating ability, and heat convection dominates the heat transfer. 2, for variation of pore density, Nusselt number of high PPI samples is lower for thermal-insulation effect at low Reynold number. However, Nusselt number of high PPI samples was higher for greater amount of penetrating air at high Reynold number. 3, a new friction factor correlation of tube bundles is proposed to describe the pressure drop by dimensionless tube pitches, Reynolds number and Darcy number with maximum ±20% deviation. 4, a new Nusselt number correlation of tube bundles were given to reflect the heat transfer mechanism by Darcy number.

Hamadouche et al., 2018, [28] described experimentally turbulent forced convection in a rectangular channel partly fitted with aluminum metallic foam blocks. Experiments were carried out on samples having a constant porosity of 93.8%, different grades of 5, 20 and 40 PPI, and three different height ratios of 0.6, 0.8 and 1. The blocks were arranged in a baffle like configuration. A constant heat flux of 2 W/cm^2 was applied on the bottom wall of the test section, while air velocity was varied from 1 to 5 $m \cdot s^{-1}$. The results showed that there was an optimal choice of the height and the grade of the metal foam for which the heat transfer and pressure drop (for an optimal design of heat exchangers) to reach the design goal. Moreover, this configuration was compared to solid fins aluminum baffles widely used in heat exchangers.

Borakhade and Mahalle, 2018, [29] visualized experimentally 40 PPI, 50 PPI, 60 PPI open cell copper metal foam for heat dissipation in forced convection. All the metal foam samples tested with various heater surface temperature and input air velocity to understand thermofluid properties of open cell copper metal foam. Effect of heater surface temperature and input air velocity on various parameters like Reynold

number, Nusselt no, solid to fluid convective heat dissipation rate studied in detail. The pore diameter and cell fiber diameter of metal foam affects the convective heat dissipation rate in forced convection. Experimental investigations showed that open cell copper metal foams are the excellent choice for forced convection heat dissipation application for power electronics devices.

Nilpueng et al., 2020 [30] presented small plate heat exchanger filled with copper foam which can be applied for small scale electronic cooling. Experimental measurements are conducted with a range of Reynolds numbers from 1200 to 2000, and copper foam pore densities varying from 30 to 50 pores per inch (PPI). The findings indicate that both the heat transfer coefficient and pressure drop increase as water velocity and pore density increase. In comparison to a conventional plate heat exchanger, the heat transfer coefficient is enhanced by 20.23%, 29.37%, and 40.28% for PHECFs with pore densities of 30 PPI, 40 PPI, and 50 PPI, respectively. The total pressure drop within the PHECF primarily arises from inertial drag pressure drop. The thermal performance of the PHECF with a pore density of 50 PPI demonstrates the highest performance, with an average thermal performance factor of 1.21.

Salari et al., 2020, [31] investigated an experimental investigation on heat transfer in a double tube heat exchanger, where the inner tube was partially filled with copper metal foam as a porous material. The study focused on laminar and turbulent flows of a nanofluid consisting of MgO nanoparticles (20 nm in size) dispersed in ethylene glycol (EG) at concentrations ranging from 0% to 1% by volume. The findings revealed a significant enhancement in the Nusselt number when using the nanofluid and porous media. The presence of the porous material improved the effectiveness of the nanoparticles in enhancing heat transfer. Additionally,

the performance evaluation criteria (PEC) parameter showed a notable increase, with the highest PEC recorded at 1.19 for a nanoparticle concentration of 1.0%.

Rajamuthu et al., 2020, [32] introduced metal foams as a promising solution for heat dissipation in forced convection cooling applications, particularly in electronics cooling. The thermal and hydraulic performance of metal foams is closely related to their pore density and porosity. The authors conducted experimental evaluations to assess the thermal-hydraulic performance of copper foam with a porosity of 0.95. The foam, with a thickness of 3mm, was placed on a heated surface. Air was employed as the working fluid, which was directed through a 3x3 array of circular nozzles (with a diameter, d j, of 1.5 mm) to enhance heat transfer. Two configurations were examined: a full foam configuration, where the metal foam covered the entire heated surface, and a foam stripes configuration, where metal foam stripes were strategically placed over the heated surface. The study investigated heat transfer, pressure drop, and thermal hydraulic performance within a Reynolds number range (Re j) of 3000 to 12000. A smooth surface, without metal foam, was used as the baseline case. Furthermore, the impact of varying the distance between the jet and the target plate (z) at ratios of z/d j = 2, 3, 5, and 7 was examined.

Rezaei and Abbassi, 2021, [33] conducted an experimental study on heat transfer and pressure drop in laminar flow within circular and flattened tubes that were partially and fully filled with copper metal foam. The experiments involved heating the tube wall with a constant and uniform heat flux, using water as the working fluid, and varying the Reynolds number from 500 to 2300. Six different configurations were considered for the tubes and porous media, and the resulting Nusselt number and pressure drop data were recorded and compared. The experimental findings

demonstrated that the presence of porous media and the flattening of the tube significantly influenced the thermal and hydrodynamic performance of the system. These effects were attributed to the heat spreading through the copper matrix, improved fluid mixing, and the increased heat transfer area. A performance evaluation was conducted, indicating that fully filled tubes exhibited the best overall performance.

Fadhala et al, 2023, [34] conducted an experimental investigation on the impact of copper foam baffles on the thermal hydraulic performance of a staggered arrangement in a duct. The experiments were conducted in a square channel (250 mm x 250 mm) manufactured specifically for this study. The bottom wall of the test section was uniformly heated. Copper foam baffles with a fixed porosity of 95% were mounted on the channel walls. The Reynolds number ranged from $3.8x10^4$ to $5.4x10^4$. To compare the effects, data from conventional copper solid baffles were also used. The results showed that compared to solid copper baffles, copper foam baffles exhibited significantly lower friction factors. The friction factor for the solid baffles was approximately 460 times higher than that for the smooth surface, while for copper foam baffles with pore per inch (PPI) values of 10, 15, and 20, the friction factors were approximately 20, 29, and 38 times higher, respectively, than for the smooth surface.

2.2. Theoretical studies

Raju and Narasimhan, 2007, [35] developed numerically the near compact heat exchanger (100-300 m^2/m^3) with cross flow coolant fluid direction. The effect of incorporating a metal foam (porous medium) in a tube-to-tube line arrangement with a square pitch (transverse to tube diameter = 2.25) was examined. The study focused on investigating the influence of transverse thickness and permeability on heat transfer and pressure drop. A numerical model was employed, utilizing the Brinkman-

Darcy flow model and an average energy equation for the energy model. The assumption of a constant wall temperature allowed for a two-dimensional analysis in the study. The flow conditions were $10<Re<100$ (laminar flow) with cooling fluid having Pr=0.7. The results showed that by increasing Re the Nu and pressure drop increased. The Darcy number increasing which leads to increase Nu, but decreases pressure drop. They chose based configurations for Nu, and pressure drop as a function of Re and permeability.

Ghosh, 2009, [36] carried out theoretically the open cell metal foam with high porosity. Metal foam was employed as an extended surface in a compact heat exchanger to enhance its thermal performance. The heat transfer and pressure drop through the metal foam were described using theoretical models. Nusselt number and pressure drop were determined using correlated equations, while the performance of the heat exchanger was evaluated using the area goodness factor. Three samples of copper metal foam with different pore per inch (PPI) values (10, 30, and 60) and a porosity of 0.88 were utilized. The porosity was varied at three levels (0.8, 0.85, and 0.9). The velocity range investigated was 2 to 9 m/s. A comparison was made between the open-cell metallic foam and offset strip and wavy fins. The results demonstrated that the open-cell metallic foam showed promise as an alternative for heat exchangers. The maximum value of the area goodness factor was approximately 0.3. Furthermore, the area goodness factor increased with an increase in porosity and porous density. The area density of heat exchanger with porous material higher than heat exchanger with conventional fins.

Xu et al., 2011, [37] noted theoretically the fully developed forced convective heat transfer in a parallel-plate channel partially filled with highly porous, open-celled metallic foam. The Navier–Stokes equation for

the hollow region was connected with the Brinkman–Darcy equation in the foam region by the flow coupling conditions at the porous–fluid interface. The energy equation for the hollow region and the two energy equations of solid and fluid for the foam region were linked by the heat transfer coupling conditions. The normalized closed-form analytical solutions for velocity and temperature were also obtained to predict the flow and temperature fields. The explicit expression for Nusselt number is also obtained through integration. A parametric study was conducted to investigate the influence of different factors on the flow resistance and heat transfer performance. The analytical solution can provide useful information for related heat transfer enhancement with metallic foams and establish a benchmark for similar work.

Odabaee et al., 2011, [38] simulated numerically the heat transfer from a metal foam-wrapped solid cylinder in cross-flow. Effects of the key parameters including the free stream velocity and characteristics of metal foam such as porosity, permeability, and form drag coefficient on heat and fluid flow are examined. Being a determining factor in pressure drop and heat transfer increment, the porous layer thickness was changed systematically to observe that there was an optimum layer thickness beyond which the heat transfer does not improve while the pressure drop continues to increase. This has been verified by the application of Bejan's Intersection of Asymptotes method. Results have been compared to those of a finned-tube heat exchanger to observe much higher heat transfer rate with reasonable excess pressure drop leading to a higher area goodness factor for metal foam-wrapped cylinder.

Hugo and Topin, 2012, [39] consisted metal foams heat exchangers design. The effective properties of metal foams such as thermal conductivity and heat transfer coefficient used to model heat transfer,

permeability, and inertial coefficient used to model flow pattern through foams are presented. All these properties constitute basic inputs for the homogeneous equivalent porous media approach widely used to design heat exchangers. Methods are presented which allow for the determination of thermo-physical and geometrical properties of foams. A numerical approach is used to get better understanding of solid matrix geometry influence on transport properties.

Dai et al., 2012, [40] suggested open-cell aluminum foam with a highly compact replacement for conventional louver fins in brazed aluminum heat exchangers. A model based on the ϵ-NTU method is developed to compare the flat-tube, serpentine louver-fin heat exchanger to the flat-tube metal-foam heat exchanger. The two heat exchangers are subjected to identical thermal-hydraulic requirements, and volume, mass, and cost of the metal-foam and louver-fin designs were compared. The results showed that the same performance was achieved using the metal-foam heat exchanger, but a lighter and smaller heat exchanger was required. However, the cost of the metal-foam heat exchanger is currently much higher than that of the louver-fin heat exchanger, because of the high price of metal foams. If the price of metal foam falls to equal that of louver-fin stock (per unit mass), then the metal-foam heat exchanger will be less expensive, smaller, and lighter than the louver-fin heat exchanger, with identical thermal performance.

Huisseune et al., 2015, [41] developed a comparison of the performance of metal foam heat exchangers to the performance of a bare tube bundle and the performance of an existing conventional louvered fin heat exchanger. A macroscopic model consisting of the Darcy–Forchheimer–Brinkman flow model and the thermal non-equilibrium energy model is used to perform two-dimensional simulations on metal

foam heat exchangers. The foamed heat exchangers show up to 6 times higher heat transfer rate than the bare tube bundle at the same fan power. If the fins are replaced by metal foam while keeping the overall dimensions the same, the finned heat exchanger shows in all cases the best performance. However, a metal foam heat exchanger can outperform the finned heat exchanger if the frontal area was changed. Optimization is required to select the best foam parameters, material and dimensions. This clearly shows the potential of open-cell metal foam for high performance heat exchanger designs.

Anuar et al., 2017, [42] explained theoretically the porous foam structure would have better transfer heat through conduction and convection processes. However, the exhaust gases that enter the cooler would carry particulate matter, which may deposit within the foam structure. The existing fouling studies cannot explain the underlying mechanisms of particulate deposition thoroughly within the foam structure. This study reviews the particulate fouling of heat exchangers, particularly in the exhaust gas recirculation system. Some past approaches to investigate fouling, particle transport, and deposition in the metal foam heat exchangers for many different applications are also included. In addition, this study also includes the challenges that lie ahead in implementing the metal foam heat exchangers in the industries.

Buonomo et al., 2018, [43] studied numerically the thermal and fluid dynamic behaviors of a tubular heat exchanger in aluminum foam. A plate in metal foam with a single array of five circular tubes is the geometrical domain under examination. Darcy–Forchheimer flow model and the thermal non-equilibrium energy model are used to execute two-dimensional simulations on metal foam heat exchanger. The foam is characterized by porosity and (number) pores per inch respectively equal to

0.935 and 20. Different air flow rates are imposed to the entrance of the heat exchanger with an assigned surface tube temperature. The results are provided in terms of local heat transfer coefficient and Nusselt number evaluated on the external surface of the tubes. Furthermore, local air temperature and velocity profiles in the smaller cross section, between two consecutive tubes are given. Finally, the Energy Performance Ratio (EPR) is evaluated in order to demonstrate the effectiveness of the metal foam.

Kotresha and Gnanasekaran, 2019, [44] calculated numerically the metal foam heat exchanger system by a commercial software. A metal foam layer is attached to the bottom of the heat exchanger to absorb heat from the exhaust hot gas leaving the system. Two types of metal foams with two different pores per inch (PPI) values were considered for heat transfer enhancement. Similarly, two different materials Aluminum and copper, that poses high thermal conductivity, metal foams are considered for the present numerical simulations. The heat exchanger system was simulated over a range of 6–30 m/s fluid velocity. It has been noticed that the velocity of the fluid decreases as PPI increases at the expense of its pressure drop. The copper metal foam gives a maximum increase of 4–10% heat transfer rate compared to aluminum metal foams for a fluid velocity of 30 m/s.

Wang and Guo, 2019, [45] investigated the heat transfer in metal foams by assuming that all the foam cells were cubic. An improved model for the volumetric convective heat transfer coefficient of metal foam was obtained by considering the convective heat transfer and the thermal conduction in the connected foam ligaments. Numerical simulations of a metal foam-filled channel were performed using the local thermal non-equilibrium model to evaluate the model. The volumetric convective heat transfer coefficient significantly increases as the pore density increases.

However, the relationship between the volumetric convective heat transfer coefficient and the porosity was not linear. As the porosity increases, the volumetric convective heat transfer coefficient first increases and then decreases. The effect of the solid thermal conductivity on the volumetric convective heat transfer coefficient has an upper limit with a critical value of the solid thermal conductivity for the present conditions.

Buonomo et al., 2020, [46] analyzed numerically the behavior of heat exchangers with metal foam. A numerical study was conducted to analyze the thermal-fluid dynamic performance of a system using a laminar steady-state two-dimensional model. The system consists of an aluminum foam block with an array of five circular tubes, each assigned a uniform temperature. The aluminum foam block is considered as an open-celled porous medium in local thermal non-equilibrium (LTNE) using the Darcy-Forchheimer-Brinkman model. The metal foam used in the study has a porosity of 0.9353 and a pore density of 20 pores per inch (PPI). The numerical simulations were performed using air as the cooling fluid with varying mass flow rates and an assigned temperature for the tube surface. The study focuses on the thermal performance of the metal foam heat exchanger, aiming to find optimal geometrical configurations using conventional parameters commonly employed in the analysis of porous medium heat exchangers

Buonomo et al., 2021, [47] studied numerically metal porous structures with Kelvin cell model with water/Al_2O_3 nanofluids using the single-phase model. Foams with a porosity of 0.95 and different cells per inch (CPI) values, specifically 10 and 20 CPI, were examined in this study. The influence of Al2O3 nanoparticle volume concentrations, including 0%, 2%, and 4%, was also investigated. The main focus was on the pressure drop between the inlet and outlet sections of the foam samples. The

obtained results were analyzed and discussed, and a correlation was developed to determine the permeability and drag coefficient of the metal porous structures being studied. It was observed that these properties were independent of the type of fluid used but solely depended on the geometric characteristics of the foam.

2.3. Experimental and Theoretical studies

Hwang et al. 2002, [48] explained the effect of aluminum foam on convection heat transfer coefficient and friction of drag. Foam with porosity values of 0.7, 0.8, and 0.95, and a pore density of 10 PPI, was utilized in the study. The flow conditions ranged from $1900 < Re < 7800$. The heat transfer coefficient was determined using an experimental and thermal non-equilibrium two-equation model. It was observed that as the porosity decreased, both the friction factor and heat transfer coefficient increased. At a porosity of 0.8, the heat exchanger exhibited optimal performance. Empirical correlations were developed to relate the friction coefficient and heat transfer coefficient to the Reynolds number for different porosity values.

Lu et al., 2005, [49] reviewed the thermal characteristics for all metallic sandwich structures such as prismatic diamond, louvered fins, trusses, copper textile, metallic foams, and corrugated ducts. The relation between Reynolds number, Nusselt number, and friction factor was determined through a combination of experimental and numerical investigations. The study also examined the impact of material topological features on the thermal and dynamic performance. It was observed that the highest pressure was achieved when metallic foams, prismatic cores, and corrugated ducts were employed as the materials. The highest heat flux obtained when the material was truss core, and prismatic cores.

Han et al., 2012, [50] explained the recent advances in manufacturing methods open the possibility for broader use of metal foams and metal matrix composites (MMCs) for heat exchangers, and these materials can have tailored material properties. Metal foams in particular combine a number of interesting properties from a heat exchanger's point of view. The material properties of metal foams and MMCs are surveyed, and the current state of the art was reviewed in terms of heat exchanger applications. Four different applications are considered, including liquid-liquid, liquid-gas, and gas-gas heat exchangers, as well as heat sinks. Manufacturing and implementation issues are identified and discussed, leading to the conclusion that these materials show promise for both heat exchangers and heat sinks. However, it was acknowledged that some key issues still need to be resolved before their widespread application can be realized.

Tsolas and Chandra, 2012, [51] achieved a thermal spray coating process to deposit dense 2 mm thick metal skins on the surfaces of square cross-section channels (300 mm × 20 mm × 20 mm) of nickel and copper foams with 10 and 40 PPI (pores per inch) pore densities. The foam was modeled as a porous medium and properties such as permeability K and inertial coefficient C_F were determined from the experimental data. Local and average convective heat transfer coefficients were calculated from air and foam temperature measurements. Nusselt numbers were calculated and correlated in terms of the Reynolds, Prandtl, and Darcy numbers. Heat transfer to air flowing through a 10 PPI foam channel was shown to have an increase nearly seven times compared to that of hollow tube with the same dimensions.

Jaeger et al., 2013, [52] explained the influence of the geometry of open-cell aluminum foam on the thermohydraulic behavior in channel

flow. The flow arrangement and the operating conditions are fixed. A numerical model is implemented in a commercial solver, based on volume averaging theory. An ordinary Kriging model was used for this, indicating that the root mean square error of interpolated results was lower than 0.6 and 3% for, respectively, heat transfer and total pressure. The resulting heat transfer and total pressure difference were non dimensionalized by dividing them by the results obtained from an empty channel. The relative increment of the pressure drop was an order of magnitude higher than the increment observed for heat transfer. Consequently, the applied performance evaluation criterion (defined as the ratio of dimensionless heat transfer versus total pressure) was mainly influenced by the hydraulic performance. For the given application, a clear optimum was found. The proposed method allows performing the parameter study with acceptable computational cost with a sufficient level of detail from an engineering perspective.

Mancin et al., 2013, [53] experimentally characterizes twenty-one aluminum and copper foam samples. The samples varied in terms of the number of pores per linear inch (PPI) ranging from 5 to 40 and the porosity which varied between 0.896 and 0.956. Additionally, samples with different heights of 20 and 40 mm were investigated. The results of the experiments were analyzed with respect to various performance parameters including overall and interstitial heat transfer coefficients, foam finned surface efficiency, normalized mean wall temperature, pumping power per area density, and pressure gradient. Based on the experimental measurements, two correlations were developed to calculate the heat transfer coefficient and pressure drop. These correlations were validated and are now proposed for use in optimizing foam heat exchangers for various applications. The developed models offer a valuable tool for

enhancing the performance of foam heat exchangers in specific application scenarios.

Amori and Khalaf, 2015, [54] conducted a numerical and experimental investigation on the influence of Aluminum metal foam on the thermal characteristics of a confined impinging air jet on a hot plate. The study considered several parameters, including the jet Reynolds number (ranging from 14,000 to 70,000), the angle of impingement jet. The researchers employed the finite volume method to solve the two-dimensional continuity, Navier-Stokes, and energy equations with the (k-ε) turbulence model. The experimental and computational results demonstrated that increasing the jet angle led to a decrease in the Nusselt number, while an increase in the Reynolds number resulted in an increase in the Nusselt number. The application of a layer of metal foam on the hot plate enhanced the heat transfer through jet cooling by 33% compared to jet cooling on a bare hot plate under the same conditions.

Chen et al., 2020, [55] studied heat exchangers embedded with metal foam were drawing increasing attention in the thermal application field, due to the performance of low density, large ratio of surface area to volume as well as high thermal conductivity. The review focuses on empirical and theoretical models that have been developed for evaluating pressure drop, heat transfer coefficient, and performance criteria of compact heat exchangers utilizing metal foam. The discussion particularly emphasizes different optimized configurations that have been investigated. It was important to note that there exists a trade-off between heat transfer enhancement and the associated increase in pressure drop. The paper also introduces some exploratory work conducted by the authors, which takes into account the manufacturing process, heat transfer characteristics, and flow behavior of tube bundles wrapped with metal foam. The optimization

of heat exchangers is considered, and it has been confirmed that heat conduction plays a dominant role in the heat transfer process, especially at high permeability.

2.4. Summary of Literature Review

Some studies that used metallic foam to improve heat transfer can be summarized through the table (2-1) which shows the type of foam that was used as well as the specifications of the heat exchanger.

Table (2-1) Summary of literature review.

Study	Materials of metal foam	Foam Properties	Study type	Boundary conditions	Main findings
Klett et al., 2000, [13]	Graphite Foam	Density (0.2-0.6 g/cm^3)	Experimental	-Air flow rate 140LPM to 420LPM -Water flow rate 11.34 LPM	The heat transfer coefficient of heat exchanger with foam can be up to two orders of conventional heat exchanger
Kim, 2000, [14]	6101-Aluminum alloy foam	-PPI (10-40) -porosity (0.89-0.96)	Experimental	270<Re< 2050	friction factor is much lower for low permeable porous fins. At high Re the f is high in porous fin. j decrease as PPI increased.
Hwang et al. 2002, [48]	aluminum alloy 6101-T6 Foam	-porosity (0.7,0.8,0.95) - 10 PPI	Experimental and Theoretical	1900<Re< 7800	Both f and h increased with decreasing foam porosity porosity =0.8 had best thermal performance

Study	Materials of metal foam	Foam Properties	Study type	Boundary conditions	Main findings
Boomsma et al., 2003, [15]	aluminum alloy 6101-T6 Foam	-PPI (40) -Thermal conductivity of 218 W/m-K	Experimental	Velocity (0 to 2 m/s)	The heat exchanger with foam thermal resistance were two to three times lower than commercial heat exchanger with same pumping power.
Tadrist et al., 2004, [16]	-Stacked fibers (Copper, Bronze) -Foam (Aluminum)	-fiber (0.38 <porosity< 0.92) -foam (10,20,30PPI)	Experimental	The transport properties are analyzed for both materials: permeability, friction factors and the effective thermal conductivity.	Fibrous strong increase of thermal performance with low pressure drop
Tian et al., 2004, [17]	-metal foam (copper) -periodic cellular metal (copper) -Textile laminate (copper) -Brazed wire screen (copper)	-wire screen (0.69<porosity <0.8) -foam (0.822< porosity <0.917)	Experimental	700 < Re < 10000	-friction factor depend mainly on pore size, open area ratio, flow direction -heat transfer depend mainly on solid conduction, forced convection, porosity, and surface area.
Lu et al., 2005, [49]	-metallic foam - Louvered		Review (experimental and theoretical)		-The high pressure drop materials was foams, prismatic cores, corrugated ducts. -The high heat flux material

Study	Materials of metal foam	Foam Properties	Study type	Boundary conditions	Main findings
	fins - prismatic diamond -Trusses -Copper textile - Corrugated ducts				was truss core, prismatic cores.
Raju and Narasimhan, 2007, [35]	aluminum Foam	-porosity (0.58, 0.8, 0.95)	Theoretical	10<Re<100	As Re increased the Nu and pressure drop increased as Darcy number increase the pressure drop decrease and Nu increase
Jamin and Mohamad, 2007, [18]	-Carbon foam - Aluminum fins	porosity (0.61)	Experimental	7000<Re<40 000	aluminum fins gives Nu three time heights than carbon foam
Tzeng, 2007, [19]	- aluminum foam with copper pipe	-porosity (0.97) -PPI (10)	Experimental	883 < Re < 4416	conductive pipe with aluminum foam was very effective thermal performance
Bonnet et al., 2008, [20]	-Copper -Nickel -Nickel-Chrome	0.87< porosity <0.94	Experimental	-air (0<v<20 m/s) -water (0<v<0.1 m/s)	-Compressibility strongly effect on the flow parameter -permeability and inertia coefficient don't depend on natural of flow -Permeability proportional to (pore size)^2, inertia coefficient proportional to (pore size)$^{-1}$

Study	Materials of metal foam	Foam Properties	Study type	Boundary conditions	Main findings
Cavallini et al., 2008, [21]	-Aluminum	-40 PPI (porosity =0.93) -5 PPI (porosity =0.921)	Experimental	air mass flow rate range from 0.01 to 0.025 kg/s	They found that heat transfer coefficient is depend on mass flow rate but doesn't depend on the heat flux for both 40 PPI and 5 PPI samples. Al foam with 40 PPI gave better thermal performance than 40 PPI. The wall temperature is higher for 40 PPI samples than 20 PPI sample. The samples with 40 PPI gives higher pressure drop than 5 PPI sample
Ghosh, 2009, [36]	-Copper	-10, 30, 60 PPI -(porosity =0.8, 0.85, 0.9	Theoretical	air velocity (2 to 6 m/s)	They found that maximum value of area goodness factor was near 0.3. The area goodness factor increased by increase porosity and porous density. The area density of heat exchanger with porous material higher than heat exchanger with conventional fins
T 'Joen et al., 2010, [22]	-Aluminum	PPI (10,20) porosity (0.91,0.93, 0.95)	Experimental	air velocity (1 to 8 m/s)	the results showed that increasing the foam height leads to increase the pressure drop but at the same time the thermal resistance will decreases. They found that air penetrates the foam only for external small layer so that by increasing the foam height that reduced the thermal performance.

Study	Materials of metal foam	Foam Properties	Study type	Boundary conditions	Main findings
Kamath et al., 2010, [23]	Aluminum metal foams	porosity in the range of 0.9 to 0.95	Experimental	100<Re<10000	The enhancement ratio is always more than one which clearly indicates that metal foams have good heat transfer enhancement capability.
Mancin et al., 2011, [24]	Aluminum metal foams	10 PPI	Experimental	the air mass velocity between 0.005 and 0.025 kg m^{-2} s^{-1}	From the experimental results it appears that the Aluminum foam exploits interesting heat transfer properties at the expense of pressure drops which are orders of magnitude higher than the ones of traditional air cooling solutions
Xu et al., 2011, [37]	Aluminum metal foams	porosity (0.85,0.9,0.95)	Theoretical	100<Re<3000	Flow resistance can be reduced by increasing porosity, reducing pore density, and decreasing hollow ratio
Muley et al., 2012, [25]	Ni-Cr plate foam	5, 10 , 20 PPI	Experimental	Air flow (4 to 14 Ib/min)	that metal foam heat exchangers provide some heat transfer improvements; however, the associated pressure-drop penalty is quite high,
Odabaee et al., 2011, [38]	Aluminum metal foams	porosity $0.9 < \varepsilon < 0.95$	Theoretical	9700 < Re < 19400.	Results have been compared to those of a finned-tube heat exchanger to observe much higher heat transfer rate with reasonable excess pressure drop leading to a higher area goodness factor for metal foam-wrapped cylinder
Hugo and Topin, 2012, [39]	Aluminum metal foams	PPI(5 to 80)	Theoretical	$1<Re_d<1000$	that inertia coefficient increases when confinement decreases and mean solid size increases. These trend being directly linked to the pore shape stretching and ratio between pore and throat diameter

Study	Materials of metal foam	Foam Properties	Study type	Boundary conditions	Main findings
Han et al., 2012, [50]	Various types of materials have been reviewed		Review (experimental and theoretical)		it is concluded that these materials hold promise both for heat exchangers and heat sinks, but that some key issues still need to be solved before broad-scale application is possible
Dai et al., 2012, [40]	Aluminum foam	porosity= 0.9272, 40 PPI	Theoretical	air mass flow rate (0.075 to 0.45 kg/s)	The results showed that the same performance is achieved using the metal-foam heat exchanger, but a lighter and smaller heat exchanger is required. However, the cost of the metal-foam heat exchanger is currently much higher than that of the louver-fin heat exchanger
Tsolas and Chandra, 2012, [51]	nickel and copper foams	10 and 40 PPI	experimental and Theoretical	air flow rates of 5–80 l/min	Heat transfer to air flowing through a 10 PPI foam channel was shown to have an increase nearly seven times compared to that of hollow tube with the same dimensions
Jaeger et al., 2013, [52]	aluminum foam	PPI=10, 20 porosity=0 .93 ,0.96	experimental and Theoretical	velocity (0 to 8 m/s)	The relative gain of heat transfer (compared to the empty channel) is an order of magnitude less than the relative increment of the required pressure to maintain the mass flow rate
Mancin et al., 2013, [53]	aluminum and copper foam	PPI =5 to 40 , porosity ranging	experimental and Theoretical	air mass velocity (2 to 6.2 kg m^{-2} s^{-1})	The results show that copper foams exhibit higher heat transfer performance e than aluminum foams by virtue of

Study	Materials of metal foam	Foam Properties	Study type	Boundary conditions	Main findings
		between 0.896 and 0.956			their high thermal conductivity
Huisseune et al., 2015, [41]	Aluminum metal foam	PPI (10 to 40) porosity (0.9 to 0.95)	Theoretical	air mass flow rate (0.15 to 0.42 kg/s)	The foamed heat exchangers show up to 6 times higher heat transfer rate than the bare tube bundle at the same fan power
Amori and Khalaf, 2015, [54]	Aluminum metal foam	porosity =0.92	Experimental and Theoretical	Reynolds number (ranging from 14,000 to 70,000)	The application of a layer of metal foam on the hot plate enhanced the heat transfer through jet cooling by 33% compared to jet cooling on a bare hot plate under the same conditions
Anuar et al., 2017, [42]	Aluminum foam	10 PPI open-cell metal foam	Theoretically	2.5 to 10 m/s	This study reviews the particulate fouling of heat exchangers, particularly in the exhaust gas recirculation system. Some past approaches to investigate fouling, particle transport, and deposition in the metal foam heat exchangers for many different applications are also included
Nawaz and Jacobi, 2017, [26]	Aluminum and copper metal foam	porosity= 0.92-0.94, 20 PPI	Experimental	0.5 to 4.5 m/s	the pressure gradient was noticeably different for two samples under wet operating conditions. An obvious difference in heat transfer rate for aluminum and copper metal foam heat exchangers was observed under both dry and wet operating conditions

Study	Materials of metal foam	Foam Properties	Study type	Boundary conditions	Main findings
Chen et al., 2018, [27]	Nickel	Four types of foams with 20, 40, 60 and 80 PPI	Experimental	100 < Re < 1000	The results indicate that: 1, with increase of porosity, Nusselt number increases because of stronger penetrating ability, and heat convection dominates the heat transfer. 2, for variation of pore density, Nusselt number of high PPI samples is lower for thermal-insulation effect at low Reynold number
Hamadouche et al., 2018, [28]	Aluminum metallic foam	Porosity of 93.8%, different grades of 5, 20 and 40 PPI	Experimental	5000 < Re < 25000	The results showed that there is an optimal choice of the height and the grade of the metal foam for which the heat transfer and pressure drop (for an optimal design of heat exchangers) to reach the design goal
Kotresha and Gnanasekaran, 2019, [44]	Aluminum and copper	20, 40 PPI porosity 0.937	Theoretical	velocity 6–30 m/s	The copper metal foam gives a maximum increase of 4–10% heat transfer rate compared to aluminum metal foams for a fluid velocity of 30 m/s
Wang and Guo, 2019, [45]	Copper	was 0.918	Theoretical	3000<Re<12000	The volumetric convective heat transfer coefficient significantly increases as the pore density increases. However, the relationship between the volumetric convective heat transfer coefficient and the porosity is not linear
Buonomo et al., 2018, [43]	Aluminum foam	0.935 and 20	Theoretical	$100<Re_d<150$	The results are provided in terms of local heat transfer coefficient and Nusselt number

Study	Materials of metal foam	Foam Properties	Study type	Boundary conditions	Main findings
					evaluated on the external surface of the tubes. Furthermore, local air temperature and velocity profiles in the smaller cross section, between two consecutive tubes are given
Borakhade and Mahalle, 2018, [29]	Copper	40 PPI, 50 PPI, 60 PPI	Experimental	velocity (1 to 5 m/s)	that open cell copper metal foams are the excellent choice for forced convection heat dissipation application for power electronics devices.
Buonomo et al., 2020, [46]	Aluminum foam	0.9353 and a pore density equal to 20 pores per inch (PPI)	Theoretical	$50 < Re_d < 1120$	The study focuses on thermal performances of a metal foam heat exchanger using several conventional parameters employed in the analysis of porous medium heat exchangers to find optimal geometrical configurations
Buonomo et al., 2021, [47]	Aluminum foam	porosity of 0.95	Theoretical	0.01 to 1 m/s	the value of permeability and drag coefficient for metal porous structures under investigation. It has been possible to notice how these two properties of the foam do not depend on the type of fluid but only on the geometric properties
Nilpueng et al., 2020 [30]	Copper foam	pore density ranging from 30 to 50 pores per inch	Experimental	Reynolds number ranging from 1200 to 2000	The heat transfer coefficient is enhanced by 20.23%, 29.37%, and 40.28% for PHECF with a pore density of 30 PPI, 40 PPI, and 50 PPI as compared to a plate heat exchanger

Study	Materials of metal foam	Foam Properties	Study type	Boundary conditions	Main findings
Chen et al., 2020, [55]	Copper , Aluminum, nickel, Stainless steel		Review study		Compact heat exchangers partially embedded with metal foam are optimal to reduce pressure drop. The increase of permeability and porosity can reduce the heat transfer rate and pressure drop
Salari et al., 2020, [31]	Copper	porosity =0.95	Experimental	500 < Re < 4500	porous media in the tube can increase the effectiveness of nanofluids in improving heat transfer
Rezaei and Abbassi, 2021, [33]	Copper	porosity =0.82, 0.97	Experimental	500 < Re < 2800	that the porous media and flattening the tube have a significant effect on the thermal and hydrodynamic performances of the system due to the heat spreading through the copper matrix, better mixing of the fluid and extending the heat transfer area
Rajamuthu et al., 2020, [32]	Copper	high pore density (90 PPI), high porosity 0.95	Experimental	3000 < Re < 12000	It was observed that the stripes configuration had the highest heat transfer enhancement of about 1.45 times that of the smooth surface target, at the expense of a marginal increase in pumping power, thereby making it the best configuration in terms of thermal hydraulic performance
Fadhala et al, 2023, [34]	Copper foam	porosity of 0.95	Experimental	The Reynolds number ranged from $3.8x10^4$ to $5.4x10^4$	The friction factor for the solid baffles was approximately 460 times higher than that for the smooth surface

2.5. The Scope of Present Work

Heat exchangers embedded with metal foam are reviewed in this chapter. Based on thermos-hydraulic characteristics of metal foam, heat exchangers embedded with metal foam were optimized and designed for industrial applications. The exploratory work on compact heat exchanger, solar thermal facilities, and thermal energy storage are presented. The major findings are as follows.

1- Most of the previous studies focused on the use of metallic foam as a heat sink instead of conventional fins in cooling applications.

2- Previous studies dealt with the replacement of fins with metal foam in heat exchangers and did not address the process of designing a heat exchanger with metal foam.

3- the metal foam parameter such as permeability, porosity, and porous density are utilized to evaluate the heat transfer performance.

The fan coil unit heat exchanger design process depends mainly on the cooling load of the space. Through the current study, the heat exchanger tube length is determined by using ε-NTU method. The cooling load determines the tube length, water inlet temperature, and the water flow rate The performance of the heat exchanger was improved by replacing the traditional fins with copper foam. The current study will compare the performance between the two types of heat exchangers. The mathematical model will be built according to Darcy-Brinkman-Forchheimer and local thermal equilibrium model, through which the velocity, pressure, and temperature distribution through the heat exchanger will be found.

CHAPTER THREE

EXPERIMENTAL

WORK

Chapter Three: Experimental Work

This chapter describes the experimental work, which includes the experimental rig manufacturing, test room, and the measurements devices. The manufacturing and designing of the heat exchanger depends upon the cooling load of the space of test room in order to determine the capacity of heat exchanger. Hourly Analysis Program (HAP) estimates cooling and heating load for test room. Designing of heat exchanger depends upon the estimating value of cooling load for test room. The cooling load of test room in order to determine required heat capacity of heat exchanger. The cooling load of test room calculates under Iraqi/ Babylon (32°32′33″N 44°25′16″E conditions. The metal foam will be added to heat exchanger in order to increase the heat transfer efficiency for heat exchanger. This heat exchanger tests experimentally with and without metal foam. Also, the process of measurements devices is calibration, and the analyzing of the experimental results are carried out.

3.1. Experimental Rig Components

The experimental setup is consisting of fan coil, test room, and measurement devices as explained in figure (3-1). The fan coil is equipped with a series of sensors in order to measure the main parameters for a complete characterization of the hydraulic and thermal performance of the inserted heat exchanger as explained in schematic in figure (3-2). The air flow through fan coil cabinet is varied by changing the velocity regulator of fan motor. Air flow rate across the heat exchanger is monitored by using a hot-wire anemometer by means of which a series of velocity values are obtained at fan coil exit. A differential micro manometer is used to measure the air pressure drops across the heat exchanger. Moreover, the air temperature of fan coil inlet and outlet is monitored by means of a series of

K-type thermocouples. The heat exchanger supplies with 10°C cold water from the tank. The water mass flow rate is measured by using flow meter.

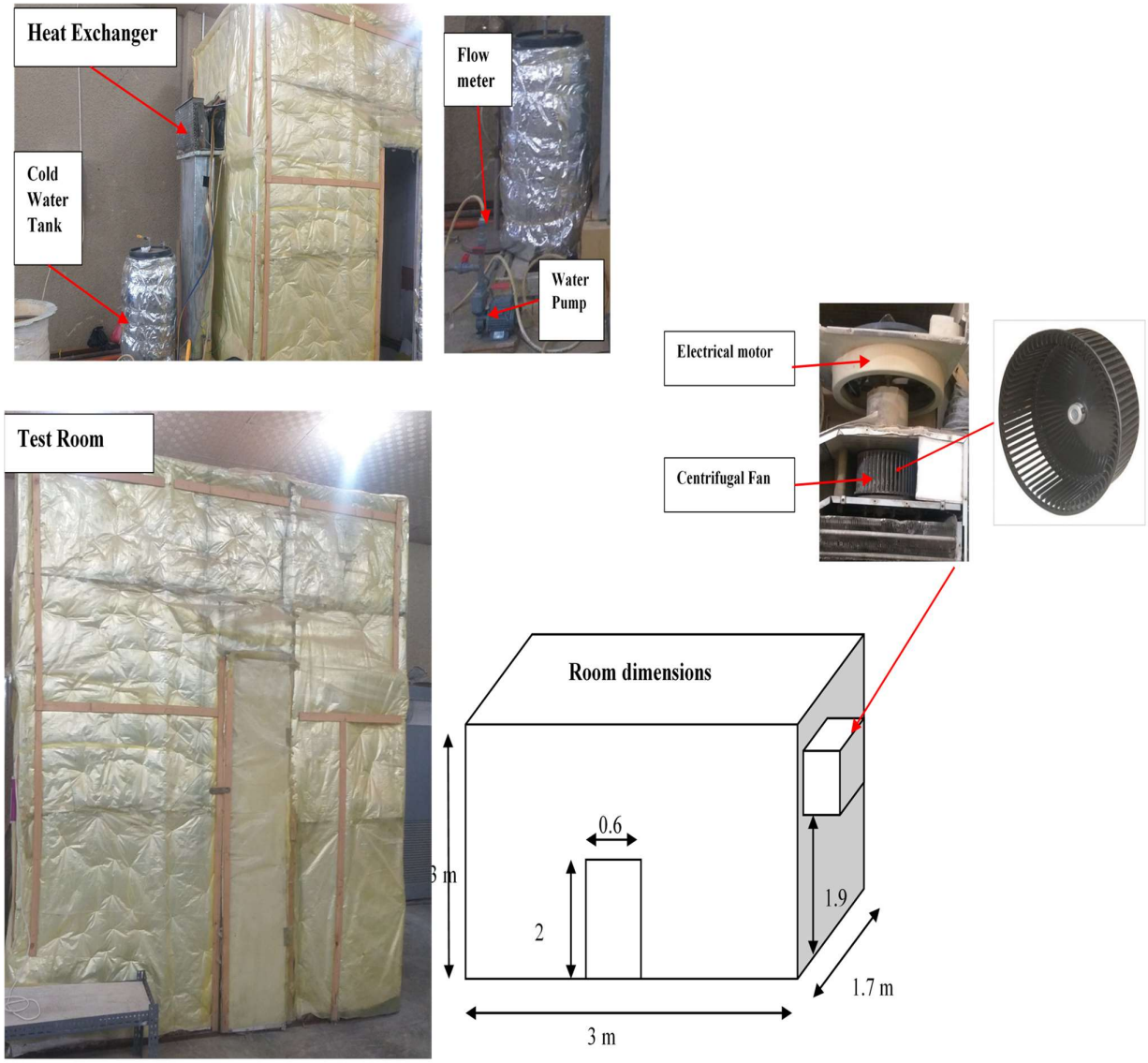

Figure (3- 1) experimental rig.

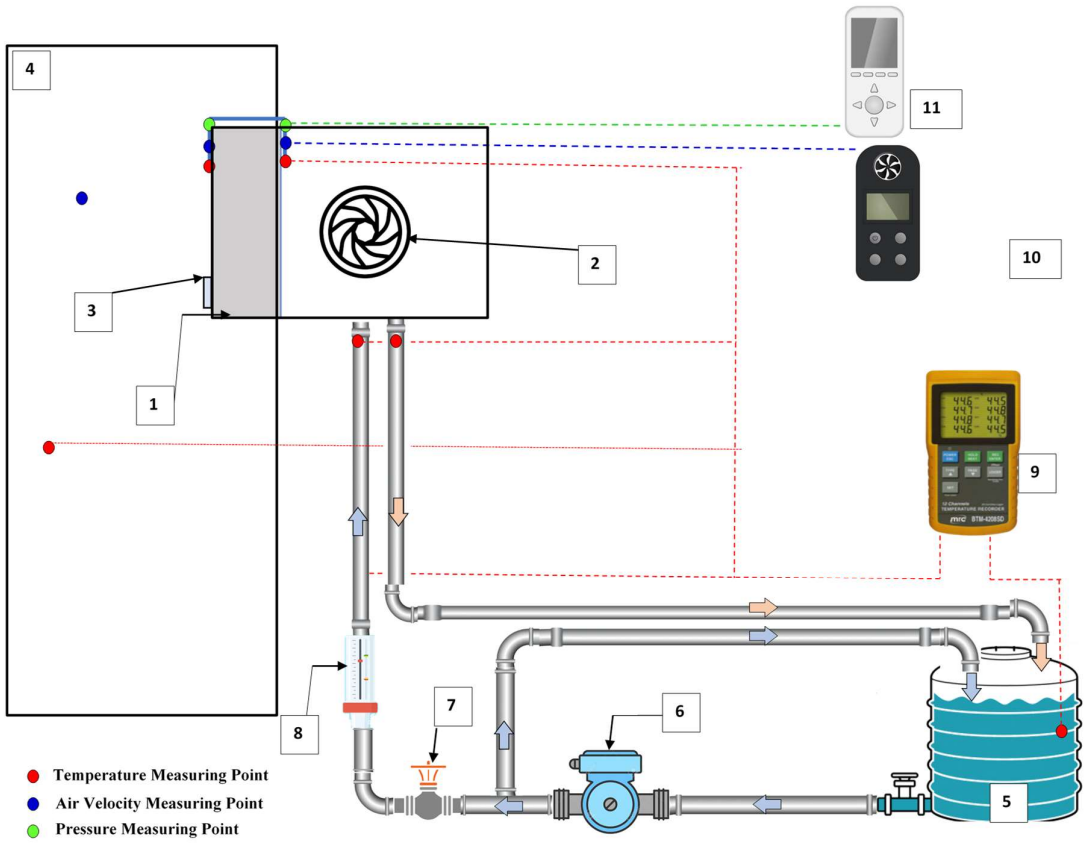

1	Cooling Coil	7	Valve
2	Air Supply Fan	8	Flow Meter
3	Air Speed Control	9	Temperature Recorder
4	Test Room	10	Hot-Wire Anemometer
5	Water Tank	11	Digital Differential Pressure Manometer
6	Pump		

Figure (3- 2) schematic diagram of experimental rig.

3.1.1. Fan coil unit heat exchanger

The cooling coil that is used in fan coil unit (FCU) consists of copper tubes arranged either in staggered pattern or non-staggered pattern. Cold water passes through these tubes and hot air passes around the tubes in a direction perpendicular to the direction of water flow. The dimensions of the heat exchanger will generally be the length of the heat exchanger, which represents the length of the single tube after adding the curvature in the form U-bends, which connects the tubes together. There are many

methods to design and determine the dimensions of the heat exchanger. Most of these methods are based on basic heat transfer equations, as well as energy and mass conservation equations. All methods for designing the heat exchanger generally depend on the overall heat transfer coefficient, and the inlet and outlet temperatures for two fluids. In present study, two methods are used to design and calculate the dimensions of heat exchanger. are the ε-NTU method and the SolidWorks software as explained in appendixes (A) and (B). The dimensions of the heat exchanger are chosen according to the design results as shown in table (3-1), and figure (3-2).

Table (3- 1) dimensions of heat exchanger

Parameter	Value
Number of rows	4
Number of tubes	52
Total tube length (m)	20.8
External surface area of tubes (m^2)	0.6008
Height of coil (m)	0.4
Width of coil (m)	0.4
Depth of coil (m)	0.12
Surface to volume ratio (m^2/m^3)	543
Fin thickness (mm)	0.12
Transvers pitch (m)	0.03
longitudinal distance (m)	0.03

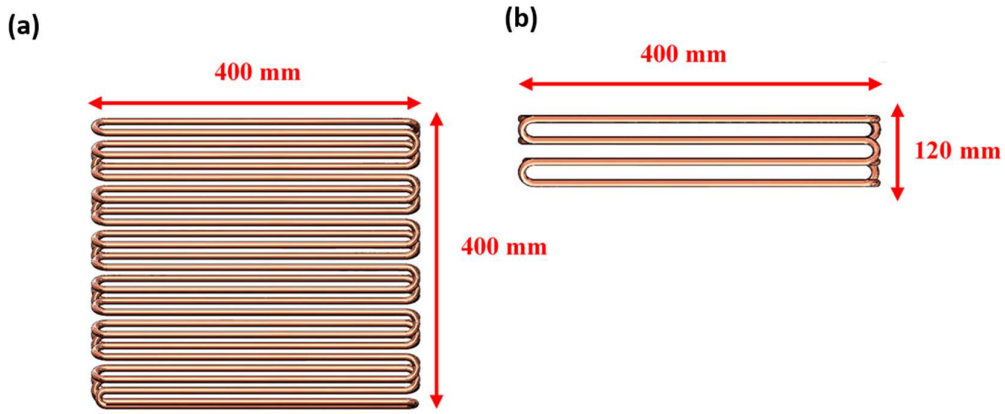

Figure (3- 3) dimensions of cooling coil, (a) front view, (b) top view.

3.1.2. Centrifugal Fan

Centrifugal fan is connected with electrical motor as shown in fig (3-4). Motor model MTR-903 (OOBEM20903) with power of 1/5 HP, 220-240V, and 50/60HZ. The maximum angular velocity is 1170 r.p.m, with 3 Speed.

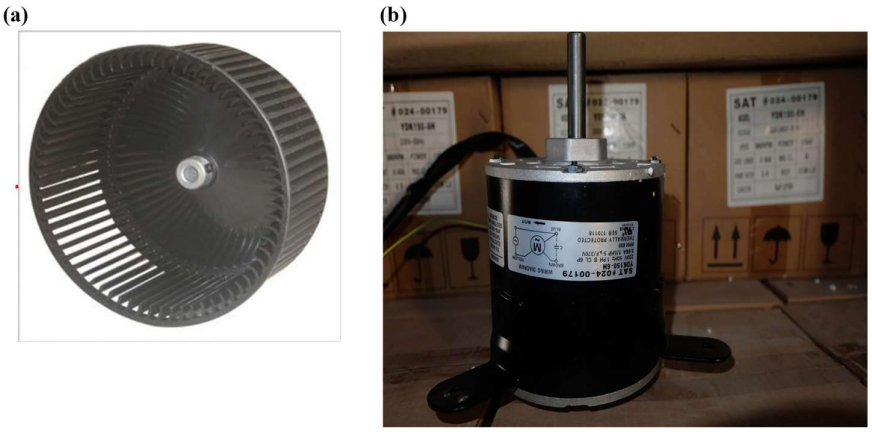

Figure (3- 4) (a) centrifugal fan, (b) electrical motor.

3.1.3. Cabinet of System

All components of the fan coil unit, which include the heat exchanger, centrifugal fan and electrical motor, are placed inside a cabinet system. This cabinet manufactures of mild steel as a rectangular box. It insulates by wrapped with glass wool to reduce heat loss.

3.1.4. Aluminum Fins

Aluminum fins play a crucial role in the heat exchanger of a fan coil unit, which is a common application in HVAC systems. aluminum fins greatly increase the surface area available for heat transfer. The extended surface area allows for more efficient heat exchange between the primary and secondary fluids, enabling effective heating or cooling of the air passing through the FCU. In the current study. The heat exchanger is purchase commercially. They are made of arrays of horizontal copper tubes with an outer diameter of 9.2 mm and tube thickness of 0.5 mm. Aluminum wavy fins with the thickness of 0.12 mm are arranged perpendicular to the horizontal tubes. During the experiments, cold water was directed through the internal flow channel of the copper tubes whereas air flows over the aluminum fins and the external tube surface. An image of aluminum fin and with dimensions is shown in figure (3-5). The thermos-physical properties of fins material are explaining in table (3-2). Figure (3-6) explained the heat exchanger with aluminum fins. It should be noted that the tube arrays are in staggered arrangement.

Table (3- 2) thermos-physical properties of fins material.

Material	ρ (kg/m^3)	c_p (J/kg.°C)	k (W/m. °C)	Thermal expansion (K^{-1})
Aluminum	2,700	900	205	23 x 10^{-6}

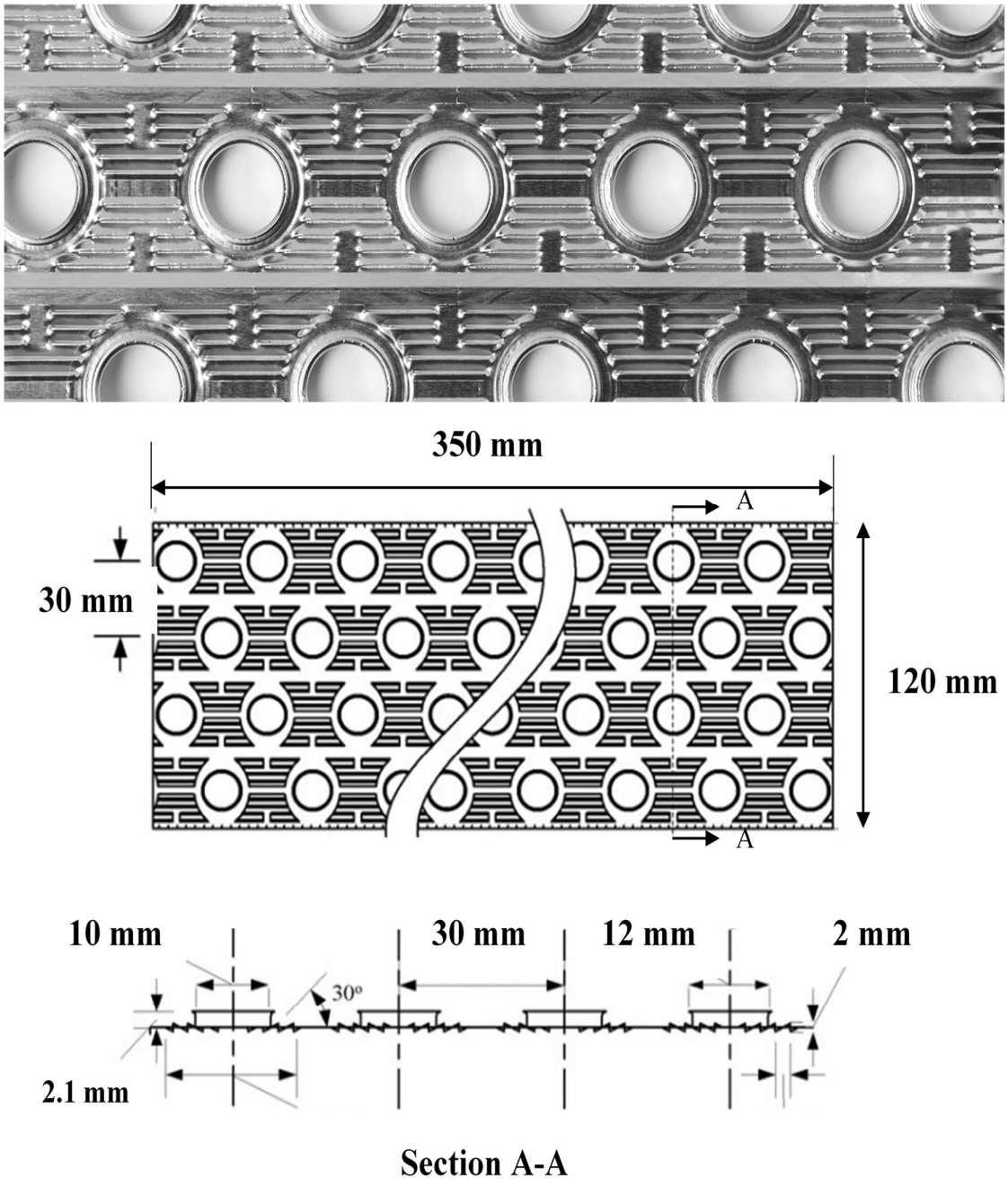

Figure (3- 5) schematics of tested aluminum fin details.

(A)

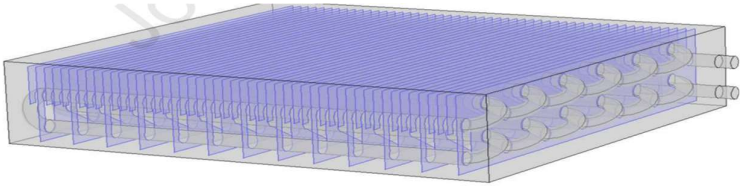

(B)

(C)

Figure (3- 6) heat exchanger, (a) tube arrays arrangement, (b) heat exchanger with fins, (c) heat exchanger tubes.

3.1.5. Metal Foam

A commercial air condition unit (Gibson-model) was used as a reference fan coil unit for the comparison between the performance of conventional fins and copper foam as shown in figure (3-7). The dimensions of the aluminum fins used in the reference heat exchanger are depicted in figure (3-7).

The metal foam with pure copper uses in this study. The porosity, permeability and thermal conductivity of copper foam is measured through this study. It finds the porosity of this copper foam 94%, and the pore density value 10 PPI. This copper foam wraps around tubes of heat exchanger depending upon the technique which details by Chen et al. [27] as shown in figure (3-8). This foam is used in the experimental work in order to increase the surface area of heat transfer. Then, the efficiency of heat exchanger improves. The heat exchanger with copper foam has the same dimensions as the heat exchanger with conventional fins, where the fins are removed and replaced with copper foam pieces as shown in the figure (3-9).

The porosity (φ) is defined as the ration of the void volume to the total volume. The solid volume determined by dividing the dry mass of copper foam on the copper density

$$V_{solid} = \frac{m_{solid}}{\rho_{solid}} \tag{3.1}$$

The metal foam is made of copper alloy which has density of 8933 kg/m^3. The metal foam is weighed using an electronic balance resolution 0.01 g. the dimensions of the copper foam are 30mm ×30mm×400mm, so the total volume of the foam can be found. The porosity is then given by [23]:

$$\varphi = \frac{V_{total} - V_{solid}}{V_{total}} \tag{3.2}$$

The mass of foam equal to 173 g, so that the solid volume equal to 1.93664×10^{-5} m^3, the copper foam porosity equal to 0.94.

The permeability is defined as a measure of the ability of a porous material to let fluids owing through it and depends only on the geometry of the media and not on the properties of the fluid. The size of the pores and their shape are characteristics that influence the permeability value.

The limiting case $K \to 0$ refers to a compact solid without void or pores. On the other hand the limiting case $K \to 1$ refers to a clear fluid as detailed by Michele [56]. Knowing that the porous media is assumed to be isotropic, therefore the permeability can be considered as a constant. Combarous and Bouries [57] using the Carman and Kozeny relationship that relates permeability and porosity, which it states as:

$$K = \frac{d^2}{172.8}\frac{\phi^3}{(1-\phi)^2} \tag{3.3}$$

In which d is the diameter of porous.

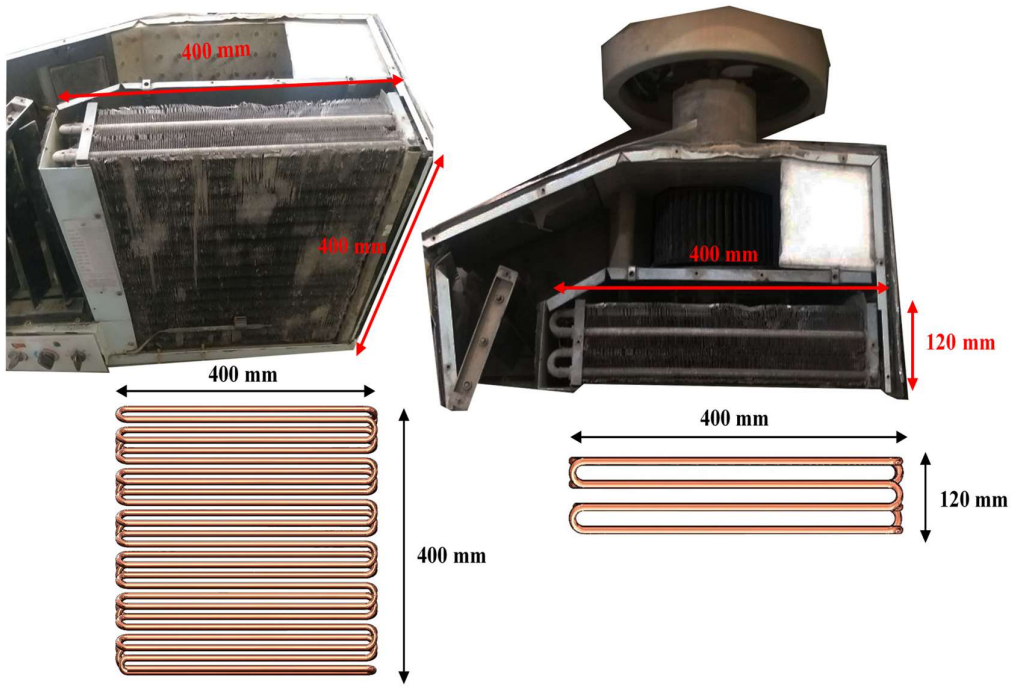

Figure (3- 7) (a) size and layout of cooling coil , (b) schematics of tested louvered fin details.

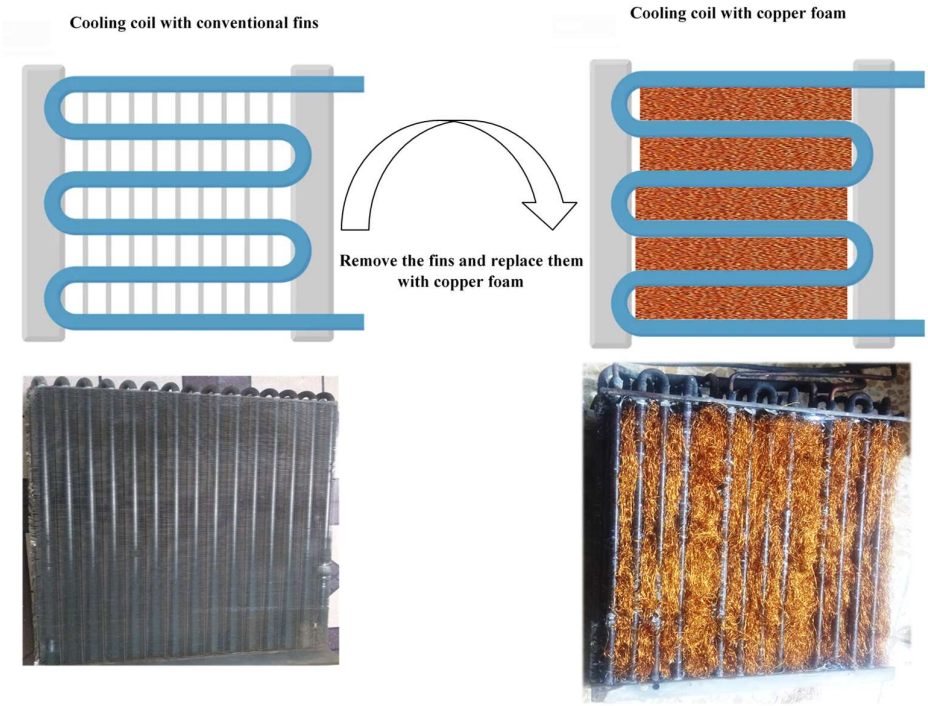

Figure (3- 8) configuration of the heat exchanger

Figure (3- 9) fan coil heat exchanger with metal foam.

3.1.6. Water Tank

The stainless steel tank uses to supply cold water. The tank capacity is 400 liters. Cooling coil used to cool the water inside the tank as shown in figure (3-10). It surrounds by a thermal insulator of glass wool. Water is cooled to 10 ^{o}C inside the tank.

3.1.7. Water Pump

The water pump has a power 0.37 kW with maximum discharge of 40 l/min and maximum head 35 m as in figure (3-11). This pump supplies the cold water to heat exchanger from the tank.

3.1.8. Test Room

The test room is designed and built of wood and is thermally insulated using pieces of wood and glass wool. The dimensions of this room are 3 m length, 1.7 m width, and 3 m height. The cooling load of this room is calculated. Then, upon this value of cooling load the heat exchanger is

designed.

Figure (3- 10) cold water tank

Figure (3- 11) Water circulator pump

3.2. Measurement Devices

3.2.1. Temperature Recorder

Temperature recorder model (BTM-4208SD) with 12-channels is used to measure temperature after calibrating as shown in figure (3-12). It has

SD card to save the temperature reading data with time, information into SD memory card and can be loaded to excel sheet. It uses for different sensor types of thermocouple such as J/K/T/R and S. It is worked as auto data logger or manual data logger sampling time range: (1 to 3600) seconds. The SD card capacity is 1 GB to 16 GB and it has Rs 232/USB computer interface, and the microcomputer circuit provides intelligent function with high accuracy. In the current study K-type thermocouples as shown in figure (3-13) used to measure the fluids, copper foam, tube temperatures

In the current experimental work two 12-chanel temperature recorder are used for temperatures measurement. Nine thermocouples are installed on the front side of the heat exchanger, and nine others are installed on the back side, as shown in figure (3-14). The temperature of the inlet and outlet water is measured through the point (1) and (2) respectively, while the air temperatures before entering and after exiting the heat exchanger is measured through the point (3) and (4) respectively, as explained in figure (3-14). One of thermocouple wires is used to monitor the temperature of the water inside the tank until its fixed at 10 ^{o}C. Another thermocouple wire used to monitor the room temperature.

Each thermocouple is individually calibrated with a digital calibration device type (PROVA123). The calibration process is done by reading the temperatures value by two devices with varying temperature range from 10 to 80 ^{o}C. As shown in figure (3-15) the connection between two devices. Then draw the relation between the temperature reading for two devices as shown in figure (3-16). Polynomial equation is obtained to correlate the temperatures measurement readings as following equation:

$$T_{calib} = -0.9481 + 1.0341T_{red} + 0.0002T_{red}^{2} - 0.000005T_{red}^{3} \quad (3.4)$$

Figure (3- 12) temperature recorder device.

Figure (3- 13) K-type thermocouple wire

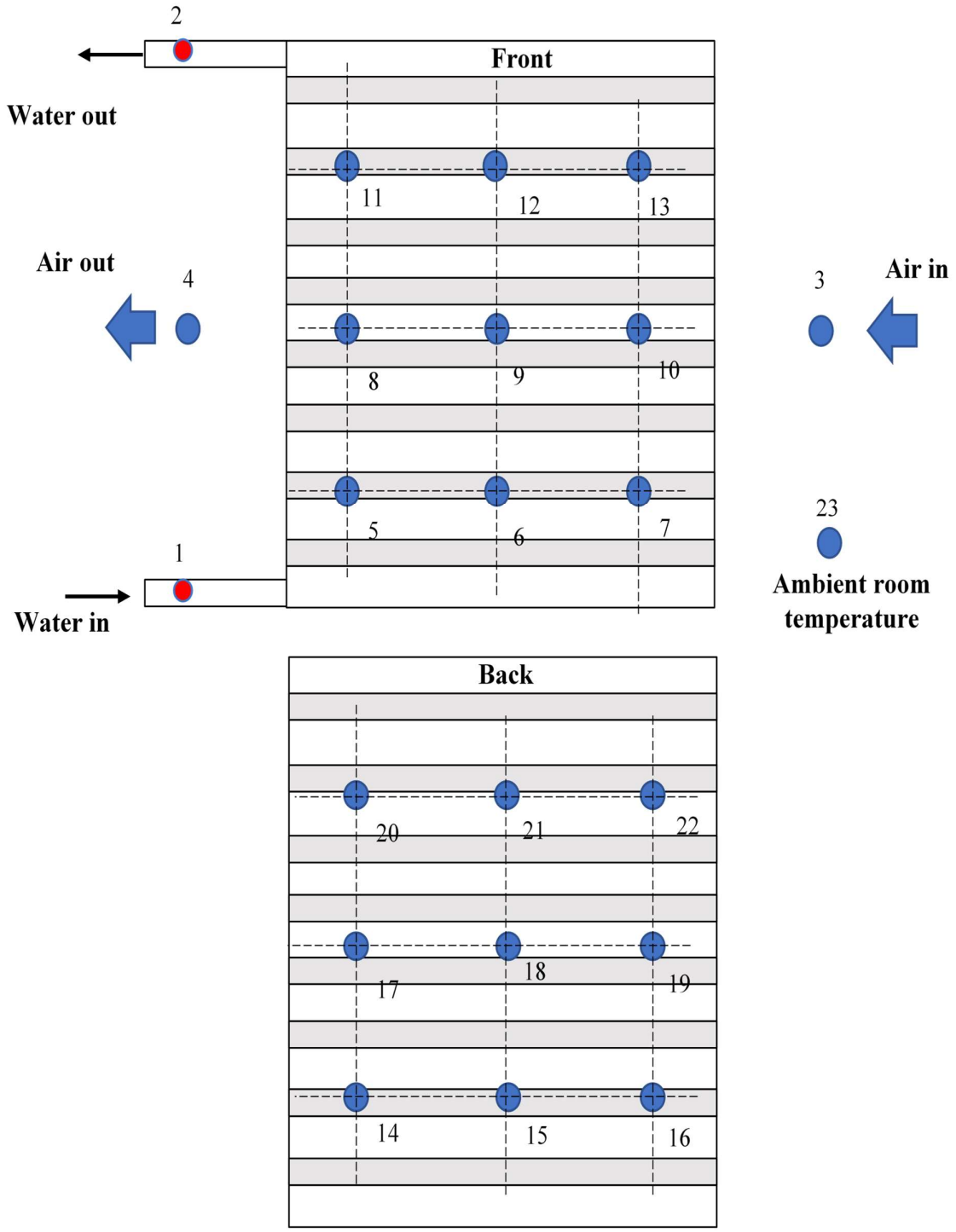

Figure (3- 14) location of thermocouples on heat exchanger

Figure (3- 15) calibration device (PROVA MODEL 123)

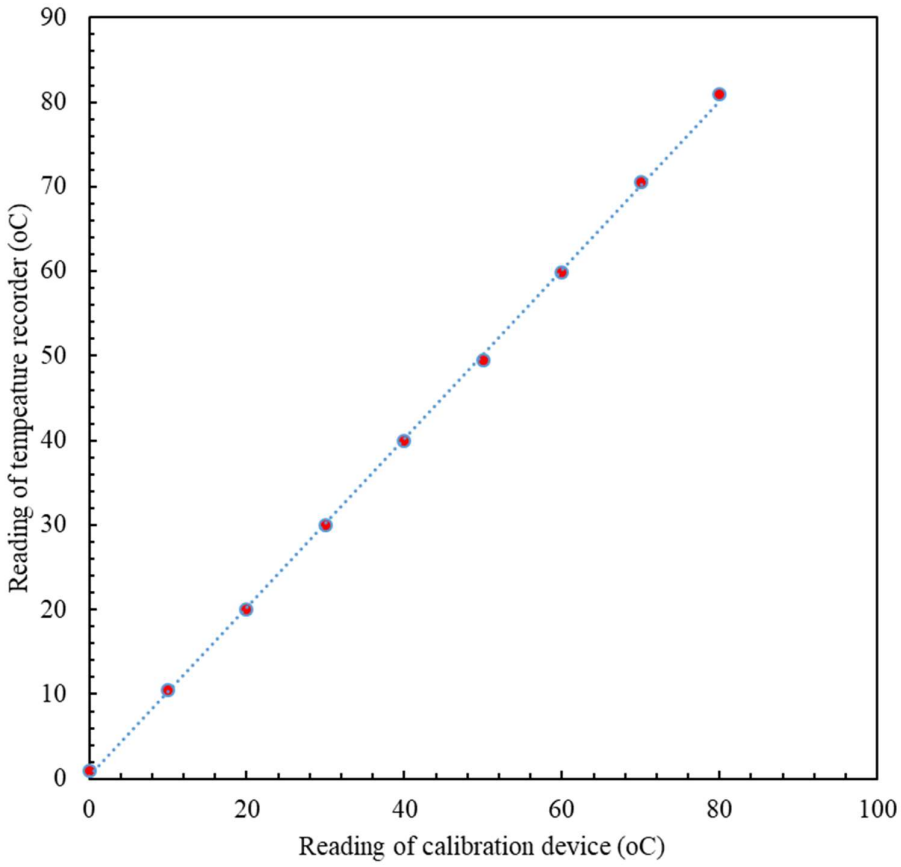

Figure (3- 16) calibration curve of temperature recorder readings

3.2.2. Water Flow Meter

Floating type flow meters Model ZYIA of range (0.5 to 4) liter per minute, are used to measure the volume flow rate of cooling water. The flow entered the bottom of the tapered vertical pipe and caused the float to move upward. The float rose to a point in the pipe, and a drag force is balanced by the weight and buoyancy force. These flow meters installed vertically with regulating valve to select the suitable flow rate according to the experimental procedure as shown in figure (3-17).

The calibration of the flow meters is performed by using a scaling volumetric flask and a stop watch to measure the time required to fill a specified volume of flask. Volumetric flask filled with the water that exits from the pipe of heat exchanger for each flow rate, and the time required for each flow rate is recorded. Figure (3-18) shows the polynomial equations are obtained to correct the flow rate measurement readings as:

$$\dot{m}_{\text{calibration}} = 0.0121\,\dot{m}^{3}_{\text{read}} - 0.058\,\dot{m}^{2}_{\text{read}} + 1.1346\,\dot{m}_{\text{read}} + 0.1786 \qquad (3.5)$$

Figure (3- 17) flow meter

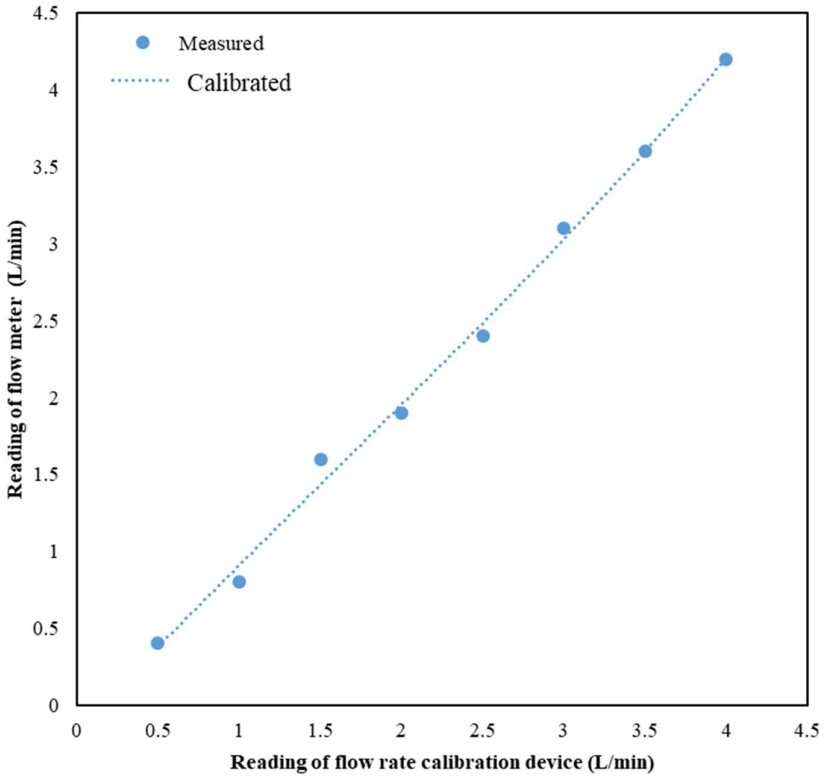

Figure (3- 18) calibration curve of flow meter readings

3.2.3. Hot Wire Anemometer

Hotwire anemometer model (YK-2005AH) device is used to measure air velocity before and after cooling coil. Thermal anemometry is the most common method used to measure instantaneous fluid velocity. The working technique of this device depends on the convective heat loss to the surrounding fluid from an electrically heated sensing element or probe. If only the fluid velocity varies, then the heat loss can be interpreted as a measure of that variable. The anemometer has thermistor type K and J thermometer used to measure ambient temperature .as shown in figure (3-19). Due to the consideration of density effect on accurate measurement of air velocity, the hot wire anemometer probe is used to measure the air velocity at 9 points at inlet section. The velocity also measured at different points through fan coil unit. The calibration process of the air velocity measuring device model (YK-2005AH) is carried out by comparing the

readings with another device model (Model AN200) shown in figure (3-20). It is noted that the error rate is within the factory limits of the device, which is 3% for air velocity and 0.2% for temperature. As shown in figure (3-21), the calibration curve between the two devices, which can be represented by the following linear relationship:

$$v_{calibration} = -0.0023\ v_{read}^{3} + 0.0421\ v_{read}^{2} + 0.8251\ v_{read} - 0.0952 \qquad (3.6)$$

Figure (3- 19) hotwire anemometer device

Figure (3- 20) thermo-anemometer for air velocity calibration.

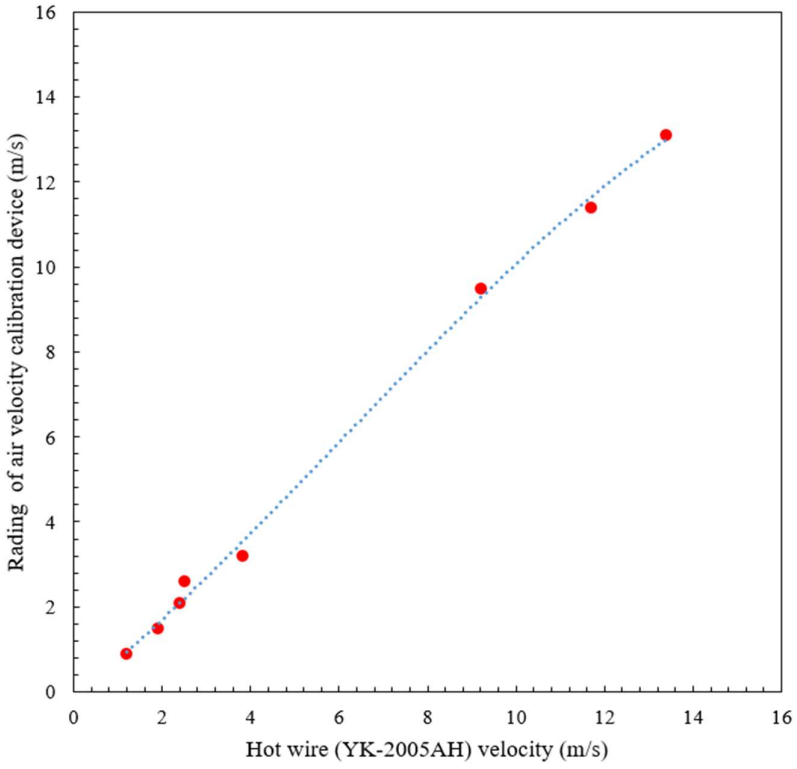

Figure (3- 21) calibration curve of air velocity readings

3.2.4. Pressure Device

The pressure drop across the airside of the heat exchanger is detected by using UT366A digital manometer as shown in figure (3-22). The manometer can measure gauge pressure and differential pressure. The measurement ranges from 0 to 15000 Pa with resolution of 1 Pa. the static pressure in range ± 0.4 to 5000 Pascal.

The readings of digital pressure different manometer are calibrated with multi tube manometer as shown in figure (3-23). The results of pressure drop for manometer and digital pressure manometer are compared and represented by calibration curve in figure (3-24). A polynomial equation for this relation is obtained to correct these readings of pressure drop as:

$$\Delta p_{calibration} = 4*10^{-3}\Delta p_{read}^{3} - 0.0132\Delta p_{read}^{2} + 2.0816\Delta p_{read} - 32.458 \quad (3.7)$$

Figure (3- 22) pressure measurement device

Wind Tunnel

Test Tube

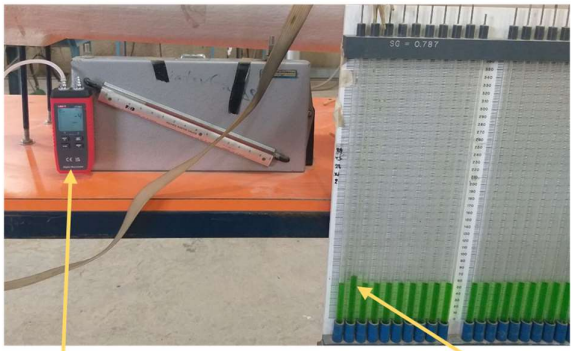

Pressure Device **Multi-tube manometer**

Figure (3- 23) calibration of pressure device with multi-tube manometer.

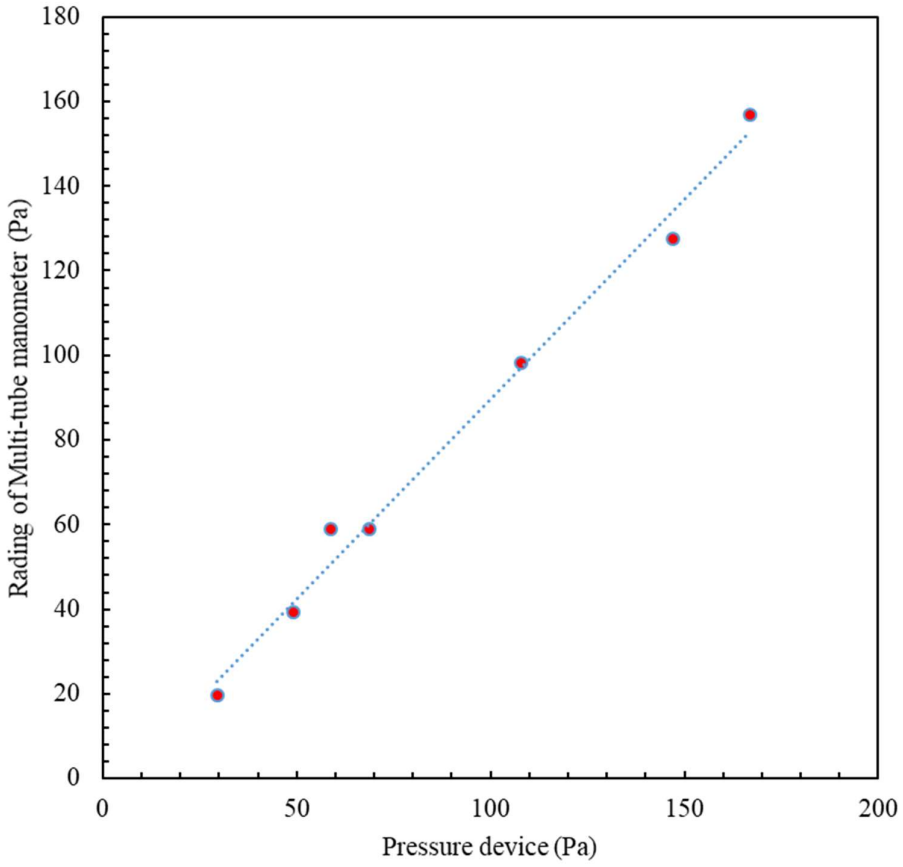

Figure (3- 24) calibration curve of pressure device

3.3. Experimental Procedures

The experiments are carried out under Iraqi a climate conditions. The experiments are conducted during the month of July, where the room temperature is between 33 ºC to 36 ºC. The steps of the experiment can be summarized through the following points:

1- Filling the tank with water, and check there are no leaks through the pipes.

2- The pump is turned on to flow the cold water with temperature of 10 ºC to heat exchanger.

3- Adjusting the water flow rate to heat exchanger by the control valves of the water flow through main and bypass pipes before the test pipe and flow meter.

4- The cooling fan is running at the desired speed and the velocity is controlled by the speed regulator.

5- Air velocity is measured using hot wire anemometer at different locations during the test section and the readings are recorded and then calibrated through the equation (3.6).

6- The pressure drop through the heat exchanger is measured using digital pressure manometer and the readings are recorded and then calibrated through the equation (3.7)

7- The cooling fan and water pump are turned on at the required flow, and then the temperature recorder starts recording temperatures for a period of 30 minutes until the temperature reaches stability.

8- The date logger with SD ram are operated to read and save the temperature readings, through the time of device operating has been measured in all selected points after calibrated by equation (3.4).

9- The experiment is repeated using a different air velocity, as well as changing the temperature of the inlet water entry and flow rate until the best value for the water flow is obtained. All measured values are shown in Appendix (D). After calibrated by equation (3.4), (3.6) and (3.7). These temperature readings are presented for case 1. The temperature readings verse time for cases 2 until 18 are reported in the appendix (C). Table (3-3) explain the test cases used in the current study.

3.4. Experimental Analysis

3.4.1. Heat transfer rate

The average air temperature of heat exchanger inlet and outlet are $T_{a,in}$, and $T_{a,out}$ respectively, which are used to determine the thermos-physical

properties of air. The heat transfer rates through air side calculated from, [3].

$$\dot{Q}_{air} = \dot{m}_{air} cp_{air} \left(T_{air,in} - T_{air,out} \right) \tag{3.8}$$

The heat transfer rates through water side calculated from

$$\dot{Q}_{water} = \dot{m}_{water} cp_{water} \left(T_{water,out} - T_{water,in} \right) \tag{3.9}$$

The mean heat transfer rate $\dot{Q}_m$ is evaluated through

$$\dot{Q}_m = \frac{\dot{Q}_{air} + \dot{Q}_{water}}{2} \tag{3.10}$$

3.4.2. Logarithmic Mean Temperature Difference (LMTD)

Shah and Sekulic [3] describe the logarithmic mean temperature difference (LMTD) for cross flow heat exchanger as following:

$$\Delta T_m = \frac{\left(T_{\text{air.in}} - T_{\text{water.out}} \right) - \left(T_{\text{air.out}} - T_{\text{water.in}} \right)}{\ln \dfrac{\left(T_{\text{air. in}} - T_{\text{water.out}} \right)}{\left(T_{\text{air.out}} - T_{\text{water.in}} \right)}} \tag{3.11}$$

Where $T_{\text{water.in}}$, $T_{\text{water.out}}$ are the averaged water temperatures at inlet and outlet, respectively.

3.4.3. Overall Heat Transfer Resistance

The overall heat transfer resistance can be separated into six parts: convection thermal resistance on air and water sides, the conductive resistance through the tube wall, and the thermal contact resistance between tube and metallic foam Chen et al [27] used equation (3.12) to evaluated overall heat transfer resistance in heat exchanger

$$R = R_{\text{ext}} + R_{f.ext} + R_{\text{bond}} + R_{\text{tube}} + R_{\text{int}} + R_{f.int} = \frac{\Delta T_m}{\dot{Q}_m} \tag{3.12}$$

3.4.4. Effectiveness of heat exchanger

The overall effectiveness of the heat exchanger which is calculated by Cengel [58] as:

$$\varepsilon = \frac{\dot{Q}_m}{\dot{Q}_{max}} \tag{3.13}$$

$$\dot{Q}_{max} = C_{min}\left(T_{air,in} - T_{water,in}\right) \tag{3.14}$$

3.4.5. Reynolds number

Reynolds number for air side pointed by Kauls [59] as following:

$$Re_{air} = \frac{\rho_{air} u_{air,in} D_{hy}}{\mu_{air}} \tag{3.15}$$

Where $u_{air,in}$ air velocity at the entrance of tube bundles. The hydraulic diameter (D_{hy}) of flow around finned surface is very complex function. Kauls [59] presents very effecting method to evaluate the hydraulic diameter from equation (3.16) depending on the porosity of the flow region and the heat transfer area

$$D_{hy} = \frac{4 \times A_c \times L}{A_s} \tag{3.16}$$

Where A_c is flow cross section area and calculated from

$$A_c = A_{front} \times \varphi \tag{3.17}$$

$$A_c = W \times H \times \varphi \tag{3.18}$$

A_s is the total heat transfer area, L is an equivalent flow length measured flow the leading edge of the first tube row to the leading edge of

a tube row that would follow the last tube row, W, and H is width and height of cooling coil, respectively.

3.4.6. Friction Factor

The friction factor of the present heat exchanger is calculated from the pressure drop across the cooling coil and inlet bulk velocity of the air and expressed by Kim et al. [14] as following:

$$f = \frac{\Delta P}{0.5 \times \rho_{air} \times u_{air}^{\ 2}} \tag{3.19}$$

Note that based on the temperature level of this study. Therefore, for time saving, the friction factor is based on the isothermal conditions.

3.4.7. Colburn Factor

The Colburn factor (j) used to evaluate the thermal performance of the heat exchanger, Kim et al [14] suggest the following equation:

$$j = \frac{h}{\rho_{air} u_{in} cp_{air}} \mathrm{Pr}^{2/3} \tag{3.20}$$

Where η_s is the surface efficiency of fine or copper foam, Pr is the Prandtel number of air. Kim et al. [14] simplify the Colburn relation for cross flow heat exchanger into the following equation:

$$j = \frac{\Delta T}{\Delta T_m} \mathrm{Pr}^{2/3} \tag{3.21}$$

$$\Delta T = T_{air,in} - T_{air,out} \tag{3.22}$$

3.4.8. Area Goodness Factor

The thermal–hydraulic performance of heat exchanger with metallic foam can be evaluated by using area goodness factor as explained by Buonomo et al. [52]

$$AG = \frac{j}{f} \tag{3.23}$$

3.4.9. The Average Nusselt Number

The average Nusselt number for air side can be calculated by Kim et al. [14] as following:

$$\overline{Nu}_{outside} = \frac{\bar{h}_{outside} \times D_{hy}}{k_{air}} \tag{3.24}$$

The heat transfer coefficient for air side calculated by Kim et al. [14]. The wall temperature measured by using thermocouples at two positions, the first position at the first row of tubes, and the second position at the last row of tubes.

$$\bar{h}_{outside} = \frac{\dot{Q}_{air}}{A_s \times (T_{air} - T_{wall})} \tag{3.25}$$

Where T_{wall}, and T_{air} calculated from:

$$T_{wall} = \frac{T_{wall\,1} + T_{wall\,2}}{2} \tag{3.26}$$

$$T_{air} = \frac{T_{air\,1} + T_{air\,2}}{2} \tag{3.27}$$

3.5. Uncertainty and Error Analysis

The error in measurement is defined as the difference between its true and measured value. However, this definition is not easy to know which the true quantity of these values is. Therefore, it is necessary to compute the uncertainty when presenting an experimental result. Generally, the uncertainty of measurement is described as the amount of errors or doubts in taking measurement. These errors or doubts are mainly due to measuring instrument, measuring process, human error (operator skills), and operating condition. For any set data, the standard uncertainty (S.U) can be calculated by equation detailed by Bell [60] as:

$$S.U = \frac{S.D}{\sqrt{N}} \tag{3.28}$$

Where,

N is the total number of measurements.

$S.D$ is the standard deviation which is calculated as:

$$S.D = \sqrt{\frac{\sum_{i=1}^{N}\left(X_i - X_{average}\right)^2}{\left(N-1\right)}} \tag{3.29}$$

$X_{average}$ is the average readings of temperature or any function in pipe. The average experimental values of readings in each pipe which are repeated N times. The value of average readings is calculated as:

$$X_{average} = \frac{1}{N}\sum_{i=1}^{N} X_i \ldots\ldots \tag{3.30}$$

Where X_i represents the values for measurements data of temperature or any function measured in each pipe. Then, all experimental analysis

depending on measuring values are uncertain. Tables (3-4), and (3-5) indicate the uncertainty for temperature, velocity, flow rate, and pressure.

Note: uncertainty propagations are carried out for all the experimental analysis parameters, which are indicated in appendix (D).

Table (3- 3) conditions of cases used during the experimental work.

	Inlet Water Temperature (°C)	**Air Inlet Velocity (m/s)**	**Water Discharge (LPM)**	**Heat Exchanger**
Case 1	10	1.5	1	Fin
Case 2	10	1.5	2	Fin
Case 3	10	1.5	3	Fin
Case 4	10	1.5	4	Fin
Case 5	18	1.5	4	Fin
Case 6	16	1.5	4	Fin
Case 7	13	1.5	4	Fin
Case 8	10	5.6	4	Fin
Case 9	10	9.3	4	Fin
Case 10	10	0.9	1	Cu/Foam
Case 11	10	0.9	2	Cu/Foam
Case 12	10	0.9	3	Cu/Foam
Case 13	10	0.9	4	Cu/Foam
Case 14	18	0.9	4	Cu/Foam
Case 15	16	0.9	4	Cu/Foam
Case 16	13	0.9	4	Cu/Foam
Case 17	10	4.8	4	Cu/Foam
Case 18	10	8.7	4	Cu/Foam

Table (3- 4) uncertainty of temperature distribution through heat exchanger.

Description	S.U Value	Description	S.U Value	Description	S.U Value
T_1	0.0972	T_9	0.0778	T_{17}	0.1051
T_2	0.0964	T_{10}	0.0811	T_{18}	0.0779
T_3	0.1288	T_{11}	0.0773	T_{19}	0.0789
T_4	0.0675	T_{12}	0.1787	T_{20}	0.0655
T_5	0.0707	T_{13}	0.0964	T_{21}	0.0500
T_6	0.0905	T_{14}	0.0895	T_{22}	0.0921
T_7	0.0625	T_{15}	0.1060	T_{23}	0.0693
T_8	0.0773	T_{16}	0.0905		0.1051

Table (3- 5) uncertainty of pressure, air velocity, and water flow rate.

Description	S.U Value
Δp (heat exchanger with fins) [Pa]	1.4752
Δp (heat exchanger with foam) [Pa]	1.6195
Air inlet velocity (heat exchanger with fins) [m/s]	0.0639
Air inlet velocity (heat exchanger with foam) [m/s]	0.0500
Water volume flow rate [L/min]	0.0726

CHAPTER FOUR

THEORETICAL WORK

Chapter Four: Theoretical Work

4.1. Introduction

This part of the study shows the mathematical model. Through this model, metal foam is used as a porous medium placed around the tubes instead of the traditional fins in order to improve the heat exchanger performance. Most of the previous studies showed the possibility of using metallic foam in heat exchanger applications, which gave good thermal performance results. On the other hand, the metal foam would generate a high pressure difference on both sides of the heat exchanger and this leads to greater energy consumption by the fan. Therefore, the choice of metal foam dimensions is an effective element in the thermal and dynamic performance of the heat exchanger. A numerical solution used to simulate the process of flow and heat transfer through the heat exchanger with the metal foam, where the finite element method (FEM) is used as a numerical method through the use of the COMSOL program. The objective of this part is to determine the dimensions of the metal foam placed around the tube, which represents a porous medium, where this foam improves heat transfer, but within a certain range of dimensions. The use of this foam is ineffective and thus leads to reduce the dynamic performance of the passage of air through the heat exchanger.

4.2. Physical Domain Description

The current study model includes a cooling coil for a cross-flow heat exchanger consisting of four rows of tubes consisting of 52 tubes arranged in a linear manner as shown in figure (4-1). Copper foam is placed around the tubes to replace a traditional fin. The geometrical specifications of heat exchanger are presented in table (4-1). The corresponding 2D computational domain is explained in figure (4-2).

Table (4- 1) dimensions of heat exchanger

Parameter	Value (mm)
Tube diameter	8
Longitudinal tube pitch	30
Transversal tube pitch	30
Heat exchanger width	400
Heat exchanger height	400
Heat exchanger depth	120

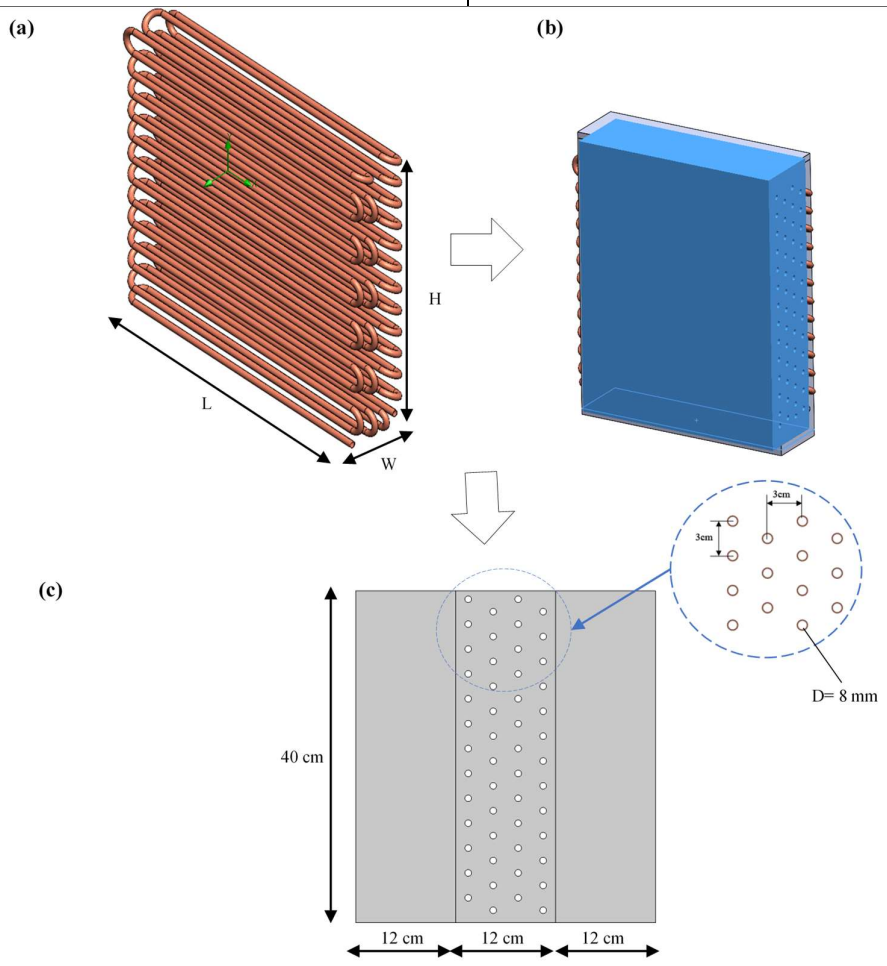

Figure (4- 1) dimensions of the fan coil heat exchanger used in this study. (a) cooling coil, (b) copper foam, (c) domain dimensions.

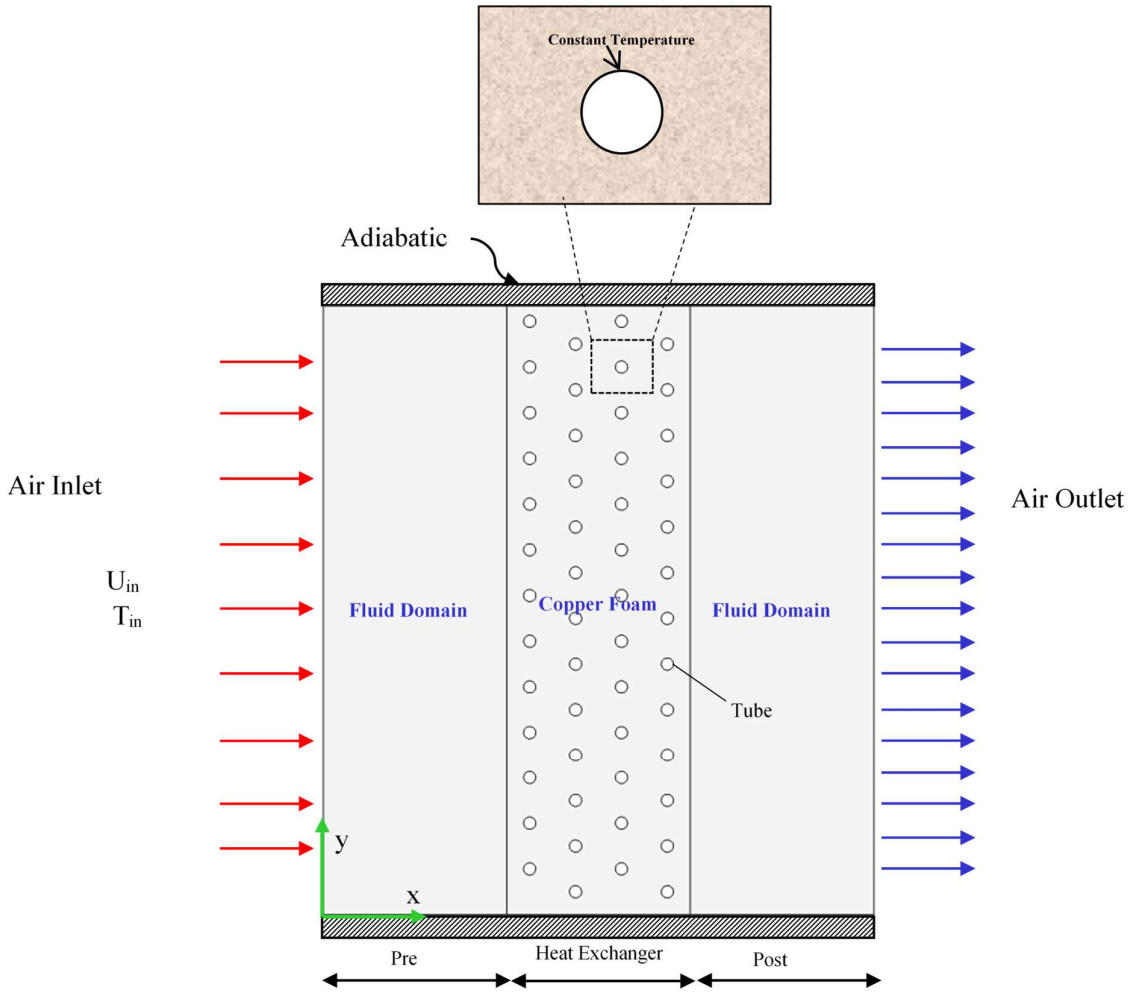

Figure (4- 2) computational domain of heat exchanger with metallic foam.

4.3. Governing Equations and Assumptions

This study is a fully numerical study, so it's need some simplifications and assumption to simplify the solution process. The following are the assumptions that are used:

1- Two dimensional study

2- Turbulent flow

3- Metal is Copper, which is isotropic and homogeneous.

4-Solid and fluid thermos-physical properties are independent on

temperature.

5-Neglected the thermal contact resistance between foam and tube surface, bouncy effect, and viscous dissipation.

6- Neglected the radiative heat transfer.

7- Tube surface has a uniform temperature.

The mathematical model is divided into two main regions, one of which consists of fluid only, which is the region before and after the tube covered with metal foam. The other regions, it includes the metal foam and the fluid that passes through it, as it is dealt with on the basis of the equations of the porous media. Two sets of governing equations are required to solve the physical problem with fluid=porous interface; one for the porous region, another for the clear fluid region for turbulent flow, these sets are:

1. Fluid Domain

The equations governing air flow through the channel is in the basic form of the equations of conservation of momentum and conservation of mass and energy. These equations are applied to pre and post fluid domain as shown in figure (4-2).[54]:

1-Continuity Equation:

$$\frac{\partial \rho}{\partial t} + \frac{\partial(\rho \mathrm{u})}{\partial \mathrm{x}} + \frac{\partial(\rho \mathrm{v})}{\partial \mathrm{y}} = 0 \qquad (4.1)$$

2-Momentum Equation:

$$\rho_f \left(\frac{\partial \mathrm{u}}{\partial \mathrm{t}} + \mathrm{u}\frac{\partial \mathrm{u}}{\partial \mathrm{x}} + \mathrm{v}\frac{\partial \mathrm{u}}{\partial \mathrm{y}}\right) = -\frac{\partial \mathrm{p}}{\partial \mathrm{x}} + \frac{\partial}{\partial \mathrm{x}}\left(\mu_\mathrm{f}\frac{\partial \mathrm{u}}{\partial \mathrm{x}}\right) + \frac{\partial}{\partial \mathrm{y}}\left(\mu_\mathrm{f}\frac{\partial \mathrm{u}}{\partial \mathrm{y}}\right) \qquad (4.2)$$

$$\rho_\mathrm{f} \left(\frac{\partial \mathrm{v}}{\partial \mathrm{t}} + \mathrm{u}\frac{\partial \mathrm{v}}{\partial \mathrm{x}} + \mathrm{v}\frac{\partial \mathrm{v}}{\partial \mathrm{y}}\right) = -\frac{\partial \mathrm{p}}{\partial \mathrm{y}} + \frac{\partial}{\partial \mathrm{x}}\left(\mu_\mathrm{f}\frac{\partial \mathrm{v}}{\partial \mathrm{x}}\right) + \frac{\partial}{\partial \mathrm{y}}\left(\mu_\mathrm{f}\frac{\partial \mathrm{v}}{\partial \mathrm{y}}\right) \qquad (4.3)$$

3- Energy Equation:

$$\rho_f cp_f \left(\frac{\partial T_f}{\partial t} + u\frac{\partial T_f}{\partial x} + v\frac{\partial T_f}{\partial y}\right) = \frac{\partial}{\partial x}\left(k_f \frac{\partial T_f}{\partial x}\right) + \frac{\partial}{\partial y}\left(k_f \frac{\partial T_f}{\partial y}\right) \quad (4.4)$$

4-Turbulence Model: The turbulence kinetic energy (K) and its rate of dissipation (ε) are obtained from the following transport equations. For the case of a constant fluid property, the differential transport equations in nonconservative form are expressed as[54]

$$\frac{\partial K}{\partial t} + u\frac{\partial K}{\partial x} + v\frac{\partial K}{\partial y} = \frac{\partial v_T \partial K}{\partial x \sigma_k \partial x} + \frac{\partial v_T \partial K}{\partial y \sigma_k \partial y} + P - D \quad (4.5)$$

$$\frac{\partial \varepsilon}{\partial t} + u\frac{\partial \varepsilon}{\partial x} + v\frac{\partial \varepsilon}{\partial y} = \frac{\partial v_T \partial \varepsilon}{\partial x \sigma_\varepsilon \partial x} + \frac{\partial v_T \partial \varepsilon}{\partial y \sigma_\varepsilon \partial y} + \frac{\varepsilon}{K} C_{\varepsilon 1} P - C_{\varepsilon 2} D \quad (4.6)$$

where the destruction term D is given by ε and the production term P is formulated as

$$P = 2v_T \frac{\partial u^2}{\partial x} + \frac{\partial v^2}{\partial y} + v_T \frac{\partial u}{\partial y} + \frac{\partial v^2}{\partial x} \quad (4.7)$$

where:

$u, v =$ component of the velocity vector in the x, and y direction. ρ: Fluid density (kg/m^3), Cp: specific heat at constant pressure (J/ (kg. K)). For the turbulent case the effective dynamic viscosity (μ_e) is defined as:

$$\mu_e = \mu_+ \mu_t \quad (4.8)$$

where

μ: laminar dynamic viscosity (fluid property)

μ_t: turbulent viscosity is turbulent model $(k - \varepsilon)$ is used to evaluate the turbulent viscosity through the expression is:

$$\mu_t = \rho C_\mu \frac{k^2}{\varepsilon} \quad (4.9)$$

where:

k : turbulent kinetic energy

ε : turbulent kinetic energy dissipation rate.

In these equations, G_K represents the generation of turbulence kinetic energy due to the mean velocity gradients. C_1 and C_2 are constants. σ_k and σ_ε are the turbulent Prandtl numbers for K and ε, respectively.

The values of turbulence model constants $C_{1\varepsilon}, C_{2\varepsilon}, C_\mu, \sigma_K$, and σ_ε are given in Table (4-2).[54]

Table (4- 2) Values of Model Constant are used in K-ε Model

Constant	$C_{1\varepsilon}$	$C_{2\varepsilon}$	C_μ	σ_K	σ_ε
Value	1.44	1.92	0.09	1	1.3

2. Porous Media Domain

In porous media, the Dupuit-Forvhheimer relation is well utilized, and if (*v)* is the average fluid velocity, then may derive the intrinsic average velocity (*V)* from it. [61] :

$$v = \varphi V \tag{4.10}$$

-Continuity equation

The general form of mass conservation equation in porous media is, [61]

$$\varphi \frac{\partial \rho_f}{\partial t} + \nabla \cdot \left(\rho_f U \right) = 0 \tag{4.11}$$

-Momentum equation

Darcy-Brinkman-Forchheimer model is used to describe the fluid movement within the porous medium [43]. The choice of this model comes

due to the possibility of using the model when there is an external flow and a porous medium, so the normal Darcy model cannot use.

The general form of this equation is:[10]

$$\nabla p = -\frac{\mu}{K}U + \mu^{*}\nabla^{2}U \tag{4.12}$$

In this study the gravity force neglected so that the form of the equation can be written in the direction of (x) as follows:

$$\frac{\partial p}{\partial x} = -\frac{\mu_f u}{K} + \frac{\mu_f}{\varepsilon}\left(\frac{\partial^2 u}{\partial x^2} + \frac{\partial^2 u}{\partial y^2}\right) - \frac{C_F}{K^{1/2}}\rho_f \sqrt{u^2+v^2}\,u - \rho_f\left(\frac{u}{\varepsilon^2}\frac{\partial u}{\partial x} + \frac{v}{\varepsilon^2}\frac{\partial u}{\partial y}\right) \tag{4.13}$$

The Momentum equation in (y) direction is:

$$\frac{\partial p}{\partial y} = -\frac{\mu_f v}{K} + \frac{\mu_f}{\varepsilon}\left(\frac{\partial^2 v}{\partial x^2} + \frac{\partial^2 v}{\partial y^2}\right) - \frac{C_F}{K^{\frac{1}{2}}}\rho_f \sqrt{u^2+v^2}\,v - \rho_f\left(\frac{u}{\varepsilon^2}\frac{\partial v}{\partial x} + \frac{v}{\varepsilon^2}\frac{\partial v}{\partial y}\right) \tag{4.14}$$

The third part of right hand side in equations (4.13) and (4.14) is called Forchheimer effect, where C_F is drag constant, and K is permeability [10]. There are several studies that set equations that are extracted through experiments to calculate these two factors. In the current study the permeability and drag constant it is taken from the experimental work, as it is measured in chapter three.

-The energy equation for porous medium

Local Thermal Equilibrium (LTE) is used, by assuming the solid and fluid mediums are in equilibrium $T_f=T_s=T$. Thus, the general form of the equation is as follows:[54]

$$\left(\rho c_p\right)_f\left(\frac{\partial T}{\partial t} + u\frac{\partial T}{\partial x} + v\frac{\partial T}{\partial y}\right) = k_e\left(\frac{\partial^2 T}{\partial x^2} + \frac{\partial^2 T}{\partial y^2}\right) \tag{4.15}$$

In general, (k_e) is a complex function of the geometry of the medium. Hans [62] describes the parallel law of effective thermal conductivity as following:

$$k_e = \varphi.k_f + (1-\varphi)k_s \tag{4.16}$$

4.4. Boundary Conditions

To simplify the solution process and to get rid of the complications of the growth of the boundary layer through the channel, the inlet air is fully developed and with velocity equal to (u_{in}). The exit area is atmospheric pressure, so the value of the gage pressure is zero, so the pressure change (Δp) can be calculated by calculating the inlet pressure only. The surface of the tube, assumed that the temperature is constant, and the rest of the surfaces of the channel are adiabatic surfaces. The boundary conditions for this study can be summarized in table (4-2).

Table (4- 3) boundary conditions for air.

Location	Momentum	Energy
Inlet	$u = u_{a,in}$ $v = 0$	$T = T_{a,in}$
Outlet	$p = p_o = 0$ p_o is the relative pressure at the boundary.	$T = T_{out}$
Tube wall	$u = v = 0$	$T = T_{water}$
Channel wall's	$\frac{\partial u}{\partial y} = 0, v = 0$	$\frac{\partial T}{\partial y} = 0$

At the interface between the porous flow region and the external flow domain, the boundary conditions for the numerical calculations pointed by Zhao and Cheng [63] as following:

(1) Mass conservation

$$(\mathrm{u}\cdot\mathrm{n})_f = (\varphi\,\mathrm{u}\cdot\mathrm{n})_p \tag{4.17}$$

$$(\mathrm{u}\cdot\mathrm{t})_f = (\mathrm{u}\cdot\mathrm{t})_p \tag{4.18}$$

Where the subscripts (*f* and *p)* represent the open fluid domain and porous domain, respectively. n and t are the unit vector normal to the interface and tangent to the interface, respectively.

(2) Continuity of the pressure

$$(p)_f = (p)_p \tag{4.19}$$

(3) Continuity of the normal stress and the shear stress

$$(\mathrm{n}\cdot\mathrm{n}\cdot\sigma)_f = (\mathrm{n}\cdot\mathrm{n}\cdot\sigma)_p \tag{4.20}$$

$$(\mathrm{t}\cdot\mathrm{n}\cdot\sigma)_f = (\mathrm{t}\cdot\mathrm{n}\cdot\sigma)_p \tag{4.21}$$

where the stress tensor (σ_{ij}) is defined as

$$\sigma_{ij} = v\left(\partial\mathrm{u}/\partial\mathrm{v} + \partial\mathrm{u}/\partial\mathrm{v}\right) \tag{4.22}$$

4.5. Material

In this study, copper foam is used as a porous medium, as it is assumed that this material is homogeneous. The physical properties of copper shown in table (4-4). Copper foam working as the porous media and its parameters are listed in the table (4-5). The air is the working fluid and its thermos-physical are listed in table (4-6).

Table (4- 4) porous medium properties. [64].

Property	Copper
Density (kg/m^3)	8933
Thermal conductivity (W/m.^{o}C)	401
Specific heat (J/kg.^{o}C)	385

Table (4- 5) copper foam parameters.

Property	PPI	Porosity	Permeability (m^2)	Fiber diameter *df* (m)	*CF*
Value	40	0.94	7×10^{-7}	$2.62*10^{-4}$	0.0113

Table (4- 6) working fluid (air) properties at 300 K. [64].

Property	Value
Thermal conductivity (W/m.^{o}C)	26.3×10^{-3}
Density (kg/m^3)	1.1614
Specific heat (J/kg.^{o}C)	1.007
Dynamic viscosity (Pa.s)	184.6×10^{-7}
Prandtl Number	0.707

4.6. Mesh Generation.

After building the geometry of the problem and determining the physical models, which included the flow model and the heat transfer model, the next step in the solution process is to build the mesh by using COMSOL software. Where the mesh is formed depending on the nature of the geometric shape used in this study, and since the current study is two-dimensional. So the shape of the elements is of two basic types: triangle and quadrilateral. The Delaunay Triangular method is used to discretize the computational domain into unstructured triangles in this numerical procedure. The Delaunay triangulation is a geometric structure that has

been widely used in mesh production from the early days of mesh creation. The Delaunay triangulation of a vertex set maximizes the least angle between all feasible triangulations of that vertex set in two dimensions. The mesh mode of the current numerical computation is shown in figure (4-3). The mesh generating process has been thoroughly carried out.

There are elements of the triangular type that contain three sides and are considered the simplest types of mesh that can be used and the fastest in the generation process as shown in figure (4-4). It can also be noted that the other type of mesh that is used in this study is the quadrilateral elements, which consists of four sides. In general, whenever the angles of the element are narrow or one of the sides is short, this element is considered a poor element. The elements close to the wall are many in order to cover the entire boundary layer area, and thus a faster convergence occurs in the solution process. To get optimum solution's a five sets of grid numbers used in this study as shown in table (4-7). They consisted elements of 45896, 65822, 76014, 112568, and 128282, respectively. In corresponding of inlet velocity equal to 5m/s, the evaluation of friction factor, Colburn factor, and temperature difference as shown in table (4-7). As demonstrated in figure (3-4) that mesh 4 had less value of error than extremely fine mesh. Therefore, to keep a balance between solution accuracy and convergent time, the 112568 element number is chosen in the current study.

Table (4- 7) grid independent study results.

Grid Type		Number of element	Skewness	f	j	ΔT
1	Normal	45896	0.7794	10.470	0.019547	2.6635
2	Fine	65822	0.7974	10.325	0.019088	2.4599
3	Finer	76014	0.8056	10.306	0.018977	2.3857
4	Extra fine	112568	0.834	10.227	0.018641	2.2759
5	Extremely fine	128282	0.8481	10.225	0.018617	2.2234

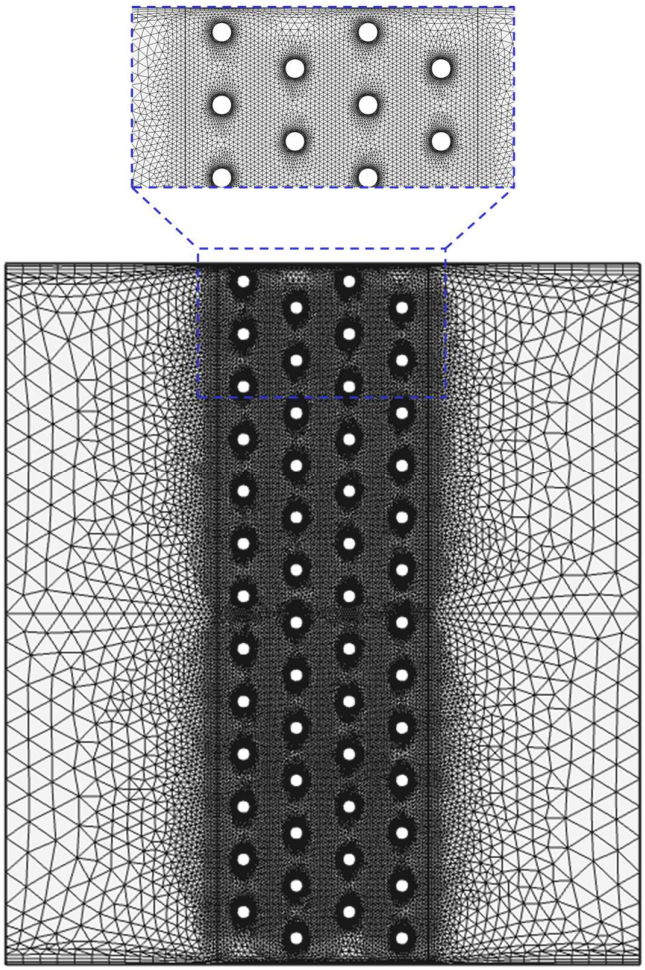

Figure (4- 3) the mesh used in the current study.

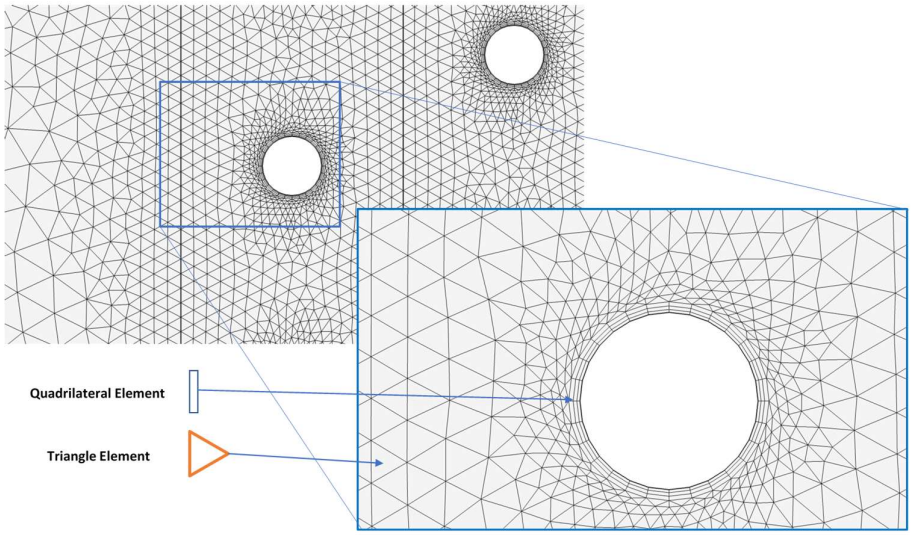

Figure (4- 4) mesh element types

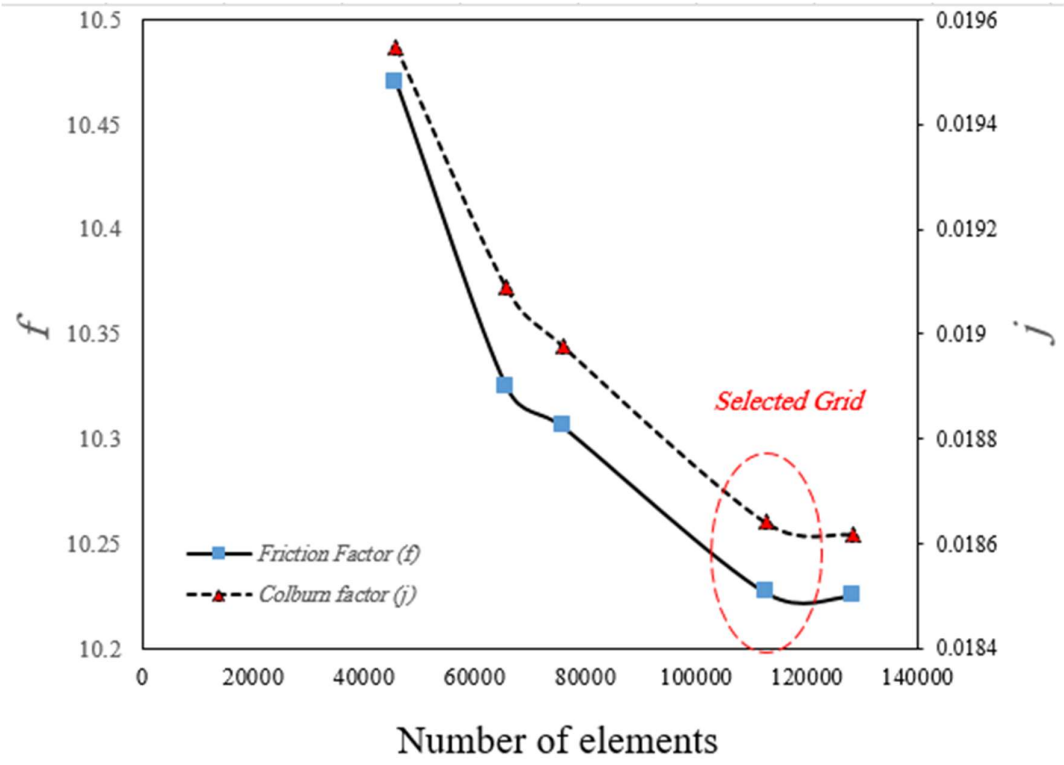

Figure (4- 5) grid independence

4.7. Numerical Methods

The widely available COMSOL Multiphysics 5.5 software is used for the two-dimensional numerical simulation. The working fluid is air, and

the turbulent flow model is employed for both porous and non-porous regions [54]. Air moves through the channel and the metal foam sections. The governing equations for the open zone are comparable to those for open pipe flow, and the governing equations for the metal foam region take into consideration the effects of permeability, porosity, and form drag coefficient. [41]

4.7.1. Finite Element Method

The finite element method is a numerical tool for determining approximate solutions to a large class of engineering problems. Recently, heat transfer engineers have sensed that finite element methodology has considerable power and versatility for solving many types of problems encountered in the field of heat transfer and have used this method very successfully to solve many heat transfer problems including heat exchangers. Among the various numerical methods that have evolved over the years, the most commonly used techniques are the finite difference, finite volume and finite element methods. The finite difference is a well-established and conceptually simple method that requires a point-wise approximation to the governing equations. The model, formed by writing the difference equations for an array of grid points, can be improved by increasing the number of points. Although many heat transfer problems may be solved using finite difference methods as descripted by Özişik et al. [65], as soon as irregular geometries or an unusual specification of boundary conditions are encountered, the finite difference technique becomes difficult to use.

4.7.2. Convergence Criteria

The iterative process is repeated until the change in the variable from one iteration to the next becomes so small that the solution can be

considered converged. At convergence all discrete conservation equations (momentum, energy, etc.) are obeyed in all cells to a specified tolerance, the solution no longer changes with additional iterations, and mass, momentum, energy and scalar balances are obtained. The governing equations are approximated in order to derive the residuals conservation equations. To make the nonlinear momentum equations easier to solve, the Newton-Raphson technique is applied. Solution convergence is predicted if the following prerequisites are met.

$$\left|\frac{\xi^{m+1}-\xi^{m}}{\xi^{m+1}}\right| \leq 10^{-6} \tag{4.23}$$

ξ Any independent variables, where m denotes the number of iterations (velocity, temperature or pressure). The convergence limit for continuity and the momentum equations is set below 10^{-4} and for energy equation is 10^{-6} as pointed by Wang [45]. Figure (4-8) shows the convergence plots for fluid flow and heat transfer. The solution runs for this testing case until a maximum 50, 40 iterations for fluid flow and heat transfer solutions or until satisfied the percentage error for all variables. Also, to obtain stable convergence behavior for the solution, various under-relaxation parameters are used. For the (U), (V)-velocities, pressure, and the energy equations, the under-relaxation parameters adopted for the most cases were 0.2, 0.2, 0.3, and 0.5, respectively. At each iteration, at each cell, a new value for variable (ψ) in cell (P) can then be calculated from equation (4. 19). It is common to apply relaxation that showed by Marshall et al.[66] as:

$$\psi_P^{\text{new,used}} = \psi_P^{\text{old}} + U\left(\psi_P^{\text{new, predicted}} - \psi_P^{\text{old}}\right) \tag{4.24}$$

where (U) is the relaxation factor, (U < 1) is under relaxation. This may slow down speed of convergence but increases the stability of the

calculation, i.e. it decreases the possibility of divergence or oscillations in the solutions. (U = 1) corresponds to no relaxation. One uses the predicted value of the variable. (U > 1) is over relaxation. It can sometimes be used to accelerate convergence but decreases the stability of the calculation.

In the solution of coupled systems of equations, different basis functions may be used for different dependent variables. A typical example is the solution of the Navier-Stokes equations, where the pressure is often more smooth and easy to approximate than the velocity. Methods where the basis (and test) functions for different dependent variables in a coupled system belong to different function spaces are called mixed finite element methods. The software adapts the order of the numerical integration to the element orders for the physics in the model. Some physics interfaces use special element types or a reduced element order for some of the field variables. Select the Shape function type and the Element order as, in most cases, Linear, Quadratic, Cubic, Quartic, or Quintic (for order 1–5, respectively). Figure (4-6) explains the linear function used for pressure and third-order function used for velocity component in this study. For the temperature, there are several functions that can be worked on, as shown in figure (4-7). In the current study, a Quadratic function is chosen

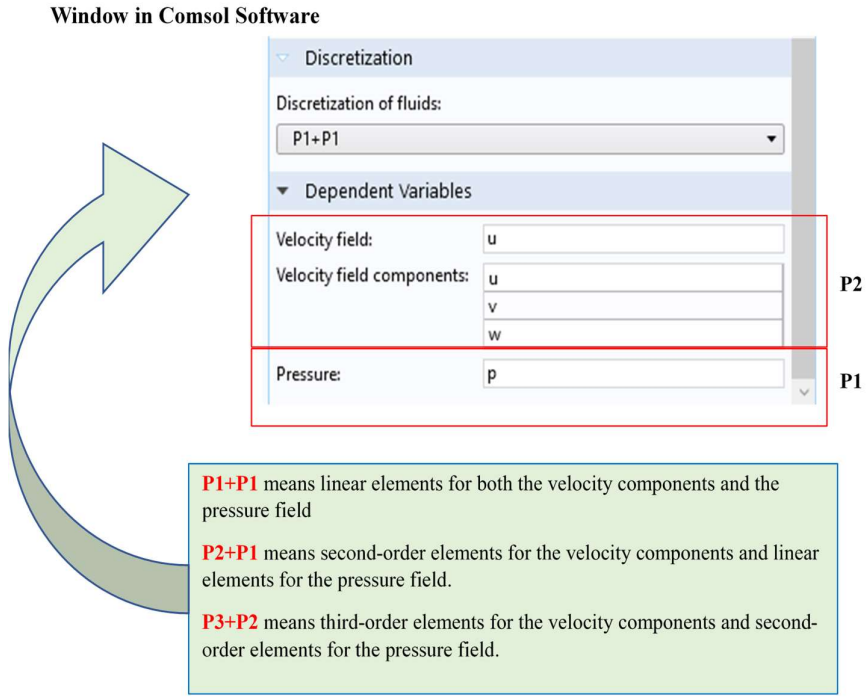

Figure (4- 6) element order and shape function type for calculating velocity components and pressure in COMSOL software.

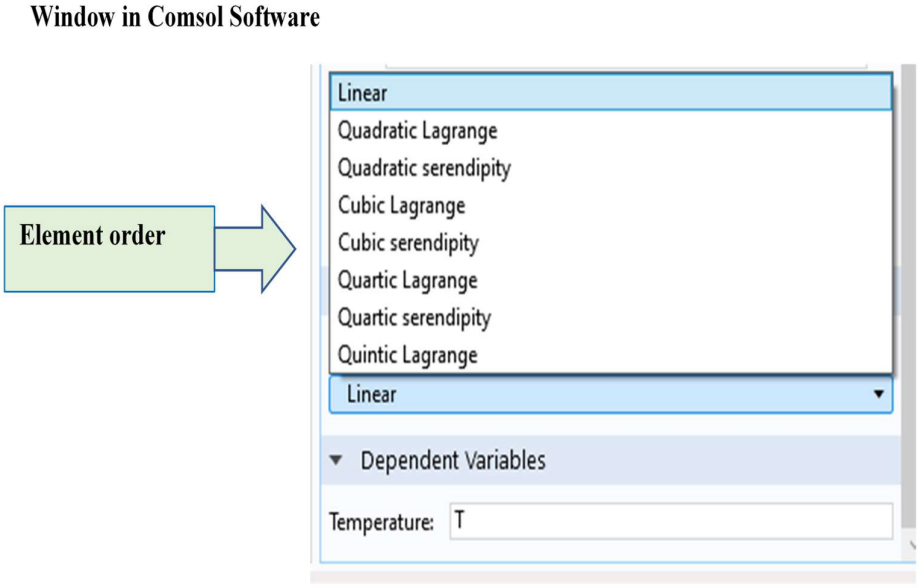

Figure (4- 7) element order and shape function type for calculating temperature in COMSOL software.

4.8. Data Analysis

There are several parameters through which it is possible to analyze the thermal and dynamic performance of the heat exchanger in the presence of metallic foam through a numerical solution, including the heat transfer coefficient (h)

$$h = \frac{\dot{Q}}{A\left(T_{\text{tube}} - T_{\text{in ,air}}\right)} \tag{4.25}$$

Where ($\dot{Q}$)is the heat transfer rate and can be calculated from:

$$\dot{Q} = \dot{m}\ cp\ (T_{in} - T_{out}) \tag{4.26}$$

Since the pressure difference can be calculated, so that the coefficient of friction calculated from the following equation:

$$f = \frac{2\Delta p}{\rho_f u_{in}^2} \tag{4.27}$$

In cross-flow heat exchangers, the Colburn factor (j) is often used to represent the thermal performance of heat exchanger, where it can be defined as follows, [46] :

$$j = \frac{hA}{\dot{m}c_p} Pr_{\text{air}}^{2/3} \tag{4.28}$$

Thus, the ratio between the Colburn factor (j) and the coefficient of friction (f) represents a new coefficient as described by Buonomo et al. [46] called Area Goodness factor (AG) for the heat exchanger

$$AG = \frac{j}{f} \tag{4.29}$$

In this study the dimensionless Reynolds number defined respect to the hydraulic diameter as the flowing equations, [41]:

$$Re = \frac{\rho u_{in} D_h}{\mu} \tag{4.30}$$

The Nusselt number is based on hydraulic diameter:

$$Nu = \frac{h D_h}{k} \tag{4.31}$$

In the current study, the height of the channel is expressed as the hydraulic diameter because the flow is a two-dimensional flow.

CHAPTER FIVE

RESULTS AND

DISCUSSION

Chapter Five: Results and Discussion

5.1. Experimental Results

5.1.1. Temporal change in temperatures.

Figures (5-1) to (5-9) represent the temporal changer in the inlet and outlet temperatures of the heat exchanger with conventional fins. The red color represents the entry temperatures of the cooling water. The water entry temperature is fixed at 10 ^{o}C, as in the figure (5-1). It can be seen that the water entry temperature fluctuates 1 ^{o}C due to the return of water during the closed cycle to the cooling tank. The blue color represents the water outlet temperature from the tube. It can be seen that the water outlet temperature decreases over time as a result of the decrease in the air temperature inside the room over time, and thus the difference between the entry and exit temperature of the water decreases. The green color represents the temperature of the inlet air to the heat exchanger. It can be seen that the inlet temperature of the air ranges from 34 ^{o}C to 36 ^{o}C at the beginning of the experiment, then the temperature decreases over time as a result of the heat exchange between the air and the cooling water, which subtracts the heat outside the system. The black color represents the temperature of the air leaving the heat exchanger to the room atmosphere. The room temperature decreases over time until it reaches the comfortable temperature. The speed at which the air temperature reaches the comfort temperature depends on several factors, including water flow rate, water inlet temperature, and air inlet velocity. Figures (5-1), (5-2), (5-3), and (5-4) show the temperature variation with time for the volumetric flow of water from 1, 2, 3, and 4 LPM, respectively. Outlet air temperature decreases as the water flow rate increase, this is due to the entry of a larger amount of cold water, and thus drawing a larger amount of heat from inside the room in a less time.

Figures (5-5), (5-6), and (5-7) show the temporal change of temperatures when the inlet water temperature 18 ºC, 16 ºC, and 13 ºC, respectively. Increasing the temperature of the inlet water leads to a slower drop in the temperature of the air leaving the heat exchanger, and thus means that the cooling time of the room increases.

Figures (5-8), and (5-9) describe the temporal change of air inlet and exit temperatures at air velocity values 5.6 m/s and 9.3 m/s respectively. It can be seen that the temperature of the exiting water increases with an increase in the air velocity, that due to outlet water draws a large amount of heat when the velocity of the exiting air increases.

Figures (5-10) to (5-18) represent the temporal change of the inlet and exit temperatures through a heat exchanger in the presence of copper foam. Figures from (5-10) to (5-13) show different values of the volumetric flow of water, where it is possible to notice the effect of increasing the flow on accelerating the process of bringing the room temperature to a comfortable level. Figures (5-14), (5-15), and (5-16) explain the temperature variation for different cases of water inlet temperature. It can be noted that an increase in the water temperature leads to a delay in the cooling process, because the difference between the temperature of the water and the air decreases, and therefore the cooling process is slower.

Figures (5-17), and (5-18) illustrate the temporal change of temperature when the incoming air velocity is increased to 4.8 m/s, and 8.7 m/s, respectively. It can be seen that increasing the air velocity reduces the heat exchange time, thus the difference between the inlet and outlet temperature of the air is less.

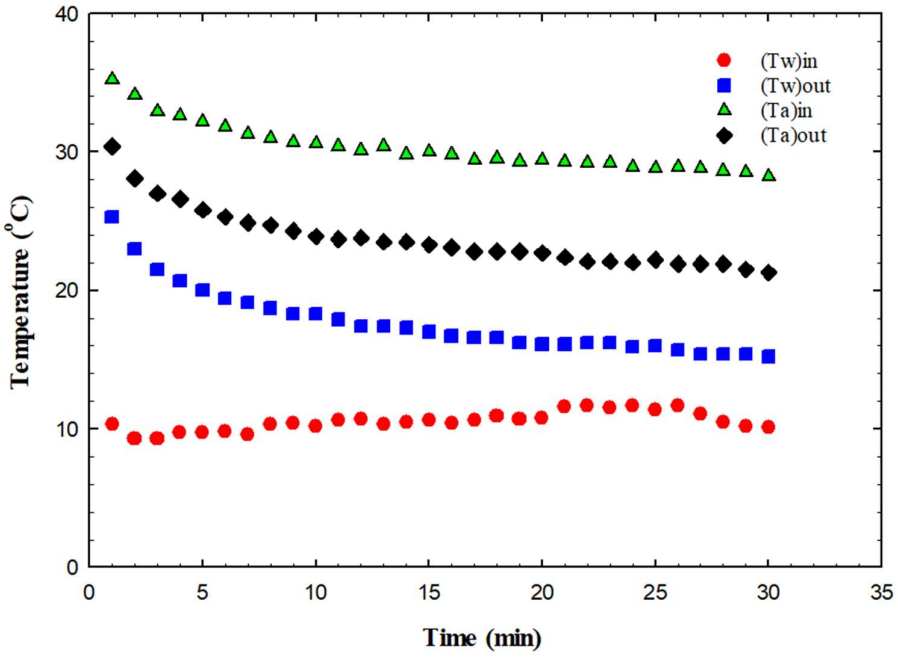

Figure (5- 1) temporal change in the inlet and outlet temperatures of the heat exchanger for case 1.

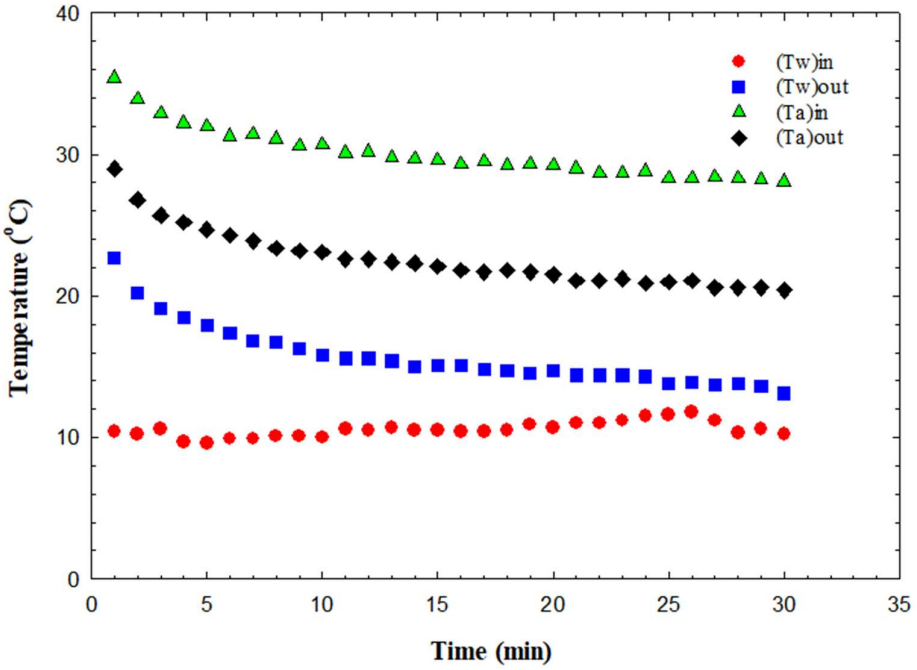

Figure (5- 2) temporal change in the inlet and outlet temperatures of the heat exchanger for case 2.

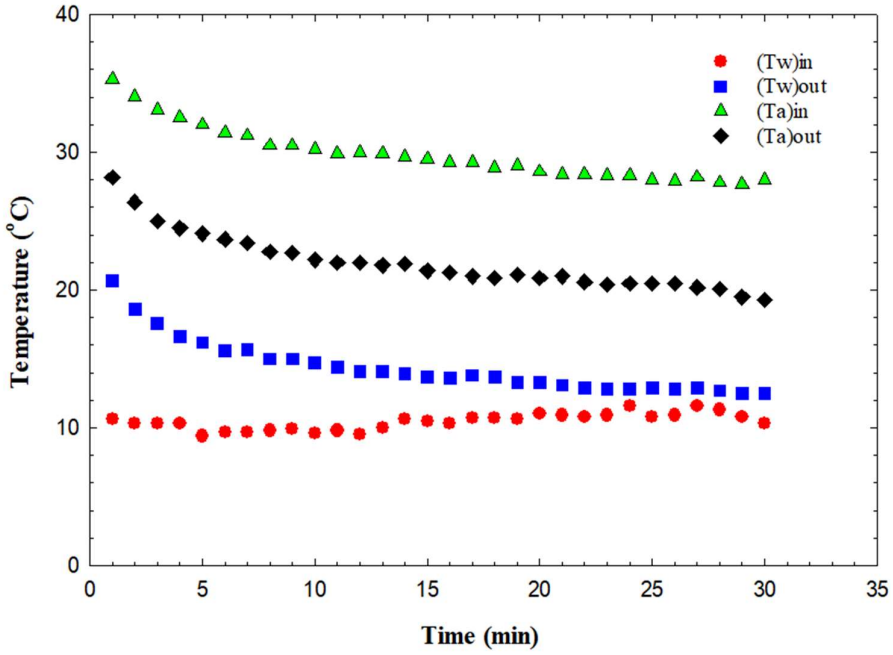

Figure (5- 3) temporal change in the inlet and outlet temperatures of the heat exchanger for case 3.

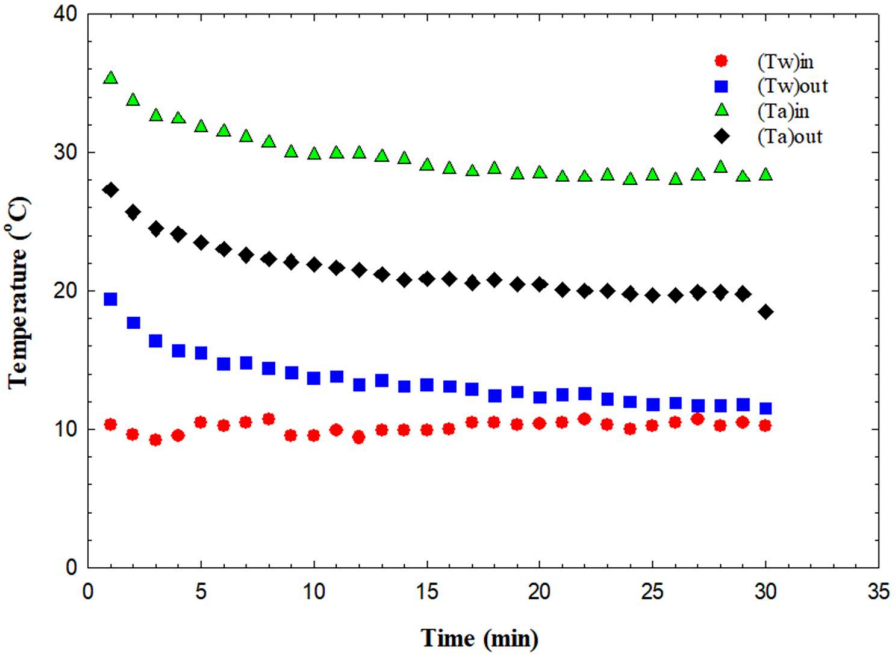

Figure (5- 4) temporal change in the inlet and outlet temperatures of the heat exchanger for case 4.

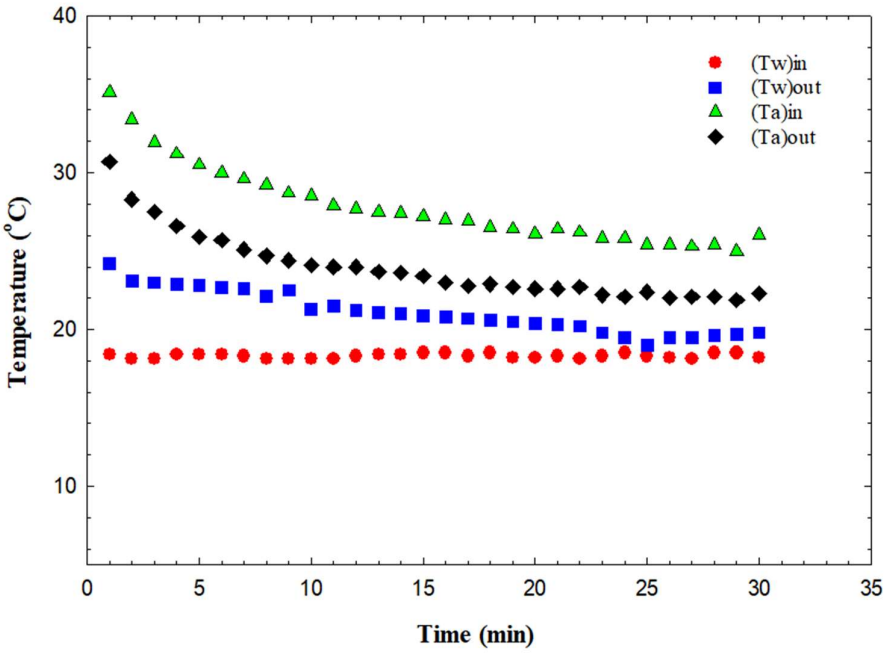

Figure (5- 5) temporal change in the inlet and outlet temperatures of the heat exchanger for case 5.

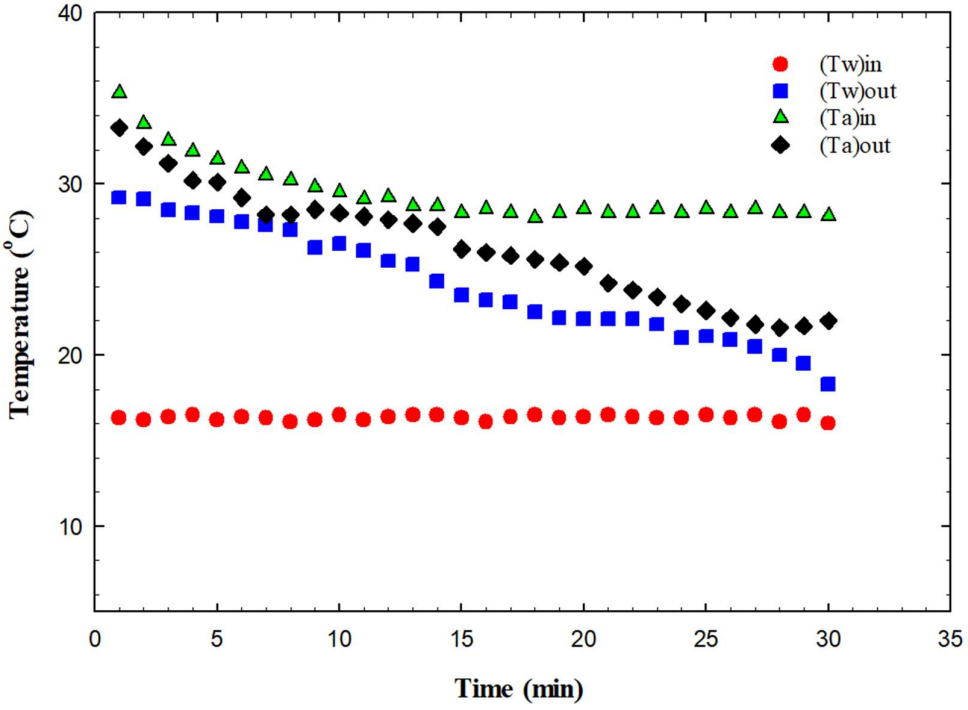

Figure (5- 6) temporal change in the inlet and outlet temperatures of the heat exchanger for case 6.

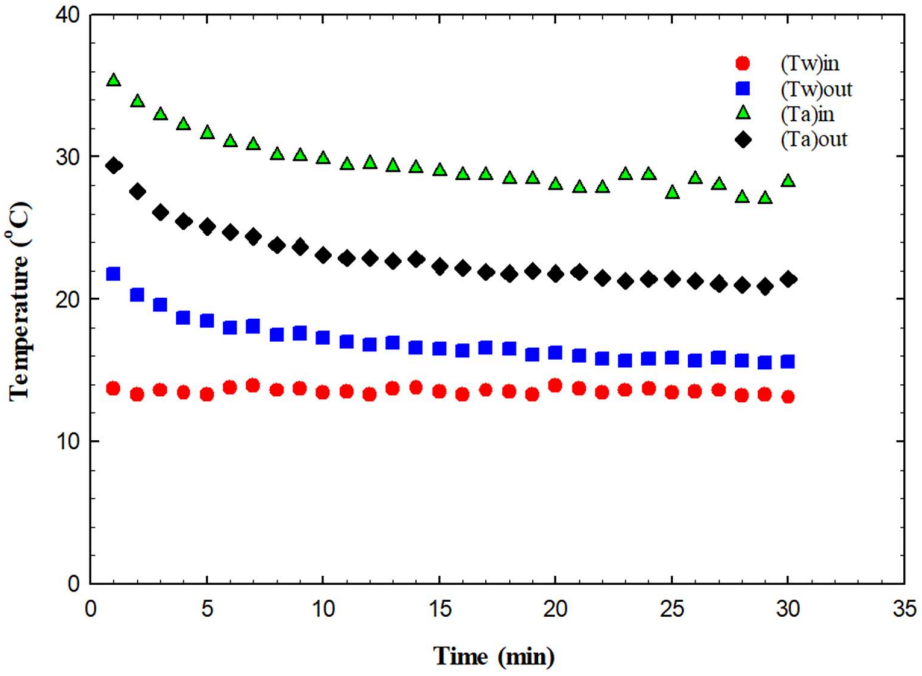

Figure (5- 7) temporal change in the inlet and outlet temperatures of the heat exchanger for case 7.

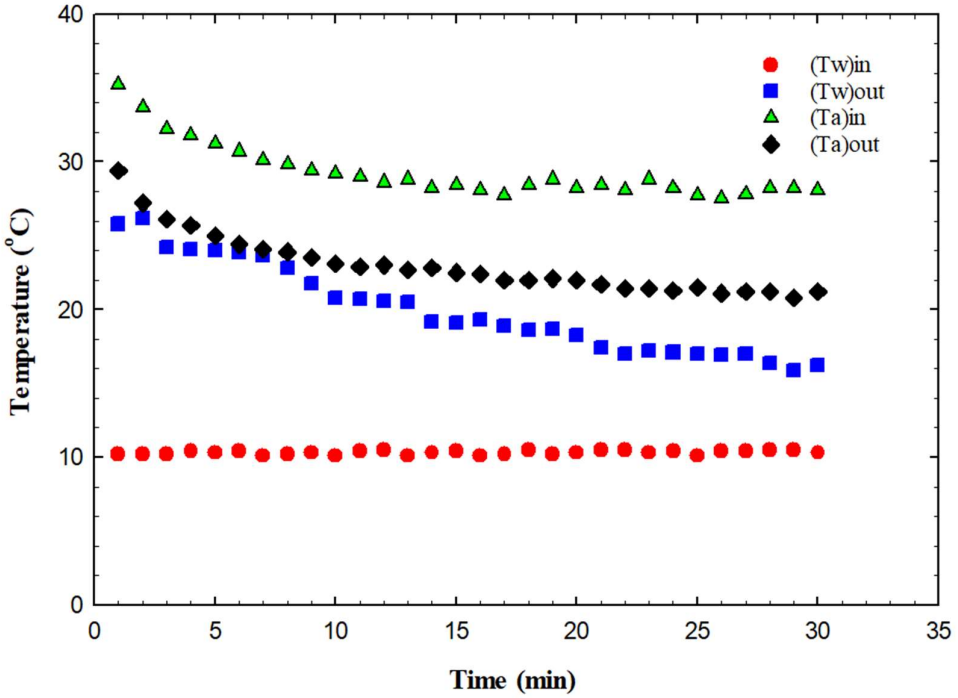

Figure (5- 8) temporal change in the inlet and outlet temperatures of the heat exchanger for case 8.

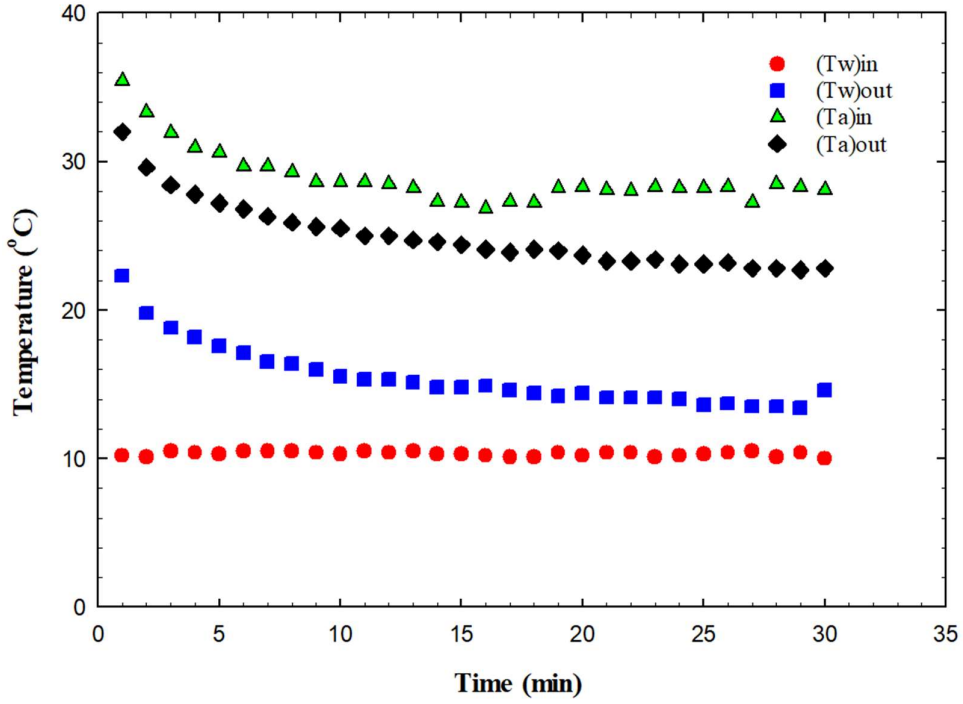

Figure (5- 9) temporal change in the inlet and outlet temperatures of the heat exchanger for case 9.

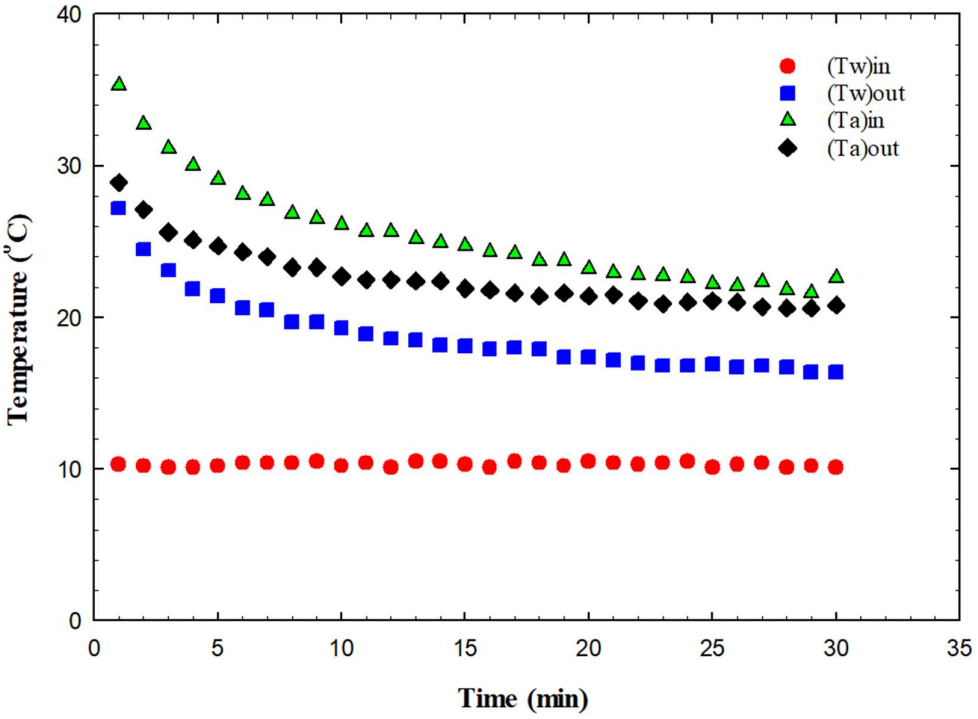

Figure (5- 10) temporal change in the inlet and outlet temperatures of the heat exchanger for case 10.

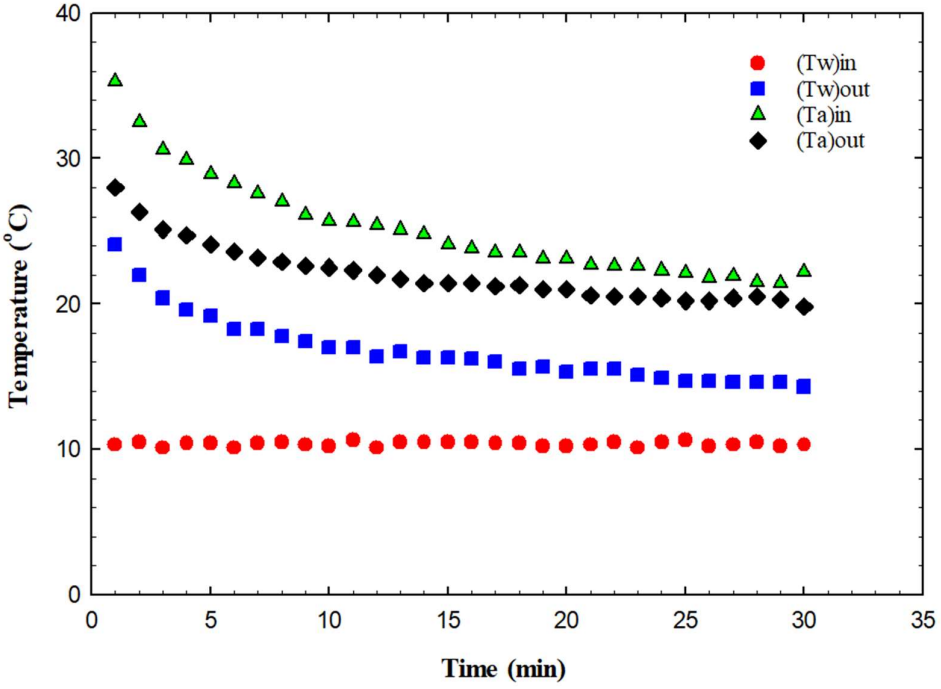

Figure (5- 11) temporal change in the inlet and outlet temperatures of the heat exchanger for case 11.

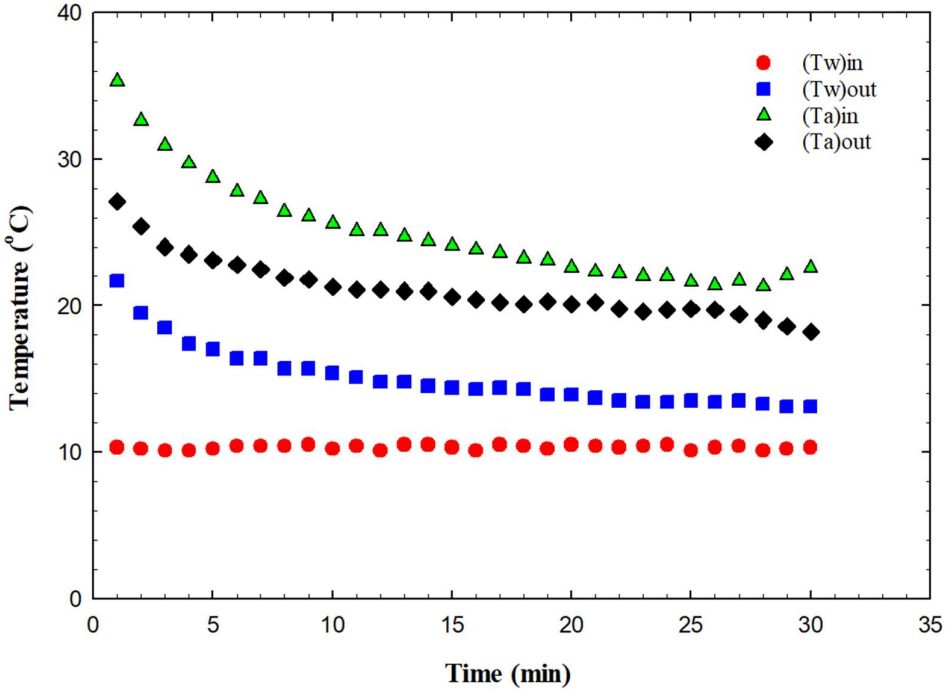

Figure (5- 12) temporal change in the inlet and outlet temperatures of the heat exchanger for case 12.

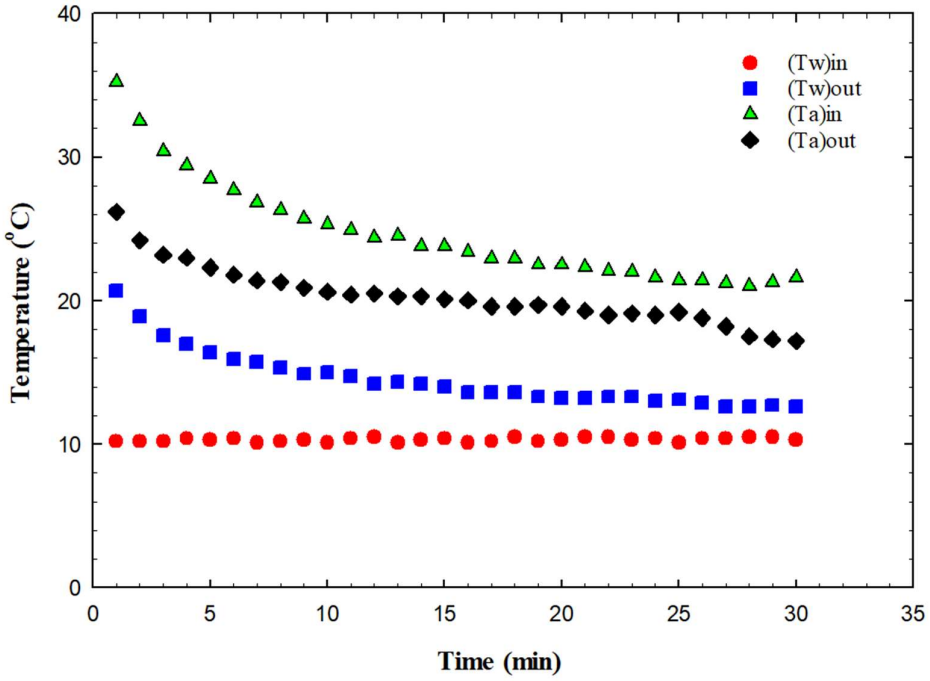

Figure (5- 13) temporal change in the inlet and outlet temperatures of the heat exchanger for case 13.

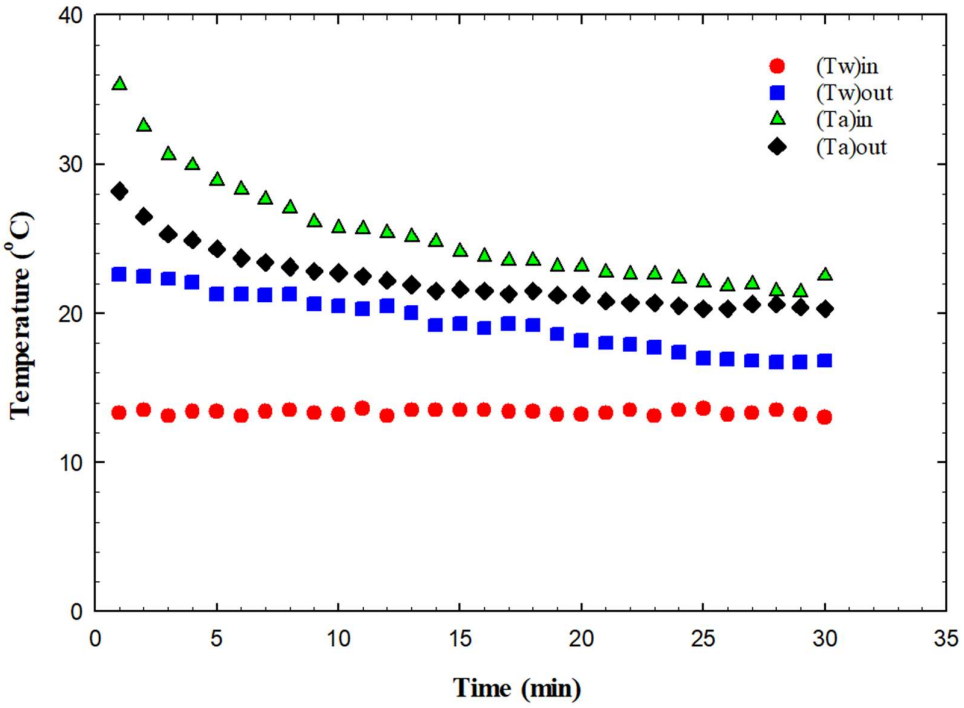

Figure (5- 14) temporal change in the inlet and outlet temperatures of the heat exchanger for case 14.

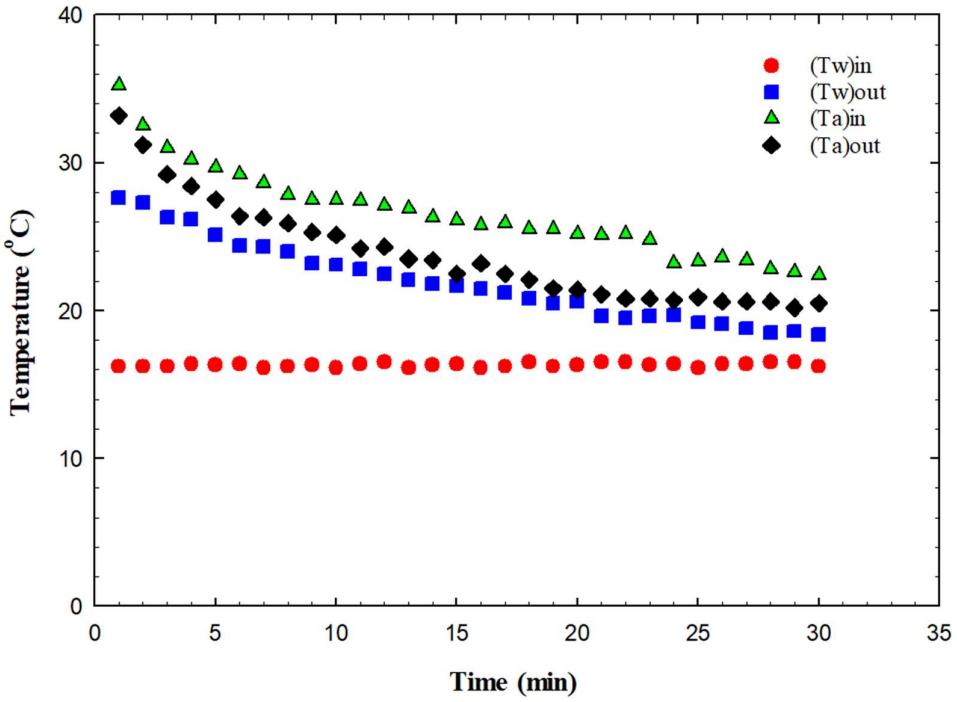

Figure (5- 15) temporal change in the inlet and outlet temperatures of the heat exchanger for case 15.

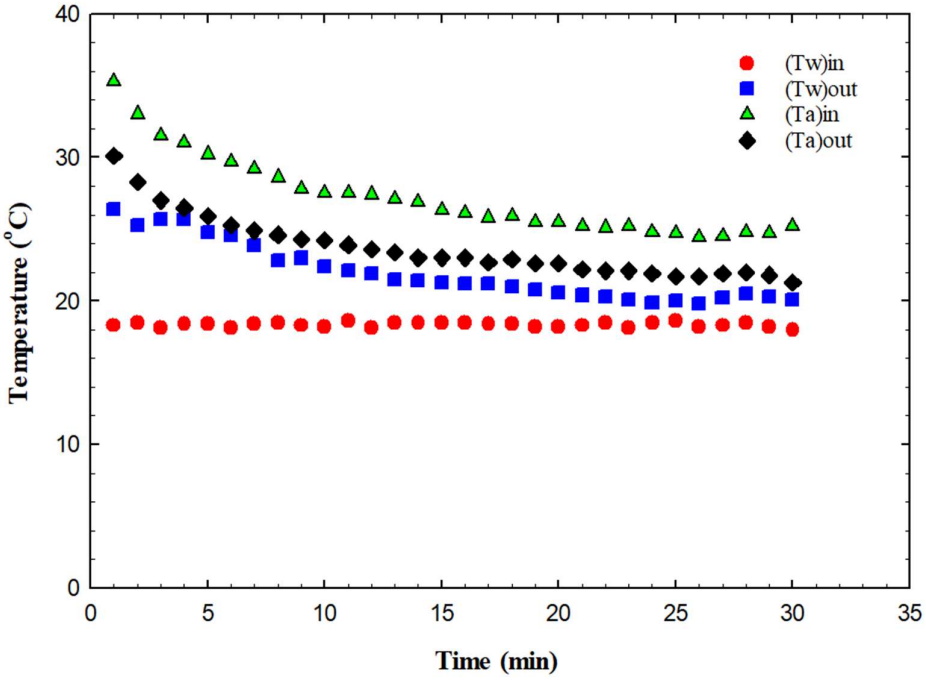

Figure (5- 16) temporal change in the inlet and outlet temperatures of the heat exchanger for case 16.

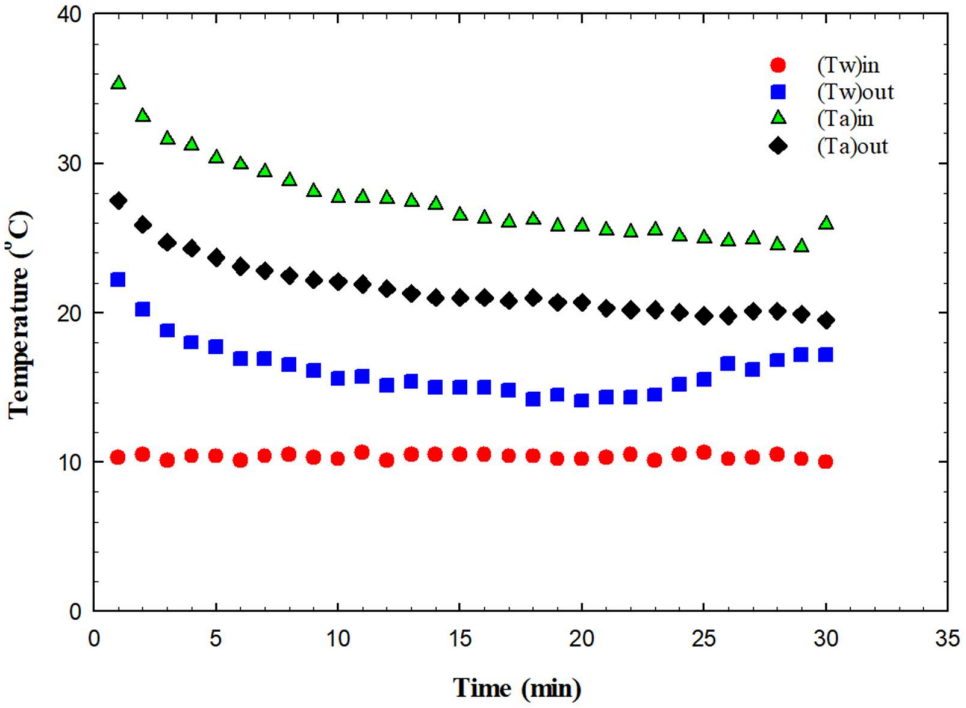

Figure (5- 17) temporal change in the inlet and outlet temperatures of the heat exchanger for case 17.

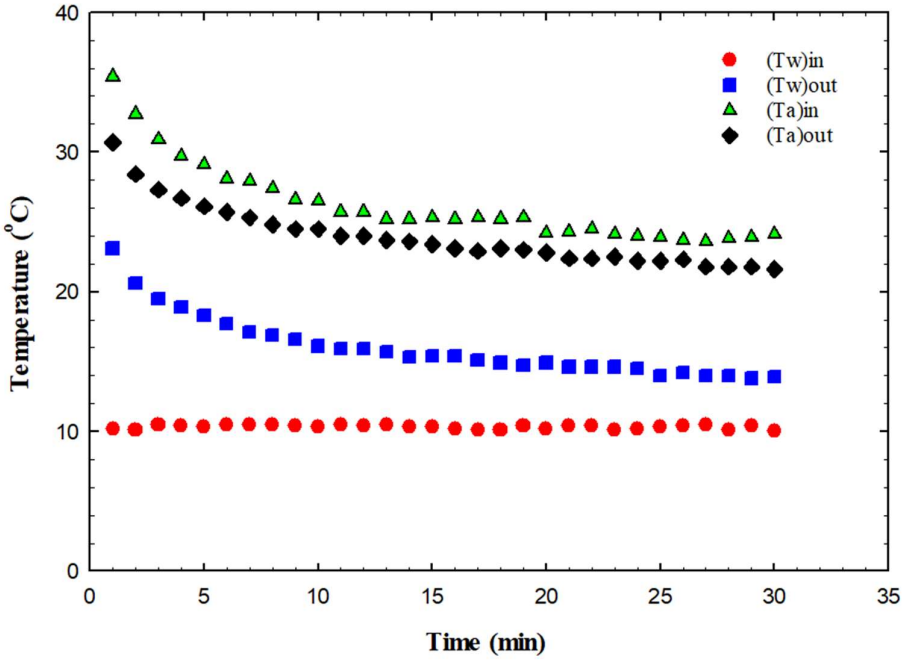

Figure (5- 18) temporal change in the inlet and outlet temperatures of the heat exchanger for case 18.

5.1.2. The effect of water inlet flow rate

Figure (5-19) shows the relation between water flow rate and heat transfer coefficient at water side when the air velocity is 1.5 m/s. The heat transfer coefficient increases with the increase in the water flow rate in both cases with fins or with copper foam. The direct relationship between them is logarithmic, where the heat transfer coefficient increases from 5403 $W/m^2.^oC$ to 7509 $W/m^2.^oC$, when increasing the flow rate from 1 to 4 LPM in the case of the heat exchanger with fins (red color), while the heat transfer coefficient increases from 6558 $W/m^2.^oC$ to 12400 $W/m^2.^oC$ for the heat exchanger with copper foam (blue color). Increasing the heat transfer coefficient, because an increase in flow means an increase in the flow velocity, and the presence of copper foam helps dissipate heat more than in traditional fins.

Figure (5-20) explains the relation between water flow rate and Nusselt number of water. The relationship between flow and Nusselt number is direct in both types of heat exchangers. The red color shows the change of Nusselt number by increasing the volumetric flow of water in the case of the heat exchanger with fins, as it increases with the increase of the mass flow to 3 LPM and then begins to stabilize. The blue color indicates the Nusselt number in the presence of copper foam, where it can be seen that the Nusselt number increases with the increase in flow. Likewise, the value of the number revealed is higher than in the case of the traditional fins, and that is because the copper foam contributed to dissipating the heat over a larger surface area.

Figure (5-21) demonstrates the relation between heat transfer rate and water flow rate. The heat transfer rate increases from 347 W to 416 W, when the flow is increased from 1 LPM to 4 LPM, then it begins to remain stable in the case of the exchanger with fins, but in the case of copper foam,

the direct relationship continues to rise until the heat transfer rate reaches 721.8 W at the flow of 4 LPM. During the current study the water volume flow rate fixed at 4 LPM to study the rest of the variables. The blue color shows the case of the heat exchanger with the fins, where it can be seen that the effect of the flow is greater in the case of the copper foam (black color). The effect of the water flow on heat transfer rate is less in the case of the fins. This is due to that the copper foam caused a greater difference in water temperatures between inlet and outlet.

Figure (5-22) observes the relations between logarithmic mean temperature difference (LMTD) and water flow rate for both types of heat exchangers at an air velocity of 1.5 m/s, and a water inlet temperature of 10 ^{o}C. It is can be noticed an increase LMTD with an increase in the water flow rate of both types of heat exchanger. The higher flow rate of water leads to a higher temperature difference and thus increases LMTD. The highest value of LMTD is 11.79 ^{o}C at flow 4 LPM in the case of copper foam, while its value is 12.52 ^{o}C in the case of fins.

Figure (5-23) explains the relation between the water flow rate and the effectiveness of the heat exchanger once with the fins and again with the copper foam. The relationship between them is a direct exponential relationship. The effectiveness increases with increasing water flow rate, as it increased from 0.56 to 0.71 in the case of fins and from 0.59 to 0.726 in the case of copper foam. The reason for the increase in the effectiveness is due to the increase in the rate of heat transfer at the increase in the volumetric flow rate of water. These results agree with experimental results of Wang et al. [67]

Figure (5-24) shows the relation between the thermal resistance of the heat exchanger and the volumetric flow of cold water at 1.5 m/s air velocity. It is possible to notice the linear inverse relationship between

them, where the heat resistance value decreases from 0.0104 °C/W to 0.00782 °C/W in the case of the heat exchanger with fins and from 0.0135 °C/W to 0.00849 °C/W in the case of the heat exchanger with copper foam. This is due to the fact that an increase in the water flow rate leads to an increase in the value of the heat transfer rate, and also the difference in temperature between the outlet and inlet of water decreases, and then the thermal resistance decreases.

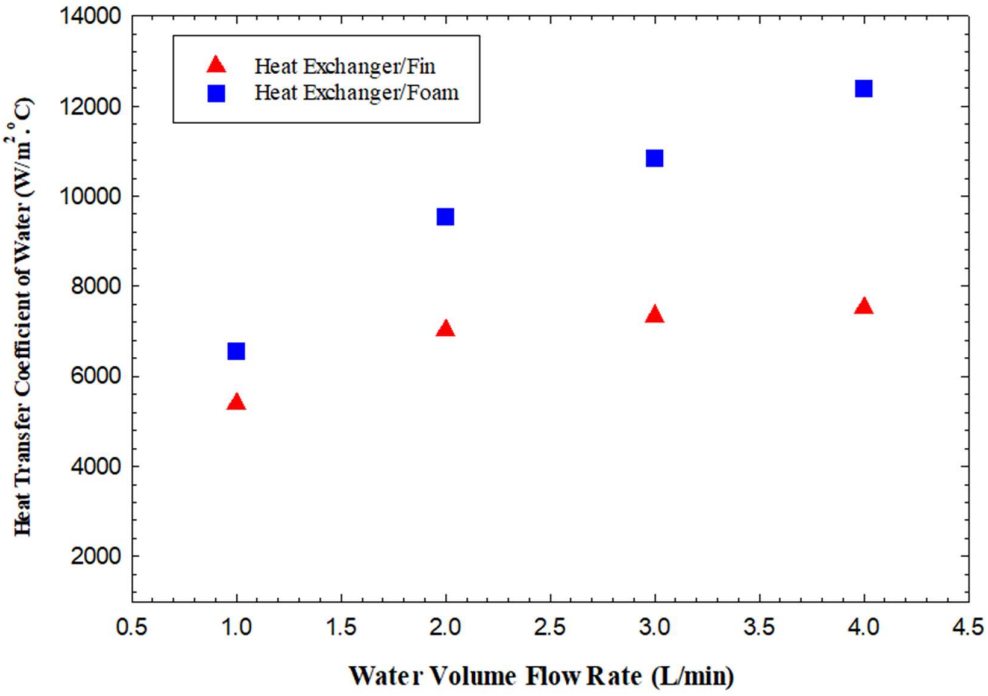

Figure (5- 19) water volume flow rate versus heat transfer coefficient of water at $(Tw)_{in}$=10°C, $(Ua)_{in}$=1.5m/s.

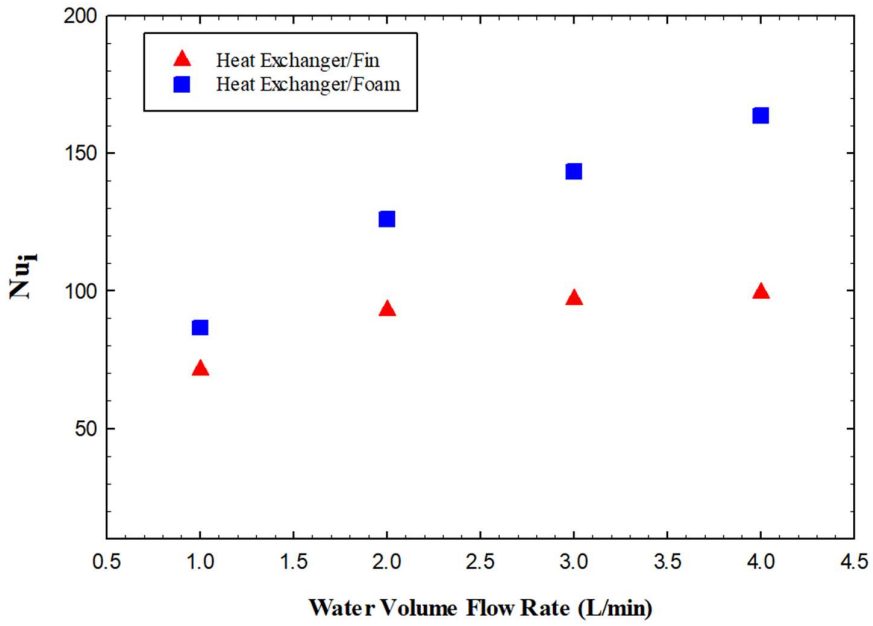

Figure (5- 20) water volume flow rate versus water side Nusselt number at $(Tw)_{in}$=10°C, $(Ua)_{in}$=1.5m/s..

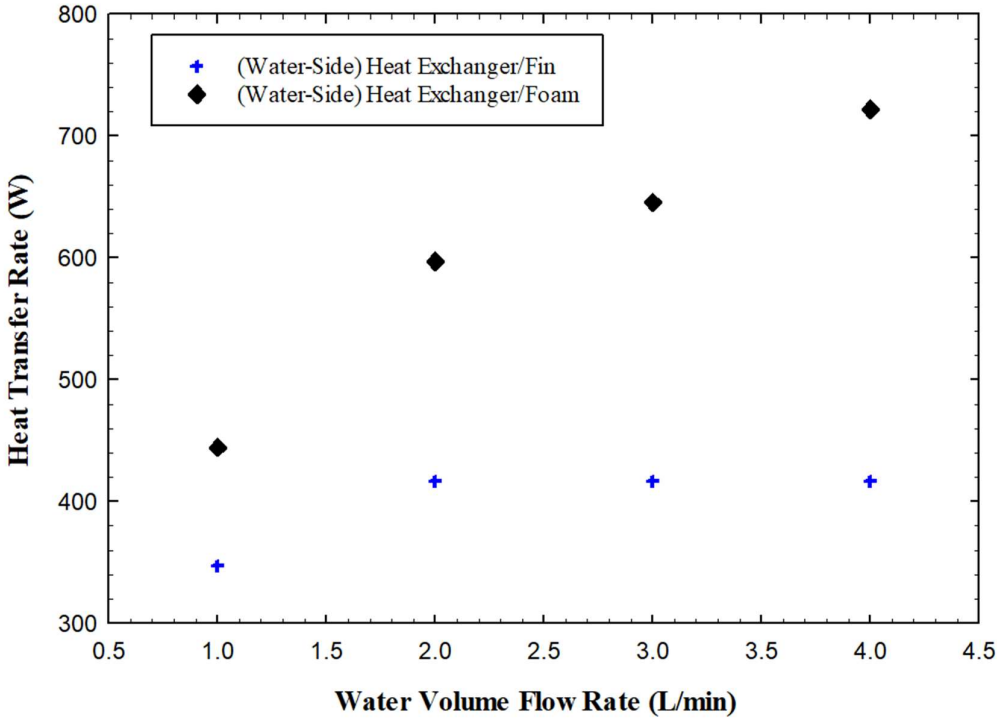

Figure (5- 21) water volume flow rate versus water heat transfer rate at $(Tw)_{in}$=10°C, $(Ua)_{in}$=1.5m/s.

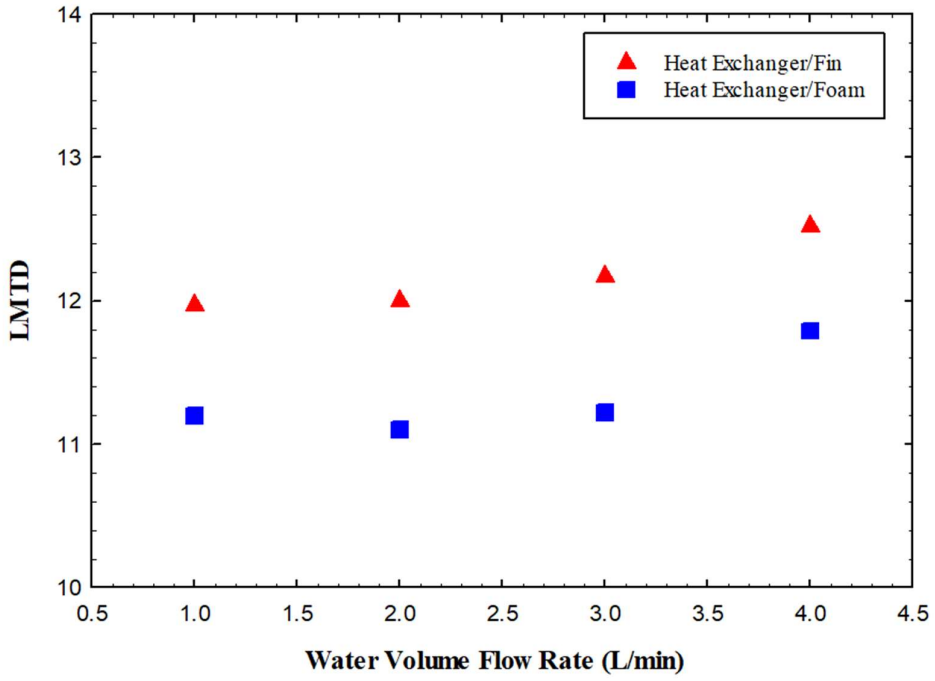

Figure (5- 22)) water volume flow rate versus LMTD of heat exchanger at $(Tw)_{in}$=10°C, $(Ua)_{in}$=1.5m/s.

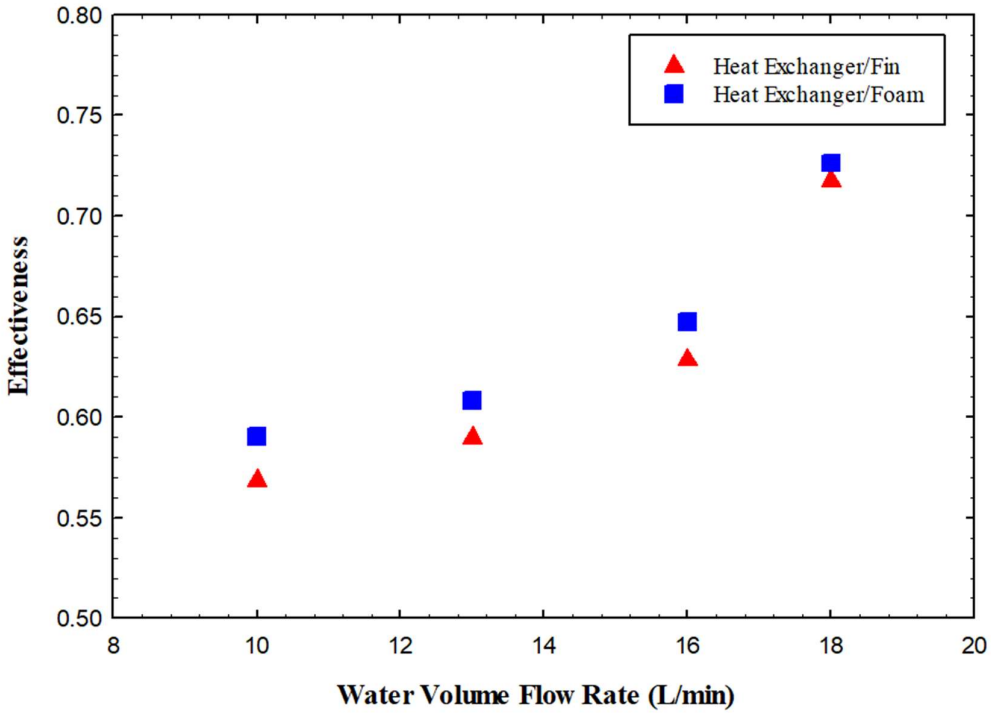

Figure (5- 23) water volume flow rate versus effectiveness of heat exchanger at $(Tw)_{in}$=10°C, $(Ua)_{in}$=1.5m/s.

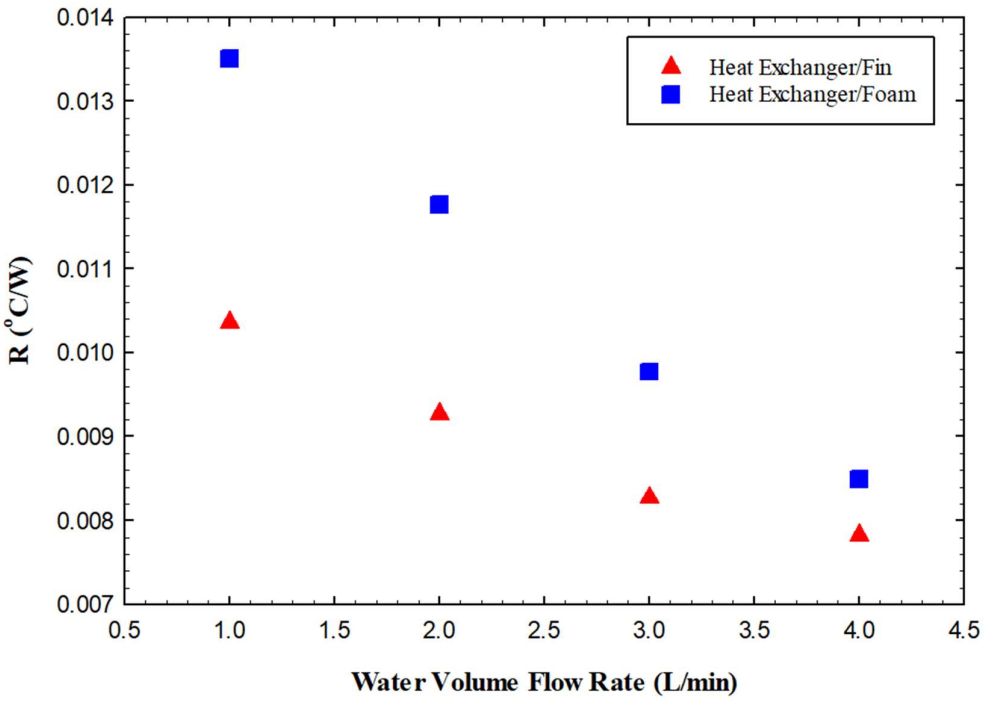

Figure (5- 24) effect water volume flow rate on thermal resistance of heat exchanger at $(Tw)_{in}$=10°C, $(Ua)_{in}$=1.5m/s.

5.1.3. The effect of water inlet temperature

Figure (5-25) shows the relations between LMTD and water inlet temperature for both types of heat exchanger. The blue color shows the change in LMTD values with the change in the water inlet temperature in the case of the heat exchanger with fins. It can be seen that the relationship is linear, as water inlet temperature increases, the LMTD decreases. The red color that represents the LMTD values in the case of the heat exchanger with the copper foam. The value LMTD is higher in the case of the foam as a result of the higher thermal dispersion through the porous medium, which causes a temperature difference between the inlet and outlet of the two fluids.

Figure (5-26) observes the effect of cold water inlet temperature on the effectiveness of heat exchangers once with fins and again with copper foam. It can be seen that the increase in the water inlet temperature from 10

°C to 18 °C leads to a decrease in the effectiveness of the heat exchanger from 0.66 to 0.61 for the exchanger with fins, while it decreases from 0.69 to 0.62 in the case of the exchanger with copper foam. This is due to the fact that an increase in the cold water temperature leads to a decrease in the heat transfer rate, and thus the effectiveness of the heat exchanger decreases.

Figure (5-27) explains the relation between water inlet temperature and the thermal resistance of the heat exchanger. The inverse relations between water inlet temperature and thermal resistance can be observed. Because an increase in the inlet water temperature leads to a decrease in the heat transfer rate, but the value of LMTD decreases, and therefore the effect of temperature is reversed on the thermal resistance of the heat exchanger. Through the same figure, the difference between the thermal resistance can be seen when using the copper foam and when using the fins. The thermal resistance of the copper foam is less than that of the fins, and this difference between them decreases with the increase in the cold water inlet temperature.

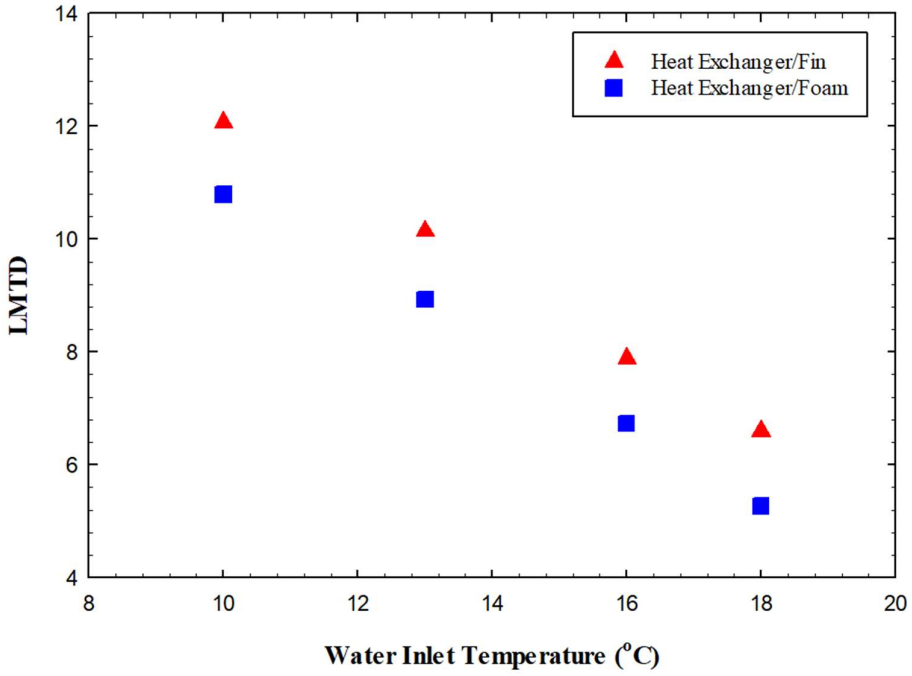

Figure (5- 25) effect of water inlet temperature on LMTD of heat exchanger, at water flow 4 LPM, and $(Ua)_{in}$=1.5m/s.

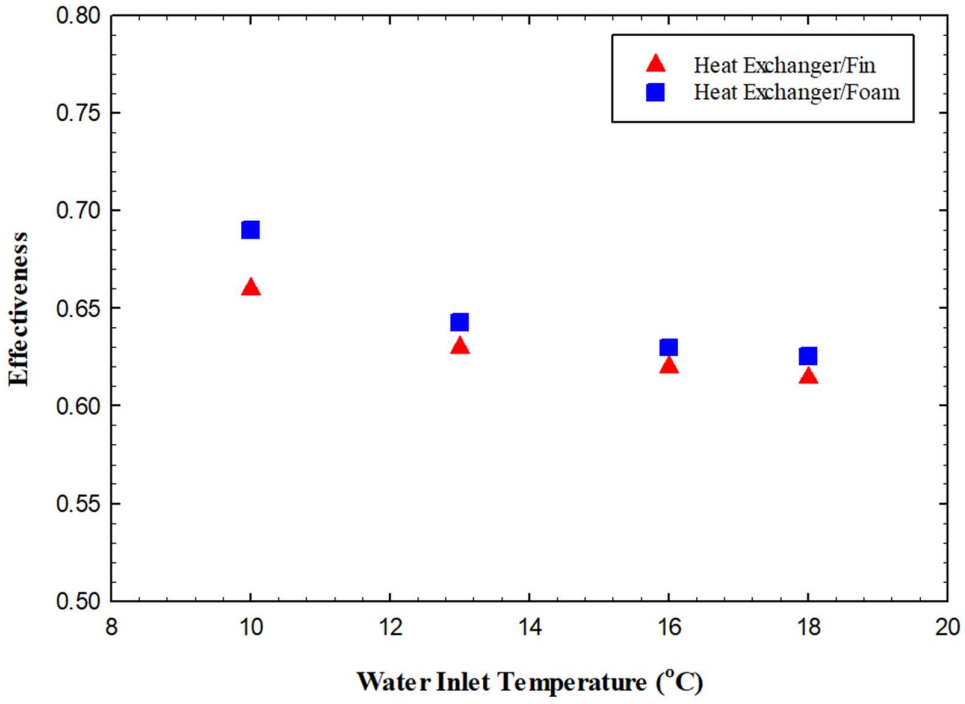

Figure (5- 26) effect of water inlet temperature on effectiveness of heat exchanger, at water flow 4 LPM, and $(Ua)_{in}$=1.5m/s.

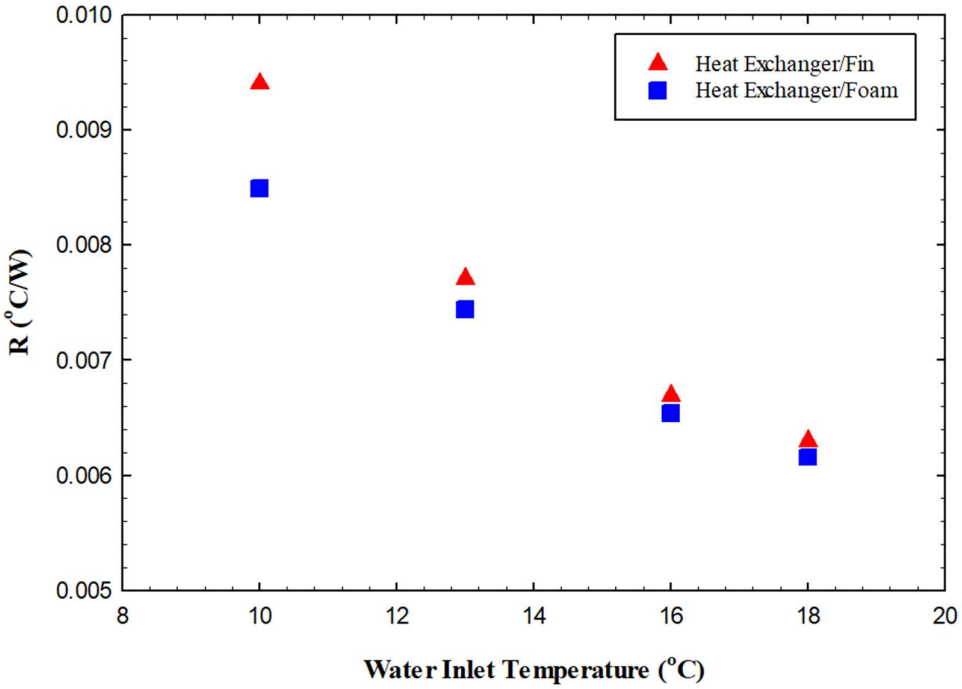

Figure (5- 27) effect of water inlet temperature on thermal resistance of heat exchanger, at water flow 4 LPM, and $(Ua)_{in}$=1.5m/s.

5.1.4. The effect of air Reynolds number

Figure (5-28) introduces the relation between the Reynolds number and heat transfer coefficient for both types of heat exchangers. The direct logarithmic relationship can be observed between the heat transfer coefficient and Reynolds number. The heat transfer coefficient increases from 263 W/m^2.°C to 950 W/m^2.°C when Reynolds number increases from 37750 to 234040 in the case of aluminum fins. The heat transfer coefficient increases from 260.3 W/m^2.°C to 1118 W/m^2.°C, when increasing the Reynolds number from 22650 to 218990 in the case of the exchanger with copper foam. The heat transfer coefficient is greatly affected by the flow conditions and the nature of the porous medium, so when the Reynolds number is increased, the velocity of the air molecules is higher through the pores, and this leads to greater heat exchange between porous material and air molecules, which increases the heat transfer coefficient. It can be seen

that the heat transfer coefficient for the copper foam is higher than that of the aluminum fins, this is due to the high thermal dispersion present through the porous medium, which distributes air molecules and passes them through larger heat exchange areas than in the fins. As a result of the high heat transfer coefficient. These results agree with experimental results of Nawaz and Jacobi [26], and Mancin et al [53].

Figure (5-29) shows the relations between air Reynolds number and heat transfer rate of air. The direct relations between heat transfer rate and the air velocity can be observed. The heat transfer rate in the case of using copper foam is higher at medium and high Reynolds number, while the difference between the rate of heat transfer at low Reynolds number tended in favor of the aluminum fins. At medium air Reynolds number, the heat transfer rate is 7635 W for the copper foam and 6392 W for the conventional fins. At the higher Reynolds number, the heat transfer rate for copper foam is 10419 W and 9049W for fins. The reason for the difference in the rate of heat transfer is because metallic foam has greater conductivity and heat dissipation than conventional fins. These results agree with experimental results of Nawaz and Jacobi [26], and Huisseune et al. [41]

Figure (5-30) explains the relations between the Reynolds number and Nusselt number for both types of heat exchangers. The direct relationship between Reynolds number and Nusselt number is logarithmic. The difference between the value of the Nusselt number for both exchangers can be seen once with the traditional aluminum fins and again with the copper foam, as this difference increases with the increase in the velocity of the inlet air. The Nusselt number increases from 4013 to 14450 when the air speed is increased from 1.5 m/s to 9.3 m/s in the case of heat exchanger with fins. While it rises from 3977 to 17000 in the case of the heat exchanger with copper foam. This is because Nusslet's number is

directly affected by the value of the heat transfer coefficient. The increase in the Reynolds number leads to an increase in the heat transfer coefficient, and thus the Nusselt number increases. Nusselt number in the case of heat exchanger with copper foam is greater by 38.7% when the Reynolds number is equal to 140930 and by 17.6% when Reynolds number is equal to 234040. At lower value of Reynolds number, the difference between the foam and the fins is small in Nusselt number. These results agree with experimental results of Chen et al. [27].

Figure (5-31) shows the Colburn factor as a function of Reynolds number. The linear inverse relations between the two variables can be observed for both types of heat exchangers. The Colburn factor decreases by 42% in the case of increasing the Reynolds number from 37750 to 234040 in the case of the heat exchanger with fins. In the case of the heat exchanger with copper foam, Colburn factor coefficient is higher, but it is affected by the change in Reynolds number which is greater, as it decreases by 55. 7% when increasing Reynolds number from 22650 to 218940. The difference in the value of Colburn factor is due to the increase in the heat transfer coefficient when using the copper foam compared to the aluminum fins. Colburn factor is higher in the case of the heat exchanger with copper foam than in the conventional fins, where it is equal to 0.1959 for the copper foam and 0.1186 for the fins. This difference between them is reduced by increasing the inlet velocity of air. The reason for the difference between the two heat exchangers in the value of Colburn factor because the fins pass a larger amount of air than the copper foam, but the copper foam disperses the heat by slowing the air through the pores, so it is noted that Colburn factor is higher in the case of foam than the fins. These results agree with experimental results of Wang et al. [68]

Figure (5-32) introduces the relations between Reynolds number and the thermal resistance of the heat exchanger. It is possible to notice the decreasing exponential relationship between the two variables, because an increase in the value of the Reynolds number means that a larger amount of air passes through the porous medium, and thus the thermal resistance value decreases. The thermal resistance is less in the case of the copper foam than in the fins, and this is due to the increase in the heat exchange area in the case of the copper foam. It can be noted that the thermal resistance decreases with the increase in Reynolds number of the inlet air. This is due to that the increase in Reynolds number of the air means a greater heat exchange between the porous medium and the air, and thus the heat resistance decreases. These results agree with experimental results of Schampheleire et al. [69], and Ho et al. [70].

Figure (5-33) shows the relation between Reynolds number and LMTD of the heat exchanger. Increasing the air Reynolds number that causes a temperature difference between the inlet and outlet of cold water, and thus increases the value of LMTD. This effect is clear on the value of the effectiveness of the heat exchanger, which can be seen in through figure (5-34). The effectiveness of the heat exchanger is affected relatively slightly when changing the value of the Reynolds number, as it can be seen that the effectiveness increases from 0.61 to 0.70 in the case of heat exchanger with fins when Reynolds number increases from 37750 to 234040 and increases from 0.625 to 0.712 in the case of copper foam.

Figure (5-35) explains the pressure gradient as a function of Reynolds number. The relations between $\Delta P/L$ and Re is a direct logarithmic. It can be observed that the value of $\Delta P/L$ increases by 650% when the Reynolds number increases from 37750 to 234040, in the case of the heat exchanger with fins. The value of $\Delta P/L$ increases by 457% when

the value of Reynolds number increases from 22650 to 218990 in the case of the heat exchanger with copper foam. The difference in the value of ΔP/L can be seen between the two heat exchangers, where the heat exchanger with copper foam is 75% higher at the lower Reynolds number values. This is due to the obstruction to the passage of air through the copper foam is higher, so the pressure difference on both sides of the heat exchanger increases. These results agree with experimental results of Schampheleire et al. [69].

Figure (5-36) explains the relations between Reynolds number and friction factor for both types of heat exchanger. It can be noted that increasing the air Reynolds number reduces the friction factor, and that the coefficient of friction reached 148 in the case of copper foam at the Reynolds number of 22650, and the friction coefficient decreases with the increase in the velocity of the inlet air. The copper foam has higher value of friction factor than aluminum fins, due to its complex form, which causes multiple air paths inside the porous and this causes greater friction compared to the aluminum fins, which have a regular shape that allows air to pass through them. These results agree with experimental results of Chen et al. [27], and Schampheleire et al. [69].

Figure (5-37) shows the relations between area goodness factor (AG) and Reynolds number. The AG factor increases with increasing air Reynolds number from 37750 to 140930 and then decreases between 140930 and 234040 by a small amount. It can be seen that the value of AG factor is higher in the case of fins than its value in the case of copper foam, and this is due to the high value of friction in the heat exchanger with the copper foam. It can be seen that the highest value of AG factor is 0.01244 at 140930 Reynolds number in the case of fins, while it is equal to (0.010691) at 120800 Reynolds number in the case of copper foam. This

means that the comparison between the dynamic and thermal performance through AG factor shows that the traditional fins gave a better dynamic performance compared to the copper foam. Increasing AG factor because an increase in Re means an increase in air flow inside the porous medium, which increases the rate of heat transfer as well as reduces the friction coefficient, and thus AG factor increases.

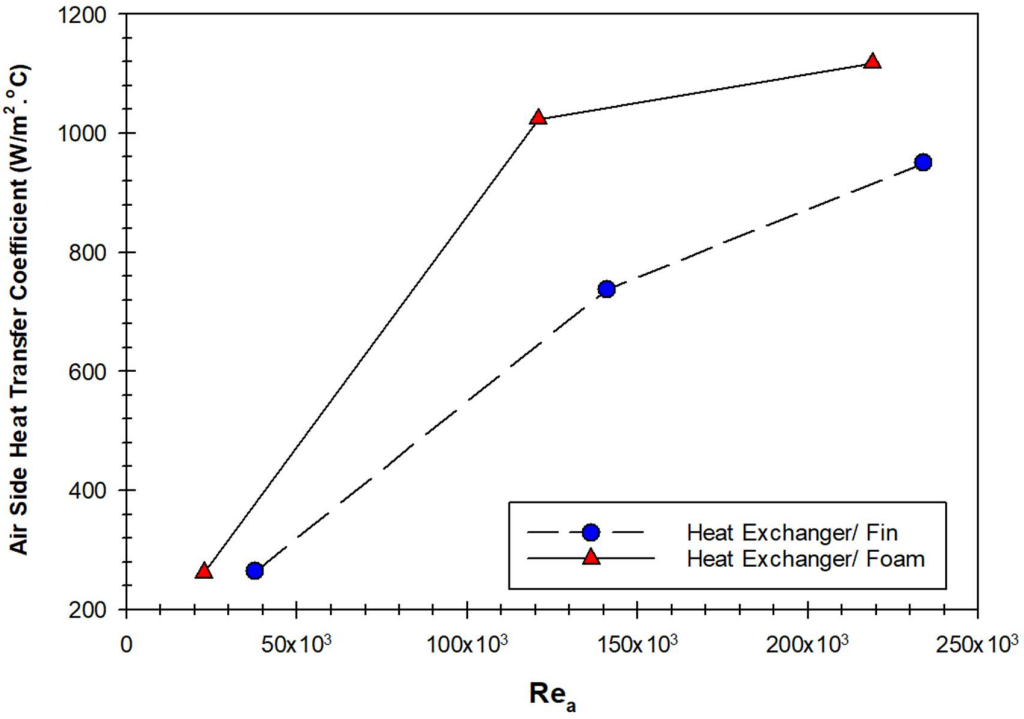

Figure (5- 28) the relation between Reynolds number and heat transfer coefficient.

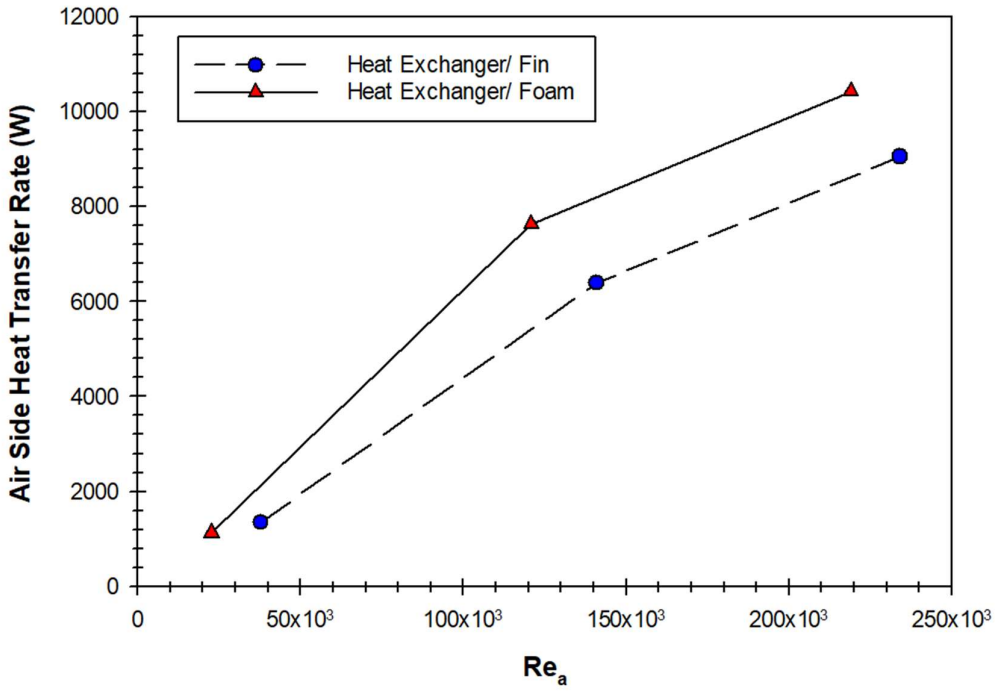

Figure (5- 29) the relation between Reynolds number and heat transfer rate.

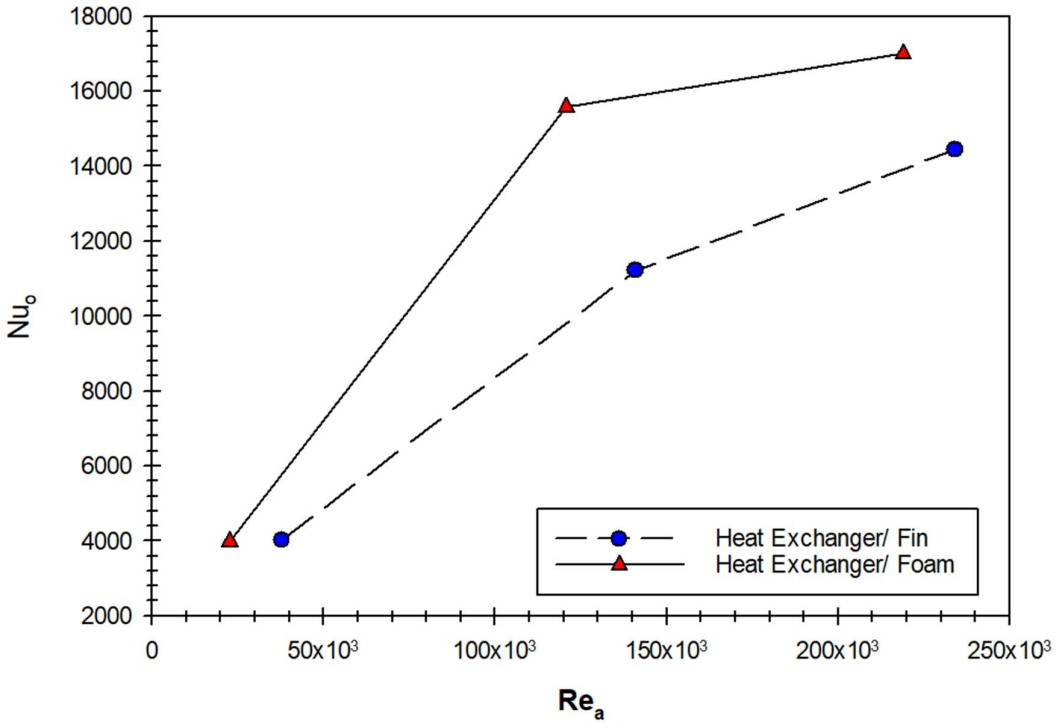

Figure (5- 30) the relation between Reynolds number and Nusselt number.

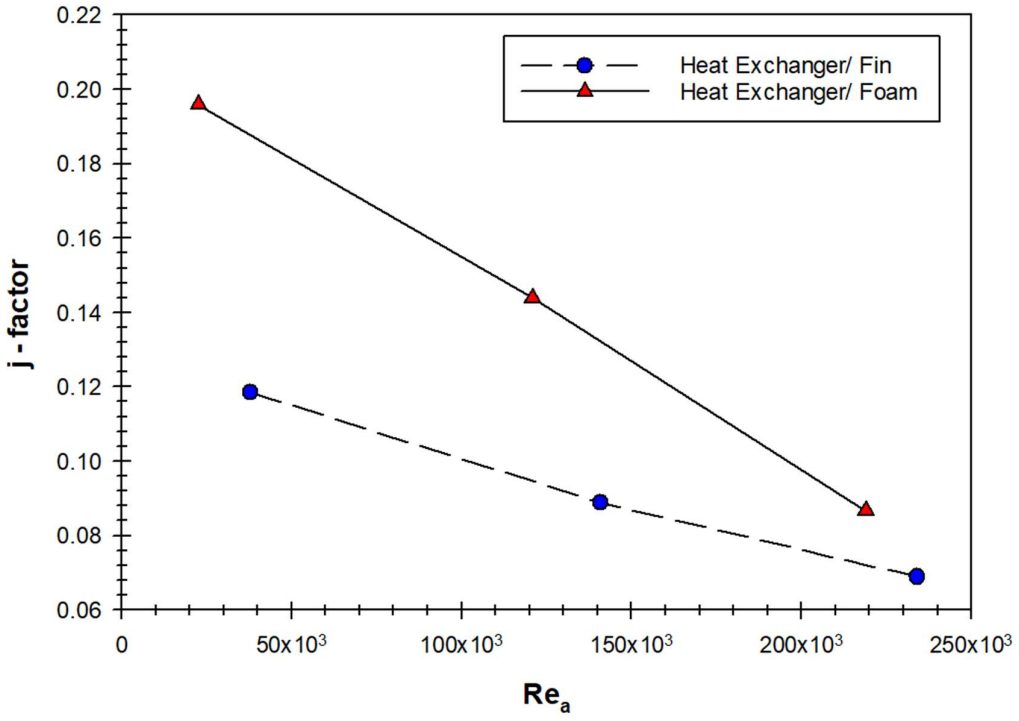

Figure (5- 31) the relation between Reynolds number and Colburn factor.

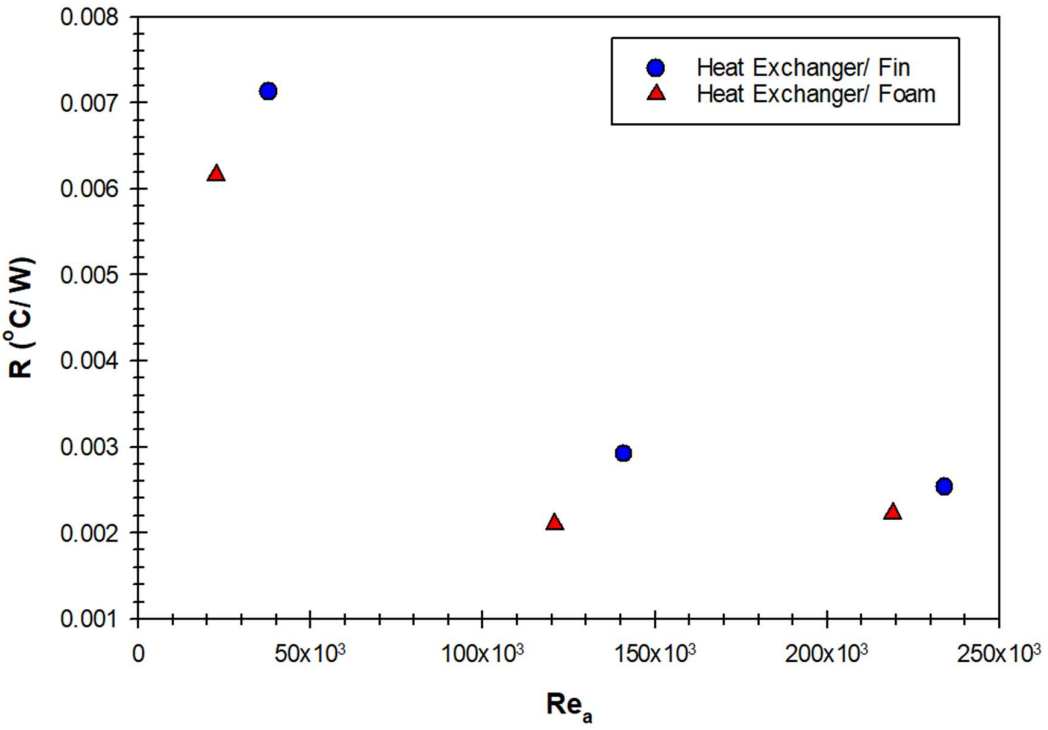

Figure (5- 32) the relation between Reynolds number and thermal resistance.

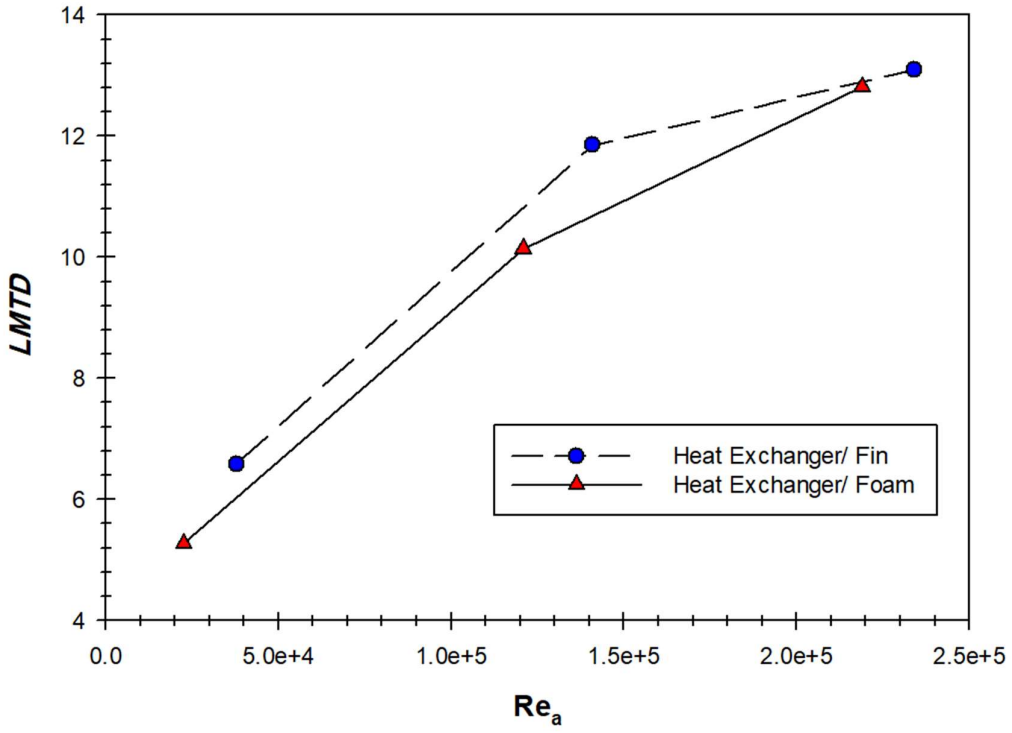

Figure (5- 33) the relation between Reynolds number and LMTD.

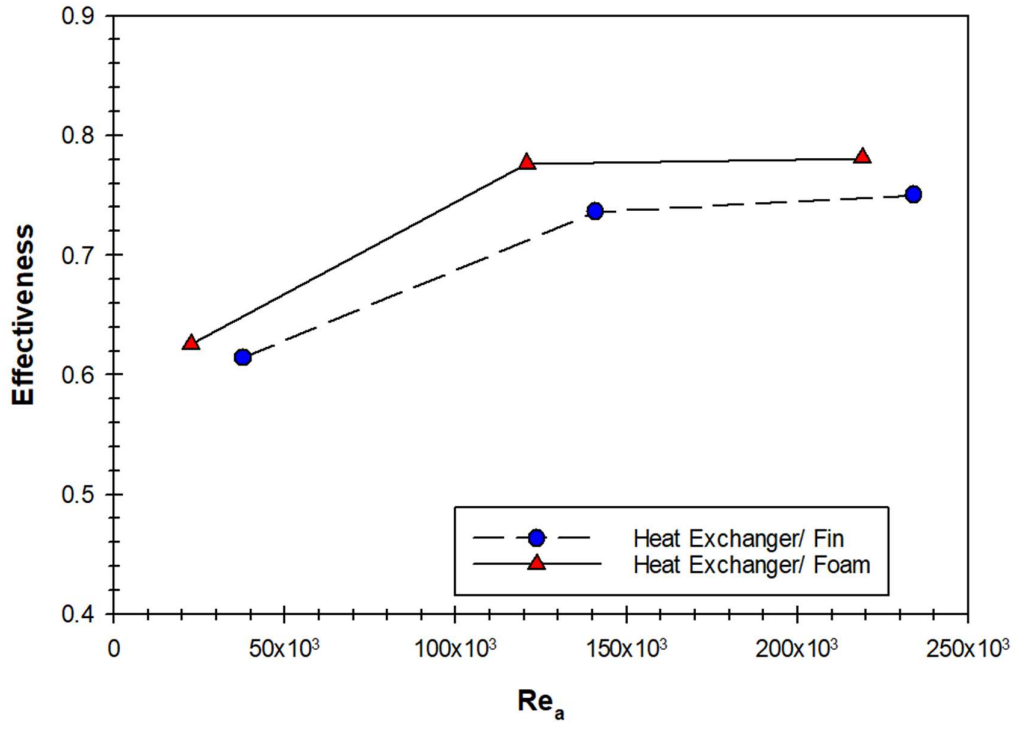

Figure (5- 34) the relation between Reynolds number and heat exchanger effectiveness.

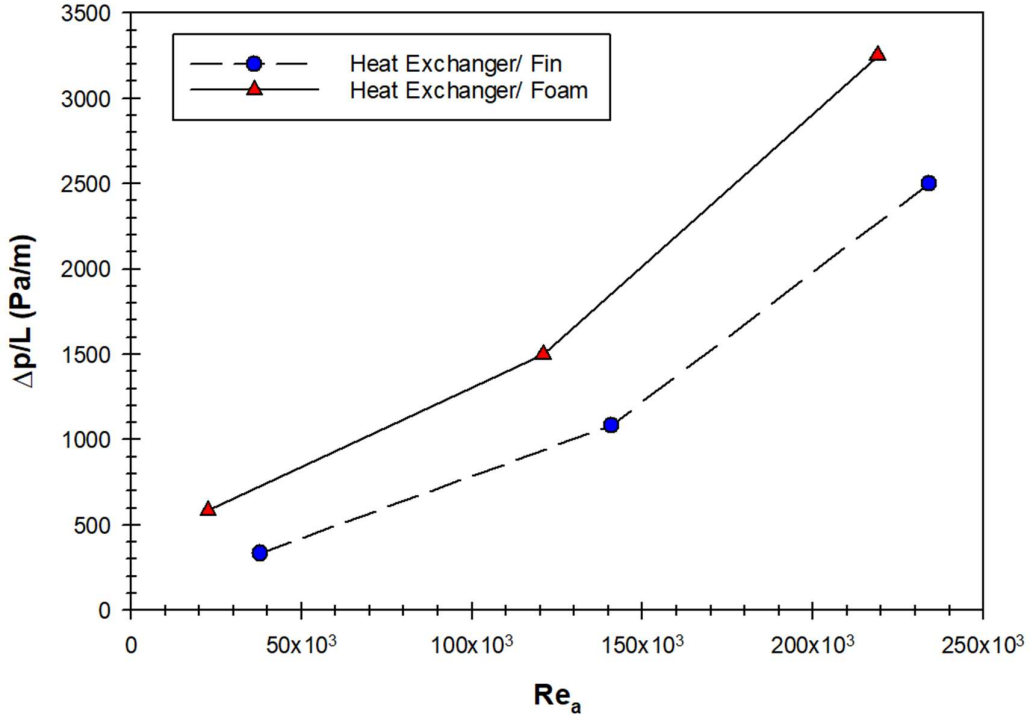

Figure (5- 35) the relation between Reynolds number and pressure gradient through heat exchanger.

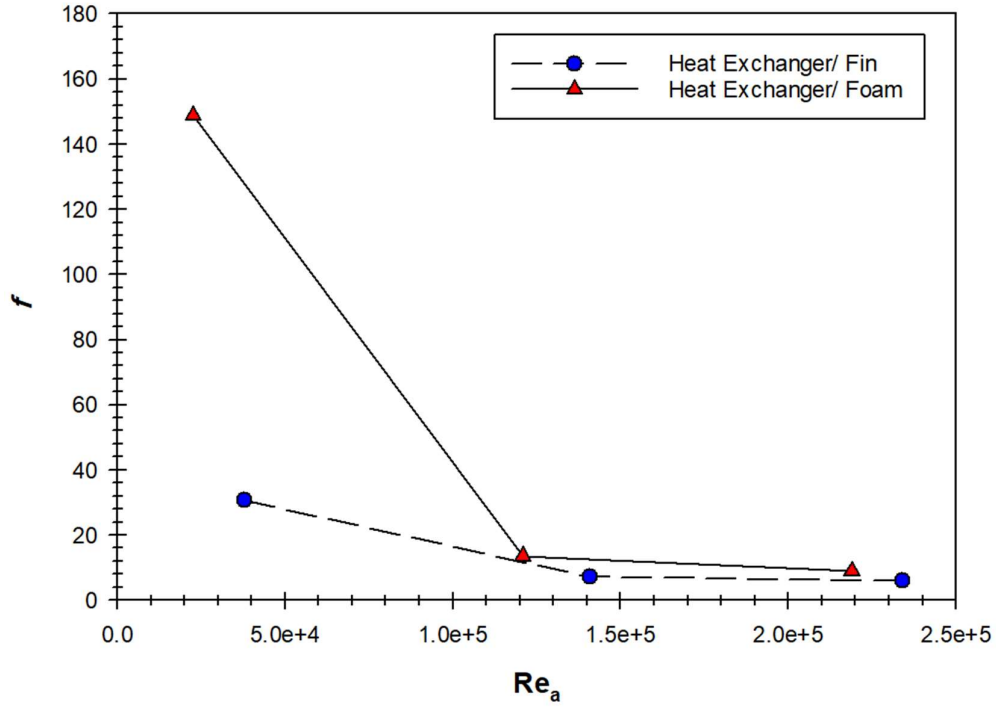

Figure (5- 36) the relation between Reynolds number and friction factor.

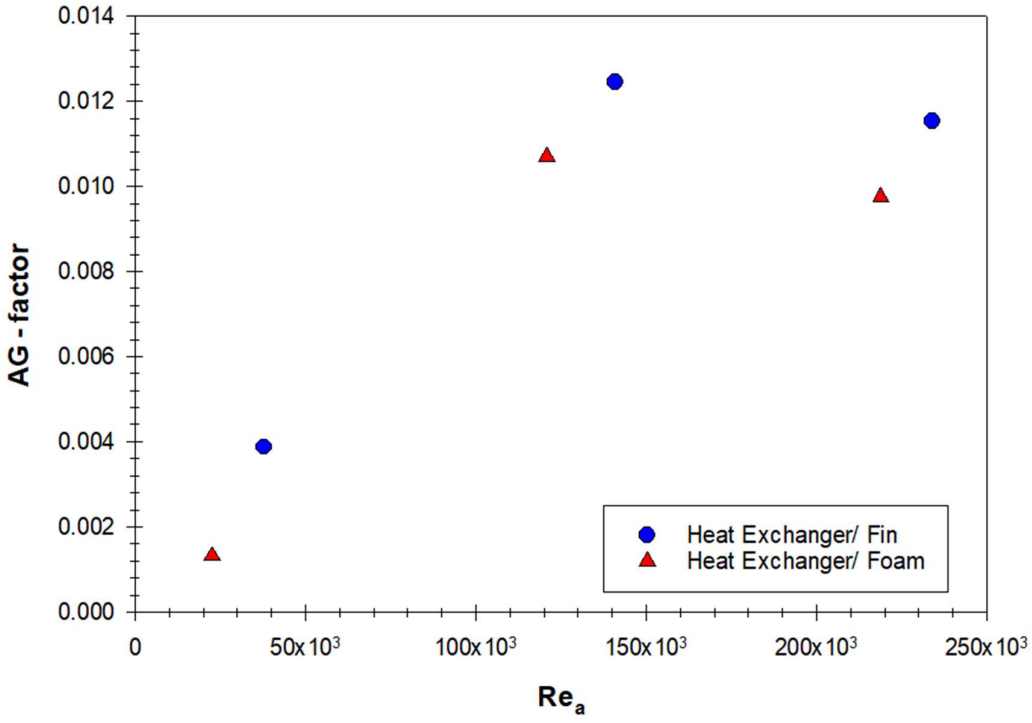

Figure (5- 37) the relation between Reynolds number and area goodness factor.

5.2. Theoretical Results

5.2.1. Validation of Numerical Solution

Figure (5-81) depicts the pressure contour map for the current numerical model and Buonomo et al. [43] model. The similar behavior can be seen as the pressure decreases while passing through the metal foam in both models. During Buonomo et al. [43] study, they used Darcy – Forchheimer – Brinkman model to analyze the distribution of velocity and pressure through the porous medium, which is the same model that was used during the current study.

Figure (5-82) and (5-83) explains the isothermal contour for the current numerical model and Buonomo et al. [43] model. In the present study LTE used to solve energy equation through metallic foam, while Buonomo et al. [43] used LTNE model. It can be noted that the thermal behavior is similar and the temperature distribution around the tube is similar between both models.

Figure (5-84) shows the numerical validation results of area goodness factor verses L/d ratio. Buonomo et al. [46] changed the ratio of foam length to pipe diameter (L/d) to study the effect of foam on AG factor. The maximum deviation error between Buonomo et al. [46] model and the current study model was ranged from 5.5% to 8%.

Figure (5-85) represents the numerical validation results of area goodness factor verses Reynolds number. The deviation between Buonomo et al. [46] results and the current study results is 5% for $Re<300$, and 7.3% for $Re>300$. The numerical results show the same response of the previous study results.

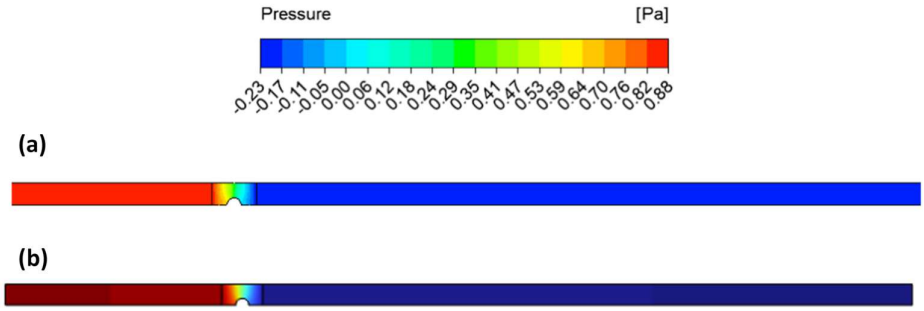

Figure (5- 38) pressure contour map for (a) Buonomo et al [43] study, and (b) current study

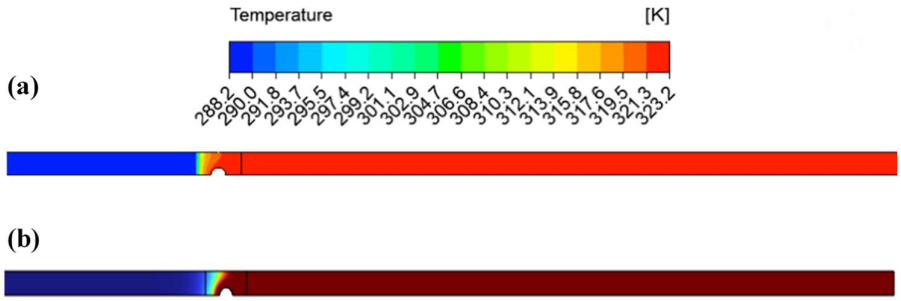

Figure (5- 39) isothermal contour for (a) Buonomo et al [43] study, and (b) current study

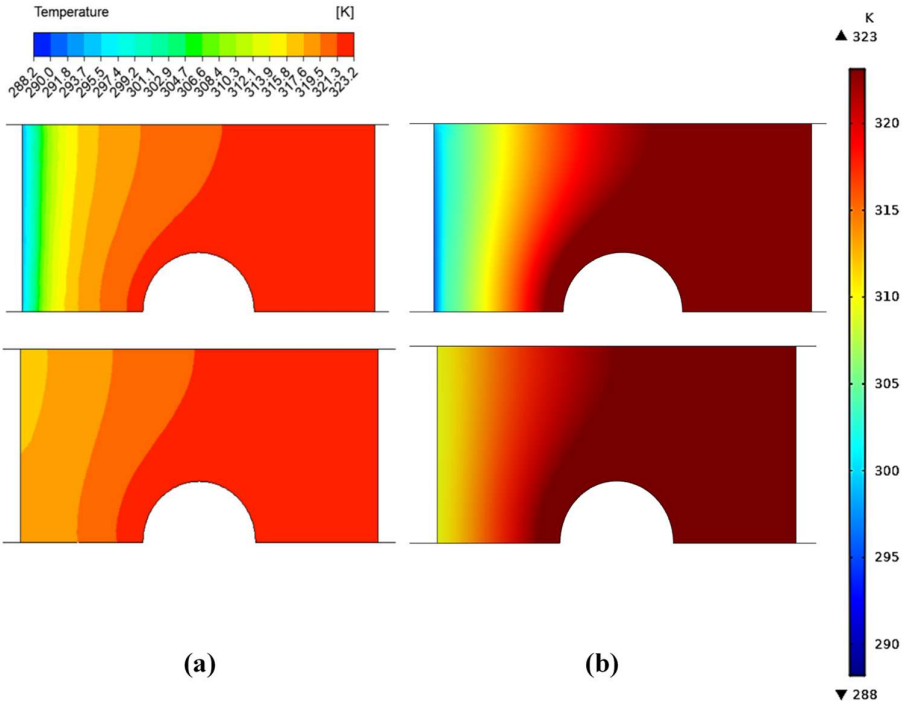

Figure (5- 40) isothermal contour in porous region for (a) Buonomo et al [43] study, and (b) current study

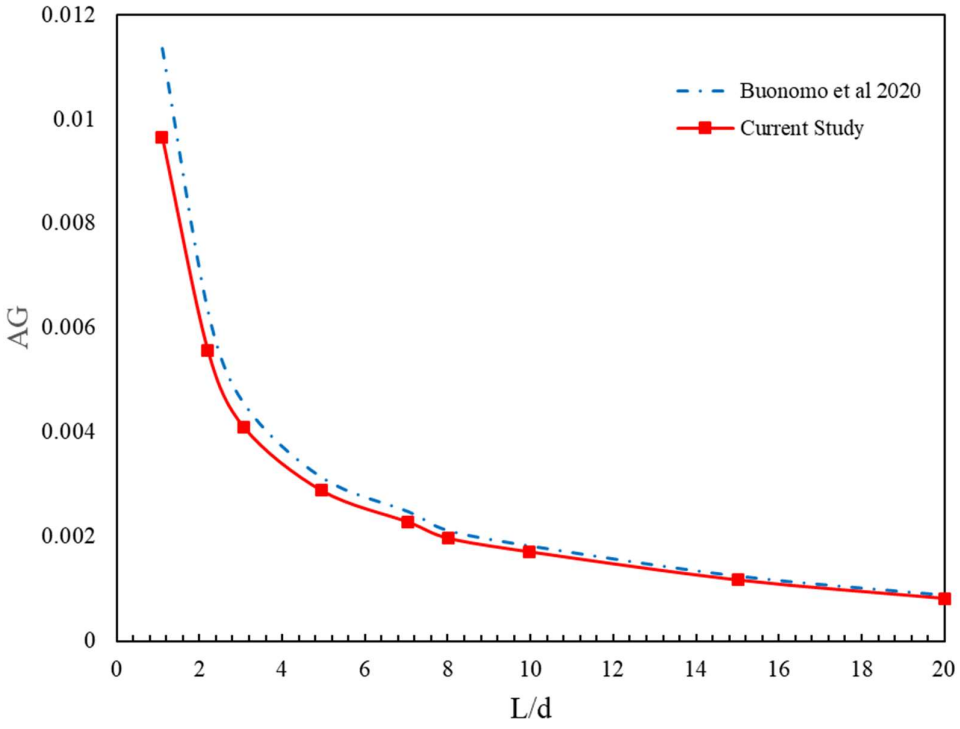

Figure (5- 41) validation of numerical model with Buonomo et al [46].

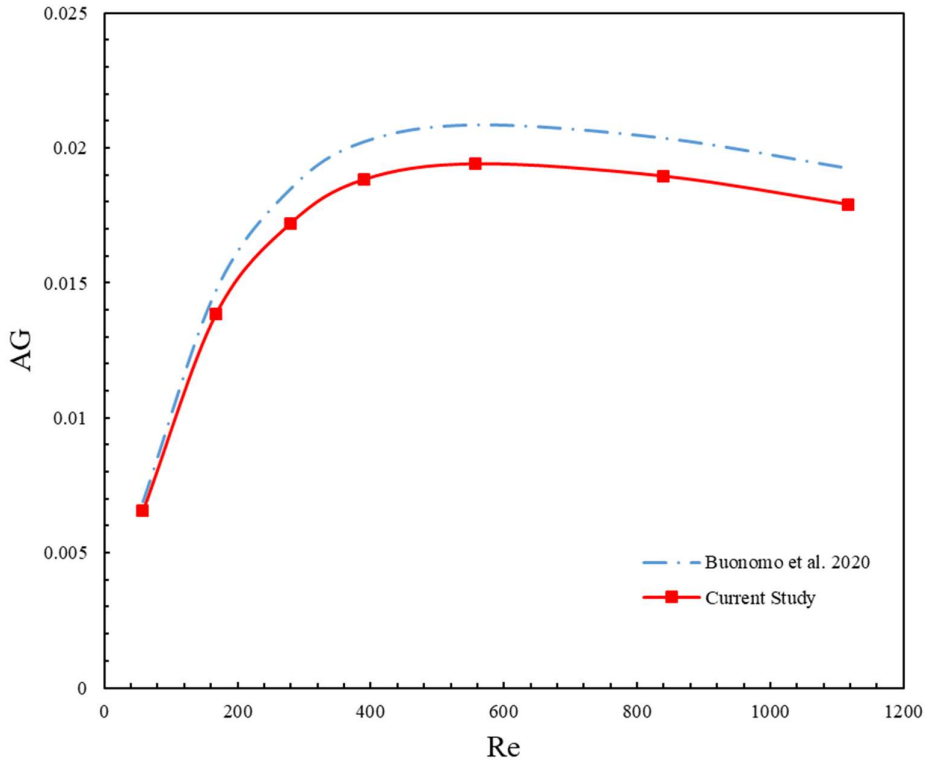

Figure (5- 42) AG vs Re validation of numerical model with Buonomo et al [46]

5.2.2. Temperature, velocity, and pressure distribution

Figure (5-43) demonstrates the isothermal contour of the numerical results of heat exchanger with 0.96 porosity copper foam. It can be seen that the temperature distribution around the tubes varies with the increase in the inlet air velocity to the heat exchanger. It can be noted that increasing the air velocity reduces the air temperature difference between the inlet and outlet of heat exchanger. High-speed air does not give enough time for heat exchange between the surface of the tube, the porous surface, and the air molecules, so the difference between the tube temperature and the air temperature is high. It can be seen that the temperature difference is 3.89 ^{o}C at an air velocity of 1 m/s, and this difference decreases until it reaches 1.818 ^{o}C at an air velocity of 9 m/s. It can also be noted through isotherm map that the distribution of temperatures is greater in the case of low air velocity.

Figure (5-44) represents the velocity contour map through the heat exchanger around the tubes and for different air inlet velocity. Where it can be seen that the higher value of velocity in the areas between the tubes in the vertical direction due to the convergence of the area and thus the velocity increases. As for the areas behind the pipe, the velocity is low due to the separation of the boundary layer around the pipe, but in general, the porous medium works to reduce the separation by dispersing air through the pores and thus destroying the boundary layer.

Figures (5-45) to (5-47) explain the pressure profile through the heat exchanger for three different types of porosity of the copper foam and at different air entry velocities ranging from 1 m/s to 10 m/s. It is possible to notice a gradual decrease in pressure until it reaches atmospheric pressure in the exit area. In some areas, it is possible to notice the fluctuation of the curve as a result of passing through areas between the tubes, which causes

an increase in air velocity and thus a decrease in pressure. The increase in air velocity leads to a higher pressure difference through the heat exchanger. As it can be noted that the increase in porosity as in the figure (5-47) led to a decrease in pressure drop because the high porosity means the passage of air with less obstruction.

Figure (5-48) shows contour map of air pressure through the heat exchanger with copper foam. It is possible to notice the effect of obstruction generated during the passage of air from the metal foam, which causes a pressure difference between the two faces of the heat exchanger. It can be seen that the pressure difference increases with the increase in the velocity of the incoming air. It can be seen that ΔP reaches 19.032 Pa at inlet velocity 1m/s, but ΔP begins to rise until it reaches 335.76 Pa when the air inlet velocity is doubled to 10 times.

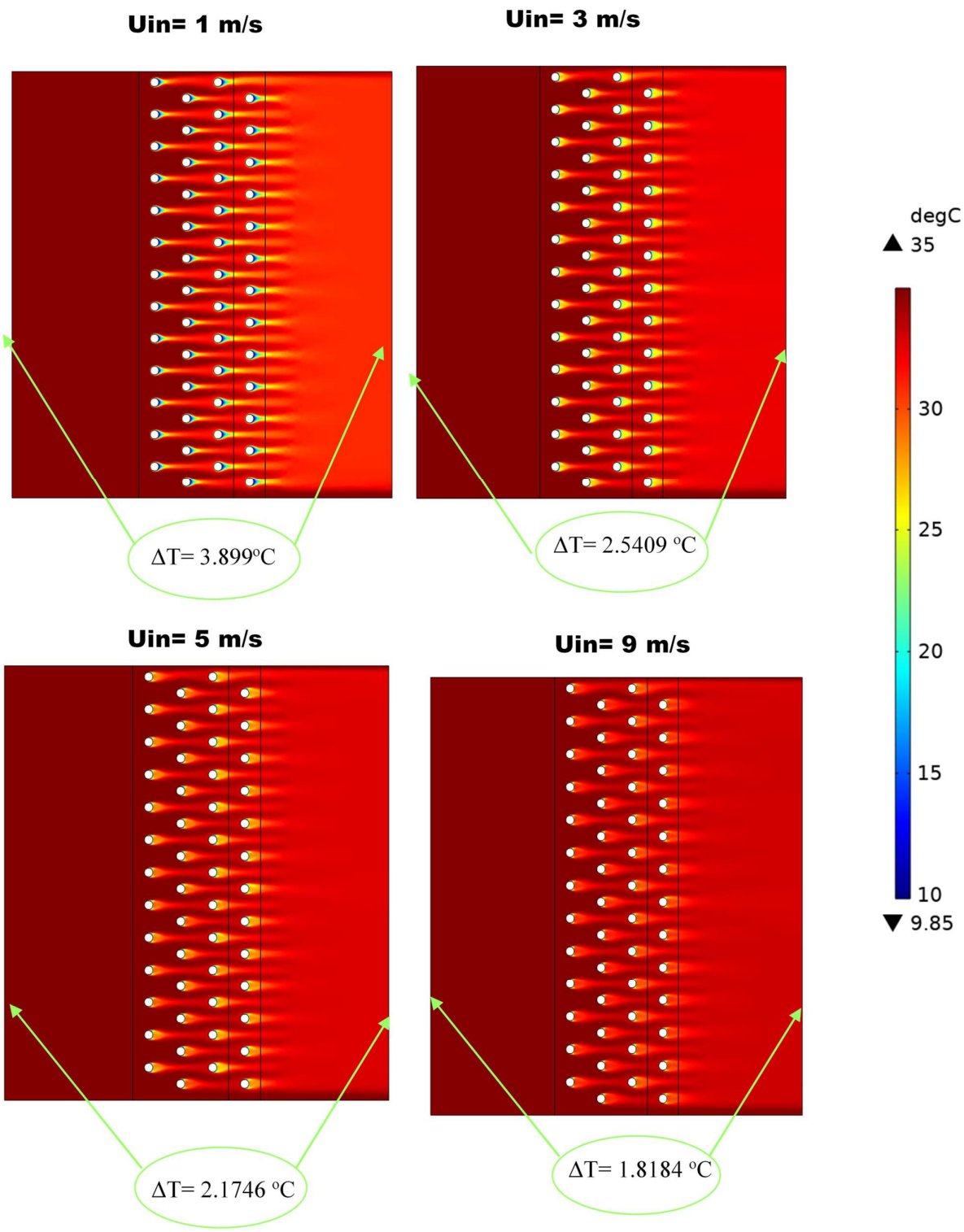

Figure (5- 43) isothermal contour of heat exchanger with 0.96 porosity copper foam at different value of air inlet velocity.

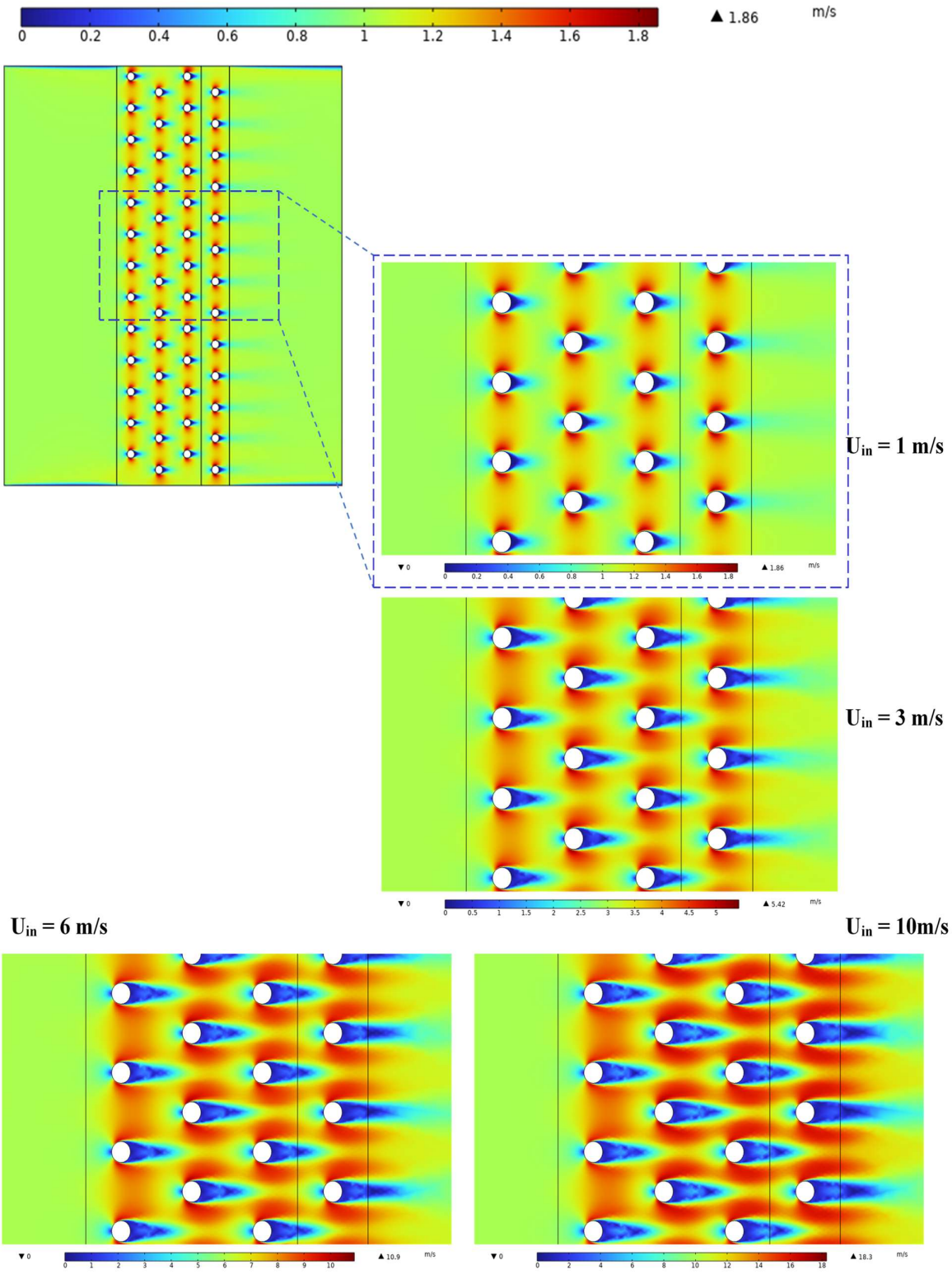

Figure (5- 44) velocity contour map around tubes with metal foam.

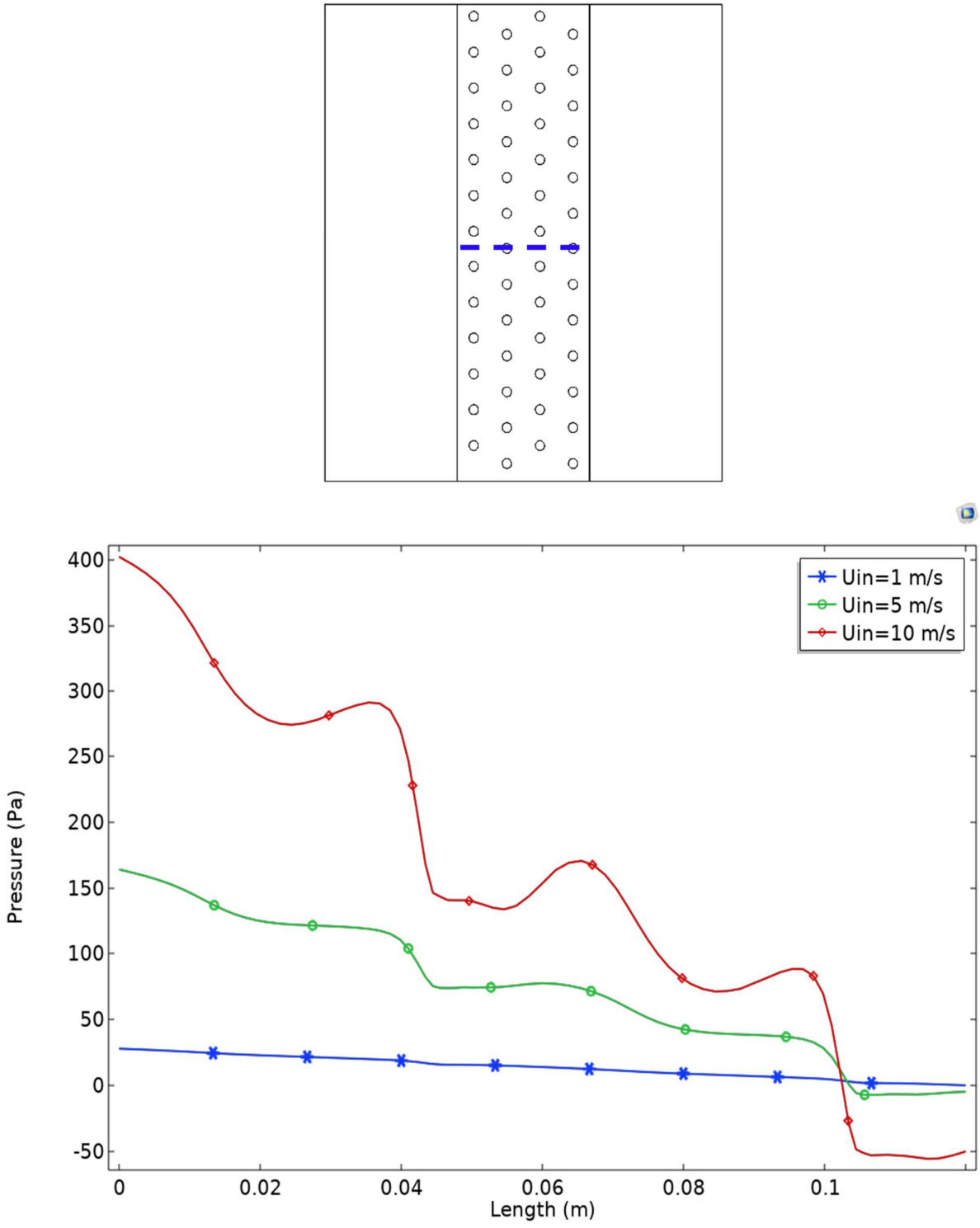

Figure (5- 45) pressure profile at centerline through heat exchanger with 0.88 porosity copper foam.

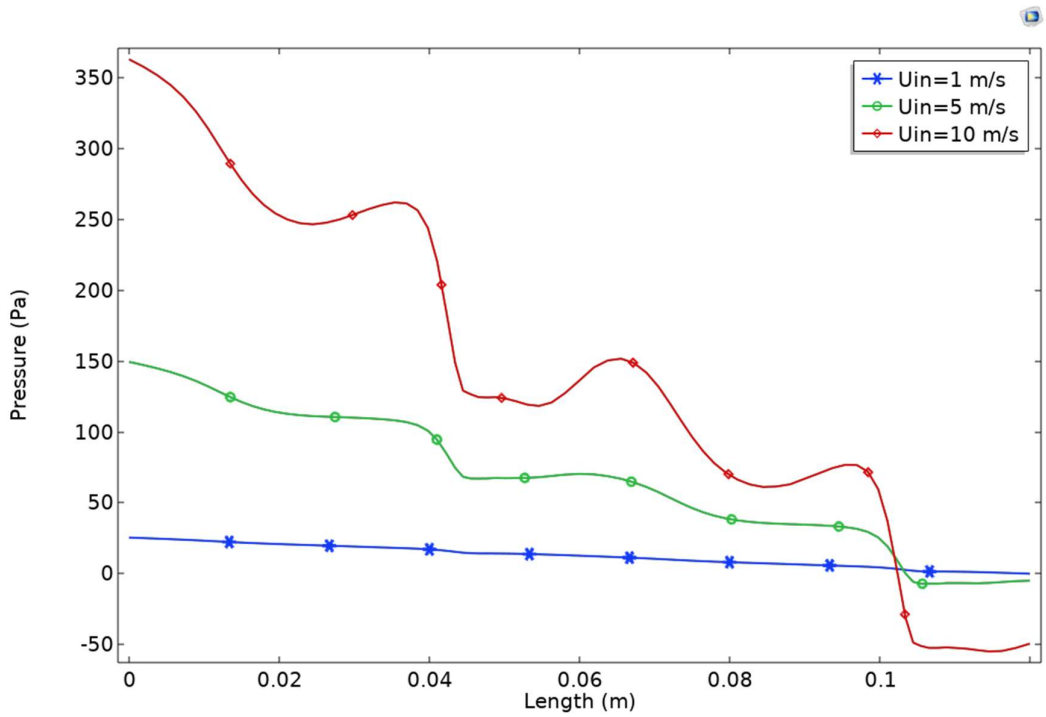

Figure (5- 46) pressure profile at centerline through heat exchanger with 0.92 porosity copper foam.

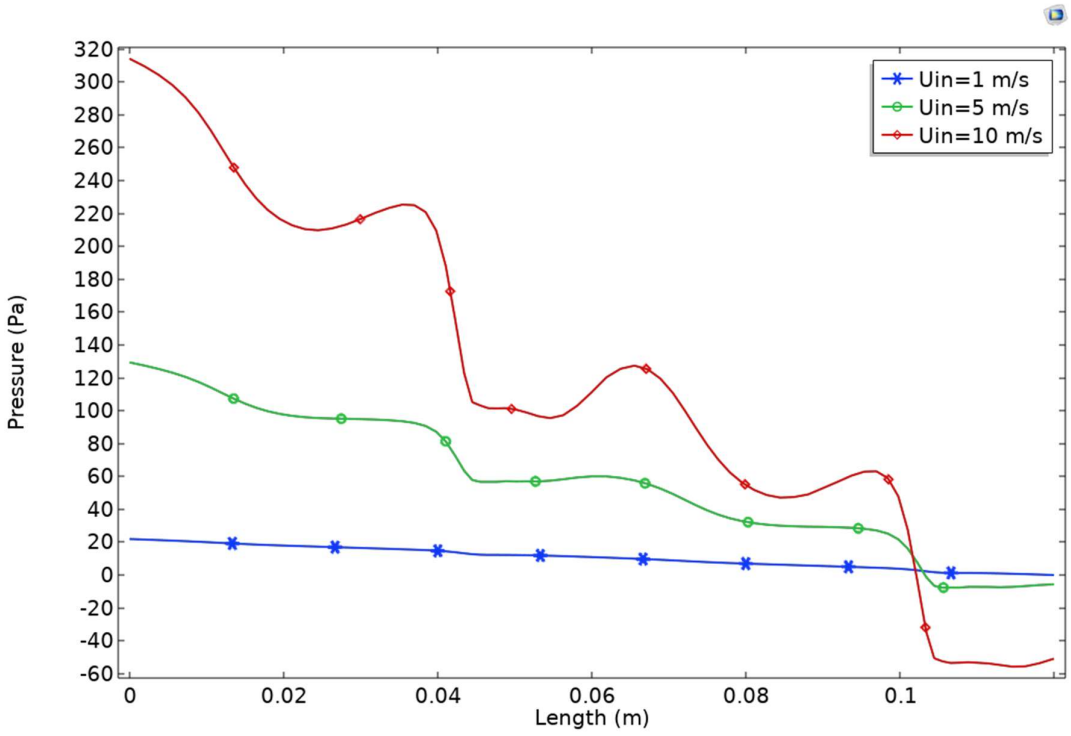

Figure (5- 47) pressure profile at centerline through heat exchanger with 0.96 porosity copper foam.

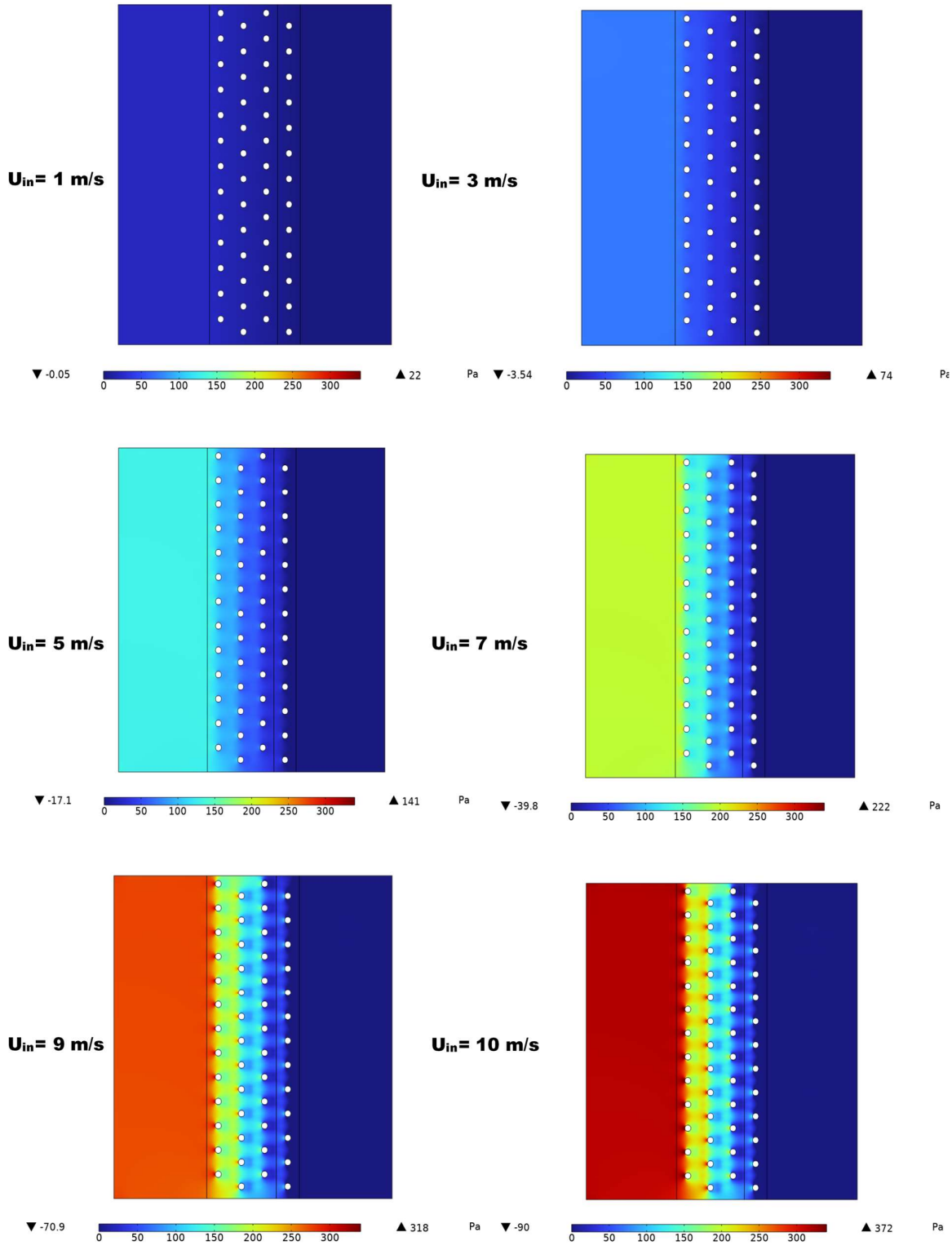

Figure (5- 48) pressure contour map for heat exchanger with 0.96 porosity copper foam at different value of inlet velocity.

5.2.3. The effect of air inlet velocity

Figure (5-49) represents the effect of velocity on the temperature difference (ΔT) between the inlet and outlet air for three different values of porosity. Increasing the velocity leads to a decrease in ΔT and this is because the higher velocity does not give the fluid enough time for the heat exchange process, so the temperature of the outlet air decreases. Increased porosity means that air passes through the porous medium faster and means less heat exchange time. Therefore, it is possible to observe the opposite effect of increasing the porosity on the value of ΔT.

Figure (5-50) shows the effect of air inlet velocity on the heat transfer rate for three different values of porosity. It can be noticed the exponential logarithmic relations between the air velocity and the rate of heat transfer. An increase in air velocity means an increase in kinetic energy and thus an increase in heat exchange between the porous medium and the air molecules. The heat transfer rate increases by 309% when air inlet velocity increases 10 times in the case of copper foam with a porosity of 0.88, while the percentage increase in the cases of porosity of 0.92 and 0.96 is 328% and 353%, respectively.

Figure (5-51) introduces the relation between the inlet air velocity and the heat transfer coefficient. The direct relation between the two variables can be observed. The heat transfer coefficient increases from 271.78 $W/m^2.^oC$ to 1112 $W/m^2.^oC$, when air inlet velocity increases from 1m/s to 10 m/s at 0.88 foam porosity. Increasing the air velocity leads to an increase in the amount of heat transferred by convection, and thus means a higher heat transfer coefficient. The heat transfer coefficient is also affected by the nature of the porous medium, so it can be noted that the heat transfer coefficient is higher in the case of the medium with lower porosity.

Figure (5-52) depicts the relations between air inlet velocity and Nussult number for different value of porosity. Nusselt number increased from 4133 to 16903 when the air inlet velocity is increased from 1 m/s to 10 m/s. An increase in the inlet velocity of air to the porous medium means an increase in heat transfer by convection, and thus an increase in the Nusselt number can be observed. The green color shows the heat exchanger with a porosity of 0.96, where it can be noted that the high porosity means a faster passage through the porous medium, and thus the heat exchange period decreases, and then the Nusselt number decreases. The red color shows the heat exchanger with a foam with a porosity of 0.85, where it can be seen that the Nusselt number increases with the increase in the porosity.

Figure (5-53) shows the relations between the inlet air velocity and the Colburn factor of the heat exchanger at three different values of the porosity of the copper foam. The inverse relationship that shows the decrease of Colburn factor can be seen with the increase in the inlet air velocity. Colburn factor decreases sharply between an air velocity of 1 m/s to 6 m/s, then the decrease begins gradually between an air velocity of 6 m/s to 10m/s. This is because the increase in air velocity represents an increase in mass transfer at the expense of heat transfer. Therefore, Colburn factor decreases by 59% in the case of porosity equal to 0.88.

Figure (5-54) explains the direct relations between the inlet air velocity of and the pressure drop through the heat exchanger, where it can be observed that a rise Δp from 27 Pa to 449 Pa is observed in the case of an increase in the air velocity from 1 m/s to 10 m/s. This is due that the pressure is produced due to the random movement between the gas molecules, and when the gas accelerates, some of this random energy is used to move the gas faster in the direction of the gas movement. This

results in a decrease in pressure in some areas, which causes a higher pressure difference according to Bernoulli's principle.

Figure (5-55) gives the effect of the inlet air velocity on friction factor through the copper foam. An inverse relationship can be seen between the two variables. The friction factor decreases sharply when the velocity increases from 1 m/s to 4 m/s, then it begins to gradually decrease. The reason for the decrease in the friction factor is because the friction factor is inversely proportional to the square of the velocity. Therefore, it can be observed that the friction factor decreases by 84% when the velocity is increased 10 times.

Figure (5-56) shows the effect of the air inlet velocity on area goodness factor (AG) of the heat exchanger. AG represents the ratio between the j- factor to the friction factor. Therefore, it can be observed that AG factor increases with a logarithmic function when the air velocity increases. It can be noted that an increase in air velocity greater than 9 m/s will have an insignificant effect on the AG factor. Air velocity range between 7 m/s to 9 m/s gives the best AG factor.

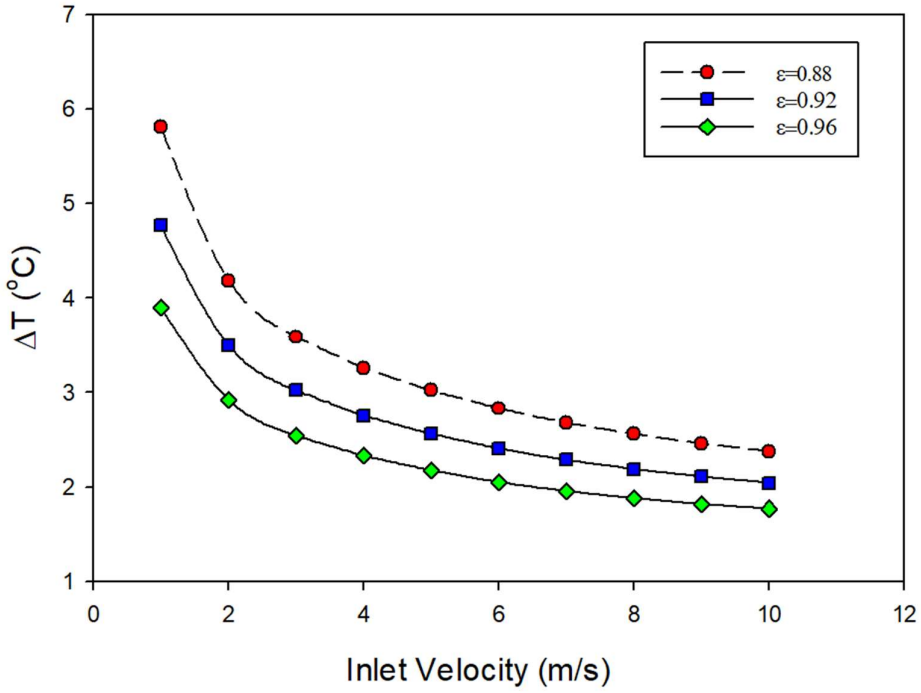

Figure (5- 49) effect of air inlet velocity on the temperature difference through heat exchanger.

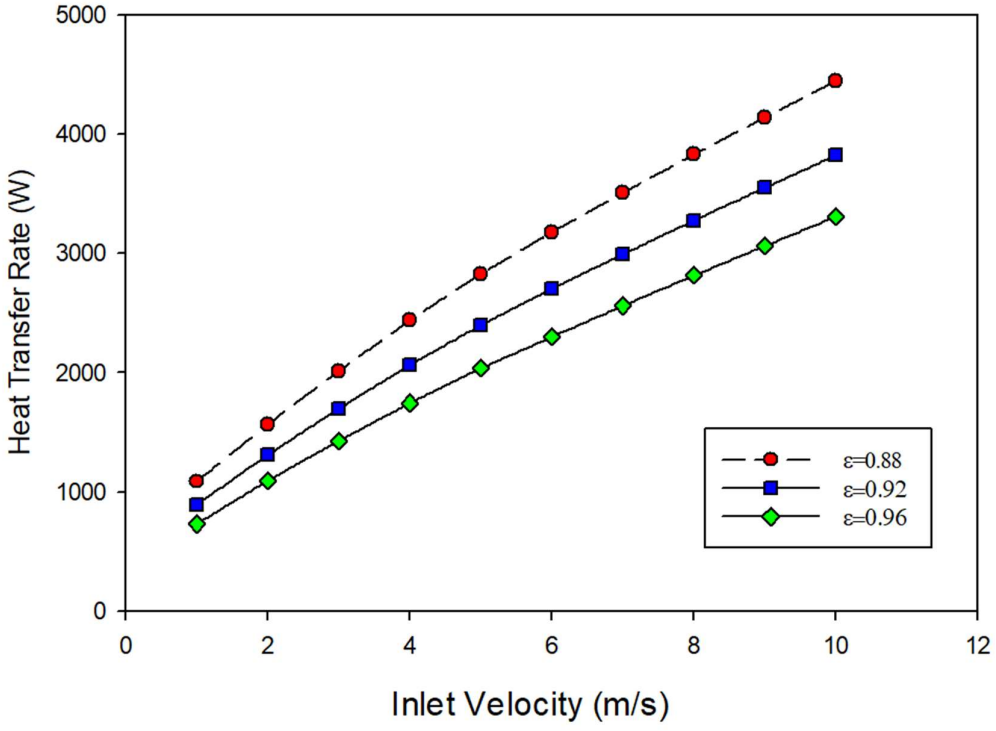

Figure (5- 50) effect of air inlet velocity on heat transfer rate.

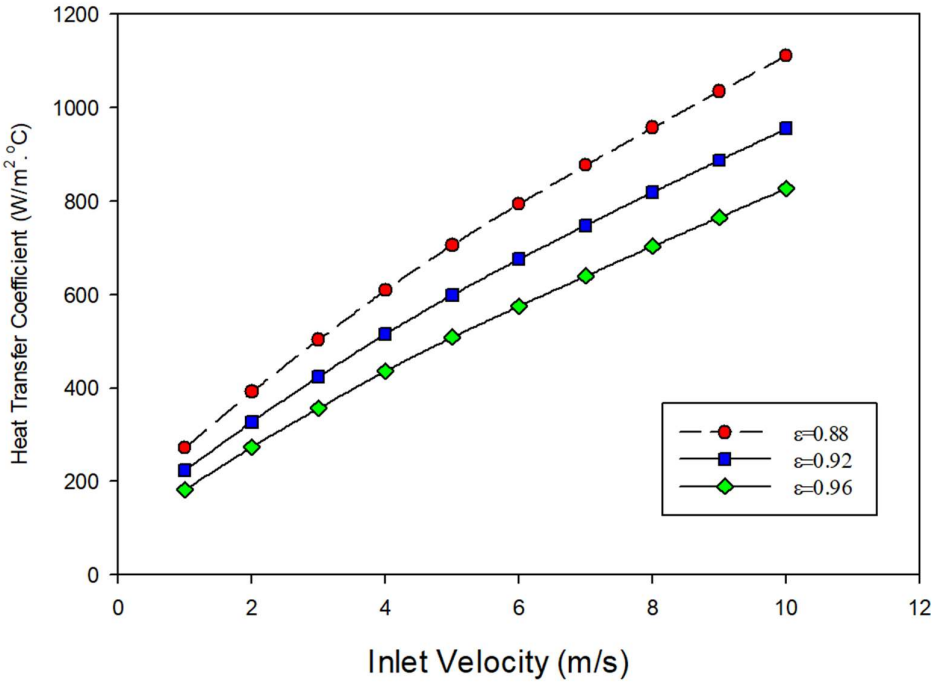

Figure (5- 51) effect of air inlet velocity on heat transfer coefficient.

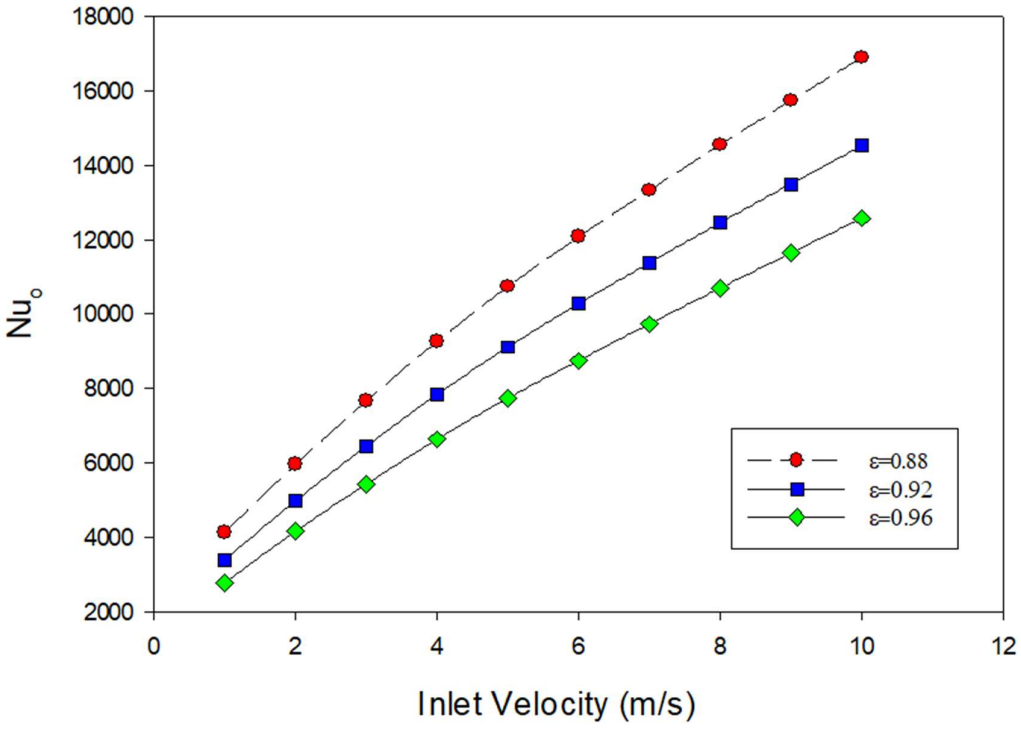

Figure (5- 52) effect of air inlet velocity on Nusselt number.

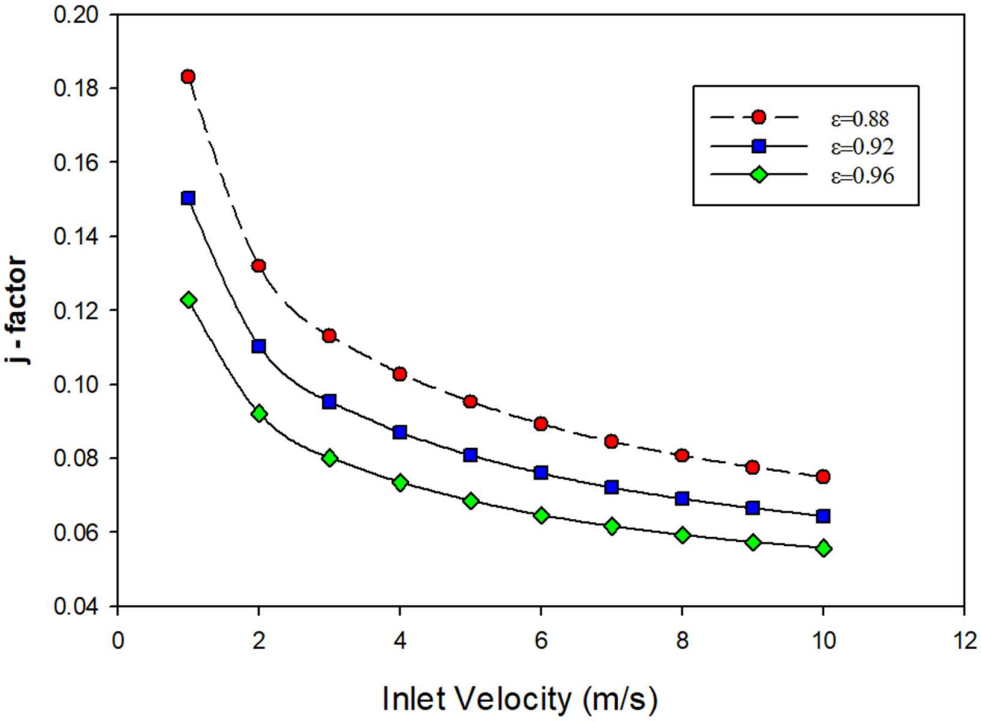

Figure (5- 53) effect of air inlet velocity on Colburn factor.

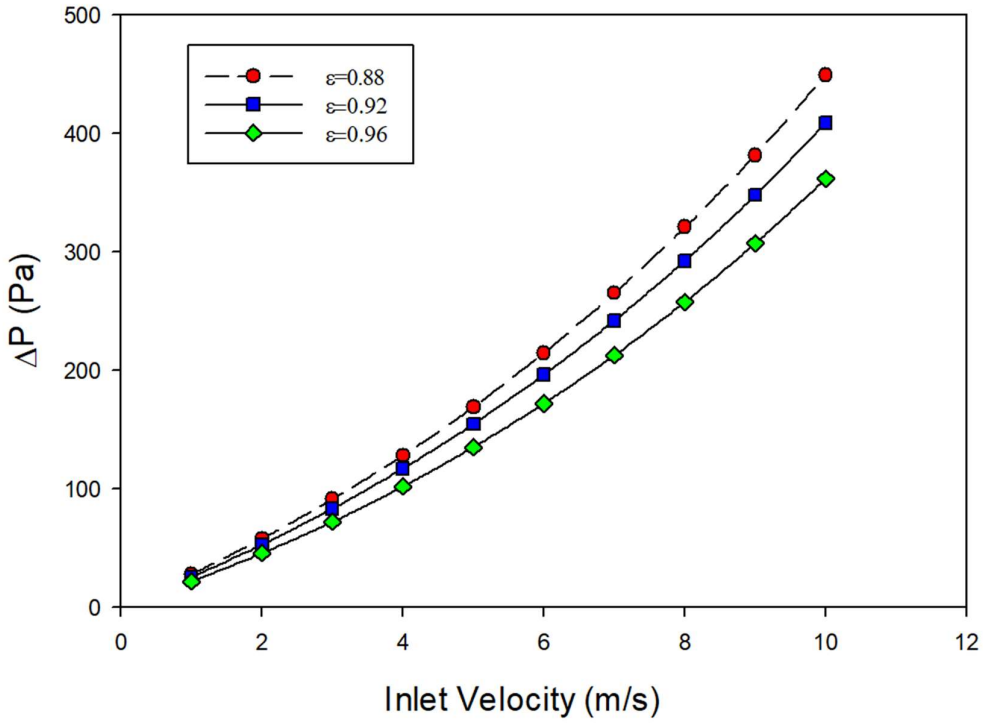

Figure (5- 54) effect of air inlet velocity on pressure drop.

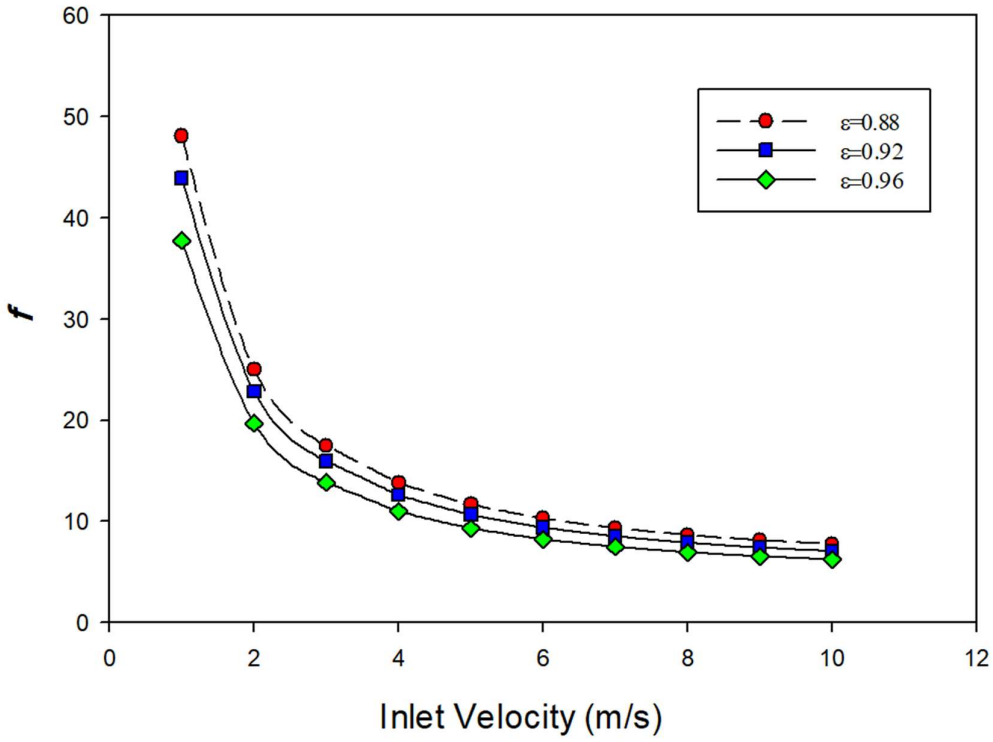

Figure (5- 55) effect of air inlet velocity on friction factor.

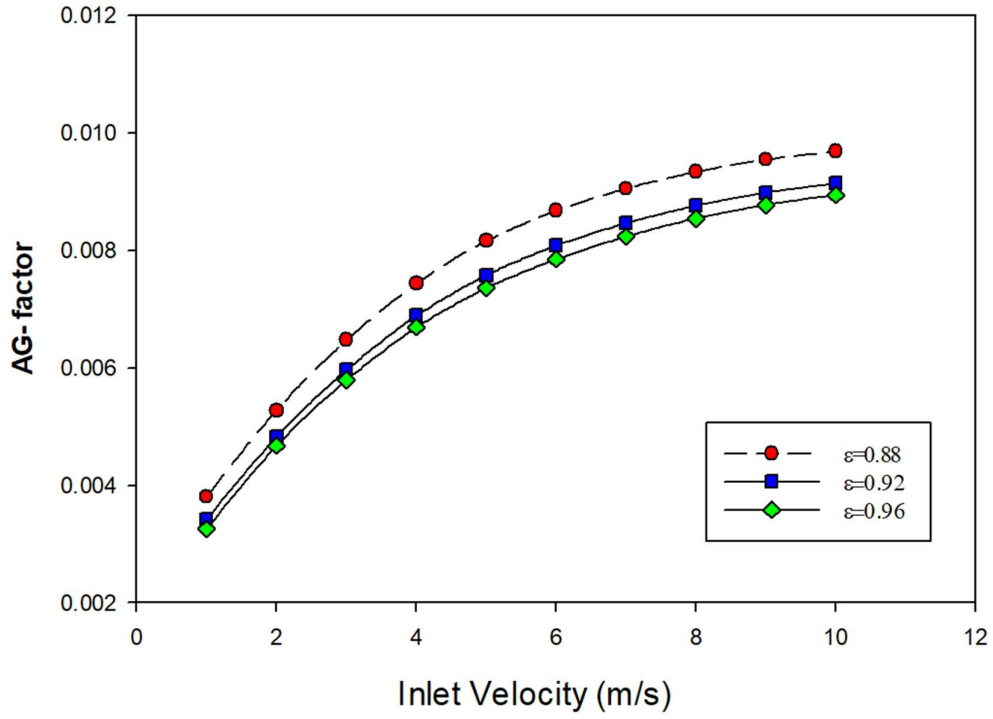

Figure (5- 56) effect of air inlet velocity on area goodness factor.

5.2.4. Fitting relation

Figure (5-57) shows the relations between Reynolds number and the air temperature difference during its passage through the heat exchanger. Increase in Reynolds number means an increase in the initial force of the fluid, and this leads to less time for heat exchange between the air and the porous medium, so that the temperature difference between the inlet and outlet of the air decrease by increase Reynolds number. The temperature difference is higher in the case of copper foam with low porosity, as it decreases from 5.8 °C to 2.37 °C when increasing Reynolds number from 25666 to 257000 at foam porosity of 0.88. The power relations between Re and temperature difference can be found by using curve fitting as following:

$$\Delta T = aRe^{-b} \tag{5.1}$$

Where a=261.13 and b=0.379 for φ =0.88, a=177.14 and b=0.36 for φ =0.92, while a=114.97 and b=0.337 for φ =0.96.

Figure (5-58) explains the empirical results of heat transfer rate with Reynolds number. It is possible to notice an increase in the heat transfer rate when Reynolds number is increased for all the different porous samples. The heat transfer rate is higher in the case of copper foam with low porosity. Increase in the Reynolds number means an increase in the air particles motion and thus the heat exchange process increases between the fibers of the porous medium and the air, and then the heat transfer rate increases. The power relations can be concluded by using curve fitting for different value of copper foam porosity

$$Q = aRe^{b} \tag{5.2}$$

Where a=1.905 and b=0.6213 for φ =0.88, a=1.2923 and b=0.6403 for φ =0.92, while a=0.8387 and b=0.6632 for φ =0.96.

Figure (5-59) shows the relations between Nusselt number and Reynolds number. The empirical results showed the power relationship between Reynolds number and Nussult number at different values of copper foam porosity. The direct relationship that can be represented through the following power equation:

$$Nu = aRe^{b} \tag{5.3}$$

Where a=3.1891 and b=0.6632 for φ =0.88, a=4.9136 and b=0.6403 for φ =0.92, while a=7.2435 and b=0.6213 for φ =0.96.

This is due to an increase in Reynolds number leads to an increase in the velocity of the inlet air to the heat exchanger, and thus the heat transfer coefficient increases, and then the Nusselt number increases.

Figure (5-60) gives the relations between Reynolds number and Colburn factor, which is an inverse logarithmic relationship that can be represented through the following equation:

$$j = -a\ln(Re) + b \tag{5.4}$$

Where a=0.044 and b=0.6197 for φ =0.88, a=0.035 and b=0.4984 for φ =0.92, while a=0.028 and b=0.3968 for φ =0.96.

It is possible to notice a decrease in the value of Colburn factor by 48% when increasing in Reynolds number from 25666 to 128000, then the decrease is gradual and returns. The increase in Reynolds number means an increase in the mass flow of air inside the porous medium, and thus the part related to mass transfer increases, which causes a decrease in Colburn factor.

Figure (5-61) shows the direct relations between Reynolds number and the pressure drop through heat exchanger. The pressure difference rise can be observed with a polynomial function that can be represented through the following equation:

$$\Delta p = a Re^2 + b Re + c \quad (5.5)$$

Where a=3×10^{-9}, b=0.0006, c=6.038 for φ =0.88, a=3×10^{-9}, b=0.0008, c=5.2833 for φ =0.92, while a=3×10^{-9}, b=0.0008, c=4.5465 for φ =0.96.

Increasing the pressure difference depends on the velocity of the incoming air, as the increase in the velocity of the air creates an obstruction due to the collision of the air with the copper foam, which causes a difference in pressure on both sides of the heat exchanger.

Figure (5-62) moderates the relations between Reynolds number and the coefficient of friction, where the inverse power relations can be observed between the two variables. The empirical equation between Reynolds number and friction factor can be written in the following form:

$$f = a Re^{-b} \quad (5.6)$$

Where a=136210 and b=0.792 for φ =0.88, a=126178 and b=0.793 for φ =0.92, while a=94253 and b=0.779 for φ =0.96.

It is possible to notice the effect of Reynolds number increase, which leads to an increase in the flow velocity and thus an increase in the value of Δp, but the ratio between the dynamic pressure to the shear stress decreases with an increase in Reynolds number.

Figure (5-63) shows the relations between Reynolds number and area goodness factor at different values of the porosity of the copper foam. It can be observed that AG factor rises sharply when Reynolds number

between 25000 to 180000, then it starts to rise slightly. The following polynomial empirical equation shows this relation:

$$AG = aRe^2 + bRe + c \quad (5.7)$$

Where a= 3×10^{-3}, b= 6×10^{-8}, c=0.0025 for φ =0.88, a= 3×10^{-3}, b= 6×10^{-8}, c=0.0022 for φ =0.92, while a= 3×10^{-3}, b= 6×10^{-8}, c=0.0021 for φ =0.96.

Increase in Reynolds number means an increase in the difference between temperatures within the layers of the porous medium, and thus a greater heat exchange occurs, which leads to an increase in the heat transfer coefficient and at the same time an increase in Reynolds number leads to a decrease in friction factor. Therefore, an increase in AG factor can be observed.

Figure (5-64) explains the comparison between the results of empirical equation of Nussult number and experimental results. The dotted line inclined at an angle of 45° represents the experimental results, while the red points represent the results extracted from equation (5.3). Convergence can be seen between the results of the equation and the experimental results. The maximum deviations between experimental results and empirical equations results is 15.2%.

Figure (5-65) represents the comparison between the empirical equation and experimental results of Colburn factor. The empirical results based on equation (5.4) showed a good convergence with the experimental results. The maximum deviation is 22% while in the other results it ranged from 9 to 13 %.

Figure (5-66) shows the comparison between the empirical equation and experimental results of pressure gradient through heat exchanger. The empirical results based on equation (5.5) gave results close to the experimental results at medium and high air velocities. The maximum

deviation is 30% at low air velocity, while in the other results it ranged from 15 to 18 %.

Figure (5-67) explains the comparison between the empirical equation and experimental results of area goodness factor. The empirical equation gave an acceptable prediction for the AG results. The maximum deviation in the results was at low air velocity, where the deviation reached 30 %, while it ranged from 1% to 7% in the rest of the air velocities.

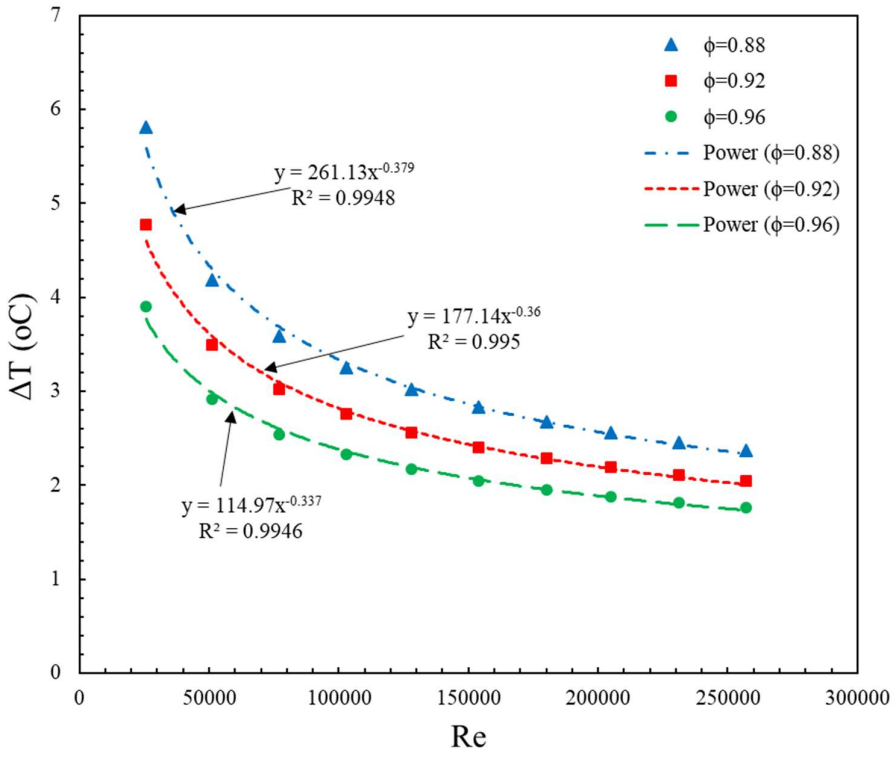

Figure (5- 57) temperature difference as a function of Reynolds number.

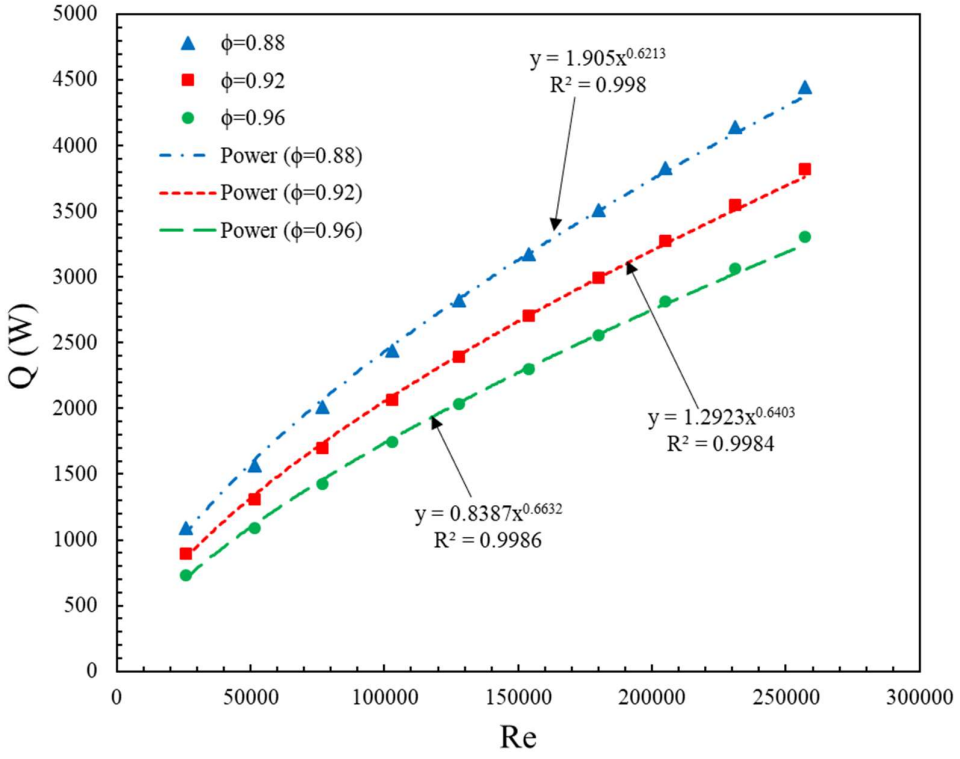

Figure (5- 58) heat transfer rate as a function of Reynolds number.

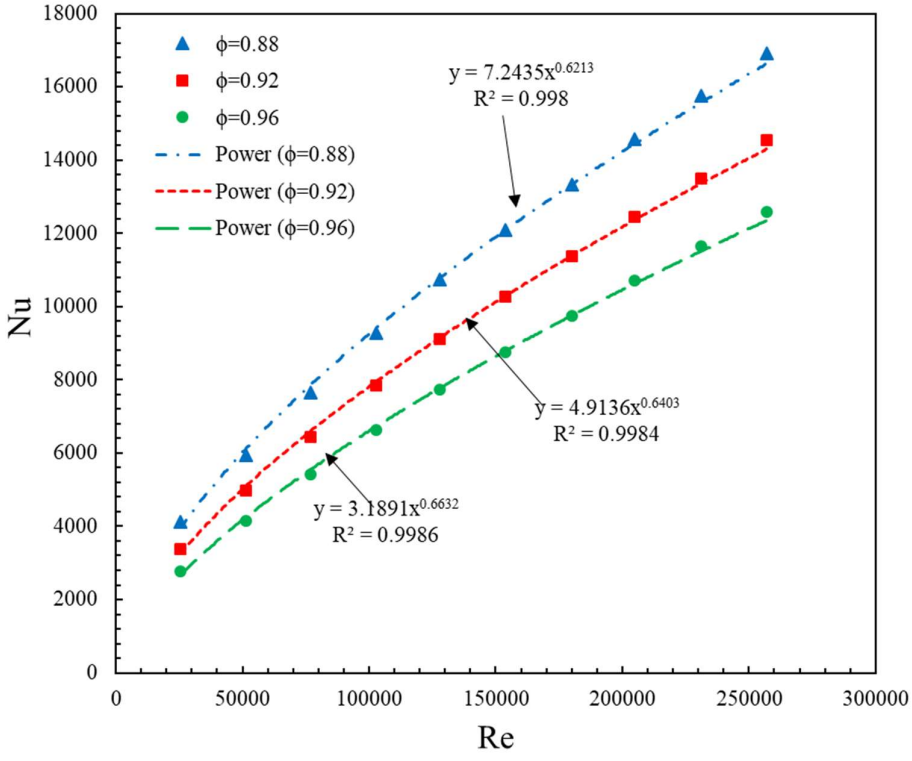

Figure (5- 59) Nusselt number as a function of Reynolds number.

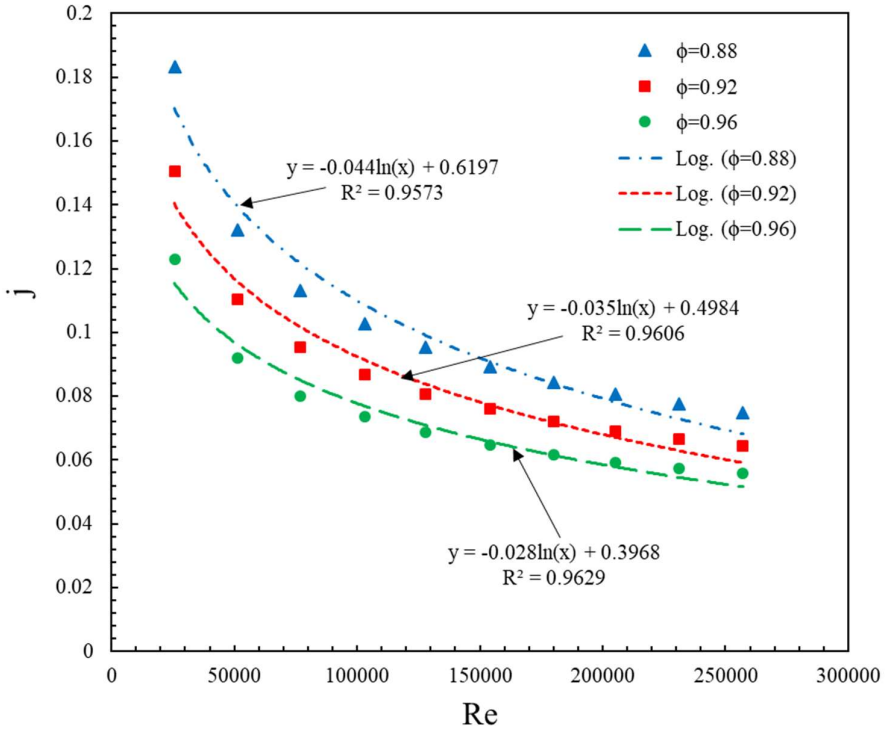

Figure (5- 60) Colburn factor as a function of Reynolds number.

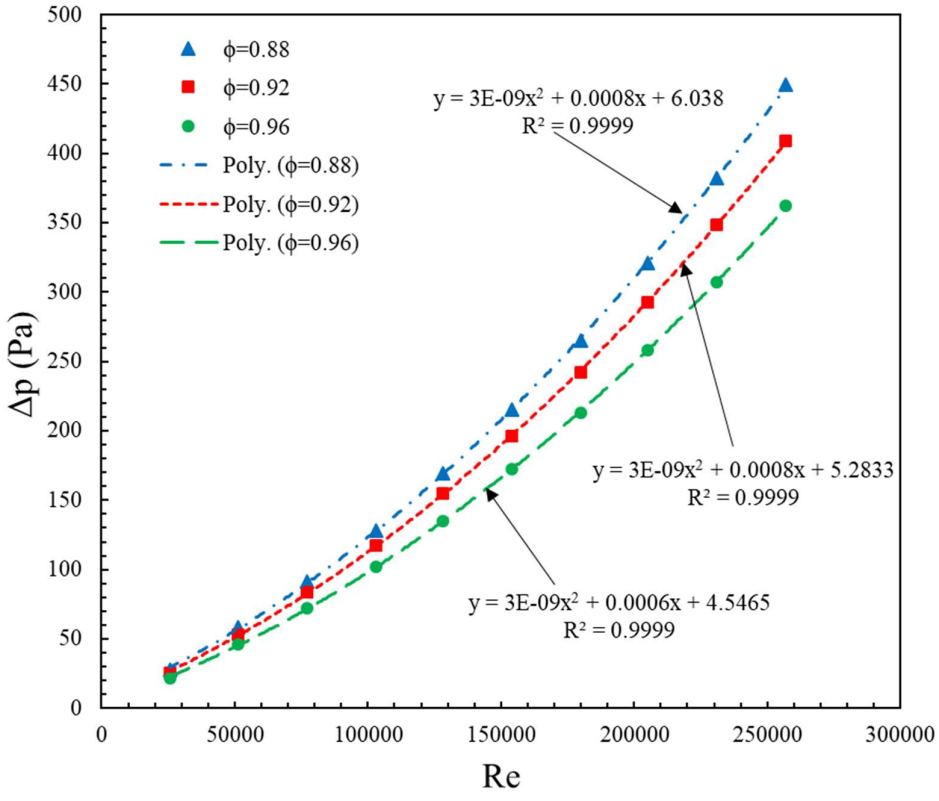

Figure (5- 61) pressure drop as a function of Reynolds number.

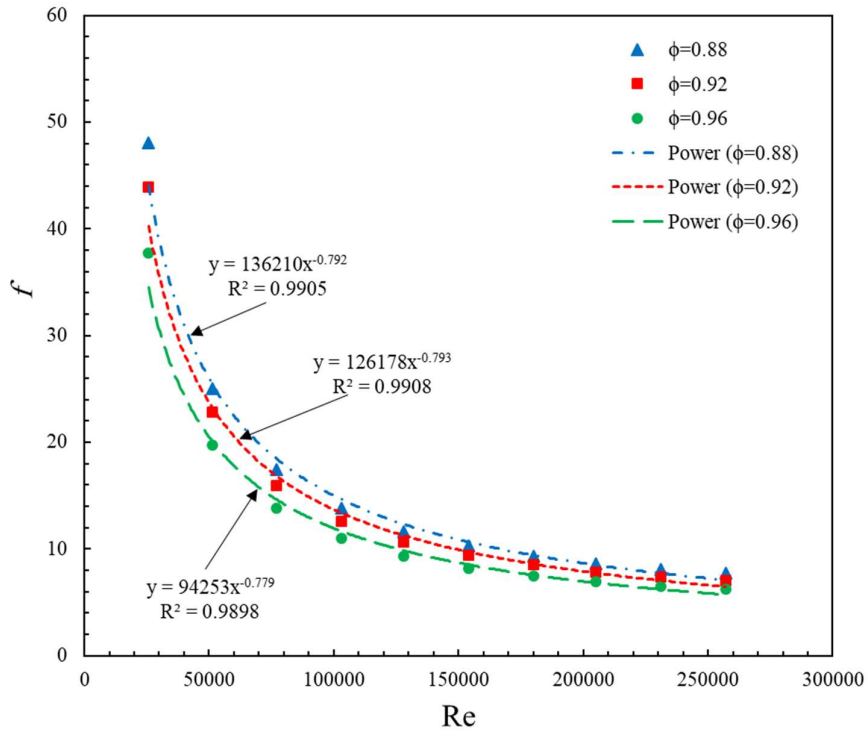

Figure (5- 62) friction factor as a function of Reynolds number.

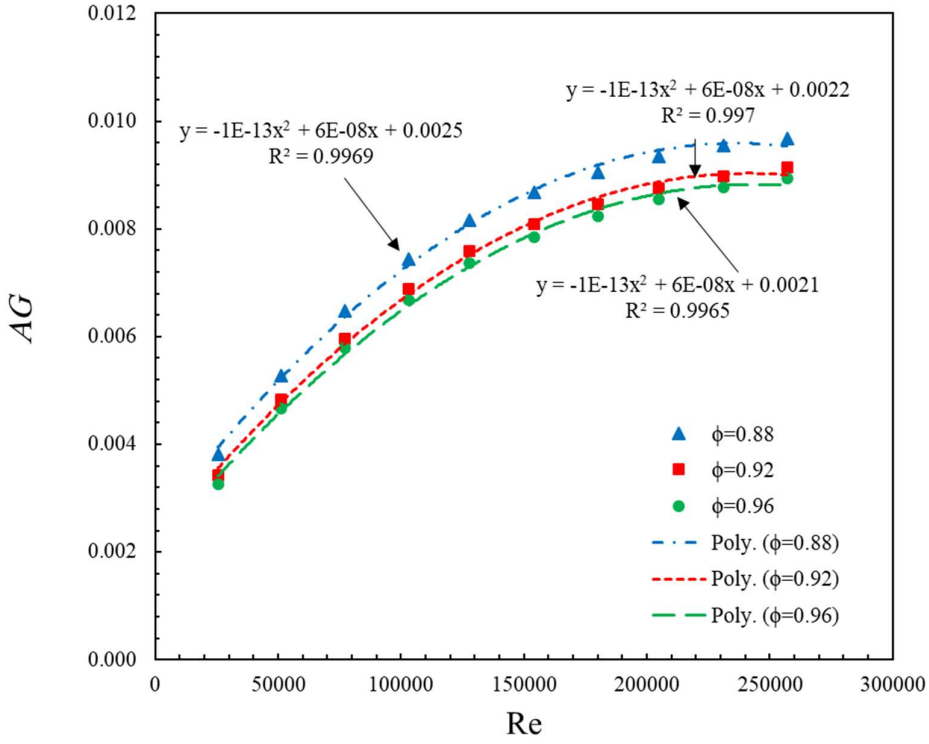

Figure (5- 63) area goodness factor as a function of Reynolds number.

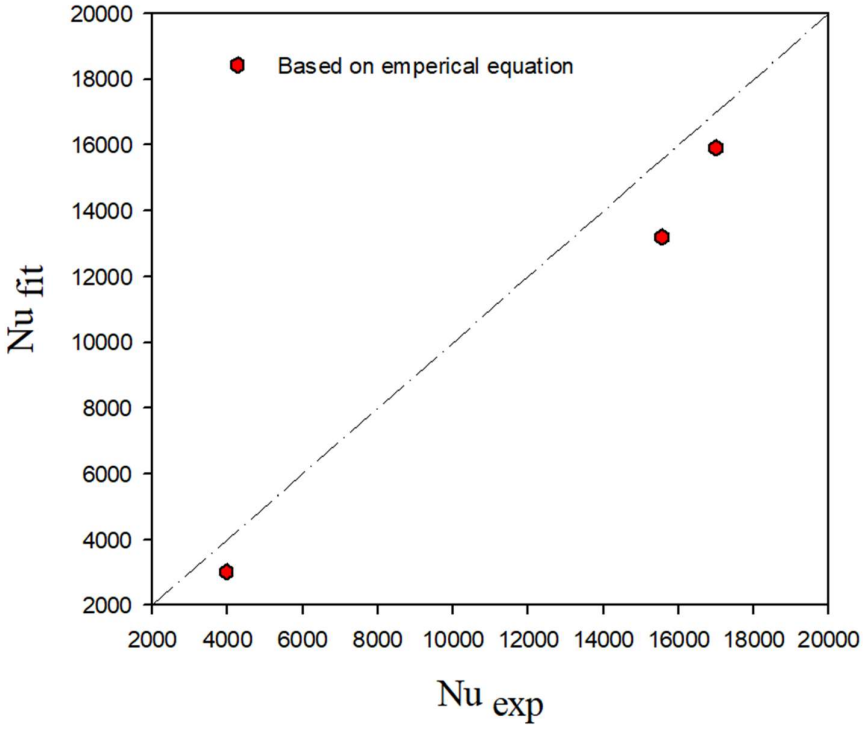

Figure (5- 64) comparison of experimental Nusselt number with empirical equation.

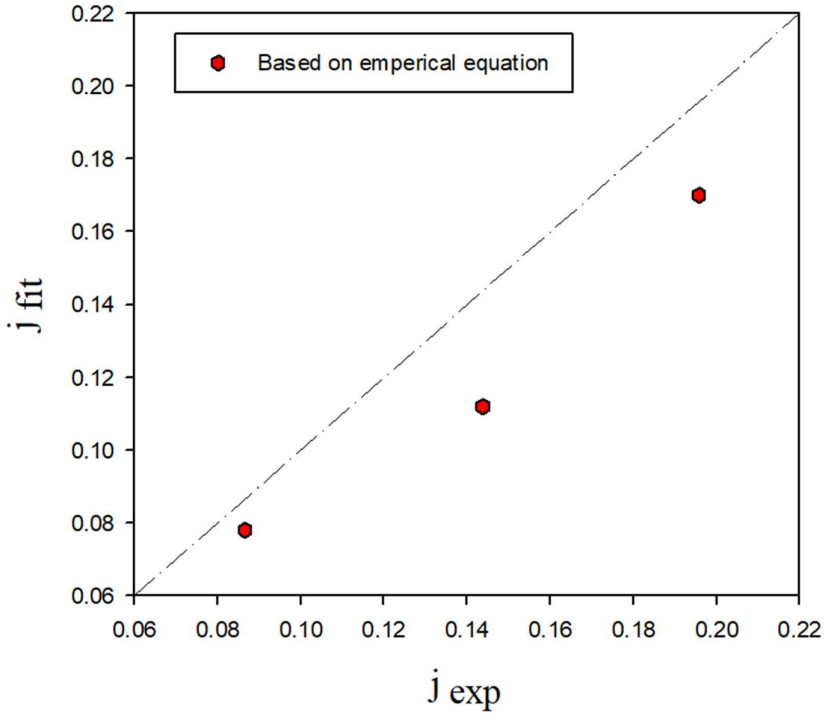

Figure (5- 65) comparison of experimental Colburn factor with empirical equation.

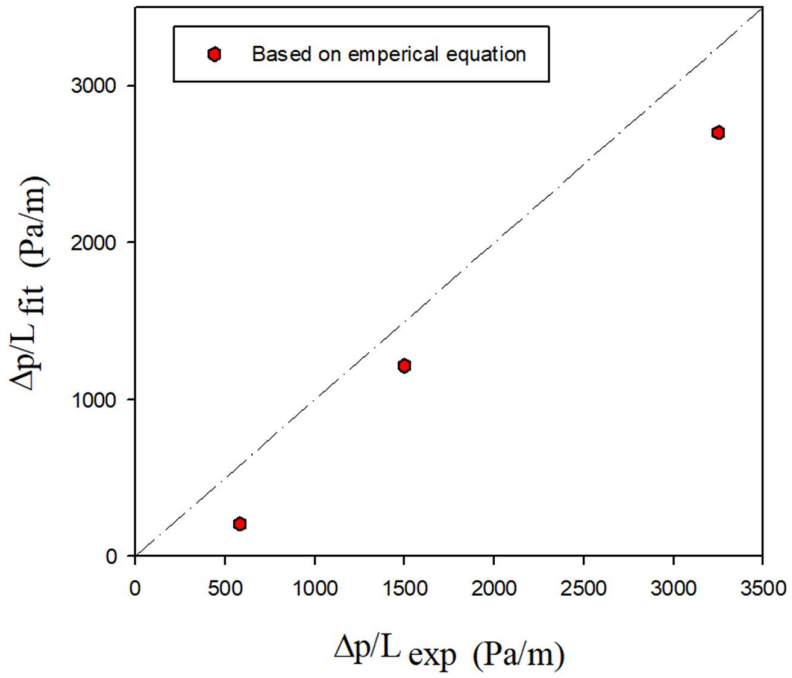

Figure (5- 66) comparison of experimental pressure gradient with empirical equation.

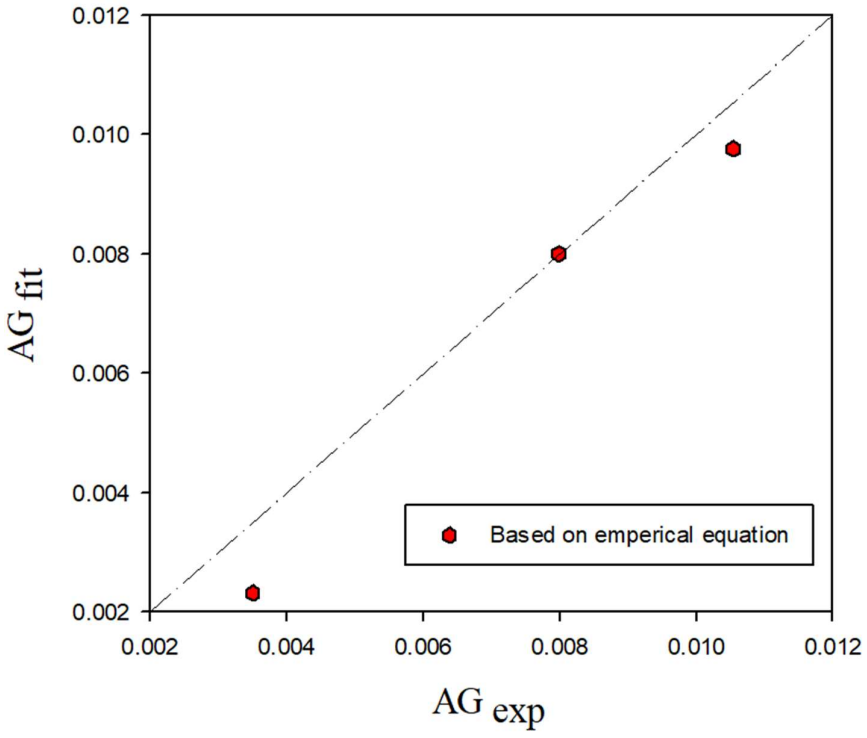

Figure (5- 67) comparison of experimental area goodness factor with empirical equation.

5.3. Comparison between Experimental and Theoretical Results

Figures (5-68) shows the comparison between experimental and numerical results of heat transfer coefficient. The theoretical results of the heat transfer coefficient with the Reynolds number showed the same response with the experimental results. The heat transfer coefficient increases with the increase in Reynolds number due to the increase in air flow inside the copper foam. The deviation error between the experimental and theoretical results was 1.7 % when Reynolds number equal to 22650. The deviation between experimental and theoretical results increases with Reynolds number increase to reach 18% at Reynolds number equal to 120800, and 19.1 % at Reynolds number equal to 218940.

Figure (5-69) indicates the comparison between experimental and theoretical results of Nussult number. The results show a similarity in the response, where Nussult number depends mainly on the value of the heat transfer coefficient. Therefore, it can be seen that the Nussult number increased with the Reynolds number. The maximum deviations error between experimental and theoretical results is at the value of the Reynolds number equal to 218940 and it was 19.1 %. This is due to that the model used during the theoretical solution is a model that assumes that the flow is laminar through the porous medium. Therefore, by increasing the Reynolds number, the difference between the experimental and theoretical results increases.

Figure (5-70) shows the comparison between experimental and theoretical results of Colburn factor. The Colburn factor depends on the heat transfer coefficient and the amount of air flow within the porous medium. An increase in the Reynolds number means an increase in the air flow, and thus a decrease in Colburn factor in both experimental and theoretical results. It can be seen that the response corresponds between

experimental and theoretical results. The maximum deviation error between experimental and theoretical results is 14% at higher value of Reynolds number (218940), while it is between 11% to 13% for $Re < 25\times10^4$.

Figure (5-71) shows the comparison between the experimental and theoretical results of the relations of Reynolds number with pressure gradient ($\Delta p/L$) through the heat exchanger. It can be noted the similarity of response between the two solutions. Increases $\Delta p/L$ by increasing Reynolds number in both solutions. The deviation error between the experimental and theoretical results is 12 % when Reynolds number equal to 22650, 12.5% at Reynolds number equal to 120800, and 13.4 % at Reynolds number equal to 218940.

Figure (5-72) describes the comparison between the experimental and theoretical results of the relations of Reynolds number with friction factor through the heat exchanger. Friction factor depend upon the inlet velcity of air and pressure drop through heat exchanger. Increasing Reynold number leads to increase the velocity of the air as well as pressure drop, so that the friction factor decrease in both experimental and theoretical results. Lower value of Reynold number gives higher deviations error which is approximately 13%. The deviation error between the experimental and theoretical results is 12.5% at Reynolds number equal to 120800, and 12.4 % at Reynolds number equal to 218940.

Figure (5-73) shows the comparison between the experimental and theoretical results of the relations of Reynolds number with AG factor. The theoretical results show a response similar to the experimental results, where the relationship between AG and Re is power in both solutions. The deviation error between the experimental and theoretical results is increasing with the increase in Reynolds number. The deviation error between the experimental and theoretical results was 15 % when Reynolds

number equal to 22650, 16 % at Reynolds number equal to 120800, and 18 % at Reynolds number equal to 218940.

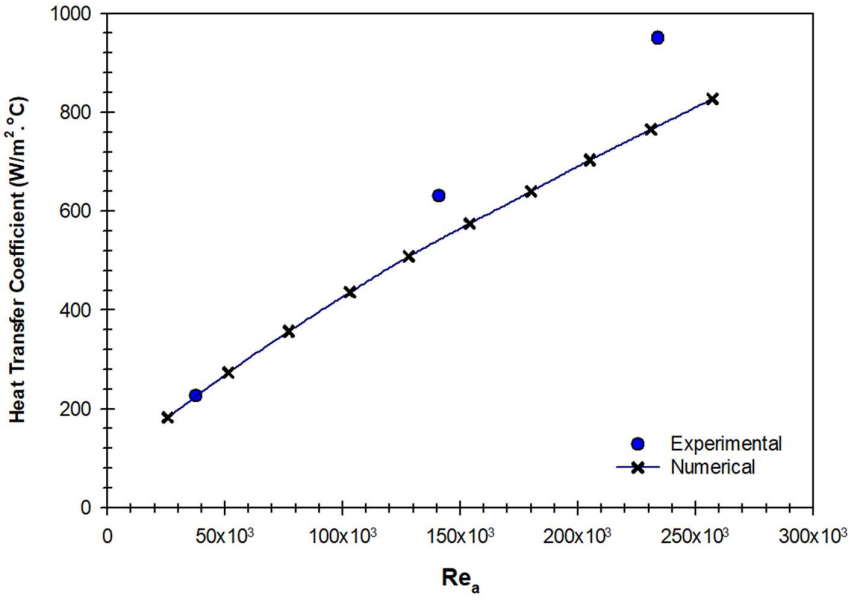

Figure (5- 68) comparison between experimental and theoretical results, the relationship of Reynolds number with heat transfer coefficient.

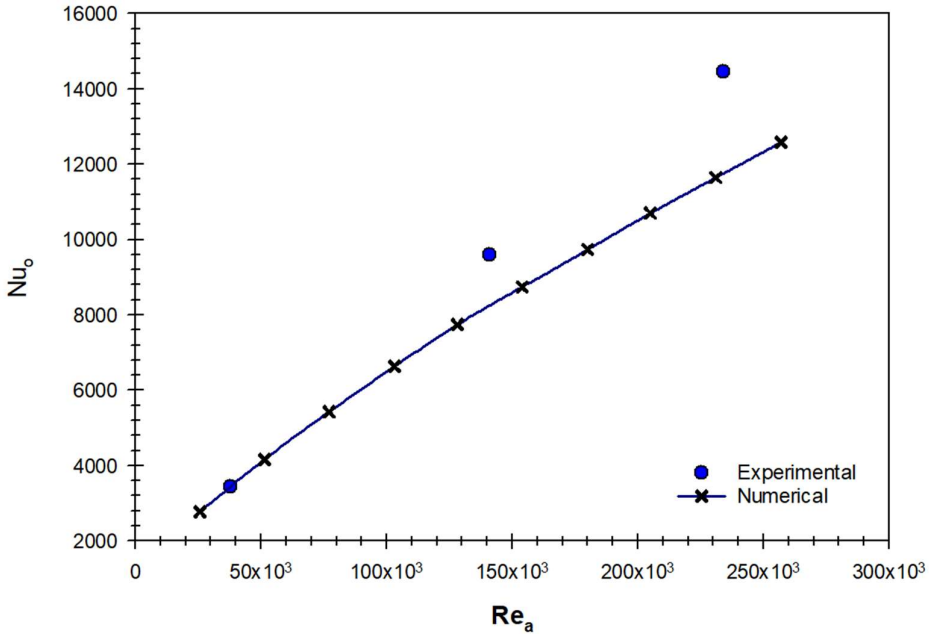

Figure (5- 69) comparison between experimental and theoretical results, the relationship of Reynolds number with Nusselt number.

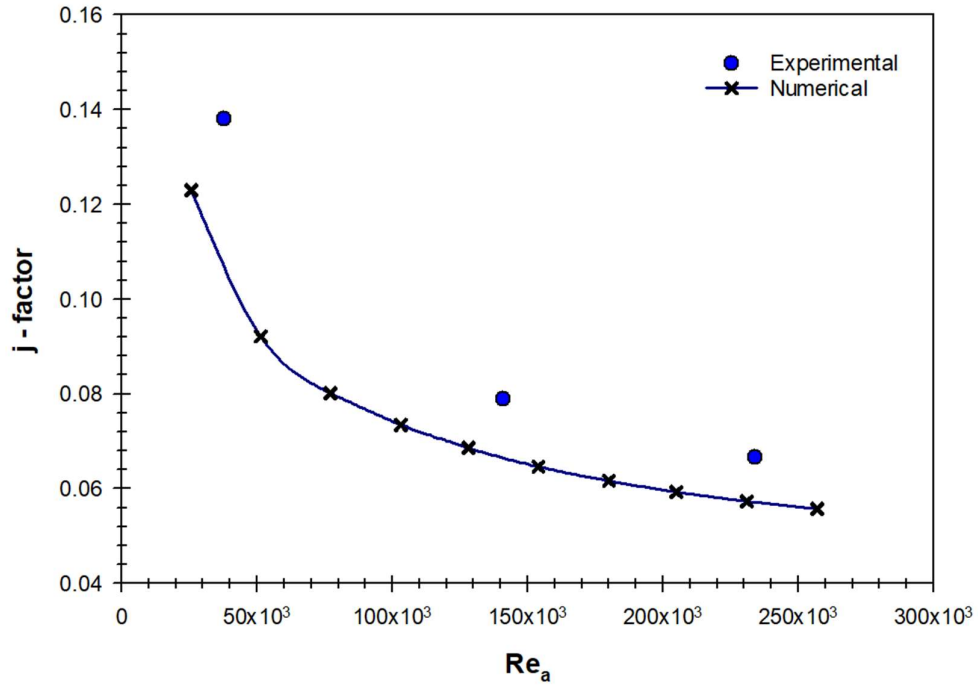

Figure (5- 70) comparison between experimental and theoretical results, the relationship of Reynolds number with Colburn factor.

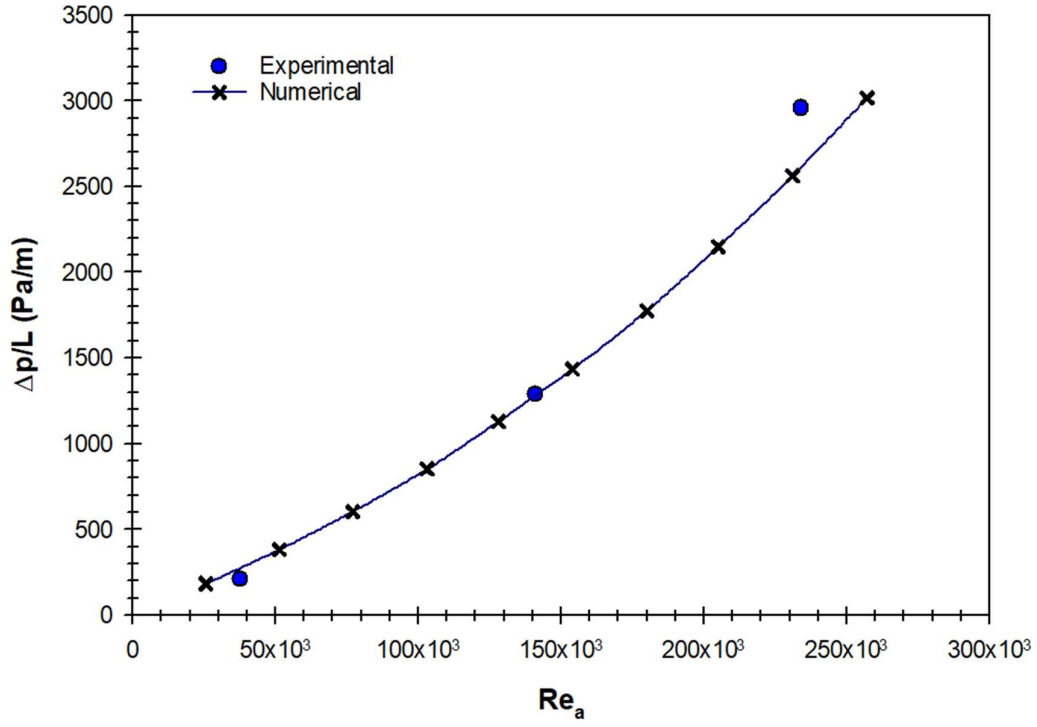

Figure (5- 71) comparison between experimental and theoretical results, the relationship of Reynolds number with pressure gradient.

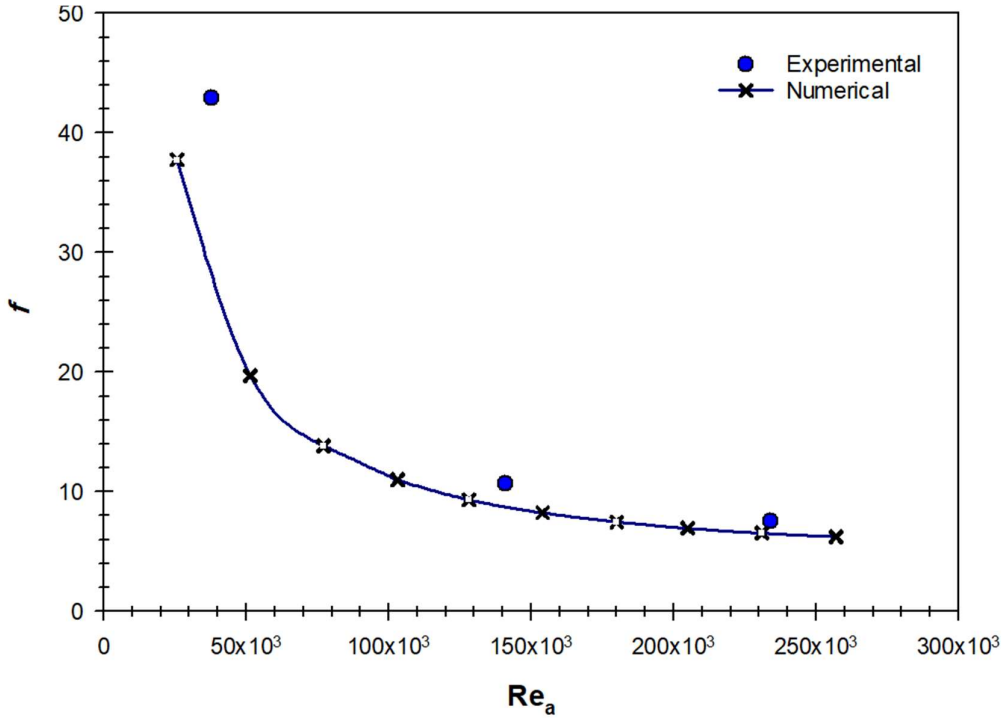

Figure (5- 72) comparison between experimental and theoretical results, the relationship of Reynolds number with friction factor.

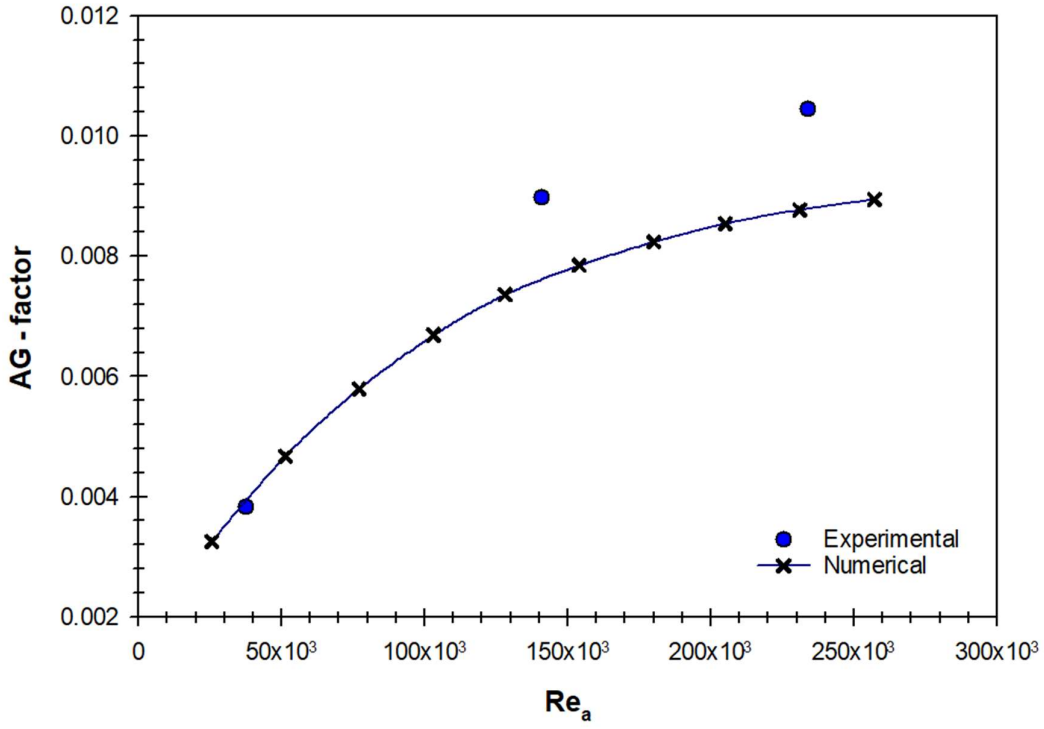

Figure (5- 73) comparison between experimental and theoretical results, the relationship of Reynolds number with area goodness factor.

CHAPTER SIX

CONCLUSIONS AND SUGGESTIONS FOR FUTURE WORK

Chapter Six: Conclusions and Suggestions for Future Work

6.1. Conclusions

In the current study, the following points can be concluded:

1- Generally the heat transfer coefficient increases by increasing the air inlet velocity for heat exchanger with fins or with copper foam. The heat transfer coefficient of the foam is higher by 17.6% than that of the conventional fins.

2- Colburn factor is higher in the case of the heat exchanger with copper foam than in the conventional fins, where it is equal to 0.1959 for the copper foam and 0.1186 for the fins. The thermal resistance is less in the case of the copper foam than in the fins, and the thermal resistance decreases with the increase in the velocity of the inlet air.

3- The pressure drop in the heat exchanger with copper foam is 75% higher than that of the heat exchanger with conventional fins at low air velocity and 30% at high air velocity. The copper foam has higher value of friction factor than fins.

4- The value of AG factor is higher in the case of fins than its value in the case of copper foam. The highest value of AG factor is 0.01244 at 5.6 m/s air velocity in the case of fins, while it is equal to 0.010691 at 4.8 m/s velocity in the case of copper foam. This means that the comparison between the dynamic and thermal performance through AG factor shows that the fins giving a better dynamic performance compared to the copper foam.

5- The porosity increases from 0.88 to 0.98, leading to a decrease in the heat transfer coefficient by 39% in the case of velocity 10 m/s and by 30%

in the case of velocity 1 m/s. The effect of porosity on Colburn factor is more effective at low air velocities. The Colburn factor decreases with an increase in porosity.

6- Pressure drop decreases by 32% when increasing the porosity from 0.88 to 0.98 at an air inlet velocity of 10 m/s. The effect of porosity is less on Δp at lower air velocities, as it decreases Δp by 25% at an air velocity of 1 m/s

7- The increase in porosity reduces j-factor and f-factor. It can be seen that the porosity slightly affects AG factor as it decreases by 14% when the porosity is increased from 0.88 to 0.98 in the case of air inlet velocity 1 m/s. The AG factor decreases 9.8 %, and 7.6 % at air inlet velocity equal to 5 m/s, and 10 m/s, respectively.

6.2. Suggestions for Future Research

The following suggestions are recommended for future work:

1- A further study with more focus on the metallic foam material type is therefore suggested.

2- Future research should be done to investigating the particulate fouling in fan coil heat exchanger with metallic foam.

3- Friction reduction during the heat exchanger with metal foam is an important issue for future research.

4- The current study examined only the air cooling, so it is possible in the future to study the air heating through a heat exchanger with copper foam.

REFERENCES

References

[1] Fakheri A., "Efficiency analysis of heat exchangers and heat exchanger networks," International Journal of Heat and Mass Transfer, vol. 76, pp. 99-104, 2014.

[2] Roetzel W., "Heat exchanger design with variable transfer coefficients for crossflow and mixed flow arrangements," International Journal of Heat and Mass Transfer, vol. 17, no. 9, pp. 1037-1049, 1974.

[3] Shah, R. K., and Sekulic, D. P. "*Fundamentals of heat exchanger design*". John Wiley and Sons, 2003.

[4] Davison, D. "the Redesign of the Amethyst Fan Coil Unit". Ph.D. dissertation. *University of Huddersfield Department of Engineering and Technology*, 2013.

[5] Naphon, P., and Wongwises, S. "A review of flow and heat transfer characteristics in curved tubes". *Renewable and sustainable energy reviews*. vol.10, PP. 463-490, 2006.

[6] Wu, F., Zhang, J., Ma, X., and Zhou, W. "Numerical simulation of gas-solid flow in a novel spouted bed: Influence of row number of longitudinal vortex generators". *Advanced Powder Technology*. vol.29, pp.1848-1858, 2018.

[7] Promvonge, P., Chompookham, T., Kwankaomeng, S. and Thianpong, C. "Enhanced heat transfer in a triangular ribbed channel with longitudinal vortex generators". *Energy Conversion and Management*, vol.51, pp.1242-1249, 2010.

[8] Mangrulkar C. K., Dhoble A. S., Chamoli S., Gupta A., and Gawande V. B., "Recent advancement in heat transfer and fluid flow

characteristics in cross flow heat exchangers," Renewable and Sustainable Energy Reviews, vol. 113, p. 109220, 2019.

[9] Parveez, B. Jamal N. A., Anuar H., Ahmad Y., Aabid A., and Baig M., "Microstructure and mechanical properties of metal foams fabricated via melt foaming and powder metallurgy technique: A review," Materials, vol. 15, no. 15, p. 5302, 2022.

[10] Chen, K., Guo, L., and Wang, H. “A review on thermal application of metal foam”. *Science China Technological Sciences*, vol.63(12), pp.2469-2490, 2020.

[11] Sertkaya, A., Altınısık, K., and Dincer, K. “Experimental investigation of thermal performance of aluminum finned heat exchangers and open-cell aluminum foam heat exchangers”. *Experimental Thermal and Fluid Science*, vol.36, pp.86-92 2012.

[12] Wadley, H. N. “Multifunctional periodic cellular metals”. *Philosophical Transactions of the Royal Society A: Mathematical, Physical and Engineering Sciences*, vol.364, pp.31-68, 2006.

[13] Klett, J., Ott, R., and McMillan, A. “Heat exchangers for heavy vehicles utilizing high thermal conductivity graphite foams”. Report No. 0148-7191, *SAE Technical Paper*, 2000.

[14] Kim, S., Paek, J., and Kang, B. “Flow and heat transfer correlations for porous fin in a plate-fin heat exchanger”. *J. Heat Transfer.* vol.122, pp.572-578, 2000.

[15] Boomsma, K., Poulikakos, D., and Zwick, F. “Metal foams as compact high performance heat exchangers”. *Mechanics of materials*. Vol.35, pp.1161-1176. 2003.

[16] Tadrist, L., Miscevic, M., Rahli, O., and Topin, F. "About the use of fibrous materials in compact heat exchangers". *Experimental thermal and fluid science*. Vol.28, pp.193-199, 2004.

[17] Tian, J., Kim, T., Lu, T. J., Hodson, H. P., Queheillalt, D. T., Sypeck, D. J., and Wadley, H. N. G. "The effects of topology upon fluid-flow and heat-transfer within cellular copper structures". *International Journal of Heat and Mass Transfer*, vol.47, pp.3171-3186, 2004.

[18] Jamin, Y. L., and Mohamad, A. A. "Enhanced heat transfer using porous carbon foam in cross flow" Part I: Forced Convection, ASME. *J. Heat Transfer*. vol.129(6), pp.735–742, 2007.

[19] Tzeng, S.-C. "Spatial thermal regulation of aluminum foam heat sink using a sintered porous conductive pipe". *International journal of heat and mass transfer*, vol.50, pp.117-126, 2007.

[20] Bonnet, J.-P., Topin, F., and Tadrist, L. "Flow laws in metal foams: compressibility and pore size effects". *Transport in Porous Media*, vol.73, pp.233-254, 2008.

[21] Cavallini, A., Mancin, S., Rossetto, L., and Zilio, C. "Heat transfer performance of Aluminum foams during single phase air flow". *IEEE Second International Conference on Thermal Issues in Emerging Technologies*, pp.405-412, 2008.

[22] T'Joen, C., De Jaeger, P., Huisseune, H., Van Herzeele, S., Vorst, N., and De Paepe, M. "Thermo-hydraulic study of a single row heat exchanger consisting of metal foam covered round tubes". *International Journal of Heat and Mass Transfer*, vol.53, pp.3262-3274, 2010..

[23] Kamath, P., Balaji, C., and Venkateshan, S. "Experimental investigation of flow assisted mixed convection in high porosity foams".

IEEE 3rd International Conference on Thermal Issues in Emerging Technologies Theory and Applications, pp.437-443, 2010.

[24] Mancin, S., Zilio, C., Rossetto, L., and Cavallini, A. "Convective Air Heat Transfer Through 10 PPI Aluminum Foams" *ASME International Heat Transfer Conference*, pp.937-946, 2011.

[25] Muley, A., Kiser, C., Sundén, B., and Shah, R. K. "Foam heat exchangers: a technology assessment". *Heat Transfer Engineering*, vol.33, pp.42-51, 2012.

[26] Nawaz, K., and Jacobi, A. M. "The Impact of Base Metal on the Thermal-Hydraulic Performance of Metal Foam Heat Exchanger for Cooling and Dehumidification Applications." *Proceedings of the ASME 2017 Heat Transfer Summer Conference*, vol.2, 2017.

[27] Chen, K., Guo, L., Xie, X., and Liu, W. "Experimental investigation on enhanced thermal performance of staggered tube bundles wrapped with metallic foam". *International Journal of Heat and Mass Transfer*, vol.122, pp.459-468, 2018.

[28] Hamadouche, A., Azzi, A., Abboudi, S., and Nebbali, R. "Enhancement of heat exchanger thermal hydraulic performance using aluminum foam". *Experimental Thermal and Fluid Science*, vol.92, pp.1-12, 2018.

[29] Borakhade, K., and Mahalle, A." Enhanced Forced Convection Heat Dissipation in Power Electronics Systems by Copper Metal Foam". *IEEE 8th Power India International Conference (PIICON)*, pp.1-5, 2018.

[30] Nilpueng, K., Asirvatham, L. G., Dalkılıç, A. S., Mahian, O., Ahn, H. S., and Wongwises, S. "Heat transfer and fluid flow characteristics in a

plate heat exchanger filled with copper foam". *Heat and Mass Transfer*, vol.56, pp.3261-3271, 2020.

[31] Salari, M., Assari, M. R., Ghafouri, A., and Pourmahmoud, N. "Experimental study on forced convection heat transfer of a nanofluid in a heat exchanger filled partially porous material". *Journal of Thermal Analysis and Calorimetry*, vol.147, pp.509–523, 2020.

[32] Rajamuthu, V. P., Panse, S. S., and Ekkad, S. V." Thermal Hydraulic Performance of High Porosity High Pore Density Thin Copper Foams Subject to Array Jet Impingement". *19th IEEE Intersociety Conference on Thermal and Thermomechanical Phenomena in Electronic Systems (ITherm)*, pp. 15-22, 2020.

[33] Rezaei, E., and Abbassi, A. "Experimental investigation of heat transfer and pressure drop in metal-foam-filled circular and flattened tubes". *Journal of Thermal Analysis and Calorimetry*, vol.146, pp.469-482, 2021.

[34] Fadhala K. G., Fayyadh E. M., and Mohammed A. F., "Effect of Copper Foam Baffles on Thermal Hydraulic Performance for Staggered Arrangement in a Duct," Engineering and Technology Journal, vol. 41, no. 01, pp. 243-256, 2023.

[35] Raju, K. S., and Narasimhan, A. "Porous medium interconnector effects on the thermohydraulics of near-compact heat exchangers treated as porous media". ASME. *J. Heat Transfer*, vol.129(3), pp.273–281, 2007.

[36] Ghosh, I. "How good is open-cell metal foam as heat transfer surface?" *ASME Journal of Heat transfer*, vol.131, 2009.

[37] Xu, H., Qu, Z., Lu, T., He, Y., and Tao, W. "Thermal modeling of forced convection in a parallel-plate channel partially filled with metallic foams". *ASME Journal of heat transfer*, vol.133 (9), 2011.

[38] Odabaee, M., Hooman, K., and Gurgenci, H. "Metal foam heat exchangers for heat transfer augmentation from a cylinder in cross-flow". *Transport in Porous Media*, vol.86, pp.911-923, 2011.

[39] Hugo, J.-M., and Topin, F. "Metal Foams Design for Heat Exchangers: Structure and Effectives Transport Properties". *Springe Heat and Mass Transfer in Porous Media*, vol.13, pp.219-244, 2012.

[40] Dai, Z., Nawaz, K., Park, Y., Chen, Q., and Jacobi, A. "A comparison of metal-foam heat exchangers to compact multilouver designs for air-side heat transfer applications". *Heat Transfer Engineering*, vol.33, pp.21-30, 2012.

[41] Huisseune, H., De Schampheleire, S., Ameel, B., and De Paepe, M. "Comparison of metal foam heat exchangers to a finned heat exchanger for low Reynolds number applications". *International Journal of Heat and Mass Transfer*, vol.89, pp.1-9, 2015.

[42] Anuar, F. S., Malayeri, M. R., and Hooman, K. "Particulate fouling and challenges of metal foam heat exchangers". *Heat Transfer Engineering*, vol.38, pp.730-742, 2017.

[43] Buonomo, B., di Pasqua, A., Ercole, D., Manca, O., and Nardini, S. "Numerical investigation on aluminum foam application in a tubular heat exchanger". *Heat and Mass Transfer*, vol.54, pp.2589-2597, 2018.

[44] Kotresha, B., and Gnanasekaran, N. "Numerical simulations of fluid flow and heat transfer through aluminum and copper metal foam heat

exchanger–A comparative study". *Heat Transfer Engineering*, vol.41, pp. 637-649, 2019.

[45] Wang, H., and Guo, L. "Volumetric convective heat transfer coefficient model for metal foams". *Heat Transfer Engineering*, vol.40, pp.464-475, 2019.

[46] Buonomo, B., di Pasqua, A., Manca, O., and Nardini, S. "Evaluation of thermal and fluid dynamic performance parameters in aluminum foam compact heat exchangers". *Applied Thermal Engineering*. vol.176, pp.115456, 2020.

[47] Buonomo, B., Pasqua, A. d., Manca, O., Sekrani, G., and Poncet, S. "Numerical Analysis on Pressure Drop and Heat Transfer in Nanofluids at Pore Length Scale in Open Metal Porous Structures with Kelvin Cells". *Heat Transfer Engineering*, vol.42, pp.1614-1624, 2021.

[48] Hwang, J.J., Hwang, G.J., Yeh, R.H., and Chao, C.H. "Measurement of interstitial convective heat transfer and frictional drag for flow across metal foams". *J. Heat Transfer*. vol.124, pp.120-129, 2002.

[49] Lu, T., Valdevit, L., and Evans, A. "Active cooling by metallic sandwich structures with periodic cores". *Progress in Materials Science*, vol.50, pp.789-815, 2005.

[50] Han, X. H., Wang, Q., Park, Y. G., T'Joen, C., Sommers, A., and Jacobi, A. "A review of metal foam and metal matrix composites for heat exchangers and heat sinks". *Heat Transfer Engineering*, vol.33, pp.991-1009, 2012.

[51] Tsolas, N., and Chandra, S., "Forced convection heat transfer in spray formed copper and nickel foam heat exchanger tubes". *Journal of heat transfer*, vol.134(6), 2012.

[52] De Jaeger, P., T'Joen, C., Huisseune, H., Ameel, B., De Schampheleire, S., and De Paepe, M. "Influence of geometrical parameters of open-cell aluminum foam on thermohydraulic performance". *Heat transfer engineering*, vol.34, pp.1202-1215, 2013..

[53] Mancin, S., Zilio, C., Diani, A., and Rossetto, L. "Air forced convection through metal foams: Experimental results and modeling". *International Journal of Heat and Mass Transfer*, vol.62, pp.112-123, 2013.

[54] Amori K. E. and Khalaf D. A., "Thermal Analysis of Metal Foam Heat Sink Subjected To Impingement Jet Cooling," Iraqi journal of mechanical and material engineering, vol. 15, no. 1, 2015.

[55] Chen, K., Guo, L., and Wang, H. "A review on thermal application of metal foam". *Science China Technological Sciences*, vol.63(12), pp.2469-2490, 2020.

[56] Michele, C. Stability, "Viscous Dissipation and Local Thermal non-Equilibrium in Fluid Saturated Porous Media". Ph.D. thesis, *University of Bologna*, 2010.

[57] Combarnous, M., and Bories, S. "Hydrothermal Convection in Saturated Porous Media1", *Advances in hydroscience, Elsevier*, vol. 10, pp. 231-307, 1975.

[58] Cengel, Y. A. "*Introduction to thermodynamics and heat transfer: Engineering*", Book, 2nd ed., Publisher: McGraw-Hill. 2008.

[59] Kays, W. M., and London, A. L. "Compact heat exchangers". Book, 3rd ed., McGraw Hill, 1984.

[60] Bell, S. A. A "beginner's guide to uncertainty of measurement". Center for Basic, *Thermal and Length Metrology National Physical Laboratory*. Measurement Practice Guide No.1, Issue 2., 2001.

[61] Ingham D., "Governing equations for laminar flows through porous media," in Emerging Technologies and Techniques in Porous Media: Springer, 2004, pp. 1-11.

[62] Hans, T. A. "The effective Thermal Conductivity of Saturated Porous Media". M.Sc. thesis, *University of Minnesota*, 1999.

[63] Zhao M. and Cheng L., "Finite element analysis of flow control using porous media," Ocean Engineering, vol. 37, no. 14-15, pp. 1357-1366, 2010.

[64] Bergman, T. L., Incropera, F. P., DeWitt, D. P., and Lavine, A. S. "*Fundamentals of heat and mass transfer*". Book 6th ed., John Wiley & Sons, 2011.

[65] Özişik, M. N., Orlande, H. R., Colaço, M. J., & Cotta, R. M. "*Finite Difference Methods in Heat Transfer*". Book, 2nd ed., Boca Raton, 2019.

[66] Marshall, E. M., and Bakker, A. "*Computational fluid mixing*". Handbook of industrial mixing: science and practice (Wiley), pp.257-343, 2004.

[67] Wang, T., Luan, W., Liu, T., Tu, S.-T., and Yan, J. "Performance enhancement of thermoelectric waste heat recovery system by using metal foam inserts". *Energy conversion and management*, vol.124, pp.13-19, 2016.

[68] Wang, Y., Tian, H., Shu, G., Yu, G., Ma, X., and Li, X. "Simulation and optimization of metal-foam tube banks for heat transfer enhancement

of exhaust heat exchangers". *Energy Procedia*, vol.142, pp.3863-3869, 2017.

[69] De Schampheleire, S., De Jaeger, P., Huisseune, H., Ameel, B., T'Joen, C., De Kerpel, K., and De Paepe, M. "Thermal hydraulic performance of 10 PPI aluminium foam as alternative for louvered fins in an HVAC heat exchanger". *Applied Thermal Engineering*, vol.51, pp.371-382, 2013..

[70] Ho, J., Leong, K., and Wong, T. "Additively-manufactured metallic porous lattice heat exchangers for air-side heat transfer enhancement". *International Journal of Heat and Mass Transfer*, vol.150, 119262, 2020.

[71] Xia, L., Chan, M., Deng, S., and Xu, X. "Analytical solutions for evaluating the thermal performances of wet air cooling coils under both unit and non-unit Lewis Factors". *Energy Conversion and Management*, vol.51, pp.2079-2086, 2010.

[72] Mansour, M. K., and Hassab, M. "Novel approach of thermal modeling of partially dry–wet chilled water cooling coil under unit and nonunit Lewis number conditions". *Numerical Heat Transfer*, Part B: Fundamentals, vol.70, pp.164-181, 2016.

[73] Bergman, T. L., Bergman, T. L., Incropera, F. P., Dewitt, D. P., and Lavine, A. S. "*Fundamentals of heat and mass transfer*". John Wiley & Sons, 2011.

[74] Holman, J. P. "*Heat transfer*". Book,10th ed., McGraw Hill Higher Education, 2010.

[75] Bejan, A., and Kraus, A. D. "*Heat transfer handbook*". John Wiley & Sons, vol.1, 2003.

APPENDICES

Appendix (A): Effectiveness –NTU Method

The ε-NTU-method will be used to calculate the dimensions of the cross flow heat exchanger. These calculation depends upon the data assumption in table (A-1). [71]. The physical and thermal properties of the materials use in this study are shown in table (A-2).

1- calculating of the length of heat exchanger

The length of cooling coil tube can be calculated based on the water side heat transfer area (Ai) as pointed by Mansour and Hassab [72]

$$L_t = \frac{A_i}{\pi * d_i} \tag{A.1}$$

Where Ai pointed by Mansour and Hassab [72] as following:

$$A_i = A_o / 24 \tag{A.2}$$

A_o is the overall air side heat transfer area calculated from:

$$A_o = \frac{\text{NTU } C_{\min}}{\text{U}} \tag{A.3}$$

Where NTU is number of transfer units and calculated through the following equation as explained by Bergman et al. [73]:

$$\text{NTU} = -\ln\left[1 + \left(\frac{1}{C_r}\right)\ln\left(1 - \varepsilon C_r\right)\right] \tag{A.4}$$

The cooling load that will be 2 TR in order to find the appropriate FCU dimensions. First, the heat capacity rates will be calculated from the following equation:

$$C_c = \dot{m}_c c_{p,c} \tag{A.5}$$

$$C_h = \dot{m}_h c_{p,h} \tag{A.6}$$

Where the subscript (c) is for the cold fluid, which is water, and (h) for the hot, which is air. Through the above equations, the maximum and minimum value of the rate of heat capacity is determined, then it is found on the maximum heat transfer as explained by Bergman et al. [73] through the following equation:

$$q_{max} = C_{min}\left(T_{h,in} - T_{c,in}\right) \tag{A.7}$$

effectiveness is found by Bergman et al. [73] as following:

$$\varepsilon = \frac{q_{\text{actual}}}{q_{max}} \tag{A.8}$$

Where q_{actual} represents the cooling load required to design the fan on its basis. The ratio of specific heat C_r found by Bergman et al. [73] as following:

$$C_r = \frac{C_{\text{h}}}{C_{\text{c}}} \tag{A.9}$$

Where C_c represents the heat capacity of water, which is the water that does not mix during the flow in the tubes of the cross flow heat exchanger, while C_h represents the heat capacity of the air, which is the fluid that mixes during the flow around the tubes of the cross flow heat exchanger.

Estimation of the overall heat transfer coefficient from the following equation:

$$U = \left[\frac{1}{h_i} + \frac{1}{h_o}\right]^{-1} \tag{A.10}$$

$$h_i = \frac{Nu_{di} * k}{d_i} \tag{A.11}$$

$$Nu_{di} = \frac{h_i D}{k} = 0.023 \mathrm{Re}_{di}^{0.8} \; Pr_w^{0.4} \tag{A.12}$$

$$\mathrm{Re}_{di} = \frac{u_{in,w} \, d_i}{v_w} = \frac{4\left(\dot{m}_w\right)_i}{\pi d_i \mu_w} \tag{A.13}$$

$$h_o = \frac{Nu_o * k}{d_o} \tag{A.14}$$

$$\mathrm{Re}_{o,\max} = \frac{u_{\max} d_o}{v_a} \tag{A.15}$$

As for the staggered arrangement, the maximum air velocity is calculated by

$$u_{max} = u_{a,in} \frac{S_T}{2\left[\sqrt{S_L^2 + \left(\frac{S_T}{2}\right)^2} - d_o\right]} \tag{A.16}$$

S_T and S_L is the vertical and horizontal distance between tubes and they assumed to 3cm.

The outer Nusselt number for air side can be calculated by the following equation was proposed by Holman [74].

$$Nu_o = C_1 C_2 \, Re_{o,\max}^m Pr^{0.36} \left(\frac{Pr}{Pr_s}\right)^{0.25} \tag{A.17}$$

Where C_1, C_2, and m are constants that are extracted from figure (A-2) and table (A-3), where C_1 depends on the number rows and the

arrangement of tubes, while C_2 depends on the distance between the tubes, the arrangement of tubes.

Table (A-1) data design requirements.

Water mass flow rate (kg/s)	0.1133
inlet water temperature (°C)	10
inlet air temperature (°C)	35
Cooling load (W)	2TR=7040 (W)

Table (A-2) thermo- physical properties of materials (at 295 K). Ref. [73]

Material	ρ (kg/m^3)	c_p (J/kg.°C)	k (W/m. °C)	μ (N.s/m^2)	Pr
Water	998	4181	0.606	0.959×10^{-3}	6.62
Air	1.1614	1007	0.0263	0.1846×10^{-3}	0.707
Copper	8933	385	401	-	-

The model is based on the initial assumption shown in table (A-1), and solved by using ε-NTU method with EES software. This software is compact tool integrated in many technical books so the EES software easy to used and developed further. In this approach one parameter is updated while the other remain constant, and the location of variable and constant parameter are changed until the optimization procedure cover all potential configuration, as illustrated in the flow chart in figure (A-3). The final dimensions of the cross flow heat exchanger that were found by ε-NTU method can be illustrated by the table (A-4). The air and water temperatures will be recalculated based on the Solid Work software. The comparison between the results of the current study and the results of Xia et al. [71] can be seen in the table (A-5).

Table (A-3) constants C_2 and m for equation (17) Ref.[75]

Arrangement	*Re*	S_T / S_L	C_2	*m*
Aligned	10 -10^2	any	0.80	0.40
	10^2 -10^3	any	Treat as a single tubes, eq. 17	
	10^3 - 2×10^5	≥ 0.7	0.27	0.63
	10^3 - 2×10^5	< 0.7	Heat transfer inefficient, other	
	2×10^5-10^6	any	0.021	0.84
	10 -10^2	any	0.90	0.40
	10^2 -10^3	any	Treat as a single tubes, eq. 17	
Staggered	10^3 - 2×10^5	≥ 2	0.40	0.60
	10^3 - 2×10^5	< 2	$0.35\left(\frac{S_T}{S_L}\right)^{0.2}$	0.60
	2×10^5-10^6	any	0.022	0.84

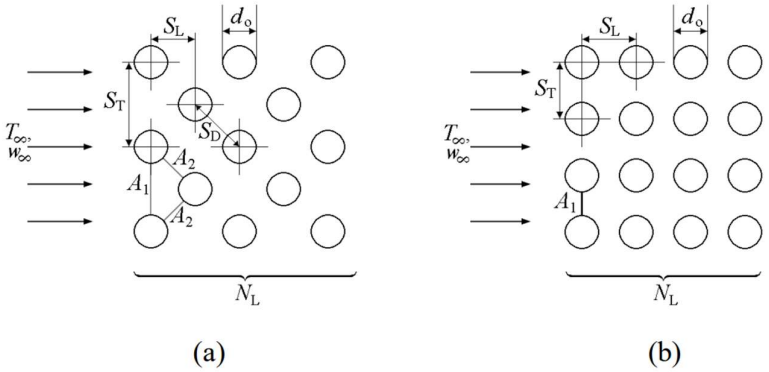

Figure (A-1) tube bank arrangements: a) staggered, b) in-line Ref. [73].

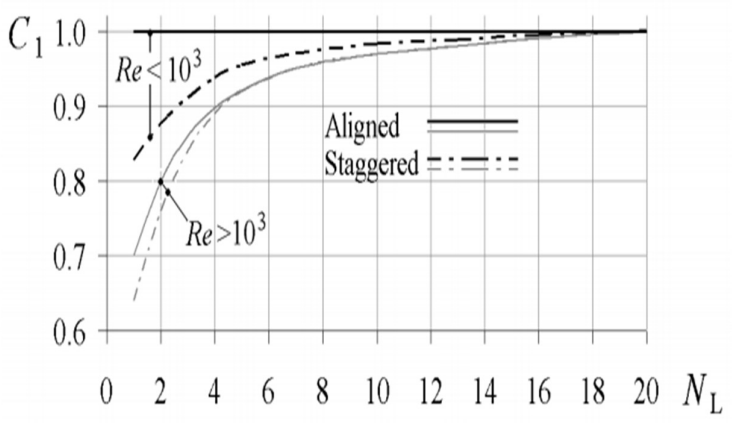

Figure (A-2) correction for equation (14). Ref.[75], and Ref. [73]

Table (A-4) Dimension of heat exchanger by using ε-NTU method for different water mass flow rate, and air velocity at 2TR.

$\dot{m}_w$ (kg/s)	Ai (m^2)	Total tube length (m)
0.05	0.6061	24.13
0.07	0.5141	20.47
0.09	0.4607	18.34
0.11	0.425	16.92
0.13	0.3992	15.89
$u_{a,in}$ (m/s)	Ai (m^2)	Total tube length (m)
1	0.7124	28.36
2	0.5404	21.51
3	0.4599	18.31
4	0.4101	16.33
5	0.3753	14.94

Table (A-5) comparison between the simulation results obtained from the present model and those of Xia et al. [71].

Parameter	Current study	Xia et al. [71]
Water inlet temperature (°C)	10	8
Air inlet temperature (°C)	35	24
Water mass flow rate (kg/s)	0.1	0.35
Air velocity (m/s)	1.5	1.2
Chilled water heat transfer coefficient ($W/m^2.°C$)	9299	8000
Air heat transfer coefficient ($W/m^2.°C$)	35.49	70
Tube inside diameter (m)	0.008	0.00886
Tube outer diameter (m)	0.0092	0.00952
Height of heat exchanger (m)	0.4	0.45
Depth of heat exchanger (m)	0.12	0.13
length of heat exchanger (m)	0.4	0.42
Tube material	Copper	Copper
Fine material	Aluminum	Aluminum

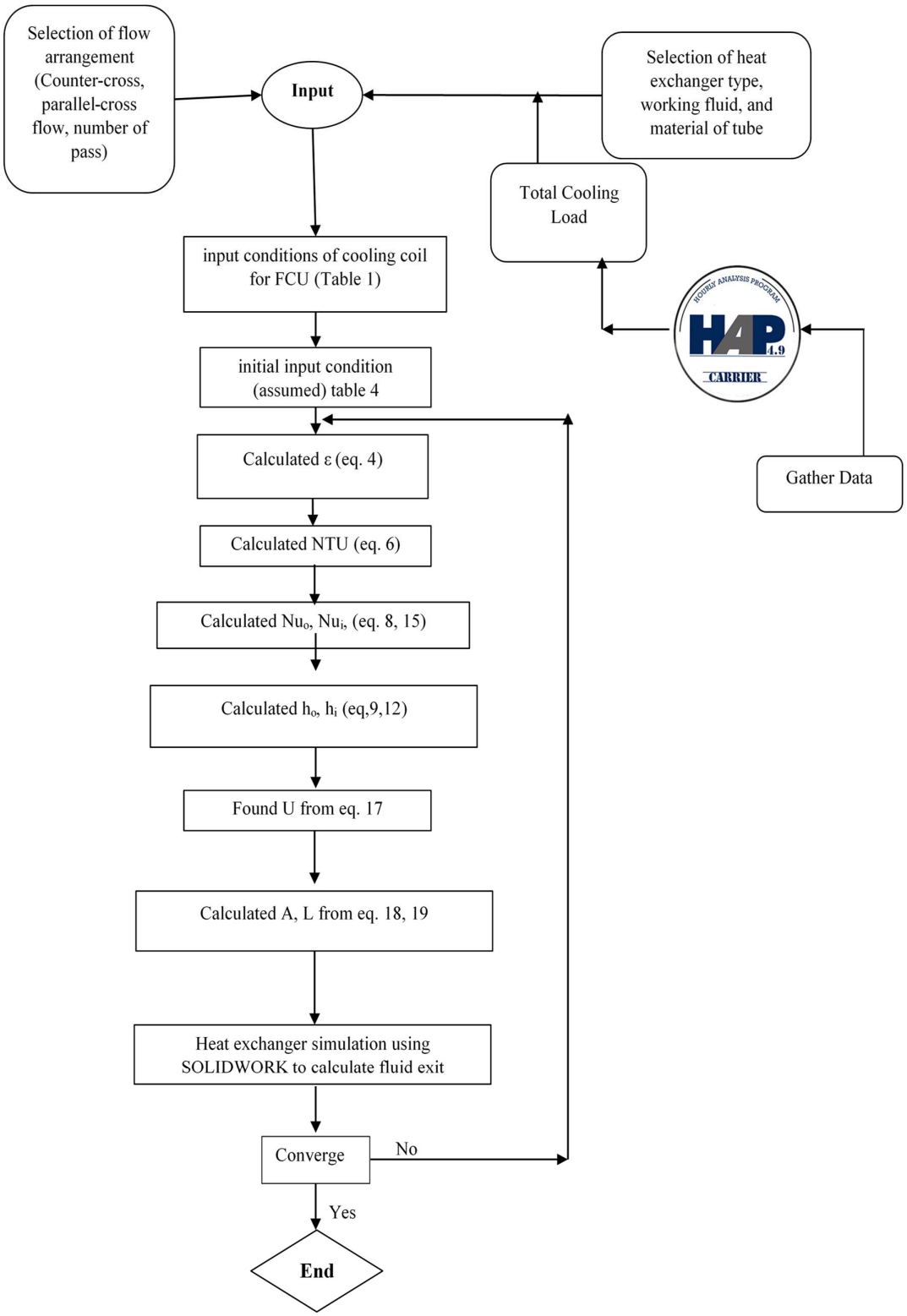

Figure (A-3) optimization algorithm for FCU heat exchanger designe flowchart.

Appendix (B): Cooling Load Estimation

Carrier's Hourly Analysis Program (HAP). HAP is a computer tool which assists engineers in designing Heating, Ventilation, and Air Conditioning (HVAC) systems for commercial buildings. HAP is two tools in one. First it is a tool for estimating loads and designing systems. Second, it is a tool for simulating energy use and calculating energy costs. (HAP) uses the ASHRAE-endorsed transfer function method for load calculations and detailed 8,760 hour-by-hour energy simulation techniques for the energy analysis. HAP estimates design cooling and heating loads for commercial buildings in order to determine required sizes for (HVAC) system components. Ultimately, the program provides information needed for selecting and specifying equipment.

The procedure for designing (HVAC) systems in (HAP) involves four steps:

1. Define the Problem: The objective of section is to design an (HVAC) system which serves one room of a house building located in Iraq. The room for which the air conditioning system is to be designed with dimensions (3×1.7×3) m^3.

2. Gather Data: The second step in the design process is to gather information necessary to model heat transfer processes in the building and to analyze operation of the (HVAC) equipment which heats and cools the building. This involves gathering data for the building, its environment and its (HVAC) equipment.

3. Enter Data into HAP: After weather, space and (HVAC) system data has been gathered, it is entered into (HAP). This is the third step in the design process. The procedure for entering data into (HAP) by using Schedule Input Data in HAP software.

4. Use HAP to Generate Design Report: The fourth step in the design process is to use the data entered in step 3 to perform system design calculations and generate system design reports.

Appendix (C): Fan coil unit heat exchanger by SOLID WORK

The process of designing the heat exchanger using the SolidWorks software is carried out through the following steps:

A- Drawing process of the model and forming the shape of the cooling coil. This process is done by using the command (Swept) after drawing two circles representing the inner and outer diameter of the tube. Then, drawing the path that determines the shape of the tube and the coils of the tube through the heat exchanger, as shown in figure (C-1). Choosing the shape of the cooling coil, the number of tubes, the arrangement of the tubes, and the formation of the heat exchanger is done using a solid work, as shown in figure (C-2).

B- Then, the numerical solution process is done using the flow simulation that includes in the SolidWorks software. Where, the flow simulation depends on the basic flow equations, which includes the Navier-Stoke equations and the mass and energy conservation equations.

C- Design processes by using SolidWorks depend on parametric study solver and flow simulation as shown in figure (C-3). The parametric study solver consists of the following steps:

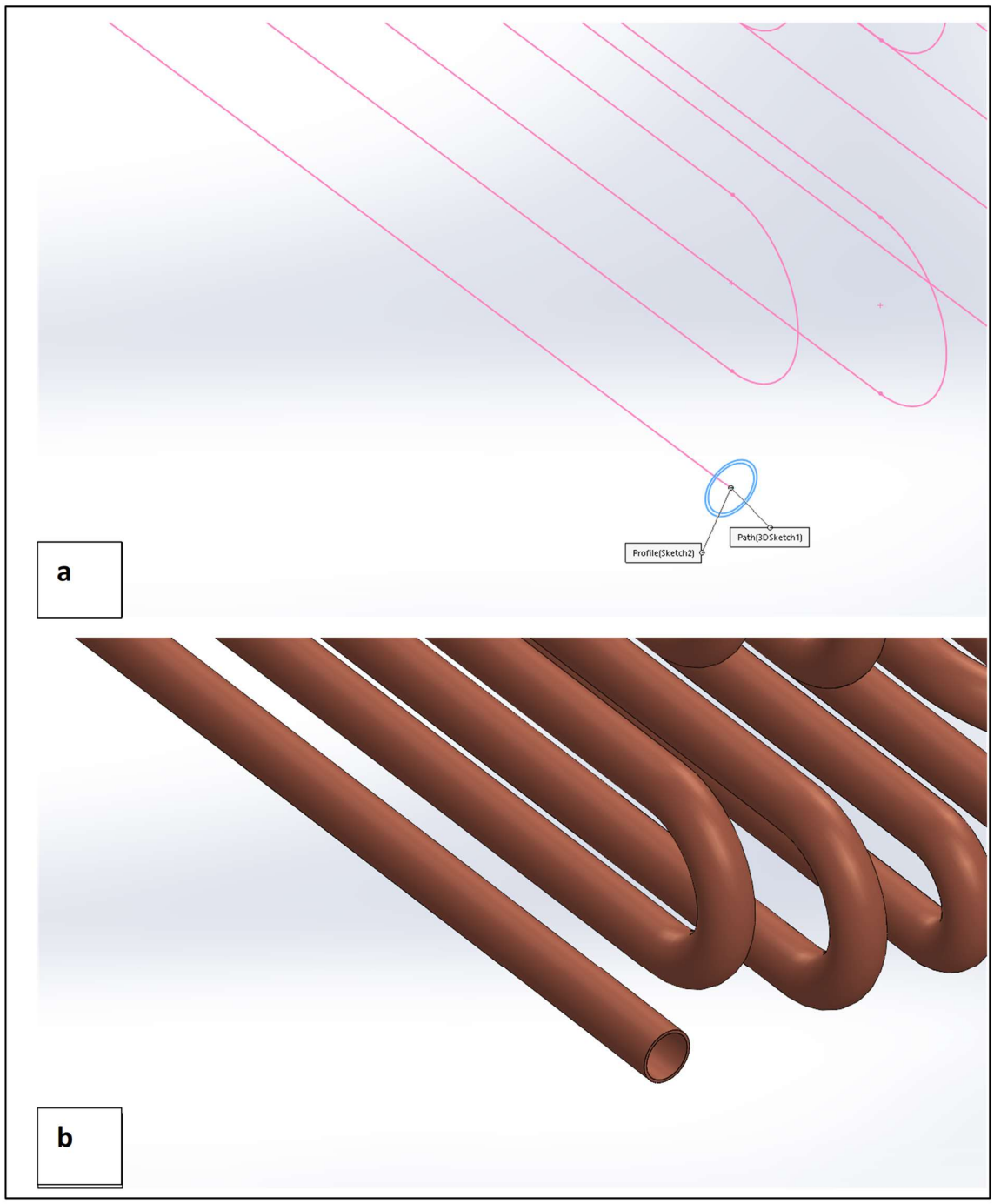

Figure (C- 1) drawing process by solid work (a) define inner and outer diameter of tube, (b) tube geometry after swept command.

I- Input variables: Through this window the water mass flow rate and tube diameter are input as a range between tow values as shown in figure (C-4).

II- Goal optimization: In this step, the target value of water and air temperature are selected as shown in figure (C-5).

III- Output parameters: In this step, the simulation and design results are presented as shown in figure (C-6).

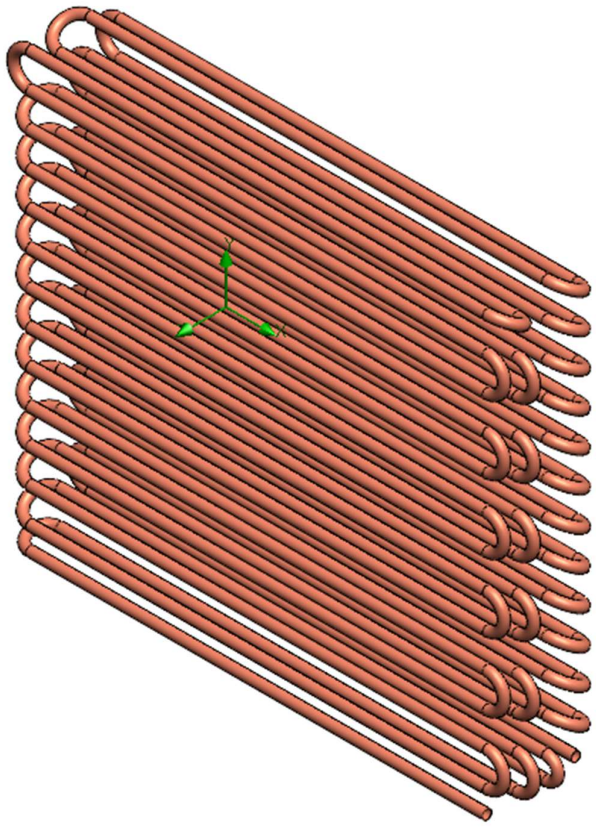

Figure (C- 2) geometry of fan coil heat exchanger.

IV- Scenario: The SolidWorks selected different scenarios to design the cooling coil, and to select the optimum tube diameter, as shown in figure (C-6). The SolidWorks suggests different design points are based on the tube diameter and mass flow rate.

The dimensions of the heat exchanger are chosen according to the design results as shown in table (C-1), and figure (C-6).

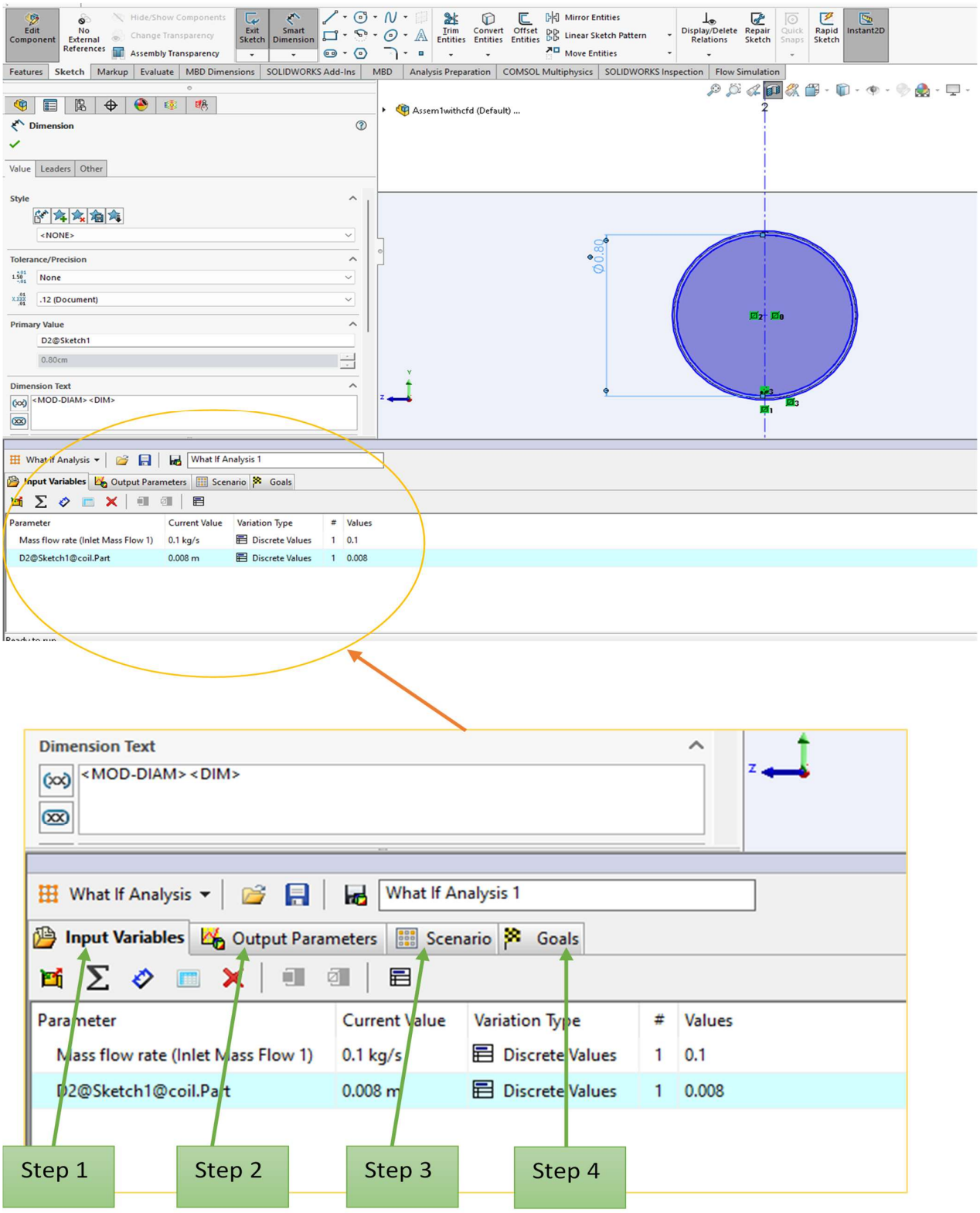

Figure (C-3) design process by using solidwork parametric study.

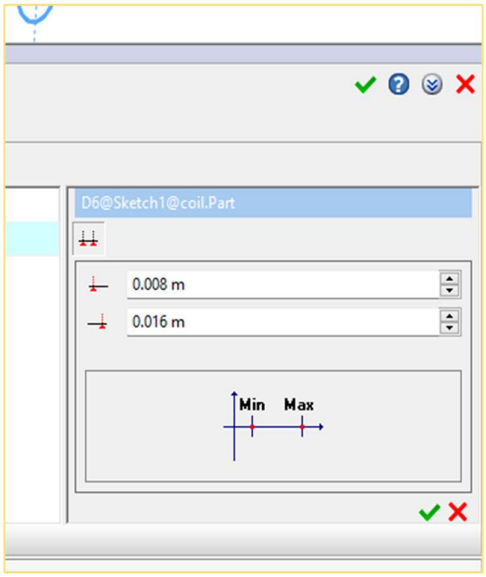

Tube Diameter range input to solid work parametric study.

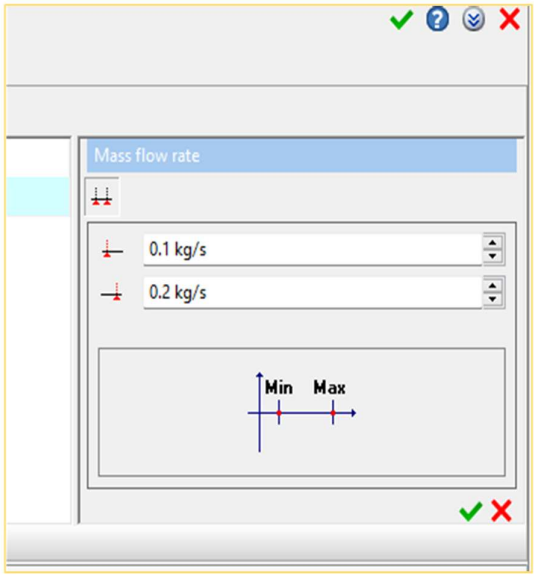

Water mass flow range input to solid work parametric study.

Figure (C-4) goal optimization process for tube diameter and water mass flow rate.

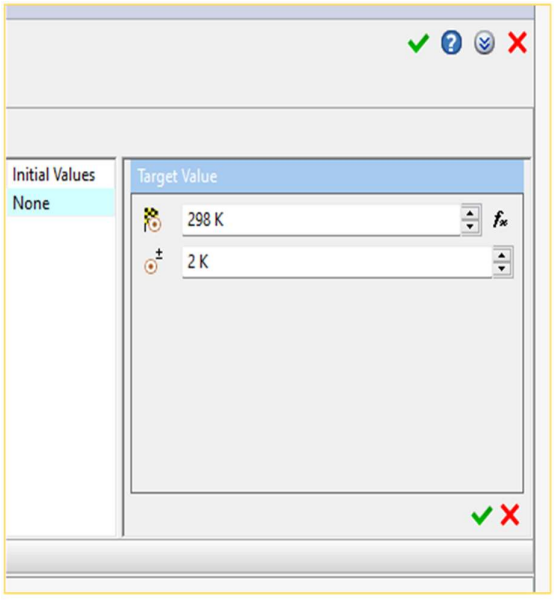

Water outlet target temperature, and deviation value in design process.

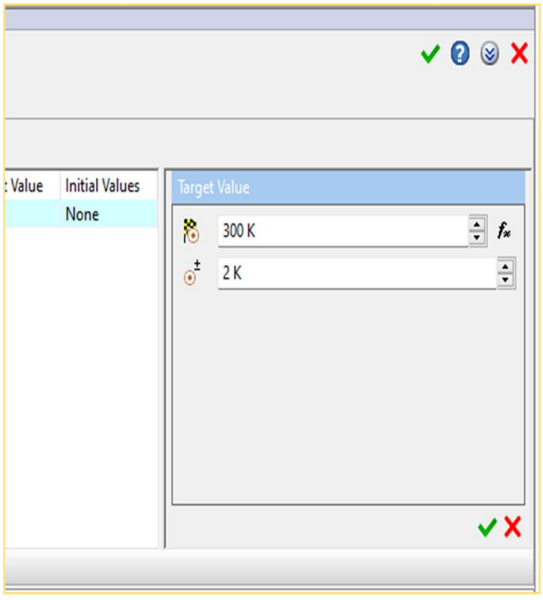

Air outlet target temperature, and deviation value in design process.

Figure (C-5) target design outlet temperatures with maximum deviation.

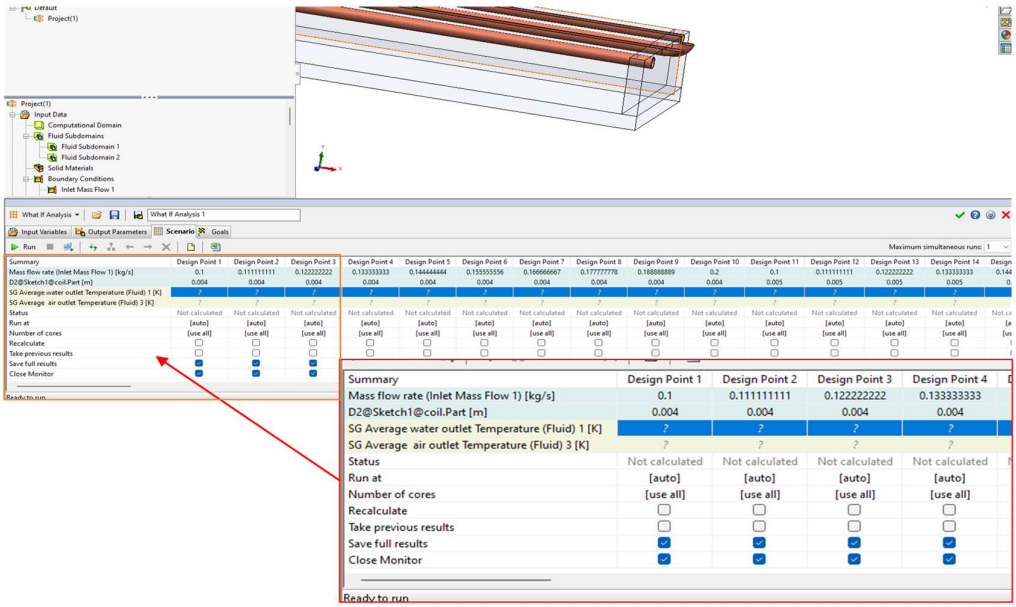

Figure (C-6) scenario window (SolidWorks suggestion for design points)

Table (C-1) dimensions of heat exchanger

Parameter	Value
Number of rows	4
Number of tubes	52
Total tube length (m)	20.8
External surface area of tubes (m^2)	0.6008
Height of coil (m)	0.4
Width of coil (m)	0.4
Depth of coil (m)	0.12
Surface to volume ratio (m^2/m^3)	543
Fin thickness (mm)	0.12
Transvers pitch (m)	0.03
longitudinal distance (m)	0.03

Appendix (D) Experimental Data

Table (D-1) inlet and outlet temperature for air and water variation with experiment time at case 2 conditions.

Time (min)	T_1 (°C)	T_2 (°C)	T_3 (°C)	T_4 (°C)
1	10.4	22.7	35.4	29.0
2	10.2	20.2	33.9	26.8
3	10.6	19.1	32.9	25.7
4	9.7	18.5	32.2	25.2
5	9.6	17.9	32.0	24.7
6	9.9	17.4	31.3	24.3
7	9.9	16.8	31.4	23.9
8	10.1	16.7	31.1	23.4
9	10.1	16.3	30.6	23.2
10	10.0	15.8	30.7	23.1
11	10.6	15.6	30.1	22.6
12	10.5	15.6	30.2	22.6
13	10.7	15.4	29.8	22.4
14	10.5	15.0	29.7	22.3
15	10.5	15.1	29.6	22.1
16	10.4	15.1	29.3	21.8
17	10.4	14.8	29.5	21.7

18	10.5	14.7	29.2	21.8
19	10.9	14.5	29.3	21.7
20	10.7	14.7	29.2	21.5
21	11.0	14.4	29.0	21.1
22	11.0	14.4	28.7	21.1
23	11.2	14.4	28.7	21.2
24	11.5	14.3	28.8	20.9
25	11.6	13.8	28.3	21.0
26	11.8	13.9	28.3	21.1
27	11.2	13.7	28.4	20.6
28	10.3	13.8	28.3	20.6
29	10.6	13.6	28.2	20.6
30	10.2	13.1	28.1	20.4

Table (D-2) front of heat exchanger temperature variation with experiment time at case 2 conditions.

T_5(°C)	T_6(°C)	T_7(°C)	T_8(°C)	T_9(°C)	T_{10}(°C)	T_{11}(°C)	T_{12}(°C)	T_{13}(°C)
11.7	12.4	12.8	11.8	12.7	13.1	12.0	12.7	13.2
11.5	11.9	12.7	11.9	12.0	12.5	12.0	12.4	13.0
12.2	12.6	13.0	12.3	12.6	13.2	12.2	13.1	13.5
11.0	11.4	12.0	11.3	11.7	12.2	11.5	12.0	12.4
10.9	11.4	12.0	11.0	11.4	11.8	11.4	11.5	12.4

11.4	11.7	12.1	11.2	12.1	12.5	11.5	12.0	12.6
11.4	11.7	12.2	11.3	11.8	12.5	11.8	12.1	12.5
11.2	11.8	12.3	11.6	12.3	12.7	11.8	12.3	12.9
11.3	11.9	12.3	11.5	12.2	12.4	11.9	12.2	12.9
11.3	11.8	12.1	11.5	12.2	12.6	11.6	12.3	12.5
11.9	12.5	13.2	12.2	12.7	13.0	12.6	12.7	13.5
12.1	12.4	13.1	12.3	12.7	12.9	12.4	13.0	13.3
12.2	12.5	13.1	12.5	12.6	13.3	12.3	13.2	13.8
11.8	12.2	12.7	11.9	12.8	12.9	12.2	12.8	13.4
12.1	12.6	12.7	12.1	12.4	13.2	12.3	12.7	13.4
11.9	12.2	13.0	12.0	12.3	12.9	12.4	12.7	13.0
11.9	12.5	12.8	12.0	12.5	13.2	12.4	12.8	13.1
11.9	12.5	12.9	12.2	12.6	13.3	12.1	12.8	13.3
12.5	12.6	13.5	12.3	13.3	13.7	12.9	13.1	13.8
11.9	12.7	13.0	12.4	12.9	13.2	12.3	13.0	13.5
12.6	12.8	13.3	12.5	13.4	13.6	12.8	13.3	14.1
12.4	13.1	13.3	12.6	13.0	13.8	12.7	13.3	13.9
12.4	13.0	13.6	13.0	13.3	13.9	13.3	13.6	14.4
13.0	13.7	13.9	13.0	13.6	14.5	13.3	14.0	14.8
13.1	13.8	14.1	13.2	14.1	14.5	13.7	14.3	14.5

13.4	13.8	14.7	13.5	14.1	14.7	13.6	14.2	14.9
12.4	13.3	13.9	13.0	13.2	13.9	13.3	13.8	14.1
11.8	11.9	12.7	11.8	12.2	12.9	12.2	12.5	12.9
12.1	12.3	13.0	12.2	12.7	13.3	12.4	13.1	13.2
11.6	11.8	12.5	11.6	12.4	12.7	12.0	12.3	13.1

Table (D-3) back of heat exchanger temperature variation with experiment time at case 2 conditions.

T_{14}(ºC)	T_{15}(ºC)	T_{16}(ºC)	T_{17}(ºC)	T_{18}(ºC)	T_{19}(ºC)	T_{20}(ºC)	T_{21}(ºC)	T_{22}(ºC)	T_{23}(ºC)
18.7	19.6	20.6	18.7	18.9	20.2	18.4	18.8	19.8	32.4
16.9	17.5	18.2	16.6	16.7	18.0	16.1	16.8	17.9	29.8
16.1	16.2	17.4	15.7	16.1	16.9	15.2	16.0	17.0	29.0
15.7	15.7	16.8	15.3	15.7	16.7	15.0	15.3	16.5	28.5
15.0	15.5	16.4	14.9	15.1	16.1	14.3	14.7	15.7	27.8
14.6	14.9	15.6	14.1	14.3	15.8	14.2	14.4	15.4	27.3
14.0	14.4	15.3	13.6	14.2	15.3	13.7	13.8	15.0	26.8
14.2	14.1	15.0	13.7	14.0	14.9	13.3	14.0	14.8	26.5
13.5	13.8	14.9	13.1	13.4	14.5	13.0	13.3	14.6	25.9
13.5	13.4	14.3	13.2	13.1	14.4	12.8	12.9	14.3	25.9
12.9	13.4	14.4	12.8	12.9	13.8	12.7	12.7	13.8	25.5
13.3	13.6	14.0	13.0	13.1	13.8	12.5	12.8	13.7	25.3
13.1	13.0	13.9	12.8	13.0	13.9	12.6	12.8	13.8	25.1

12.8	12.7	13.8	12.4	12.8	13.4	12.0	12.3	13.5	25.0
12.5	13.0	13.6	12.5	12.9	13.7	12.0	12.6	13.4	24.9
12.5	13.0	13.7	12.3	12.7	13.5	12.5	12.5	13.5	24.6
12.4	12.7	13.3	12.4	12.2	13.3	11.8	12.2	13.0	24.2
12.4	12.6	13.6	12.2	12.1	13.3	11.7	12.2	13.2	24.6
12.3	12.7	13.4	12.1	12.3	13.0	11.6	11.9	12.7	24.4
12.1	12.6	13.6	12.0	12.2	13.0	11.8	12.2	13.3	24.3
12.1	12.5	13.3	12.0	11.9	12.7	11.4	12.1	12.8	23.8
12.3	12.4	12.9	11.6	12.0	13.0	11.7	12.0	12.7	23.5
12.1	12.3	13.1	11.8	12.1	12.8	11.6	12.1	12.7	24.1
12.0	12.3	13.1	11.7	11.9	12.7	11.5	11.9	12.6	23.5
11.4	11.7	12.5	11.1	11.4	12.6	11.2	11.5	12.4	23.5
11.9	12.1	12.8	11.5	11.8	12.3	11.3	11.8	12.3	23.9
11.8	11.9	12.3	11.2	11.8	12.3	11.1	11.4	12.3	23.4
11.4	11.7	12.4	11.5	11.4	12.3	11.2	11.3	12.5	23.2
11.2	11.7	12.5	11.3	11.6	12.2	11.1	11.4	12.3	22.9
10.9	11.3	11.9	11.0	11.0	12.0	10.8	10.7	11.5	23.1

Table (D-4) inlet and outlet temperature for air and water variation with experiment time at case 3 conditions.

Time (min)	T_1 (°C)	T_2 (°C)	T_3 (°C)	T_4 (°C)
1	10.6	20.7	35.3	28.2
2	10.3	18.6	34.0	26.4
3	10.3	17.6	33.1	25.0
4	10.3	16.6	32.5	24.5
5	9.4	16.2	32.0	24.1
6	9.7	15.6	31.4	23.7
7	9.7	15.7	31.2	23.4
8	9.8	15.0	30.5	22.8
9	9.9	15.0	30.5	22.7
10	9.6	14.7	30.2	22.2
11	9.8	14.4	29.9	22.0
12	9.5	14.1	30.0	22.0
13	10.0	14.1	29.9	21.8
14	10.6	13.9	29.7	21.9
15	10.5	13.7	29.5	21.4
16	10.3	13.6	29.3	21.3
17	10.7	13.8	29.3	21.0
18	10.7	13.7	28.9	20.9

19	10.6	13.3	29.0	21.1
20	11.0	13.3	28.6	20.9
21	10.9	13.1	28.4	21.0
22	10.8	12.9	28.4	20.6
23	10.9	12.8	28.3	20.4
24	11.6	12.8	28.3	20.5
25	10.8	12.9	28.0	20.5
26	10.9	12.8	27.9	20.5
27	11.6	12.9	28.2	20.2
28	11.3	12.7	27.8	20.1
29	10.8	12.5	27.7	19.5
30	10.3	12.5	28.0	19.3

Table (D-5) front of heat exchanger temperature variation with experiment time at case 3 conditions.

T_5(ºC)	T_6(ºC)	T_7(ºC)	T_8(ºC)	T_9(ºC)	T_{10}(ºC)	T_{11}(ºC)	T_{12}(ºC)	T_{13}(ºC)
12.0	12.6	13.0	12.1	12.9	13.3	12.2	12.9	13.4
11.6	12.0	12.9	12.0	12.2	12.7	12.1	12.6	13.2
11.8	12.2	12.7	11.9	12.3	12.9	11.8	12.8	13.2
11.6	12.0	12.8	11.9	12.5	13.0	12.1	12.8	13.2
10.6	11.2	11.8	10.7	11.2	11.6	11.2	11.3	12.2
11.2	11.5	11.8	11.0	11.8	12.2	11.3	11.7	12.3

11.2	11.5	11.9	11.1	11.5	12.2	11.6	11.8	12.2
10.9	11.5	12.0	11.3	12.0	12.4	11.5	12.0	12.6
11.1	11.7	12.1	11.3	12.0	12.2	11.7	12.0	12.7
10.9	11.3	11.6	11.1	11.7	12.1	11.1	11.8	12.0
11.0	11.6	12.3	11.3	11.8	12.1	11.7	11.8	12.6
11.0	11.2	11.9	11.1	11.5	11.7	11.2	11.8	12.1
11.4	11.7	12.3	11.7	11.8	12.4	11.5	12.4	12.9
11.9	12.3	12.8	12.0	12.9	13.0	12.3	12.9	13.5
12.1	12.6	12.7	12.1	12.4	13.2	12.3	12.7	13.4
11.8	12.0	12.9	11.9	12.2	12.8	12.2	12.6	12.9
12.3	12.8	13.1	12.4	12.8	13.6	12.7	13.1	13.5
12.1	12.7	13.1	12.4	12.8	13.6	12.3	13.0	13.6
12.2	12.3	13.1	12.0	12.9	13.3	12.6	12.7	13.4
12.2	13.1	13.4	12.7	13.3	13.5	12.6	13.4	13.8
12.5	12.6	13.2	12.4	13.3	13.5	12.7	13.2	14.0
12.2	12.8	13.1	12.4	12.7	13.6	12.5	13.1	13.7
12.1	12.6	13.3	12.7	13.0	13.5	12.9	13.3	14.0
13.1	13.8	14.0	13.1	13.7	14.7	13.4	14.1	14.9
12.2	12.9	13.2	12.3	13.1	13.5	12.8	13.4	13.5
12.4	12.7	13.6	12.5	13.1	13.6	12.5	13.2	13.8

12.9	13.7	14.4	13.5	13.7	14.4	13.7	14.3	14.6
12.9	13.1	13.9	13.0	13.3	14.1	13.4	13.6	14.1
12.3	12.5	13.3	12.4	12.9	13.6	12.6	13.4	13.5
11.7	11.9	12.7	11.7	12.6	12.9	12.1	12.5	13.3

Table (D-6) back of heat exchanger temperature variation with experiment time at case 2 conditions.

T_{14}(ºC)	T_{15}(ºC)	T_{16}(ºC)	T_{17}(ºC)	T_{18}(ºC)	T_{19}(ºC)	T_{20}(ºC)	T_{21}(ºC)	T_{22}(ºC)	T_{23}(ºC)
17.1	17.9	18.8	17.1	17.3	18.4	16.9	17.2	18.1	31.5
15.5	16.1	16.7	15.3	15.3	16.6	14.8	15.5	16.5	29.4
14.8	14.9	16.1	14.5	14.8	15.6	14.0	14.8	15.7	28.2
14.1	14.0	15.1	13.8	14.1	15.0	13.5	13.7	14.8	27.7
13.6	14.0	14.9	13.5	13.7	14.6	12.9	13.4	14.2	27.1
13.2	13.4	14.0	12.7	12.9	14.2	12.8	12.9	13.9	26.7
13.0	13.5	14.3	12.7	13.2	14.3	12.8	12.9	14.0	26.3
12.8	12.7	13.5	12.4	12.6	13.4	11.9	12.6	13.3	25.8
12.5	12.7	13.8	12.1	12.4	13.4	12.0	12.3	13.5	25.4
12.5	12.4	13.3	12.2	12.1	13.4	11.9	12.0	13.3	24.8
11.9	12.4	13.3	11.8	11.9	12.7	11.8	11.7	12.7	24.8
12.0	12.3	12.6	11.8	11.8	12.5	11.3	11.6	12.4	24.6
12.1	12.0	12.8	11.8	12.0	12.7	11.6	11.7	12.7	24.5

Table (D-7) inlet and outlet temperature for air and water variation with experiment time at case 1 conditions.

Time (min)	T_1 (ºC)	T_2 (ºC)	T_3 (ºC)	T_4 (ºC)
1	10.3	25.3	35.2	30.4
2	9.3	23.0	34.1	28.1
3	9.3	21.5	32.9	27.0
4	9.7	20.7	32.6	26.6
5	9.7	20.0	32.2	25.8
6	9.8	19.4	31.8	25.3
7	9.6	19.1	31.3	24.9
8	10.3	18.7	31.0	24.7
9	10.4	18.3	30.7	24.3
10	10.2	18.3	30.6	23.9
11	10.6	17.9	30.4	23.7
12	10.7	17.4	30.1	23.8
13	10.3	17.4	30.4	23.5
14	10.5	17.3	29.8	23.5
15	10.6	17.0	30.0	23.3
16	10.4	16.7	29.8	23.1
17	10.6	16.6	29.4	22.8
18	10.9	16.6	29.5	22.8
19	10.7	16.2	29.3	22.8
20	10.8	16.1	29.4	22.7
21	11.6	16.1	29.3	22.4
22	11.7	16.2	29.2	22.1
23	11.5	16.2	29.2	22.1
24	11.7	15.9	28.9	22.0
25	11.4	16.0	28.8	22.2
26	11.7	15.7	28.9	21.9
27	11.1	15.4	28.8	21.9
28	10.5	15.4	28.6	21.9
29	10.2	15.4	28.5	21.5
30	10.1	15.2	28.2	21.3

Table (D-8) front of heat exchanger temperature variation with experiment time at case 1 conditions.

T_5(ºC)	T_6(ºC)	T_7(ºC)	T_8(ºC)	T_9(ºC)	T_{10}(ºC)	T_{11}(ºC)	T_{12}(ºC)	T_{13}(ºC)
11.6	12.2	12.7	11.7	12.6	13.0	11.8	12.6	13.1
10.5	10.9	11.7	10.9	11.0	11.4	11.0	11.4	11.9
10.7	11.1	11.5	10.8	11.1	11.6	10.7	11.6	11.9
11.0	11.4	12.0	11.3	11.7	12.2	11.5	12.0	12.4
11.0	11.6	12.1	11.1	11.5	11.9	11.6	11.6	12.5
11.3	11.6	12.0	11.1	12.0	12.4	11.4	11.9	12.5
11.1	11.3	11.8	11.0	11.4	12.1	11.4	11.7	12.1
11.4	12.0	12.6	11.8	12.6	13.0	12.0	12.6	13.2
11.6	12.3	12.7	11.8	12.6	12.8	12.3	12.6	13.3
11.5	12.0	12.3	11.7	12.4	12.8	11.8	12.5	12.7
11.9	12.5	13.2	12.2	12.7	13.0	12.6	12.7	13.5
12.3	12.6	13.3	12.5	12.9	13.2	12.6	13.2	13.6
11.7	12.0	12.7	12.0	12.2	12.8	11.8	12.8	13.3
11.8	12.2	12.7	11.9	12.8	12.9	12.2	12.8	13.4
12.2	12.7	12.8	12.2	12.5	13.3	12.4	12.8	13.5
11.9	12.2	13.0	12.0	12.3	12.9	12.4	12.7	13.0
12.2	12.7	13.0	12.3	12.7	13.4	12.6	13.0	13.3
12.3	12.9	13.4	12.6	13.1	13.8	12.5	13.3	13.8
12.3	12.4	13.2	12.1	13.0	13.5	12.7	12.8	13.6
12.0	12.8	13.2	12.5	13.0	13.3	12.4	13.2	13.6
13.3	13.4	14.0	13.2	14.1	14.4	13.5	14.0	14.9
13.2	13.9	14.1	13.4	13.8	14.7	13.5	14.1	14.8
12.8	13.3	14.0	13.4	13.7	14.2	13.6	14.0	14.8
13.2	14.0	14.1	13.2	13.8	14.8	13.5	14.2	15.0
12.8	13.6	13.9	13.0	13.8	14.2	13.5	14.1	14.2
13.3	13.7	14.5	13.4	14.0	14.6	13.4	14.1	14.8
12.3	13.2	13.8	12.9	13.1	13.7	13.2	13.7	14.0
12.1	12.2	12.9	12.1	12.4	13.1	12.5	12.7	13.1
11.6	11.8	12.5	11.7	12.2	12.8	11.9	12.6	12.7
11.5	11.7	12.4	11.5	12.3	12.6	11.9	12.2	13.0

Table (D-9) back of heat exchanger temperature variation with experiment time at case 1 conditions.

T_{14}(ºC)	T_{15}(ºC)	T_{16}(ºC)	T_{17}(ºC)	T_{18}(ºC)	T_{19}(ºC)	T_{20}(ºC)	T_{21}(ºC)	T_{22}(ºC)	T_{23}(ºC)
20.8	21.8	22.9	20.7	21.0	22.5	20.5	20.9	22.1	33.9
19.2	19.8	20.7	18.8	19.0	20.5	18.3	19.0	20.3	31.3
18.0	18.1	19.5	17.6	18.0	19.0	17.1	17.9	19.1	30.3
17.5	17.5	18.7	17.1	17.5	18.6	16.7	17.1	18.4	30.0
16.7	17.2	18.2	16.5	16.8	17.9	15.9	16.4	17.5	29.1
16.3	16.6	17.4	15.7	16.0	17.6	15.8	16.0	17.2	28.4
15.9	16.4	17.4	15.5	16.1	17.3	15.5	15.7	17.1	27.9
15.8	15.8	16.8	15.3	15.6	16.6	14.9	15.6	16.5	27.9
15.2	15.4	16.6	14.7	15.1	16.3	14.5	14.9	16.3	27.2
15.5	15.4	16.5	15.1	15.1	16.6	14.7	14.9	16.4	26.8
14.8	15.4	16.4	14.6	14.8	15.9	14.6	14.6	15.8	26.7
14.8	15.1	15.6	14.4	14.6	15.4	13.9	14.3	15.2	26.6
14.8	14.7	15.7	14.4	14.7	15.6	14.1	14.4	15.5	26.4
14.7	14.6	15.8	14.2	14.7	15.4	13.8	14.1	15.4	26.4
14.1	14.6	15.3	14.0	14.5	15.4	13.5	14.2	15.1	26.1
13.8	14.3	15.0	13.5	14.0	14.9	13.7	13.7	14.8	26.1
13.9	14.3	14.9	13.8	13.7	14.9	13.2	13.7	14.6	25.4
14.0	14.2	15.2	13.7	13.7	15.0	13.2	13.7	14.8	25.7
13.7	14.1	15.0	13.5	13.7	14.6	13.0	13.4	14.2	25.7
13.3	13.8	14.8	13.2	13.4	14.3	12.9	13.4	14.5	25.6
13.5	13.9	14.8	13.4	13.3	14.3	12.8	13.5	14.3	25.3
13.8	13.9	14.5	13.0	13.5	14.6	13.2	13.5	14.3	24.7
13.6	13.8	14.7	13.2	13.6	14.4	13.0	13.6	14.3	25.1
13.3	13.6	14.5	13.0	13.2	14.1	12.7	13.2	14.0	24.8
13.2	13.5	14.4	12.9	13.2	14.6	12.9	13.2	14.3	24.9
13.4	13.6	14.4	13.0	13.3	13.9	12.7	13.2	13.9	24.8
13.1	13.3	13.8	12.5	13.1	13.8	12.4	12.8	13.7	24.8
12.7	13.1	13.8	12.8	12.7	13.8	12.5	12.6	13.9	24.6
12.7	13.2	14.1	12.7	13.1	13.8	12.6	12.9	13.9	24.0
12.7	13.1	13.7	12.7	12.8	13.9	12.5	12.4	13.3	24.1

Table (D-10) experimental data at steady state conditions for inlet and outlet temperature

Conditions	Tw_{in}(°C)	Tw_{out}(°C)	Ta_{in}(°C)	Ta_{out}(°C)
Case 1	10	15	28	21
Case 2	10	13	28	20
Case 3	10	12	28	19
Case 4	10	11.5	28	18.5
Case 5	13	15.5	28	21.1
Case 6	16	18.3	28	22.3
Case 7	18	19.8	28	23.2
Case 8	10	16.2	28	21.9
Case 9	10	14.6	28	22.8
Case 10	10	16.4	28	20.8
Case 11	10	14.3	28	19.8
Case 12	10	13.1	28	18.2
Case 13	10	12.6	28	17.2
Case 14	13	16.8	28	20
Case 15	16	18.4	28	20.5
Case 16	18	20.1	28	21.3
Case 17	10	17.2	28	19.5
Case 18	10	13.9	28	21.6

Table (D-11) experimental data of pressure drop, air velocity, and water flow rate

Conditions	Δp (Pa)	Ua_{in} (m/s)	$\dot{V}$ w (L/min)
Case 1	40	1.5	1
Case 2	40	1.5	2
Case 3	40	1.5	3
Case 4	40	1.5	4
Case 5	40	1.5	4
Case 6	40	1.5	4
Case 7	40	1.5	4
Case 8	130	5.6	4
Case 9	300	9.3	4
Case 10	70	0.9	1
Case 11	70	0.9	2
Case 12	70	0.9	3
Case 13	70	0.9	4
Case 14	70	0.9	4
Case 15	70	0.9	4
Case 16	70	0.9	4
Case 17	180	4.8	4
Case 18	390	8.7	4

Table (D-12) experimental calculation for heat transfer rate.

Conditions	Q_m (W)	Q_a (W)	Q_w (W)
Case 1	1156	1965	347
Case 2	1331	2245	416.4
Case 3	1471	2526	416.4
Case 4	1541	2667	416.4
Case 5	1315	1937	694
Case 6	1119	1600	638.5
Case 7	923.5	1347	499.7
Case 8	4057	6392	1721
Case 9	5163	9049	1277
Case 10	828.4	1213	444.2
Case 11	988.9	1381	596.9
Case 12	1148	1650	645.5
Case 13	1270	1819	721.8
Case 14	1201	1347	1055
Case 15	964.7	1263	666.3
Case 16	855.7	1128	583
Case 17	4817	7635	1999
Case 18	5751	10419	1083

Table (D-13) experimental calculation for Reynolds number and heat transfer coefficients.

Conditions	Re	R ($W/^oC$)	h_o ($W/m^2.^oC$)	h_{in} ($W/m^2.^oC$)
Case 1	37750	0.01036	225	5403
Case 2	37750	0.009265	248.5	7033
Case 3	37750	0.008269	280.5	7343
Case 4	37750	0.007824	296.7	7509
Case 5	37750	0.00771	256.8	9447
Case 6	37750	0.007039	267.3	7217
Case 7	37750	0.007132	263.8	5122
Case 8	140930	0.002921	737.9	25601
Case 9	234040	0.002537	950.2	20199
Case 10	22650	0.01351	148	6558
Case 11	22650	0.01177	161.9	9554
Case 12	22650	0.009773	197.7	10855
Case 13	22650	0.00849	223.2	12400
Case 14	22650	0.00744	200.8	13749
Case 15	22650	0.006977	238.5	7509
Case 16	22650	0.006158	261.5	5930
Case 17	120800	0.002104	1024	28662
Case 18	218940	0.002227	1118	17614

Table (D-14) experimental calculation for area goodness factor, friction factor, and Colburn factor , LMTD, Nussult number.

Conditions	AG	*f*	*j*	LMTD (°C)	Nu_o
Case 1	0.0033033	30.61	0.101114	11.97	3421
Case 2	0.00364832	30.61	0.111675	12.33	3780
Case 3	0.00411812	30.61	0.126056	12.17	4267
Case 4	0.00435596	30.61	0.133336	12.06	4512
Case 5	0.00377017	30.61	0.115405	10.14	3905
Case 6	0.00392433	30.61	0.120124	7.878	4065
Case 7	0.00387294	30.61	0.118551	6.587	4013
Case 8	0.01244208	7.139	0.088824	11.85	11223
Case 9	0.01153082	5.973	0.068874	13.1	14452
Case 10	0.00074497	148.8	0.110851	11.2	2250
Case 11	0.00081493	148.8	0.121262	11.64	2462
Case 12	0.00099513	148.8	0.148076	11.22	3007
Case 13	0.00112349	148.8	0.167175	10.79	3395
Case 14	0.00101074	148.8	0.150398	8.936	3054
Case 15	0.0012005	148.8	0.178635	6.731	3627
Case 16	0.00131628	148.8	0.195862	5.27	3977
Case 17	0.01069196	13.45	0.143807	10.14	15574
Case 18	0.00976276	8.873	0.086625	12.81	17004

Appendix (E): Finite element method

The finite element approach is used to solve the equations (4.1 to 4.14). Using a weak formulation method, the Galerkin technique is employed to solve the governing equations of the finite element methods. The cells are divided into non-structural mesh distribution components. Interpolation algorithms are used to discretize the non-overlapping districts throughout the computational domain. For velocity, pressure, and temperature variables, Lagrange triangular finite elements of various orders are utilized throughout the computing domain.

The solution of a continuum problem by the finite element method is approximated by the following step-by-step process.

A- Discretization (Mesh): Divide the solution region into non-overlapping elements or sub-regions. The finite element discretization allows a variety of element shapes, for example, triangles, quadrilaterals as explained in figure (4-4).

B-Select interpolation or shape functions: The next step is to choose the type of interpolation function that represents the variation of the field variable over an element. A number of nodes form an element; the nature and number of unknowns at each node decide the variation of a field variable within the element.

C-Form element equations (formulation): Determine the matrix equations that express the properties of the individual elements by forming an element left hand side (LHS) matrix and load vector.

D- Assemble the element equations: To find the properties of the overall system, assemble all the individual element equations, that is, to combine the matrix equations of each element in an appropriate way such

that the resulting matrix represents the behavior of the entire solution region of the problem.

E- Solve the system of equations: The resulting set of algebraic equations may now be solved to obtain the nodal values of the field variable, for example, temperature, pressure, and velocity

F- Calculate the secondary quantities: From the nodal values of the field variable, for example, temperatures, the secondary quantities can be calculating, for example, space heat fluxes, or heat transfer coefficient.

Appendix (F): Steps to use the COMSOL Multiphysics software

1- Start a new study

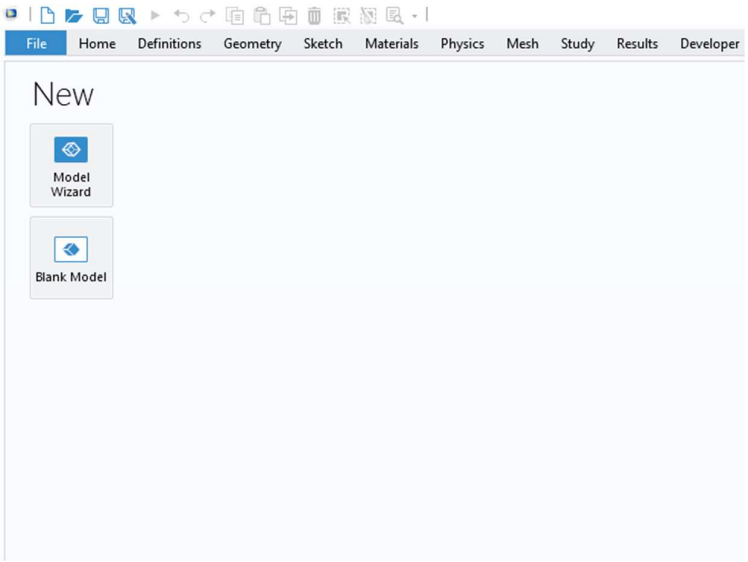

2- Define the space dimension (2-D in this study)

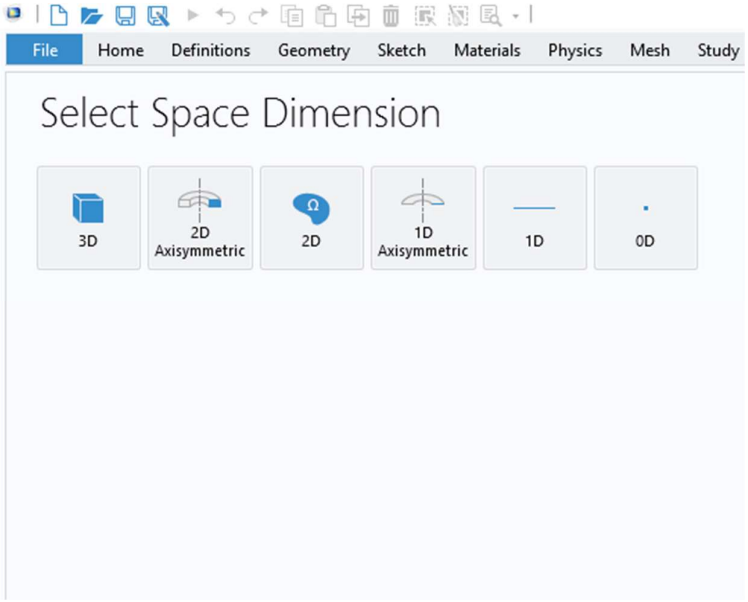

3- Define Physics: Choose the relevant physics interfaces for your problem. In this case, select the fluid flow and heat transfer physics interfaces. COMSOL provides various predefined physics interfaces, including laminar and turbulent flow, heat transfer in solids and fluids, and porous media flow.

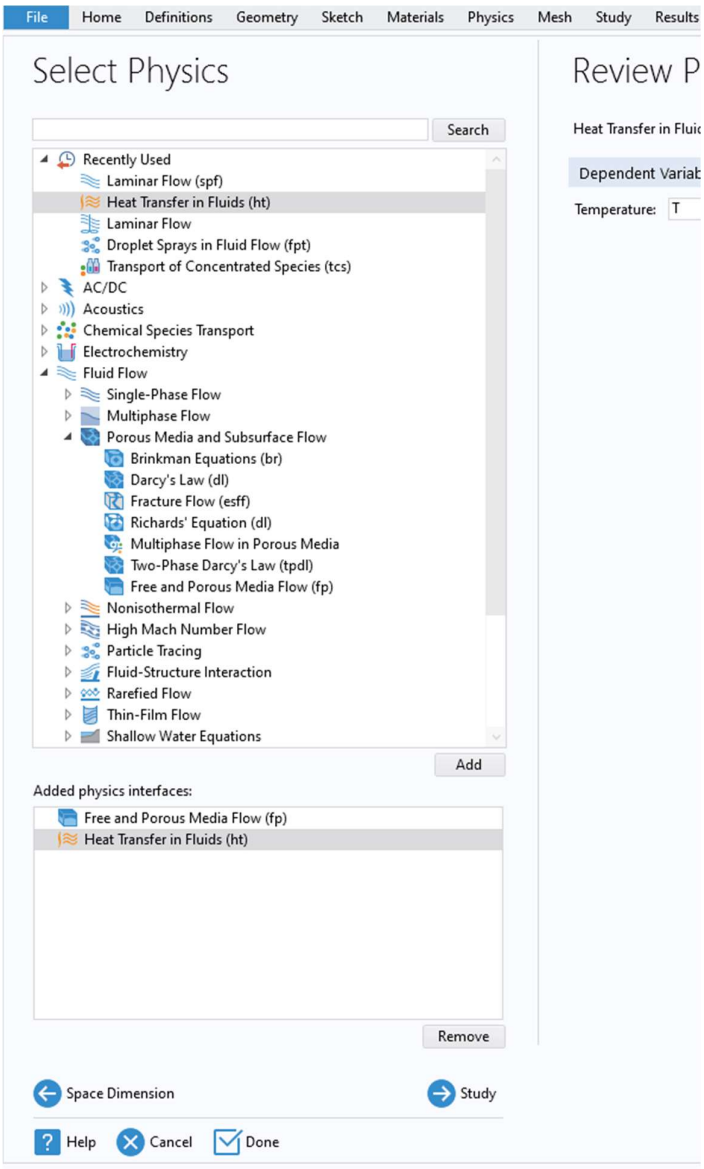

4- Defining Parameters: You can define parameters in COMSOL by assigning a value or expression to a parameter name. Parameters can represent physical constants, geometric dimensions, material properties, boundary conditions, or any other variable in your model. Parameters can be defined at different levels, such as global parameters applicable to the entire model or local parameters specific to a certain geometry, physics interface, or boundary condition.

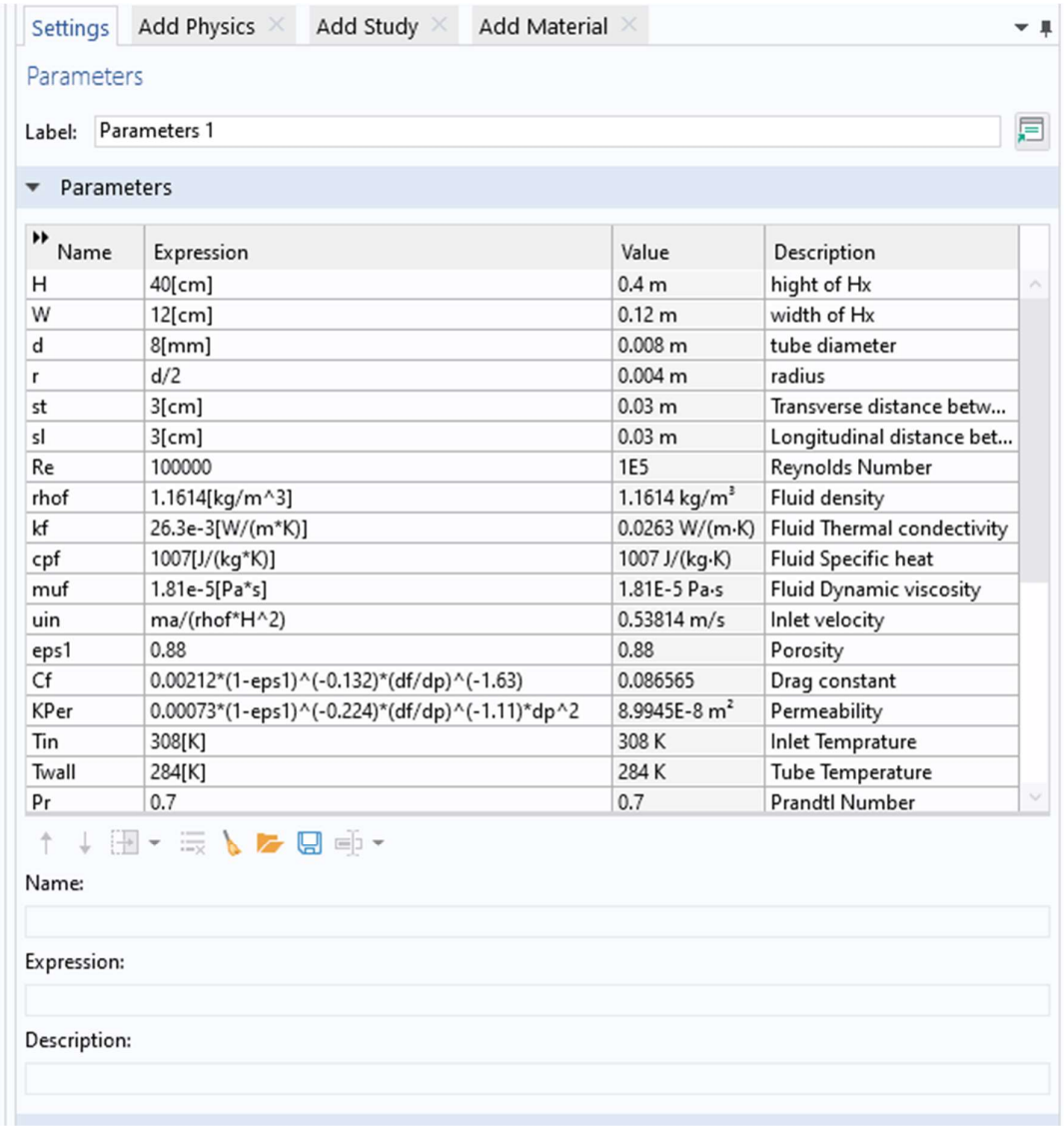

Name	Expression	Value	Description
H	40[cm]	0.4 m	hight of Hx
W	12[cm]	0.12 m	width of Hx
d	8[mm]	0.008 m	tube diameter
r	d/2	0.004 m	radius
st	3[cm]	0.03 m	Transverse distance betw...
sl	3[cm]	0.03 m	Longitudinal distance bet...
Re	100000	1E5	Reynolds Number
rhof	1.1614[kg/m^3]	1.1614 kg/m^3	Fluid density
kf	26.3e-3[W/(m*K)]	0.0263 W/(m·K)	Fluid Thermal condectivity
cpf	1007[J/(kg*K)]	1007 J/(kg·K)	Fluid Specific heat
muf	1.81e-5[Pa*s]	1.81E-5 Pa·s	Fluid Dynamic viscosity
uin	ma/(rhof*H^2)	0.53814 m/s	Inlet velocity
eps1	0.88	0.88	Porosity
Cf	0.00212*(1-eps1)^(-0.132)*(df/dp)^(-1.63)	0.086565	Drag constant
KPer	0.00073*(1-eps1)^(-0.224)*(df/dp)^(-1.11)*dp^2	8.9945E-8 m^2	Permeability
Tin	308[K]	308 K	Inlet Temprature
Twall	284[K]	284 K	Tube Temperature
Pr	0.7	0.7	Prandtl Number

5- Model Geometry: Start by creating the geometry of your porous media system. Use the built-in geometry tools in COMSOL to define the shape, size, and boundaries of your porous media domain. You can create simple or complex geometries based on your specific requirements.

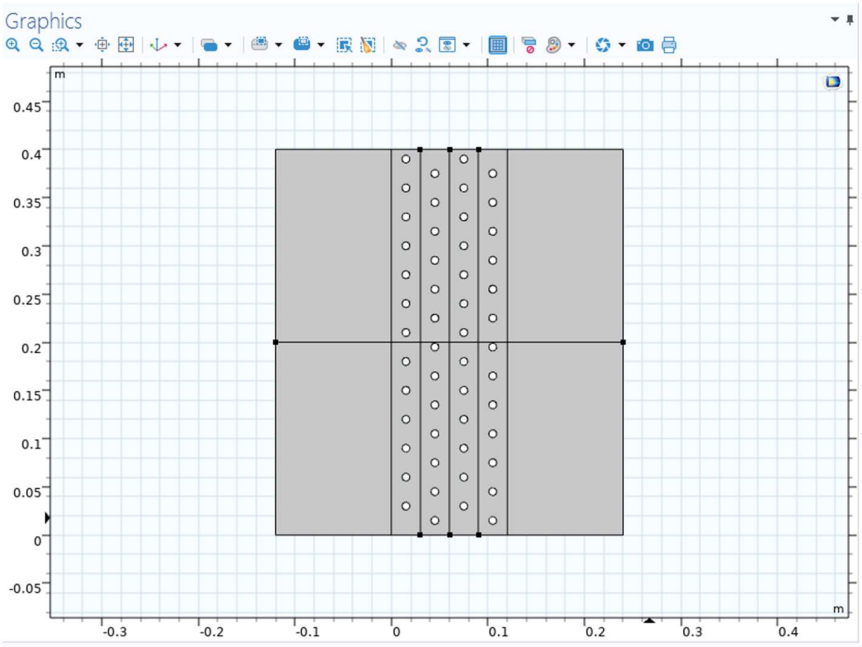

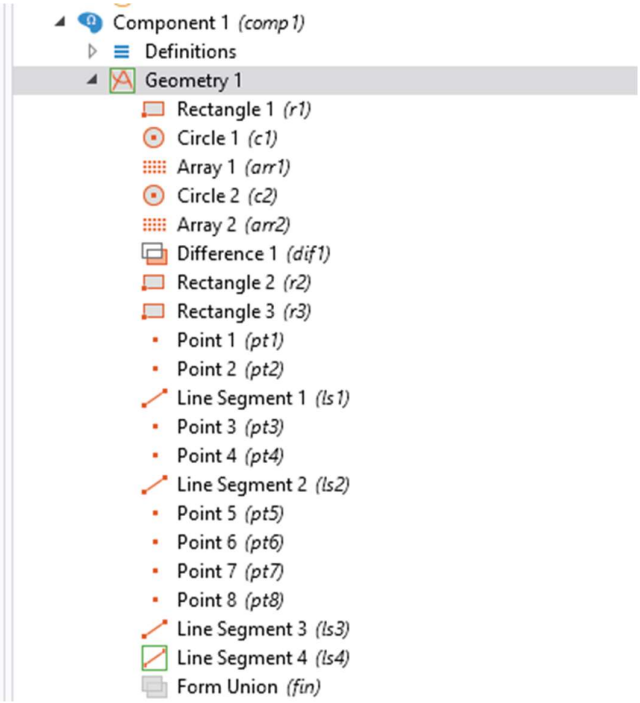

6- Free and porous media flow refers to the simultaneous flow of fluid through both a free region (such as open space) and a porous medium.

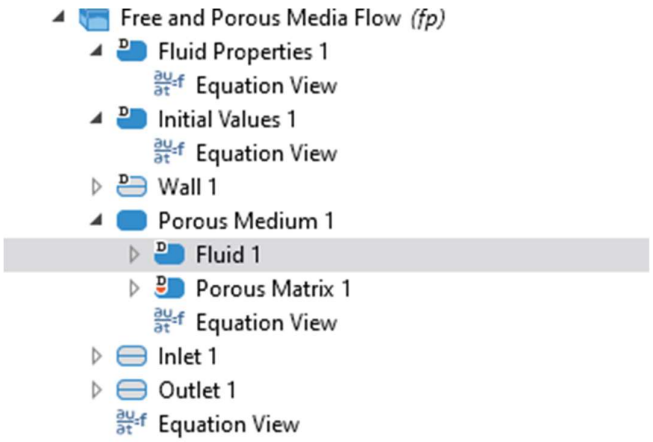

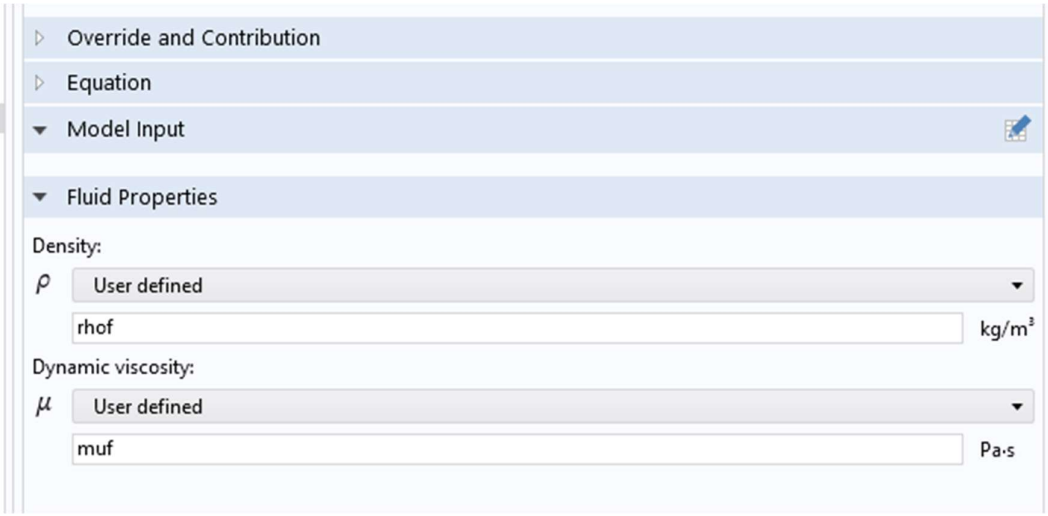

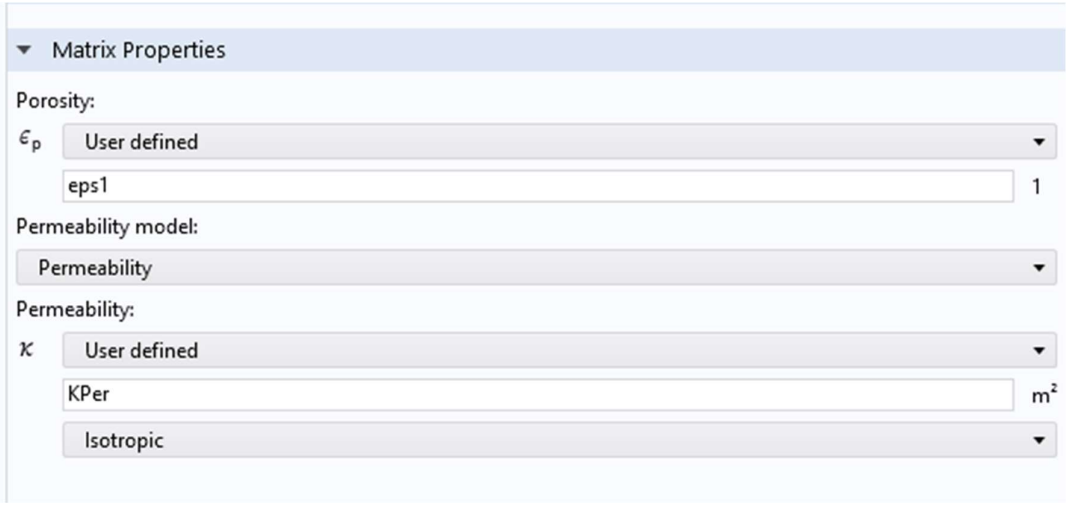

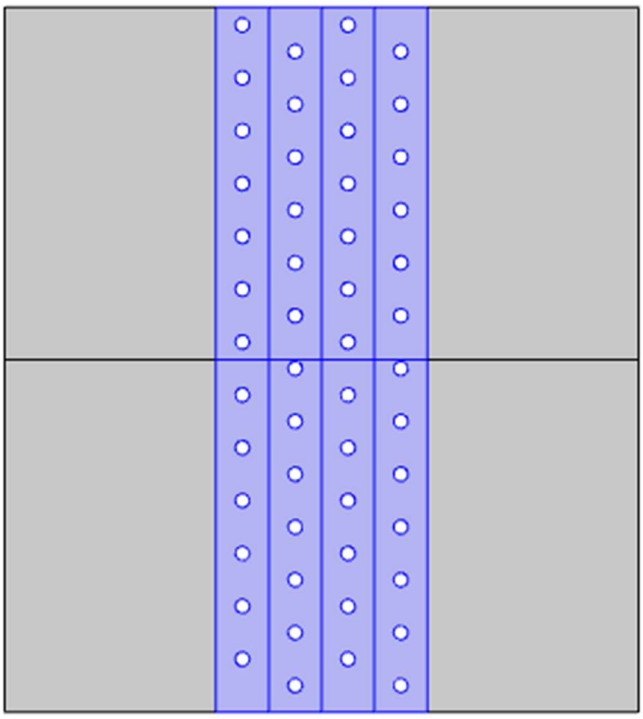

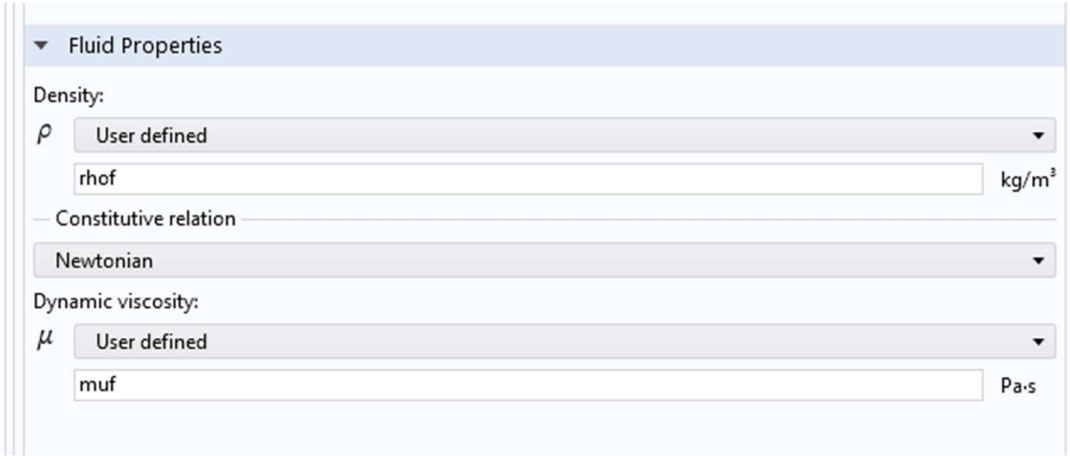
Fluid Properties
Density:
ρ
User defined
rhof
kg/m³
Constitutive relation
Newtonian
Dynamic viscosity:
μ
User defined
muf
Pa·s

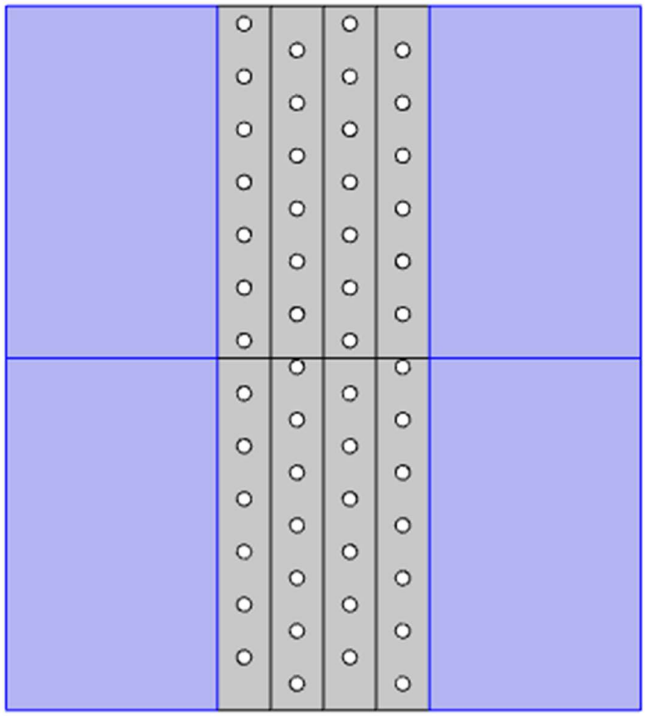

7- Heat transfer in porous media refers to the transfer of thermal energy through a porous material or medium.

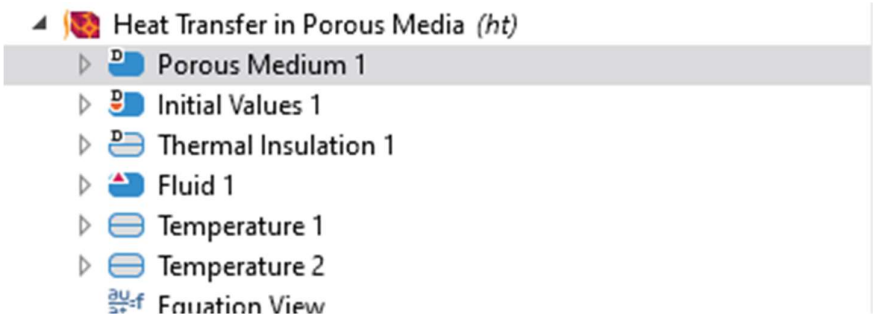

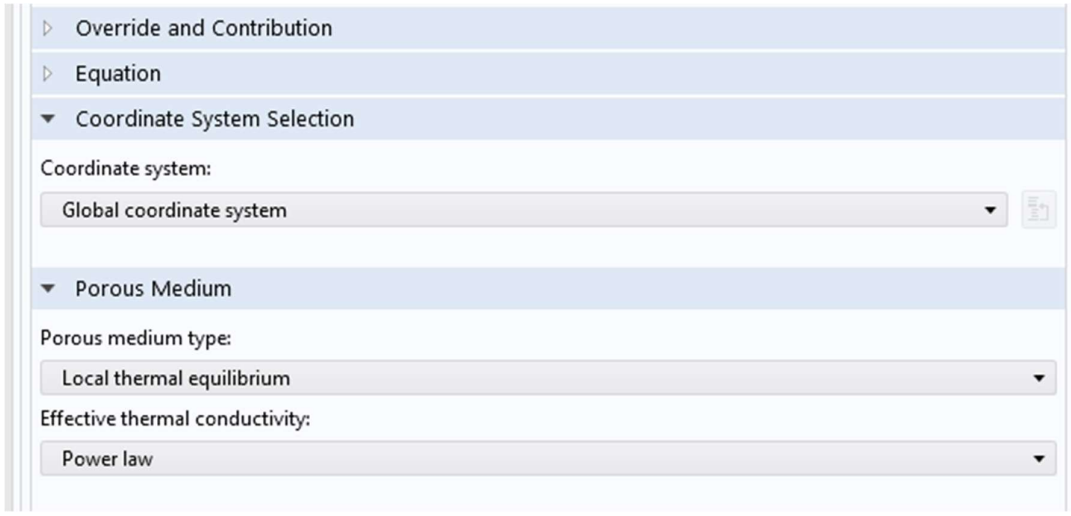
Override and Contribution
Equation
Coordinate System Selection
Coordinate system:
Global coordinate system
Porous Medium
Porous medium type:
Local thermal equilibrium
Effective thermal conductivity:
Power law

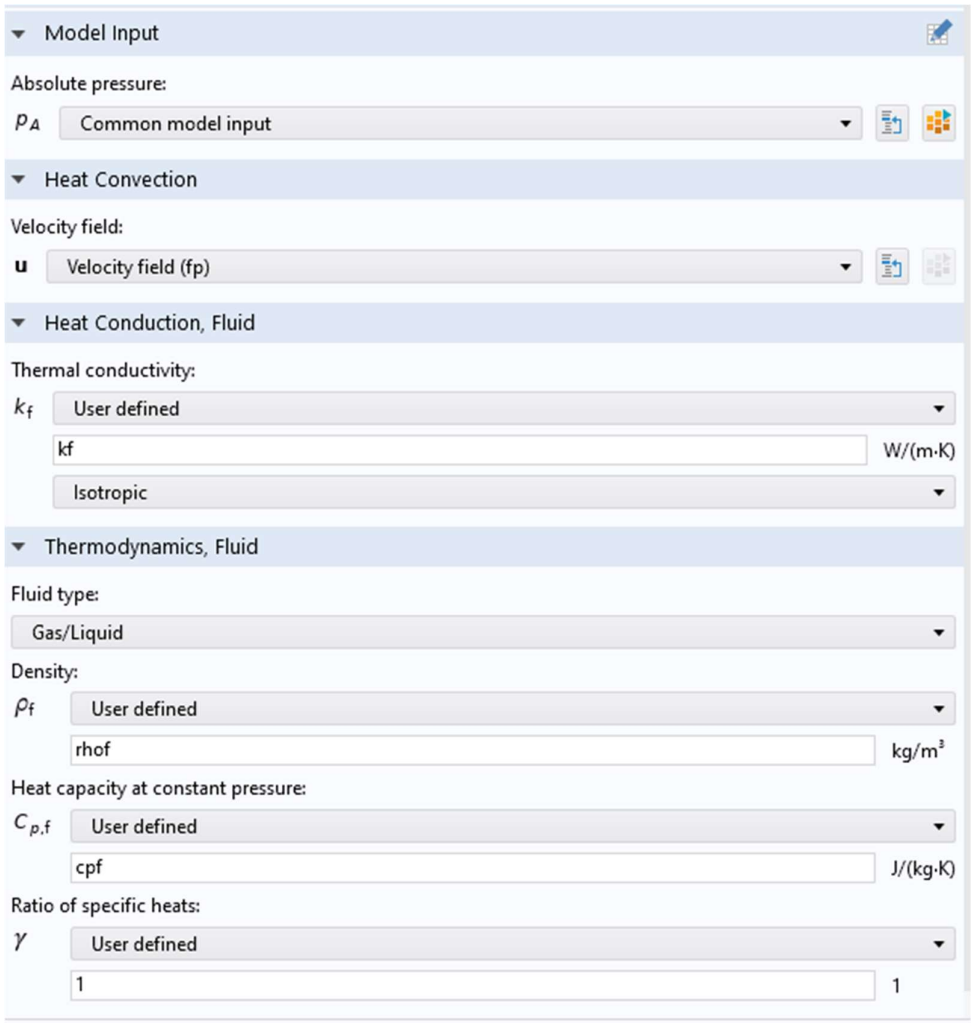
Model Input
Absolute pressure:
p_A
Common model input
Heat Convection
Velocity field:
u
Velocity field (fp)
Heat Conduction, Fluid
Thermal conductivity:
k_f
User defined
kf
W/(m·K)
Isotropic
Thermodynamics, Fluid
Fluid type:
Gas/Liquid
Density:
ρ_f
User defined
rhof
kg/m³
Heat capacity at constant pressure:
$C_{p,f}$
User defined
cpf
J/(kg·K)
Ratio of specific heats:
γ
User defined
1
1

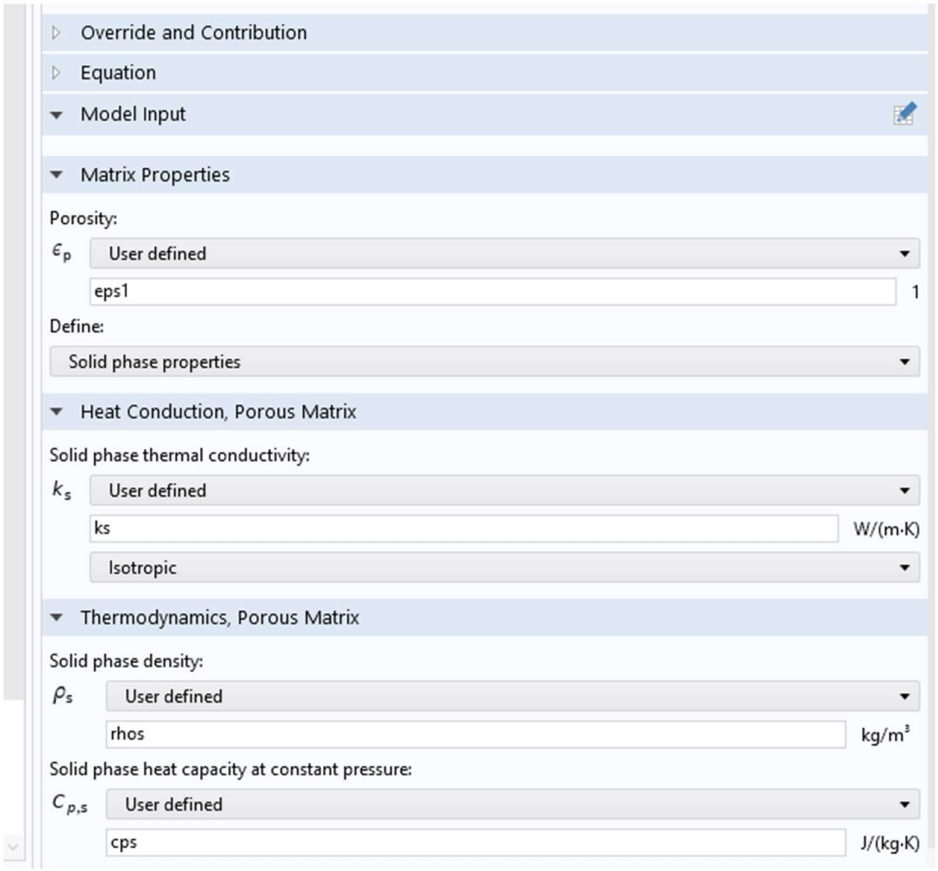

8- Mesh Generation: Generate a mesh that discretizes the porous media geometry. Ensure that the mesh is suitable for capturing the heat transfer characteristics and the porous structure. COMSOL provides automatic meshing algorithms, but you can also manually refine the mesh if needed.

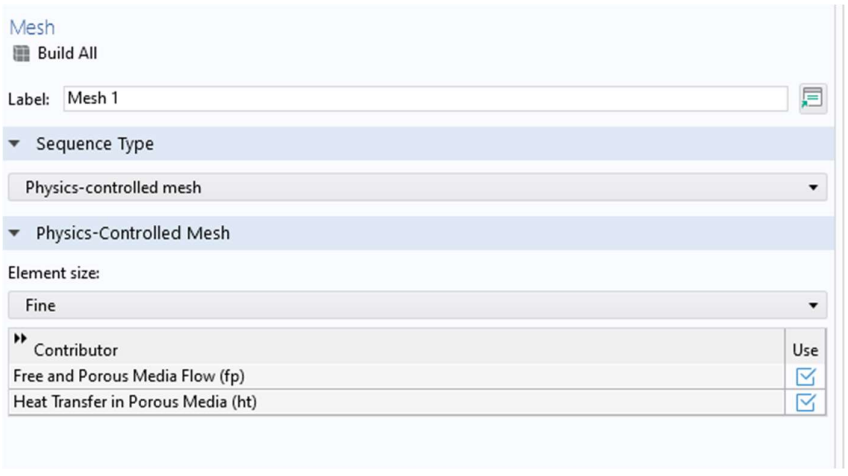

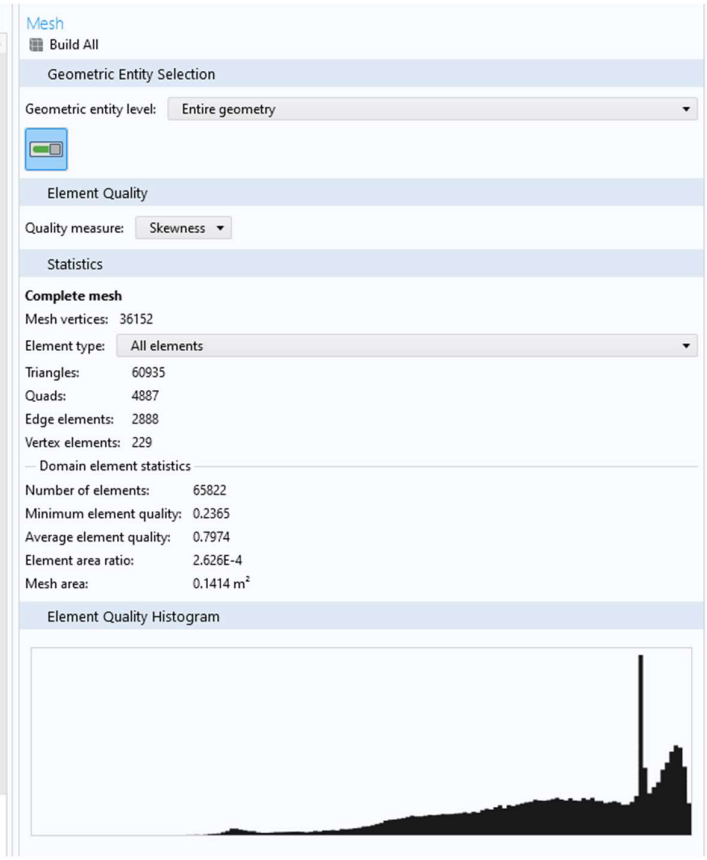
Mesh
Build All
Geometric Entity Selection
Geometric entity level: Entire geometry
Element Quality
Quality measure: Skewness
Statistics
Complete mesh
Mesh vertices: 36152
Element type: All elements
Triangles: 60935
Quads: 4887
Edge elements: 2888
Vertex elements: 229
Domain element statistics
Number of elements: 65822
Minimum element quality: 0.2365
Average element quality: 0.7974
Element area ratio: 2.626E-4
Mesh area: 0.1414 m²
Element Quality Histogram

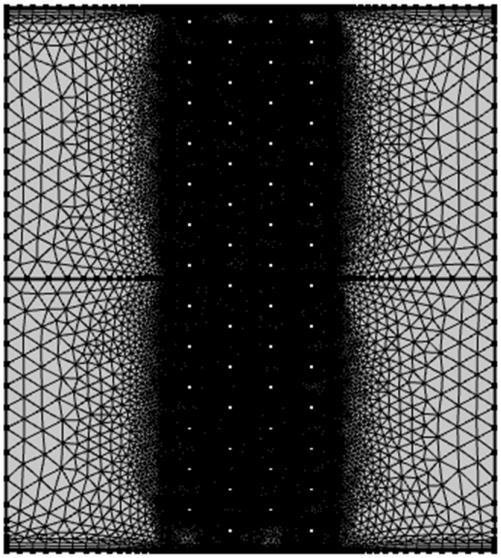

9- Parametric sweep is a powerful capability in COMSOL Multiphysics that allows you to explore the behavior of your model over a range of parameter values. It enables you to perform multiple simulations with varying parameter values automatically. Parametric sweeps are particularly useful for sensitivity analysis, design optimization, and studying the impact of different input parameters on the model's response.

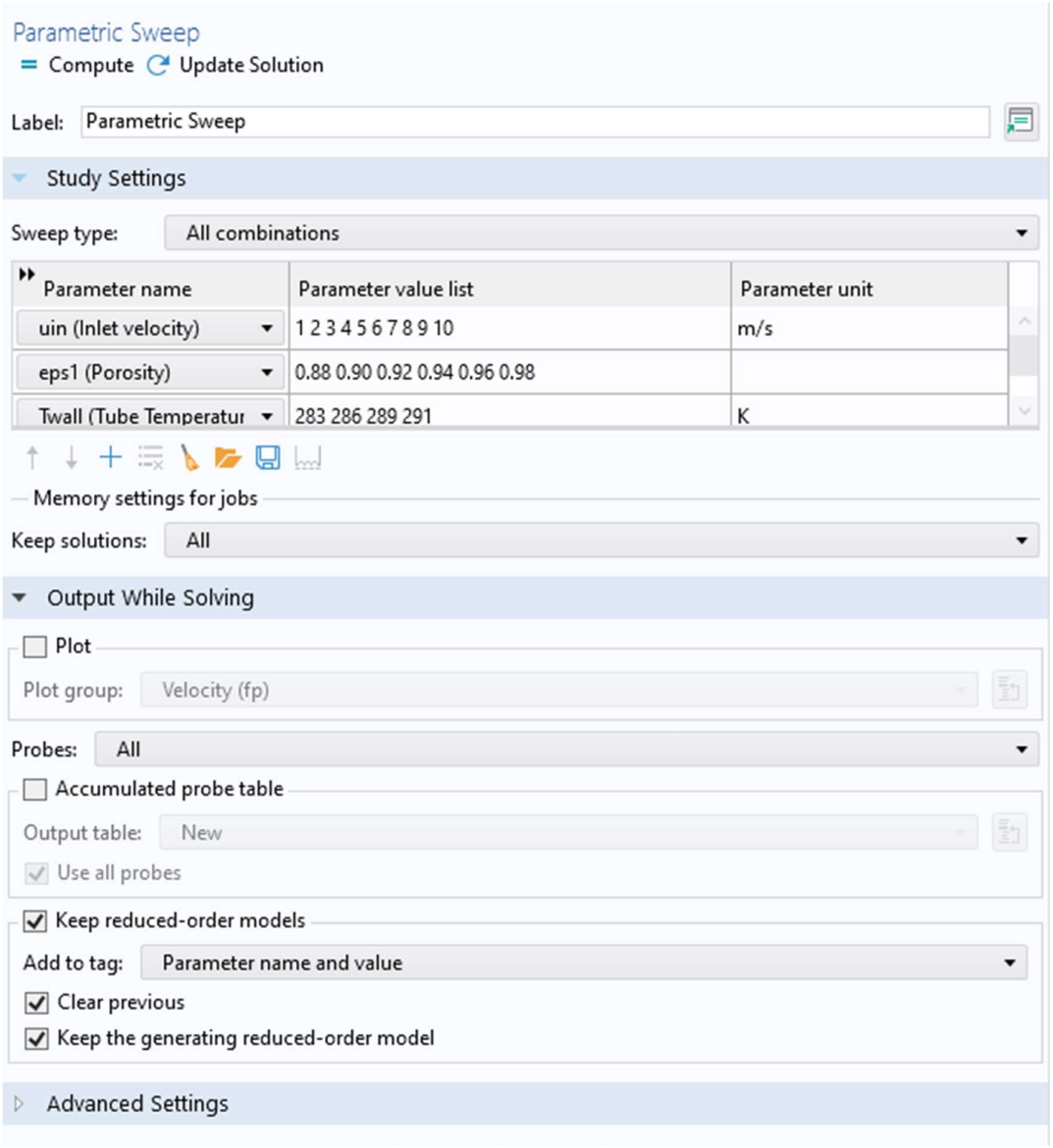

10- Analyze Results: Once the parametric sweep is complete, analyze and visualize the results. COMSOL provides various postprocessing tools to explore the data across different parameter values. You can generate plots, animations, or tables to examine how the output variables change with respect to the swept parameters.

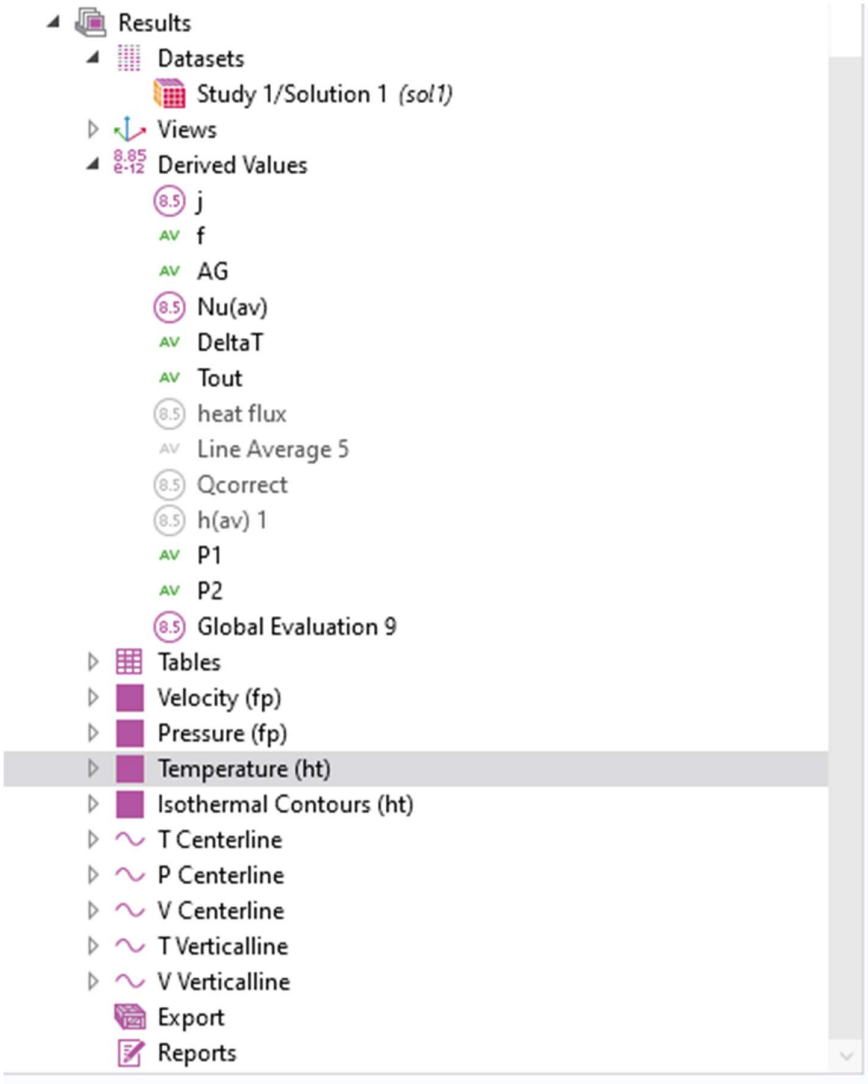

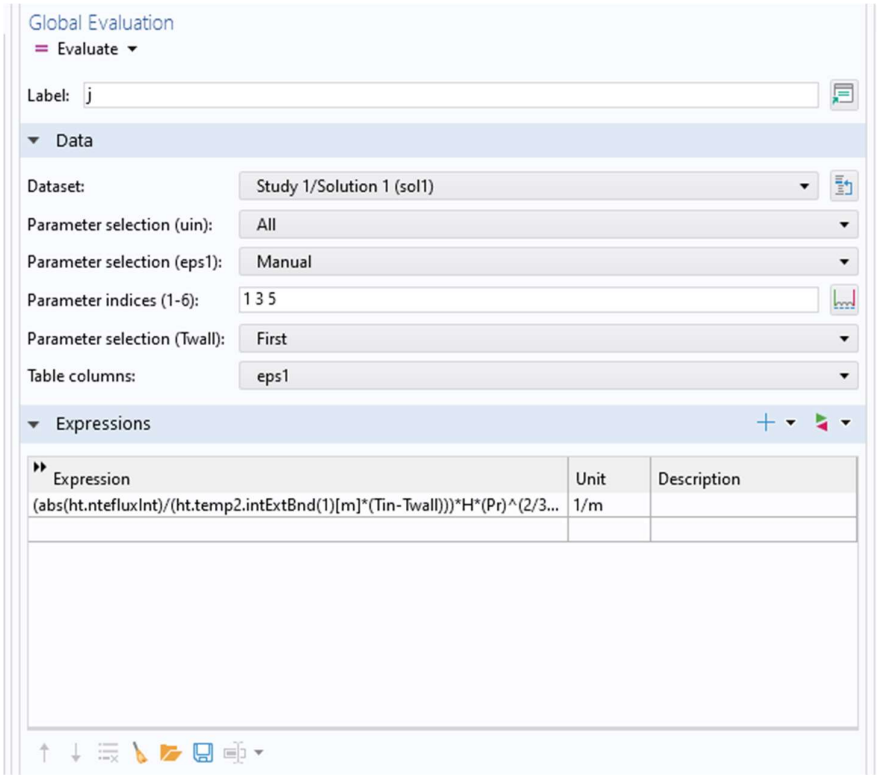
Global Evaluation
Evaluate
Label: j
Data
Dataset: Study 1/Solution 1 (sol1)
Parameter selection (uin): All
Parameter selection (eps1): Manual
Parameter indices (1-6): 1 3 5
Parameter selection (Twall): First
Table columns: eps1
Expressions
Expression
Unit
Description
(abs(ht.nteflxInt)/(ht.temp2.intExtBnd(1)[m]*(Tin-Twall)))*H*(Pr)^(2/3...
1/m

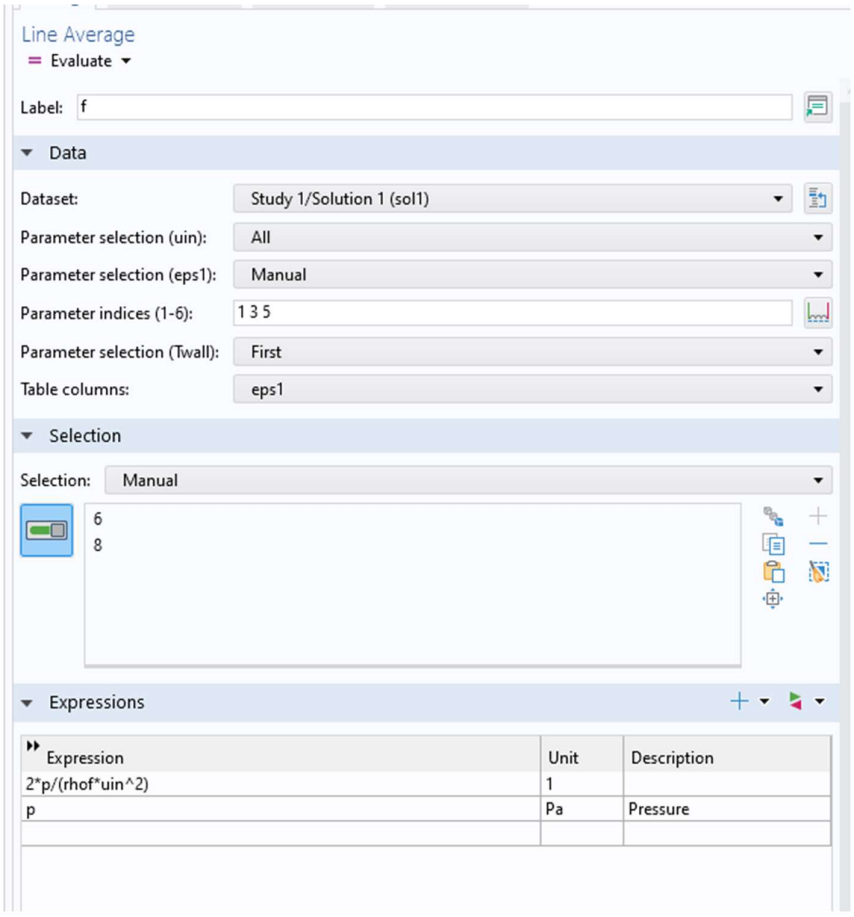
Line Average
Evaluate
Label: f
Data
Dataset: Study 1/Solution 1 (sol1)
Parameter selection (uin): All
Parameter selection (eps1): Manual
Parameter indices (1-6): 1 3 5
Parameter selection (Twall): First
Table columns: eps1
Selection
Selection: Manual
6
8
Expressions
Expression
Unit
Description
2*p/(rhof*uin^2)
1
p
Pa
Pressure

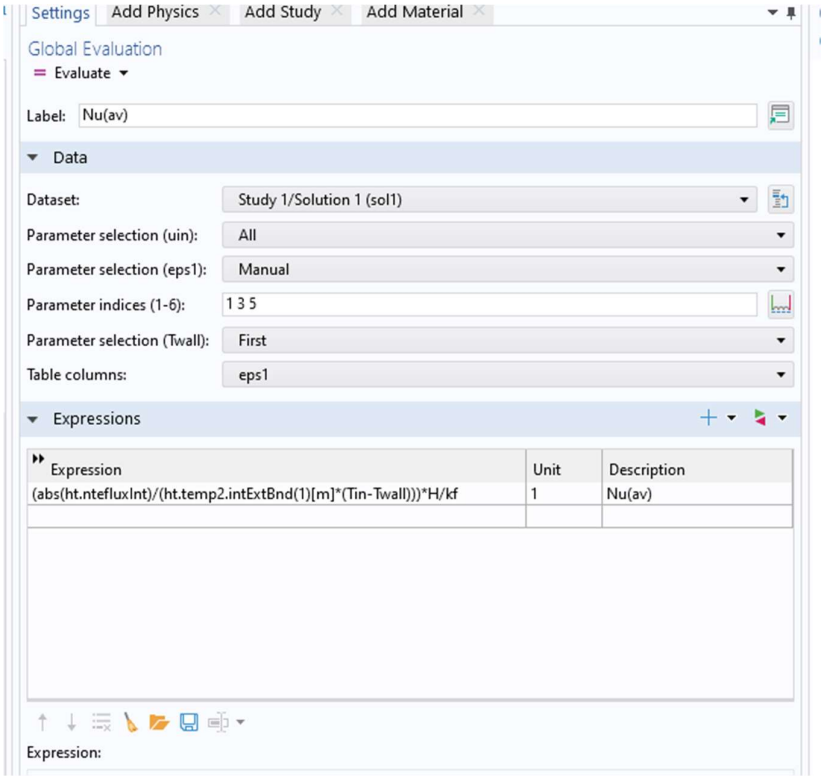
Settings
Add Physics
Add Study
Add Material
Global Evaluation
Evaluate
Label: Nu(av)
Data
Dataset: Study 1/Solution 1 (sol1)
Parameter selection (uin): All
Parameter selection (eps1): Manual
Parameter indices (1-6): 1 3 5
Parameter selection (Twall): First
Table columns: eps1
Expressions
Expression
Unit
Description
(abs(ht.nefluxInt)/(ht.temp2.intExtBnd(1)[m]*(Tin-Twall)))*H/kf
1
Nu(av)
Expression:

Appendix (G) Uncertainty Propagations

In statistics, propagation of uncertainty (or propagation of error) is the effect of variables uncertainties (or errors, more specifically random errors) on the uncertainty of a function based on them. When the variables are the values of experimental measurements they have uncertainties due to measurement limitations (e.g., instrument precision) which propagate due to the combination of variables in the function. The propagation of error due to the uncertainty of the variables in tables (3-11) and (3-12) can be calculated through the EES software as follows:

Variable±Uncertainty	Partial derivative	% of uncertainty
AG = 0.0001842±0.00001494		
DP = 300±1.47 [Pa]	$\partial AG/\partial DP$ = -6.141E-07	0.37 %
LPM = 1±0.072	$\partial AG/\partial LPM$ = 0	0.00 %
Ta_{in} = 28.1±0.12 [C]	$\partial AG/\partial Ta_{in}$ = 0.0001016	66.64 %
Ta_{out} = 26.5±0.0675 [C]	$\partial AG/\partial Ta_{out}$ = -0.0001217	30.26 %
Tw_{in} = 10±0.09 [C]	$\partial AG/\partial Tw_{in}$ = 0.000006569	0.16 %
Tw_{out} = 22.5±0.09 [C]	$\partial AG/\partial Tw_{out}$ = 0.00001354	0.67 %
$velocity_a$ = 8.9±0.05 [m/s]	$\partial AG/\partial velocity_a$ = 0.0000414	1.92 %
C_{min} = 69.4±4.997 [J/K-s]		
DP = 300±1.47 [Pa]	$\partial C_{min}/\partial DP$ = 0	0.00 %
LPM = 1±0.072	$\partial C_{min}/\partial LPM$ = 69.4	100.00 %
Ta_{in} = 28.1±0.12 [C]	$\partial C_{min}/\partial Ta_{in}$ = 0	0.00 %
Ta_{out} = 26.5±0.0675 [C]	$\partial C_{min}/\partial Ta_{out}$ = 0	0.00 %
Tw_{in} = 10±0.09 [C]	$\partial C_{min}/\partial Tw_{in}$ = 0	0.00 %
Tw_{out} = 22.5±0.09 [C]	$\partial C_{min}/\partial Tw_{out}$ = 0	0.00 %
$velocity_a$ = 8.9±0.05 [m/s]	$\partial C_{min}/\partial velocity_a$ = 0	0.00 %

$e = 0.4514 \pm 0.01047$		
$DP = 300 \pm 1.47$ [Pa]	$\partial e/\partial DP = 0$	0.00 %
$LPM = 1 \pm 0.072$	$\partial e/\partial LPM = -0.1062$	53.29 %
$Ta_{in} = 28.1 \pm 0.12$ [C]	$\partial e/\partial Ta_{in} = 0.04135$	22.44 %
$Ta_{out} = 26.5 \pm 0.0675$ [C]	$\partial e/\partial Ta_{out} = -0.06629$	18.25 %
$Tw_{in} = 10 \pm 0.09$ [C]	$\partial e/\partial Tw_{in} = -0.002687$	0.05 %
$Tw_{out} = 22.5 \pm 0.09$ [C]	$\partial e/\partial Tw_{out} = 0.02762$	5.63 %
$velocity_a = 8.9 \pm 0.05$ [m/s]	$\partial e/\partial velocity_a = 0.01192$	0.32 %

$f = 6.522 \pm 0.07995$		
$DP = 300 \pm 1.47$ [Pa]	$\partial f/\partial DP = 0.02174$	15.98 %
$LPM = 1 \pm 0.072$	$\partial f/\partial LPM = 0$	0.00 %
$Ta_{in} = 28.1 \pm 0.12$ [C]	$\partial f/\partial Ta_{in} = 0$	0.00 %
$Ta_{out} = 26.5 \pm 0.0675$ [C]	$\partial f/\partial Ta_{out} = 0$	0.00 %
$Tw_{in} = 10 \pm 0.09$ [C]	$\partial f/\partial Tw_{in} = 0$	0.00 %
$Tw_{out} = 22.5 \pm 0.09$ [C]	$\partial f/\partial Tw_{out} = 0$	0.00 %
$velocity_a = 8.9 \pm 0.05$ [m/s]	$\partial f/\partial velocity_a = -1.466$	84.02 %

$h_{in} = 10450 \pm 761.2$ [J-C/s-K-m^2]		
$DP = 300 \pm 1.47$ [Pa]	$\partial h_{in}/\partial DP = 0$	0.00 %
$LPM = 1 \pm 0.072$	$\partial h_{in}/\partial LPM = 10450$	97.70 %
$Ta_{in} = 28.1 \pm 0.12$ [C]	$\partial h_{in}/\partial Ta_{in} = -2.294E\text{-}13$	0.00 %
$Ta_{out} = 26.5 \pm 0.0675$ [C]	$\partial h_{in}/\partial Ta_{out} = 0$	0.00 %
$Tw_{in} = 10 \pm 0.09$ [C]	$\partial h_{in}/\partial Tw_{in} = -1171$	1.92 %
$Tw_{out} = 22.5 \pm 0.09$ [C]	$\partial h_{in}/\partial Tw_{out} = 520.6$	0.38 %
$velocity_a = 8.9 \pm 0.05$ [m/s]	$\partial h_{in}/\partial velocity_a = 0$	0.00 %

$h_{out} = 32.2 \pm 2.694$ [J/s-K]		
$DP = 300 \pm 1.47$ [Pa]	$\partial h_{out}/\partial DP = 0$	0.00 %
$LPM = 1 \pm 0.072$	$\partial h_{out}/\partial LPM = 0$	0.00 %
$Ta_{in} = 28.1 \pm 0.12$ [C]	$\partial h_{out}/\partial Ta_{in} = 18.79$	70.02 %
$Ta_{out} = 26.5 \pm 0.0675$ [C]	$\partial h_{out}/\partial Ta_{out} = -21.54$	29.13 %
$Tw_{in} = 10 \pm 0.09$ [C]	$\partial h_{out}/\partial Tw_{in} = 1.377$	0.21 %
$Tw_{out} = 22.5 \pm 0.09$ [C]	$\partial h_{out}/\partial Tw_{out} = 1.295$	0.19 %
$velocity_a = 8.9 \pm 0.05$ [m/s]	$\partial h_{out}/\partial velocity_a = 3.618$	0.45 %

$j = 0.001202 \pm 0.00009629$		
DP = 300±1.47 [Pa]	$\partial j / \partial DP = 0$	0.00 %
LPM = 1±0.072	$\partial j / \partial LPM = 0$	0.00 %
Ta_{in} = 28.1±0.12 [C]	$\partial j / \partial Ta_{in} = 0.0006626$	68.19 %
Ta_{out} = 26.5±0.0675 [C]	$\partial j / \partial Ta_{out} = -0.0007938$	30.96 %
Tw_{in} = 10±0.09 [C]	$\partial j / \partial Tw_{in} = 0.00004284$	0.16 %
Tw_{out} = 22.5±0.09 [C]	$\partial j / \partial Tw_{out} = 0.00008833$	0.68 %
$velocity_a$ = 8.9±0.05 [m/s]	$\partial j / \partial velocity_a = 0$	0.00 %

LMTD = 10.09±0.1184 [C]		
DP = 300±1.47 [Pa]	$\partial LMTD / \partial DP = 0$	0.00 %
LPM = 1±0.072	$\partial LMTD / \partial LPM = 0$	0.00 %
Ta_{in} = 28.1±0.12 [C]	$\partial LMTD / \partial Ta_{in} = 0.7415$	56.52 %
Ta_{out} = 26.5±0.0675 [C]	$\partial LMTD / \partial Ta_{out} = 0.3597$	4.21 %
Tw_{in} = 10±0.09 [C]	$\partial LMTD / \partial Tw_{in} = -0.3597$	7.48 %
Tw_{out} = 22.5±0.09 [C]	$\partial LMTD / \partial Tw_{out} = -0.7415$	31.79 %
$velocity_a$ = 8.9±0.05 [m/s]	$\partial LMTD / \partial velocity_a = 0$	0.00 %

$m_a = 0.1654 \pm 0.0009291$ [kg/s]		
DP = 300±1.47 [Pa]	$\partial m_a / \partial DP = 0$	0.00 %
LPM = 1±0.072	$\partial m_a / \partial LPM = 0$	0.00 %
Ta_{in} = 28.1±0.12 [C]	$\partial m_a / \partial Ta_{in} = 0$	0.00 %
Ta_{out} = 26.5±0.0675 [C]	$\partial m_a / \partial Ta_{out} = 0$	0.00 %
Tw_{in} = 10±0.09 [C]	$\partial m_a / \partial Tw_{in} = 0$	0.00 %
Tw_{out} = 22.5±0.09 [C]	$\partial m_a / \partial Tw_{out} = 0$	0.00 %
$velocity_a$ = 8.9±0.05 [m/s]	$\partial m_a / \partial velocity_a = 0.01858$	100.00 %

m_w = 0.0166±0.001195 [kg/s]

DP = 300±1.47 [Pa]	$\partial m_w / \partial DP = 0$	0.00 %
LPM = 1±0.072	$\partial m_w / \partial LPM = 0.0166$	100.00 %
Ta_{in} = 28.1±0.12 [C]	$\partial m_w / \partial Ta_{in} = 0$	0.00 %
Ta_{out} = 26.5±0.0675 [C]	$\partial m_w / \partial Ta_{out} = 0$	0.00 %
Tw_{in} = 10±0.09 [C]	$\partial m_w / \partial Tw_{in} = 0$	0.00 %
Tw_{out} = 22.5±0.09 [C]	$\partial m_w / \partial Tw_{out} = 0$	0.00 %
$velocity_a$ = 8.9±0.05 [m/s]	$\partial m_w / \partial velocity_a = 0$	0.00 %

$Nusselt_{in}$ = 138±10.05 [J-C/s-W]

DP = 300±1.47 [Pa]	$\partial Nusselt_{in} / \partial DP = 0$	0.00 %
LPM = 1±0.072	$\partial Nusselt_{in} / \partial LPM = 138$	97.70 %
Ta_{in} = 28.1±0.12 [C]	$\partial Nusselt_{in} / \partial Ta_{in} = -3.123E-15$	0.00 %
Ta_{out} = 26.5±0.0675 [C]	$\partial Nusselt_{in} / \partial Ta_{out} = 0$	0.00 %
Tw_{in} = 10±0.09 [C]	$\partial Nusselt_{in} / \partial Tw_{in} = -15.46$	1.92 %
Tw_{out} = 22.5±0.09 [C]	$\partial Nusselt_{in} / \partial Tw_{out} = 6.873$	0.38 %
$velocity_a$ = 8.9±0.05 [m/s]	$\partial Nusselt_{in} / \partial velocity_a = 0$	0.00 %

$Nusselt_{out}$ = 489.7±40.98 [J-m/s-W]

DP = 300±1.47 [Pa]	$\partial Nusselt_{out} / \partial DP = 0$	0.00 %
LPM = 1±0.072	$\partial Nusselt_{out} / \partial LPM = 0$	0.00 %
Ta_{in} = 28.1±0.12 [C]	$\partial Nusselt_{out} / \partial Ta_{in} = 285.7$	70.02 %
Ta_{out} = 26.5±0.0675 [C]	$\partial Nusselt_{out} / \partial Ta_{out} = -327.6$	29.13 %
Tw_{in} = 10±0.09 [C]	$\partial Nusselt_{out} / \partial Tw_{in} = 20.94$	0.21 %
Tw_{out} = 22.5±0.09 [C]	$\partial Nusselt_{out} / \partial Tw_{out} = 19.7$	0.19 %
$velocity_a$ = 8.9±0.05 [m/s]	$\partial Nusselt_{out} / \partial velocity_a = 55.02$	0.45 %

Q_a = 266.5±22.98 [J-C/s-K]

DP = 300±1.47 [Pa]	$\partial Q_a / \partial DP = 0$	0.00 %
LPM = 1±0.072	$\partial Q_a / \partial LPM = 0$	0.00 %
Ta_{in} = 28.1±0.12 [C]	$\partial Q_a / \partial Ta_{in} = 166.5$	75.64 %
Ta_{out} = 26.5±0.0675 [C]	$\partial Q_a / \partial Ta_{out} = -166.5$	23.93 %
Tw_{in} = 10±0.09 [C]	$\partial Q_a / \partial Tw_{in} = 0$	0.00 %
Tw_{out} = 22.5±0.09 [C]	$\partial Q_a / \partial Tw_{out} = 0$	0.00 %
$velocity_a$ = 8.9±0.05 [m/s]	$\partial Q_a / \partial velocity_a = 29.94$	0.42 %

Q_m = 567±33.57 [J-C/s-K]		
DP = 300±1.47 [Pa]	$\partial Q_m/\partial DP = 0$	0.00 %
LPM = 1±0.072	$\partial Q_m/\partial LPM = 433.8$	86.56 %
Ta_{in} = 28.1±0.12 [C]	$\partial Q_m/\partial Ta_{in} = 83.27$	8.86 %
Ta_{out} = 26.5±0.0675 [C]	$\partial Q_m/\partial Ta_{out} = -83.27$	2.80 %
Tw_{in} = 10±0.09 [C]	$\partial Q_m/\partial Tw_{in} = -34.7$	0.87 %
Tw_{out} = 22.5±0.09 [C]	$\partial Q_m/\partial Tw_{out} = 34.7$	0.87 %
$velocity_a$ = 8.9±0.05 [m/s]	$\partial Q_m/\partial velocity_a = 14.97$	0.05 %

Q_{max} = 1256±91.05 [J-C/K-s]		
DP = 300±1.47 [Pa]	$\partial Q_{max}/\partial DP = 0$	0.00 %
LPM = 1±0.072	$\partial Q_{max}/\partial LPM = 1256$	98.69 %
Ta_{in} = 28.1±0.12 [C]	$\partial Q_{max}/\partial Ta_{in} = 69.4$	0.84 %
Ta_{out} = 26.5±0.0675 [C]	$\partial Q_{max}/\partial Ta_{out} = 0$	0.00 %
Tw_{in} = 10±0.09 [C]	$\partial Q_{max}/\partial Tw_{in} = -69.4$	0.47 %
Tw_{out} = 22.5±0.09 [C]	$\partial Q_{max}/\partial Tw_{out} = 0$	0.00 %
$velocity_a$ = 8.9±0.05 [m/s]	$\partial Q_{max}/\partial velocity_a = 0$	0.00 %

Q_w = 867.6±63.09 [J-C/s-K]		
DP = 300±1.47 [Pa]	$\partial Q_w/\partial DP = 0$	0.00 %
LPM = 1±0.072	$\partial Q_w/\partial LPM = 867.6$	98.04 %
Ta_{in} = 28.1±0.12 [C]	$\partial Q_w/\partial Ta_{in} = 0$	0.00 %
Ta_{out} = 26.5±0.0675 [C]	$\partial Q_w/\partial Ta_{out} = 0$	0.00 %
Tw_{in} = 10±0.09 [C]	$\partial Q_w/\partial Tw_{in} = -69.4$	0.98 %
Tw_{out} = 22.5±0.09 [C]	$\partial Q_w/\partial Tw_{out} = 69.4$	0.98 %
$velocity_a$ = 8.9±0.05 [m/s]	$\partial Q_w/\partial velocity_a = 0$	0.00 %

Re_a = 223975±1258		
DP = 300±1.47 [Pa]	$\partial Re_a/\partial DP = 0$	0.00 %
LPM = 1±0.072	$\partial Re_a/\partial LPM = 0$	0.00 %
Ta_{in} = 28.1±0.12 [C]	$\partial Re_a/\partial Ta_{in} = 0$	0.00 %
Ta_{out} = 26.5±0.0675 [C]	$\partial Re_a/\partial Ta_{out} = 0$	0.00 %
Tw_{in} = 10±0.09 [C]	$\partial Re_a/\partial Tw_{in} = 0$	0.00 %
Tw_{out} = 22.5±0.09 [C]	$\partial Re_a/\partial Tw_{out} = 0$	0.00 %
$velocity_a$ = 8.9±0.05 [m/s]	$\partial Re_a/\partial velocity_a = 25166$	100.00 %

Re_w = 2756±198.5		
DP = 300±1.47 [Pa]	$\partial Re_w / \partial DP$ = 0	0.00 %
LPM = 1±0.072	$\partial Re_w / \partial LPM$ = 2756	100.00 %
Ta_{in} = 28.1±0.12 [C]	$\partial Re_w / \partial Ta_{in}$ = -4.626E-14	0.00 %
Ta_{out} = 26.5±0.0675 [C]	$\partial Re_w / \partial Ta_{out}$ = 0	0.00 %
Tw_{in} = 10±0.09 [C]	$\partial Re_w / \partial Tw_{in}$ = 0	0.00 %
Tw_{out} = 22.5±0.09 [C]	$\partial Re_w / \partial Tw_{out}$ = 0	0.00 %
$velocity_a$ = 8.9±0.05 [m/s]	$\partial Re_w / \partial velocity_a$ = 0	0.00 %

Rt = 0.01779±0.001041 [s-K/J]		
DP = 300±1.47 [Pa]	$\partial Rt/\partial DP$ = 0	0.00 %
LPM = 1±0.072	$\partial Rt/\partial LPM$ = -0.01362	88.80 %
Ta_{in} = 28.1±0.12 [C]	$\partial Rt/\partial Ta_{in}$ = -0.001305	2.26 %
Ta_{out} = 26.5±0.0675 [C]	$\partial Rt/\partial Ta_{out}$ = 0.003247	4.44 %
Tw_{in} = 10±0.09 [C]	$\partial Rt/\partial Tw_{in}$ = 0.0004544	0.15 %
Tw_{out} = 22.5±0.09 [C]	$\partial Rt/\partial Tw_{out}$ = -0.002397	4.30 %
$velocity_a$ = 8.9±0.05 [m/s]	$\partial Rt/\partial velocity_a$ = -0.0004697	0.05 %

Appendix (H) Articles extracted from the current study (published and under review)

Conference and Journal papers:

1- "Metallic foam with cross flow heat exchanger: A review of parameters, performance, and challenges". *(**Published** in WILEY Heat Transfer)*

2- "Numerical Study of Fan Coil Heat Exchanger with Copper-Foam". *(**Published** in International Journal of Fluid Machinery and Systems)*

3- Experimental study of thermal performance improvement in a cross-flow heat exchanger by using copper foam. *(**Published** in WILEY Heat Transfer)*

4- "Numerical Solution of Cross Flow Heat Exchanger with Metallic Foam". (***Accepted*** in AIP Publishing "4th international scientific conference of Alkafeel university, ISCKU 2022).

5- "Thermal Design of Cross Flow Heat Exchanger for Fan Coil Unit Application". (***under review*** in International Journal of Integrated Engineering).

6- "Comparing the Performance of Copper Foam and Aluminum Fins in Improving Heat Transfer of Cross-Flow Heat Exchanger: An Experimental and Numerical Study". (***under review*** in ELSEVIER International Journal of Heat and Mass Transfer) .

Received: 19 September 2022 | Accepted: 18 October 2022

DOI: 10.1002/htj.22798

ORIGINAL ARTICLE

HEAT TRANSFER WILEY

Metallic foam with cross flow heat exchanger: A review of parameters, performance, and challenges

Ahmed M. Hassan | **Adil Abbas Alwan** | **Hameed Kadhem Hamzah**

Mechanical Engineering Department, College of Engineering, University of Babylon, Hillah, Iraq

Correspondence
Ahmed M. Hassan, Mechanical Engineering Department, College of Engineering, University of Babylon, Hillah, Iraq.
Email: ahmed.abdelaris@student.uobabylon.edu.iq

Abstract

The cross-flow heat exchanger involves a tractor moving between two fluids that flow in a direction perpendicular to each other, and one of the fluids is often a liquid and the other is a gas. This type of heat exchanger has been studied in many previous studies for its importance in air conditioning applications and many industrial applications. In this type of heat exchanger, the surface area for heat transfer is very large. Therefore, many techniques have been used to improve the thermal and dynamic performance of this type of heat exchanger. In this study, previous studies that used metallic foam as one of the ways to improve the performance of heat exchangers were reviewed. The most important techniques that were used in previous studies during the process of evaluating the thermal performance of a cross-flow heat exchanger in the presence of different types of metal foam were clarified. The use of metal foam depends on important factors, including (1) the type of material, where copper and aluminum were used in most of the previous studies, due to their availability and ease of foam formation using these materials, in addition to

Abbreviations: AG, area goodness factor; *B*, surface to volume ratio (m^2/m^3); HVAC, heat ventilation and air conditions; LMTD, logarithmic mean temperature difference; LTE, local thermal equilibrium; LTNE, local thermal nonequilibrium; PPI, number of pores per inch.

International Journal of Fluid Machinery and Systems
Vol. 16, No. 1, January-March 2023

DOI: http://dx.doi.org/10.5293/IJFMS.2023.16.1.073
ISSN (Online): 1882-9554

Original Paper

Numerical Study of Fan Coil Heat Exchanger with Copper-Foam

Ahmed M. Hassan[1,2], Adil Abbas Alwan[1,2] and Hameed K. Hamzah[3]

[1] Department of Mechanical Engineering University of Babylon-Babylon-Iraq.
Babylon, Hilla, 51001, Iraq.
[2] College of Engineering, Department of Medical industry engineering, National University of Science and Technology, Dhi Qar, 64001, Iraq, ahmed.abdelaris@student.uobabylon.edu.iq,
adil_almoosway@yahoo.com, eng.hameed.hamzah1@uobabylon.edu.iq

Abstract

Due to its high porosity as well as a high specific surface area, the use of open cell metallic foam in heat transfer applications has received increasing interest. In present study, the dynamic and thermal performance of heat exchanger composed of copper foam incorporated in a fan coil was numerically analyzed. Darcy-Brinkman-Forchheimer model was used to represent the momentum equation inside the metallic foam (a porous medium). A local thermal equilibrium was used to solve the energy equation through the porous medium. Different porosity values were taken during the study, ranging from 0.88 to 0.98, while the velocity of inlet air of the heat exchanger ranged from 1 m/s to 10 m/s. The objective of current study is to compare the thermal and dynamic performance of the heat exchanger affected by several variables such as heat transfer coefficient, friction factor, pressure drop, Colburn factor, and area goodness factor. The results showed that increasing the air inlet velocity will increase the heat transfer coefficient, but on the other hand, increasing the velocity ten times will rise pressure drop from 19.032 Pa to 335.76 Pa. Also, the area goodness factor value will decrease with increasing inlet velocity. Finally, we found that increasing in medium porosity will reduce heat transfer coefficient but increase pressure drop.

Keywords: Cross flow, Heat Exchanger, Metallic Foam, Heat Transfer, Local Thermal Equilibrium (LTE), Darcy-Brinkman-Forchheimer, Colburn factor.

1. Introduction

The process of improving the performance of heat exchangers during HVAC applications as well as industrial applications has occupied many previous studies during the past decades. The fan coil unit is one of the most important parts used in air conditioning systems, which is one of the types of cross flow heat exchangers. Jacobi and Shah [1] discussed the enhancement mechanisms of air –side flow in cross flow heat exchanger by reviewing a number of methods to improve the heat transfer performance in heat exchangers such as: (1) using plain passages in plate-fin or tube-fin construction, (2) using wave passages (3) or using interrupted passages. Passive methods are the most common methods for improving heat transfer through a cross-flow heat exchanger because they do not need an external power source. They usually include the modification of the heat transfer surface area [2-5], and/or adding a vortex generator into the flow path [6-9]. As these methods provide instability in the flow, and thus improve the efficiency of heat transfer. Recently, metallic foam has been used with cross-flow heat exchangers to increase the heat exchange area as well as provide instability in the flow and thus improve heat transfer. Due to its high heat transfer area compared to its size, metallic foam has been employed extensively in studies that guarantee improved heat transfer. The metallic foam splits the boundary layer as the fluid travels through it, distributing the flow through it, and so enhancing the heat transfer coefficient. Glycol/water-air cross-flow heat exchangers made of flat aluminum foam tubes that were brazed together were employed by Tadrist et al. [10], and [11]. Three different types of foam (10, 20, and 40 PPI) were used in various exchanger systems. The tubes were also separated by two different distances, 2.5 mm and 5.3 mm. The Colburn factor did not significantly differ amongst a several recorded designs. Boomsma et al. [12] conducted an experimental study on the efficiency and pumping power of compact heat exchangers. After adding aluminum foam to the water channel. They investigated how pressure drop and heat transfer are affected by the foam compression ratio. They observed that the metal foam boosted thermal efficiency by reducing the thermal resistance in half from what it would have been with no foam.

In an experiment, Jamin and Mohamad [13] used cross-flow carbon foam to improve the heat transfer from a vertical tube. They contrasted various pipe and foam construction methods, including bare pipe, large fins, small fins, large sleeves, and small

Received October 4 2022; revised October 28 2022; accepted for publication December 13 2022; Review conducted by Guang Xi (Paper number O22038K)
Corresponding author: Ahmed M. Hassan, Dr. ahmed.abdelaris@student.uobabylon.edu.iq.

Received: 22 January 2023 | Revised: 13 March 2023 | Accepted: 30 March 2023

DOI: 10.1002/htj.22867

ORIGINAL ARTICLE

HEAT TRANSFER WILEY

Experimental study of thermal performance improvement in a cross-flow heat exchanger by using copper foam

Ahmed M. Hassan[1,2] | **Adil Abbas Alwan**[2] | **Hameed K. Hamzah**[1]

[1]Department of Mechanical Engineering, University of Babylon, Hilla, Iraq

[2]Department of Medical Industry Engineering, College of Engineering, National University of Science and Technology, Dhi Qar, Iraq

Correspondence
Ahmed M. Hassan, Department of Mechanical Engineering University of Babylon, Hilla 51001, Iraq.
Email: ahmed.abdelaris@student.uobabylon.edu.iq and ahmed.eng.mach@gmail.com

Abstract

In this study, copper foam was used as a porous medium in place of traditional aluminum fins. A comparison between the two heat exchangers—one with fins and the other with copper foam—was conducted under various conditions. The air inlet velocity ranged from 0.9 to 9.3 m/s, and the water inlet temperature ranged from 10°C to 18°C. Different water flow rates were tested. A comparison was made between the performance of copper foam and aluminum fins by calculating several parameters, including thermal resistance, heat exchanger effectiveness, Colburn factor, Nusselt number, friction factor, and area goodness factor (AG). The experimental results showed that at low air velocities, the heat transfer coefficient for both types of heat exchangers was almost equal. However, at high air velocities, the copper foam exhibited a higher heat transfer coefficient. The Colburn factor was higher for the heat exchanger with copper foam than in the conventional fins, where it was equal to 0.1959 for the copper foam and 0.1186 for the fins. On the other hand, the AG was higher in the case of fins than in the heat exchanger with copper foam.

KEYWORDS

area goodness, Colburn factor, copper foam, cross flow, fin, heat exchanger, porous media

Abbreviations: AG, area goodness factor; HVAC, heating, ventilation, and air conditioning; LMTD, logarithmic mean temperature difference; PPI, pores per inch; SD, standard deviation; SU, standard uncertainty.

Numerical Solution of Cross Flow Heat Exchanger With Metallic Foam

Ahmed M. Hassan[1,a)], Adil Abbas Alwan[2,b)], and Hameed K. Hamzah[3,c)]

[1,2,3] *Department of Mechanical Engineering University of Babylon-Babylon-Iraq,*

[a)] *Corresponding author:* ahmed.abdelaris@student.uobabylon.edu.iq
[b)] adil_almoosawy@yahoo.com
[c)] eng.hameed.kadhem@uobabylon.edu.iq

Abstract. In this study, the thermal and dynamic performance of a cross-flow heat exchanger was numerically investigated by using the Darcy-Brinkman-Forchheimer and Navier-Stokes equations. The copper foam is embedded around the tube surface to increase the heat transfer rate. The open cell copper foam was treated as a porous medium so that the Local Thermal Equilibrium (LTE) model was used in this study to find the temperature distribution. The copper foam has a pore density of 40 PPI, and a porosity of 0.93. The numerical solution used the air as a working fluid with a Reynolds number (Re) of 200 to 850. The ratio of copper foam thickness to tube diameter (L/d) varies from 2 to 20, while the ratio of tube pitch to tube diameter (H/d) varies from 2 to 20. The result showed the friction factor increased as (L/d) increased, and the highest value of the Colburn factor (j) can be obtained when (L/d) equals 2. H/r increasing leads to an increase in the friction factor and Colburn factor (j). The optimal height of metallic foam can be evaluated by using the area goodness parameter (AG), which is at H/r equal to 3 in the current study.

Keywords: Cross flow, Heat Exchanger, Metallic Foam, Heat Transfer, Local Thermal Equilibrium (LTE), Darcy-Brinkman-Forchheimer, Colburn factor.

Nomenclature

A	Cross section area [m^2]
AG	Area goodness factor
Cr	Drag factor Coefficient
c_p	Specific heat [J/kg.K]
df	Fiber diameter [m]
dp	Pore diameter [m]
f	Friction factor
g	Gravity acceleration [m/s^2]
H	Half pitch [m]
h	Heat transfer coefficient [W/m^2K]
j	Coulbourn factor
k	Thermal conductivity [W/m.K]
K	Permeability [m^2]
L	Thickness of porous medium in direction of flow [m]
LTE	Local thermal equilibrium
LTNE	Local thermal non equilibrium
$\dot{m}$	Mass flow rate
p	Pressure [Pa]
PPI	Number of pores per inch

University of AlKafeel

Acceptance Letter

Author : Ahmed M. Hassan
Affiliation : Department of Mechanical Engineering University of Babylon-Babylon-Iraq
Email : ahmed.abdelaris@student.uobabylon.edu.iq

Dear (author) We are pleased to inform you that your manuscript,
Numerical Solution Of Cross Flow Heat Exchanger With Metallic Foam
after being peer- reviewed , has been accepted for participating in the

4th INTERNATIONAL SCIENTIFIC CONFERENCE OF ALKAFEEL UNIVERSITY , ISCKU 2022

in Al-Najaf Al-Ashraf, Iraq ,December 20th -21st , 2022 . Given that your manuscript will be published after passing the conference Scopus-indexed journals requirements.

With Best Regards

N. ALDAHA
Prof. Dr. N. Al-Dahan
Rector of Alkafeel University

Scopus AIP Publishing

University of AlKafeel

Certificate of Attendance

This certificate is awarded to

Ahmed M. Hassan|Adil Abbas Alwan|Hameed K. Hamzah

for his /her attendance at the events of the Fourth International Scientific Conference of University of Alkafeel held on 20-21/12/2022 .

With Best Appreciation and Respect

N. ALDAHA
Prof. Dr. N. Al-Dahan
Rector of Alkafeel University

INTERNATIONAL JOURNAL OF INTEGRATED ENGINEERING VOL. 0 NO. 0 (2021) 1-4

IJIE

http://penerbit.uthm.edu.my/ojs/index.php/ijie
ISSN : 2229-838X e-ISSN : 2600-7916

The International Journal of Integrated Engineering

Thermal Design of Cross Flow Heat Exchanger for Fan Coil Unit Application

Ahmed M. Hassan[1*], Adil Abbas Alwan[2], Hameed Kadhem Hamzah[3]

[1,2,3] University of Babylon/College of Eng. /Mechanical Eng. Department, Iraq

*Corresponding Author: ahmed.abdelaris@student.uobabylon.edu.iq

DOI: https://doi.org/10.30880/ijie.0000.00.00.000
Received 00 Month 2000; Accepted 01 Month 2000; Available online 02 Month 2000

Abstract: Analytical and numerical solution for determine the dimensions of cross flow heat exchanger under deferent conditions are developed in this study. The analytical solution by ε-NTU method used to found the initial dimensions of cross flow heat exchanger. Numerical solution was used to validated of analytical solution and to optimized the cooling coil dimensions. The ε-NTU design results showed the effect of water mass flow rate, air inlet velocity, and the outer tube diameter of cooling coil. The distribution of air, and water temperatures through heat exchanger can be predicted by solving the basic Navier-Stoke equation, and energy equation by using numerical methods.

Keywords: Cross flow, Heat Exchanger, ε-NTU, Fan Coil Unit, Thermal Design.

1 Introduction

The increase in the cost of energy production is one of the important reasons that prompted many studies to improve the thermal performance of heat transfer systems. Perhaps the most important systems are heat exchanger systems, which constitute the main part of most industrial applications. One of the most important heat exchanger systems is the one used in air conditioning because it constitutes about 50 to 60 % of the annual rate of energy consumption [1] . The cross-flow heat exchanger is used in different parts of the air conditioning system, such as the condenser, fan coil units (FCU), and air handing unit. etc. Therefore, the good design process of the cross-flow heat exchanger will reduce energy consumption, as in the current study, which mainly relied on the design of a cross-flow heat exchanger within certain weather conditions to be used in the application of the FCU. And due to the change in heat load during the hours of the day, the air conditioning system must be designed to cover the needs of the building over all hours of the day and to provide appropriate comfort conditions for the residents inside the building. There are many studies that focused on providing comfortable conditions and a lower rate of energy consumption when designing the HVAC system such as [2]. The methods of designing the cooling coil in the cross-flow heat exchanger are divided into log mean enthalpy difference (LMED), and equivalent dry-bulb temperature method (EDTM) according to what was clarified through [3]. These two methods have been widely used in previous studies

Xia et al. [4] used the method of log mean enthalpy difference (LMED) in the process of designing and evaluated the thermal performance of the cooling coil under humid conditions, assuming the Lewis number equals 1 once and again not equal to 1. And also Thy used another method, which is modified LMED method and made a comparison between this method and a numerical method that depends on solving the equations of conservation of energy and mass and noticed that the difference between the two methods is approximately equal to 5 %. Cui et al. [5] also used the modified LMED method to study and design an indirect type heat exchanger, where this exchanger is used to reduce the air temperature by using cold water and without affecting the level of air humidity. By using this method to analyze the thermal performance of a cross-flow exchanger, they found that the results are close to the numerical solution that It takes more time to solve. There are many other studies that used methods approaching LMED, including the study [6], [7], [8], and [9] who used analytical models to calculate the thermal performance of the

*Corresponding author: author-mail@uthm.edu.my

الخلاصة

نظرًا لاستخدام الرغوة المعدنية ذات الخلايا المفتوحة في تطبيقات نقل الحرارة بسبب مساميتها العالية ومساحة سطحها النوعية العالية، فقد تلقت اهتمامًا متزايدًا. في الدراسة الحالية، تم تحليل الأداء الديناميكي والحراري لمبادل حراري يتألف من رغوة نحاسية مدمجة في وحدة ملف المروحة عملياً وعددياً.

صُمم مبادل حراري لوحدة ملف المروحة بحمل تبريد يبلغ 2 طن تثليج. اختبرات ظروف تدفق مختلفة للوصول إلى التصميم المناسب الذي يغطي حمل التبريد المطلوب. عملية تصميم المبادل الحراري تمت باستخدام طريقة (ε–NTU) وبرنامج (SOLIDWORK) لتحديد طول الأنبوب وشكل المبادل الحراري. من خلال الجانب العملي ، تم استخدام رغوة نحاسية كوسيط مسامي ، حيث تم وضعها بدلاً من زعانف الألمنيوم التقليدية. تمت المقارنة بين المبادلين الحراريين ، أحدهما بزعانف والآخر برغوة نحاسية ، تحت ظروف مختلفة. تراوح عدد رينولدز للهواء الداخل من 37000 إلى 235000. وتم إجراء مقارنة بين الأداء الحراري والديناميكي لرغوة النحاس والزعانف من خلال حساب عدة متغيرات ، منها فعالية المبادل الحراري ، والمقاومة الحرارية ، ومعامل انتقال الحرارة ، ورقم نوسلت ، ومعامل كولبيرن. ومعامل الاحتكاك وعامل جودة المنطقة. في الجانب النظري، استخدام برنامج (COMSOL Multiphysics 6.0) لتحليل الجريان وانتقال الحرارة خلال المبادل الحراري مع الرغوة المعدنية. نموذج (Darcy–Brinkman–Forchheimer)استخدمة لتمثيل معادلة الزخم داخل الرغوة المعدنية (وسط مسامي). تم استخدام موديل (توازن حراري محلي) لحل معادلة الطاقة خلال وسط مسامي.

خلال التجارب العملية ، وجد بأن درجة حرارة دخول الماء عند 10 م هي الأنسب لإعطاء أداء حراري أفضل وتعتمد بشكل أساسي على قطر الأنبوب الذي تم اختياره. يعتمد معدل تدفق الماء البارد عبر الأنبوب على حمل التبريد ، لذلك من خلال التجارب وجد أن تدفق 4 لتر/دقيقة يغطي حمل التبريد المطلوب. أظهرت النتائج العملية عند سرعة الهواء المنخفضة أن معامل انتقال الحرارة متساوٍ تقريبًا لكلا النوعين وبفارق بسيط لالزعانف ، بينما يزداد الاختلاف في معامل انتقال الحرارة مع زيادة سرعة الهواء الداخل. كان معامل كولبورن أعلى في حالة المبادل الحراري برغوة نحاسية عنه في الزعانف التقليدية ، حيث كان يساوي 0.1959 للرغوة النحاسية و 0.1186 للزعانف. يكون عامل جودة المنطقة أعلى في حالة الزعانف من قيمته في حالة الرغوة النحاسية بمقدار 16.8%. تم اختبار قيم مسامية مختلفة خلال الدراسة تراوحت من 0.88 إلى 0.98 ، بينما تراوحت سرعة الهواء الداخل للمبادل الحراري من 1 م / ثا إلى 10 م / ثا. أظهرت النتائج النظرية أن زيادة المسامية من 0.88 إلى 0.98 أدت إلى انخفاض معامل انتقال الحرارة بنسبة 39٪ في حالة السرعة 10 م / ثا وبنسبة 30٪ في حالة السرعة 1 م / ثا. ينخفض هبوط الضغط خلال المبادل الحراري بنسبة 32٪ عند زيادة المسامية من 0.88 إلى 0.98 عند سرعة دخول هواء تبلغ 10 م / ثا.

تم إجراء مقارنة بين النتائج العملية والنظرية حيث تبين أن نسبة النحراف بين النتائج لمعامل انتقال الحرارة كان 19.1٪ عندما كان رقم رينولدز يساوي 22650 ، و 19.2٪ عند رقم رينولدز يساوي 120800 ، و 19.2٪ برقم رينولدز يساوي 218940.

جمهورية العراق
وزارة التعليم العالي والبحث العلمي
جامعة بابل / كلية الهندسة
قسم الهندسة الميكانيكية

تحسين الأداء الحراري- الهيدروليكي لمبادل حراري باستخدام رغوة نحاسية

أطروحة
مقدمة إلى كلية الهندسة – جامعة بابل وهي جزء من متطلبات نيل شهادة الدكتوراه
في علوم الهندسة الميكانيكية/ قدرة

من قبل
احمد محمد حسن عبدالعريس

بأشراف

أ. د. عادل عباس علوان الموسوي

أ.د. حميد كاظم حمزه

1444هـ *2023 م*